



University
of Glasgow

Nauny, Philippe É. M. (2019) *Interpretation of biosignatures in extreme environments, and their potential impact for the search for life on Mars.*

PhD thesis.

<http://theses.gla.ac.uk/77875/>

Copyright and moral rights for this work are retained by the author

A copy can be downloaded for personal non-commercial research or study, without prior permission or charge

This work cannot be reproduced or quoted extensively from without first obtaining permission in writing from the author

The content must not be changed in any way or sold commercially in any format or medium without the formal permission of the author

When referring to this work, full bibliographic details including the author, title, awarding institution and date of the thesis must be given

Enlighten: Theses

<https://theses.gla.ac.uk/>
research-enlighten@glasgow.ac.uk

Interpretation of biosignatures in extreme environments, and their potential impact for the search for life on Mars

Philippe É. M. NAUNY
Master en Chimie et Biologie
Université Louis Pasteur, Strasbourg

*Submitted in fulfilment of the requirements for the
Degree of Doctor of Philosophy*

School of Geographical and Earth Sciences
College of Science and Engineering
University of Glasgow



Viva: 21st February 2019

Abstract

The search for life beyond Earth, and on Mars in particular, is one of the key points of astrobiology research. However, space missions are expensive and time-consuming. Simulating such missions at analogue sites on Earth can thus save time and money whilst working in natural settings. This thesis presents three studies of biosignatures from three different martian analogues. These biosignatures were linked — when possible — to environmental parameters observed at their sampling sites.

The first study was set in a hot a dry environment in the Atacama Desert in Chile. It aimed to identify biolipids and genetic material in soil samples, along a high-resolution shallow depth profile in a dry alluvial fan. Signs of microbial life were observed at the surface, despite the extreme environmental conditions, and at deeper depths — together with degraded plant material — above a layer of very fine grained sands and silts. Overall, biolipids of plant origin showed the strongest concentrations, despite the quasi-absence of plants at the surface. The poor quality of the DNA sequencing results prevented their interpretation. The sedimentation history of the sampling site seemed to be more complex than what could be observed at the surface.

The second study was on the flank of the Sairecabur, a high-altitude volcano in Chile. Soil samples, taken along four depth profiles following an altitude gradient, were analysed for their biolipids and genetic material content. Again, biolipids of plant origin showed the strongest concentrations — both at vegetated and barren sites — and the poor quality of the DNA sequencing results prevented their interpretation. Additionally, the variable environmental and physico-chemical conditions at the different sampling sites makes it more challenging to draw conclusions regarding the altitude gradient.

The third study took place inside the crater of Hverfjall, a tuff ring volcano in Iceland. Colonisation of the crater by life was studied by measuring microbial activity and biolipids in soil samples along a transect across the crater, and by considering the relationship between the results and the wind patterns over and within the crater. The results indicate that wind may be a major factor for controlling the deposition and removal of biosignatures in Hverfjall's crater.

All three sites were isolated environments. Despite this, lipid biomarkers, genetic material or microbial activity were observed at each of these sites. Molecules produced by plants were also found everywhere despite the general absence of nearby plants, implying some external source for the molecules. Aeolian input is probably the dominant factor for spreading biosignatures to these isolated locations.

The high altitude sites on the Sairecabur can serve as analogues to for a Noachian Mars, when the planet lost its global habitability, whereas the Atacama desert is an analogue for present-day Mars. Hverfall serves as an analogue for both past and present Mars, focusing on wind dispersal of biomarkers. The results obtained suggest that if any active biomarker source (i. e. life) were to be identified on Mars, downwind sampling represents an alternative means by which to sample biomarkers whilst avoiding any direct contamination of the source.

Contents

Abstract	iii
Acknowledgements	xiii
Declaration	xv
Abbreviations and symbols	xvii
1 General introduction	1
1.1 Brief historical perspective of astrobiology	2
1.1.1 The place of Earth in the Universe	2
1.1.2 A chemical origin of life	3
1.1.3 From exobiology to astrobiology	3
1.1.4 Astrobiology today	3
1.2 Mars from an astrobiology perspective	4
1.2.1 Geological and hydrological history	4
1.2.2 Mars today	6
1.3 Terrestrial analogues for Mars	7
1.3.1 Atacama Desert	9
1.3.2 Antarctic Dry Valleys	9
1.3.3 Iceland	9
1.3.4 Río Tinto	10
1.3.5 Yellowstone National Park	10
1.4 Biosignatures	10
1.4.1 Lipids	10
1.4.2 Pigments	11
1.4.3 Amino acid	11
1.4.4 Nucleic acids	12
1.5 PhD project	12
1.5.1 Motivation	12
1.5.2 Contributions	13
2 Methodology	15
2.1 Fieldwork	16

2.1.1	Sample collection	16
2.1.2	Environmental readings	16
2.2	Inorganic content	18
2.2.1	Water content	18
2.2.2	Carbonate content	18
2.2.3	pH	20
2.2.4	Grain size measurement	20
2.2.5	X-ray diffraction	20
2.2.6	Energy-dispersive X-ray spectroscopy	21
2.3	Organic content	21
2.3.1	Loss on ignition	21
2.3.2	Organic geochemistry	21
2.4	Genomic analyses	24
2.4.1	DNA extraction	24
2.4.2	DNA amplification	25
2.4.3	Library preparation and sequencing	26
2.4.4	Bioinformatics	27
2.5	ATP activity	27
2.5.1	Sample preparation	28
2.5.2	Bioluminescence measurement	28

3 Atacama 29

3.1	Introduction: The Atacama Desert	30
3.1.1	Climate	30
3.1.2	Life	31
3.2	Rationale	32
3.3	Hypotheses	33
3.4	Methods	33
3.4.1	Sampling strategy	33
3.4.2	Planned analyses	35
3.5	Results	35
3.5.1	Soil physico-chemistry	35
3.5.2	Environmental readings	38
3.5.3	Organic content	41
3.5.4	Plant sample	46
3.5.5	DNA content	46
3.6	Discussion	49
3.6.1	Soil physico-chemistry	49
3.6.2	Environmental readings	50
3.6.3	Organic content	50
3.6.4	Plant sample	52

3.6.5	DNA content	52
3.6.6	General discussion	53
3.7	Relevance to Mars	56
3.8	Conclusion	56
4	Sairecabur	59
4.1	Introduction: The Central Andean Dry Puña	60
4.1.1	Climate	60
4.1.2	Life	61
4.2	Rationale	61
4.3	Hypotheses	62
4.4	Methods	63
4.4.1	Sampling strategy	63
4.4.2	Planned analyses	65
4.5	Results	65
4.5.1	Soil physico-chemistry	65
4.5.2	Environmental parameters	70
4.5.3	Organic content	70
4.5.4	Plant and lichen samples	82
4.5.5	DNA content	84
4.6	Discussion	90
4.6.1	Soil physico-chemistry	90
4.6.2	Environmental parameters	91
4.6.3	Organic content	93
4.6.4	Plant and lichen samples	97
4.6.5	DNA	97
4.6.6	General discussion	99
4.7	Relevance to Mars	104
4.8	Conclusion	105
5	Iceland	107
5.1	Introduction: The Hverfjall crater	108
5.1.1	Climate	109
5.1.2	Life	110
5.2	Rationale	110
5.3	Hypothesis	111
5.4	Methods	111
5.4.1	Sampling strategy	111
5.4.2	Planned analyses	112
5.5	Results	112
5.5.1	ATP	112
5.5.2	Lipids	112

5.5.3	pH	115
5.6	Discussion	115
5.7	Relevance to M ars	117
5.8	Conclusion	118
6	Summary	119
6.1	Studied sites	120
6.2	Relevance to Mars exploration	122
A	X-ray diffraction spectra	123
A.1	Atacama samples	124
A.2	Sairecabur samples	127
A.2.1	4296 m	127
A.2.2	4782 m	130
A.2.3	5056 m	131
A.2.4	5269 m	132
B	Plant and lichen samples	133
B.1	Sample description	134
B.2	Comments on plants	137
B.3	Comments on lichens	138
	Bibliography	139

List of Tables

1.1	Planetary analogues for Mars	9
3.1	Atacama: air T and RH, and UV measurements	38
3.2	Atacama: (under)ground T and RH measurements	40
3.3	Atacama: metagenomics – Kraken results	48
3.4	Atacama: metagenomics – Kaiju results	48
4.1	Sairecabur: air temperature and relative humidity, and UV levels	70
4.2	Sairecabur: (under)ground T and RH measurements	74
4.3	4 296 m: metagenomics – Kraken results	87
4.4	4 296 m: metagenomics – Kaiju results	88
4.5	5 056 m: metagenomics – Kraken results	88
4.6	5 056 m: metagenomics – Kaiju results	89
4.7	5 269 m: metagenomics – Kraken results	89
4.8	5 269 m: metagenomics – Kaiju results	90
6.1	Comparative table for the main results	121
A.1	Minerals identified by XRD	124
B.1	Analysis of the plant and lichen samples	134

List of Figures

1.1	Geological periods on Mars	5
1.2	Water on Mars	8
2.1	Bioinformatics analysis strategy	27
3.1	The Atacama Desert and the factors influencing its aridity	31
3.2	Atacama field images	34
3.3	Atacama: minerals observed by EDX	36
3.4	Atacama samples: grain sizes	37
3.5	Atacama: water-related physio-chemistry	38
3.6	Atacama: air T and RH measurements	39
3.7	Atacama: organic content	40
3.8	Atacama: unresolved complex mixture	41
3.9	Plant lipid inputs at the Atacama sampling site.	42
3.10	Microbial lipid inputs at the Atacama sampling site.	43
3.11	Atacama: <i>n</i> -alkanes-related indices	44
3.12	Atacama: <i>n</i> -alkanols	45
3.13	Atacama: DNA concentrations	46
3.14	Atacama: bacterial 16S rDNA PCR gel	47
3.15	Atacama sediment deposit	49
3.16	Atacama results summary	54
4.1	Map of the area near the Sairecabur volcanic massif	64
4.2	Soil sampling sites near the Sairecabur volcano	66
4.3	Sairecabur samples: grain sizes	67
4.4	Sairecabur samples: water content	68
4.5	Sairecabur samples: carbonate content	69
4.6	Sairecabur samples: pH	69
4.7	4 296 m: ground and underground measurements	71
4.8	4 782 m: ground and underground measurements	72
4.9	5 056 m: ground and underground measurements	73
4.10	Sairecabur: LOI ₅₅₀	75
4.11	Sairecabur: TLE	76
4.12	Plant lipid inputs at 4296 m	77

4.13	Plant lipid inputs at 4782 m	78
4.14	Plant lipid inputs at 5056 m	79
4.15	Plant lipid inputs at 5269 m	79
4.16	Microbial lipid inputs at 4296 m	80
4.17	Microbial lipid inputs at 4782 m	81
4.18	Microbial lipid inputs at 5056 m	81
4.19	Microbial lipid inputs at 5269 m	81
4.20	Atacama: <i>n</i> -alkanes-related indices	83
4.21	Sairecabur plants and lichens: CPI vs ACL	84
4.22	Sairecabur: DNA content	85
4.23	4 296 m results summary	100
4.24	4 782 m results summary	101
4.25	5 056 m results summary	102
4.26	5 269 m results summary	102
5.1	Sampling points within Hverfall's crater	109
5.2	Examples of Hverfjall flora	110
5.3	Hverfjall data: ATP levels	113
5.4	Hverfjall data: TLE concentrations	113
5.5	Hverfjall data: even-numbered short chain <i>n</i> -alkanes	114
5.6	Hverfjall data: odd-numbered long chain <i>n</i> -alkanes	114
5.7	Hverfjall data: ACL values	114
5.8	Hverfjall data: CPI values	115
5.9	Putative wind patterns leading to the observed biomarker repartition	117

Acknowledgements

First of all, I would like to thank my family for their moral and financial support. Doing a four-years self-funded PhD eventually turned out to be more challenging — one can also say stupid — than anticipated. I could not have finished without their help.

Then I would like to thank the jury members, Dr Iain Neill, Dr Lydia Hallis and Dr Karen Olsson-Francis for taking time out of their schedules to take place in my PhD jury and read my thesis.

This research has been partly funded by the *Sir Alwyn Williams postgraduate scholarship* and the *Michael Golden postgraduate scholarship* from the University of Glasgow — to buy DNA extraction and sequencing kits — and by the *Scottish Alliance for Geoscience, Environment & Society small grant scheme* from SAGES — to pay for XRD analyses.

I am grateful to Prof. Vernon Phoenix for letting me start working in his group on such an interesting topic, to Prof. Jaime Toney for taking the first supervisor role when Vern switched institutes, and to Prof. Martin Lee for taking the role of second supervisor and for helping me to zap rock dust for EDX analyses.

I extend my gratefulness to Prof. William Sloan and Dr Linas Mažutis for letting me use their facilities and material.

Thanks to my two fellow astrobiology colleagues Nick and Rory and to the BECS people, especially Nono, Jill, and Julien for sharing their experience and knowledge. Thanks also to Harry, Ali, Peter, John, Robert, and Kenny for their technical help and wisdom.

Thanks to Dr Jose Rico, Prof. Justin Hargreaves, Dr Claire Wilson and Dr Tizi Marocco for helping me carry out the XRD analyses and interpret the results. Thanks to Prof. Michael Richter and Dr Scott Paine for sharing the meteorological data they recorded on the Sairecabur. Thanks to Prof. Claudio Latorre for helping me identify the Chilean plants.

Working in Vilnius was the best experience during this PhD after Iceland (sorry guys, but it's hard to beat that one). Thanks again Linas for bringing me back to the world of droplets after all these years; I'm sorry that the results ended up being far less interesting what we hoped. Thanks a lot to your team too (Dalius, Greta S., Greta Z., Juozas, Karolis G., Karolis L., Karolis S., Valdemaras) who were very welcoming, and especially Karolis S., Juozas, and Valdemaras for training and helping me. Ačiū visiems!

Thanks to Prof. Wolf Geppert, Prof. Karen Meech, and Dr David Cullen for letting me attend workshops and fieldwork in Iceland twice and bearing with me when I took some extra time to finish collecting my samples. Thanks to my all my colleagues from the HAMCOM and the TEAMC teams, and all the other attendees too. One question will probably never get

a definitive answer: cheese or dog?

Thanks also to the other former souls trapped in the *Corridor of Doom* at the begin of our PhD (Annemarie, Jessica, Jonny, Sapphire, and Rory), and to the others we assimilated (Ash and Jorge), for sharing these four years.

Thanks to Nicolas and Julien for the rubbish French chats, and to Uli for testing my German level. I'll miss the beer and wine and crisps and film nights in the office.

Extra credit to my former flatmates Annemarie and Jorge. Thanks for the nerdy chats, for making fun of each other's country, and for the Exploding Kittens and the Zombicide games. Additional thanks to Annemarie for proofreading my English (my hovercraft is full of eels), and for answering my never-ending questions about rocks and trying to make me a geologist (but my padawan training is not complete yet).

Thanks to all the others — work mates, professors, internship supervisors, scientists from the lab next door, conference and workshop organisers and participants — who helped me to shape my "carrier" in science — from stepping into academic research, to working on prebiotic chemistry, directed evolution, and ultimately astrobiology: Dr Claire Courson, Dr Nigel Ribeiro, late Prof. Guy Ourisson, Prof. Catherine Grosdemange, Prof. Michel Rohmer, Prof. Andrew Griffiths, Dr Michael Ryckelynck, Agnès Gaudry, Dr Oliver Miller, Dr Lucia Granieri, Dr Joël Boeglin, Dr Linas Mažutis, Dr Shigeyoshi Matsumura, Dr Christoph Merten, Dr Kerstin Blank, Dr Lucas Frenz, Dr Dave van Ditmarsch, Dr Gabrielle Woronoff, Dr Ashleigh Theberge, Prof. Claudia Höbartner, Dr Elisabeth Zielonka, Prof. Patrice Soumillion, Prof. Bernard Hallet, Dr Bruno Baudoux, Laurence Bausier, Prof. Muriel Gargaud, Prof. Hervé Cottin, Prof. Lena Noack, Dr Petra Schwendner, Dr Mickael Baqué, Dr Ruth-Sophie Taubner, Prof. James Head, Prof. David Des Marais, Prof. Ernst Hauber, Dr Petr Brož, Dr Morgan Cable, Đorđe Marković, Dr Brandi Carrier, Dr Michael Wong, and Dr Julie Mitchell. The best (i.e. most interesting) science is done in an international and interdisciplinary environment. If it involves some cool fieldwork, it's not bad either.

Merci aux joueurs Belges; au clan Malden (Ol, Ju, Caro et feu Sto) et aux autres qui se sont rajoutés (Olaf et Steph, Nico et Laurence, Pirlouit); à PY, Émeline et Eusèbe le descendant du Lapin de Caerbannog. Parce que résoudre des problèmes (mathématiques, la plupart du temps) pour le fun et en s'insultant joyeusement, c'est toujours bien, même si dit comme ça, ça n'en a pas l'air :) Et merci Ju pour l'impression de ce manuscrit !

Merci à Philippe, Estelle, Eve et Léon pour les soirées pizza et jeux, et pour m'avoir montré que les probabilités aux dés ne s'appliquent pas aux enfants !

Merci à ma famille, une fois encore, pour leur soutien.

Declaration

I declare that, except where explicit reference is made to the contribution of others, that this dissertation is the result of my own work and has not been submitted for any other degree at the University of Glasgow or any other institution.

Philippe Nauny

Abbreviations and symbols

Abbreviations and acronyms

ATP	a denosine t riphosphate
ddMDA	d igital d roplet m ultiple d isplacement a mplification
DNA	d eoxyribo n ucleic a cid
dNTP	d eoxyribo n ucleoside t riphosphate
EDX	e nergy d ispersive X -ray spectroscopy
ESA	E uropean S pace A gency
\overrightarrow{F}	f orward primer
GC-FID	g as c hromatography - f lame i onisation d etector
GC-MS	g as c hromatography - m ass spectrometry
LOI	l oss o n i gnition
MDA	m ultiple d isplacement a mplification
NASA	N ational A eronautics and S pace A ministration
PCR	p olymerase c hain r eaction
PDMS	p oly d imethylsiloxane
\overleftarrow{R}	r everse primer
rDNA	r ibosomal d eoxyribo n ucleic a cid
RH	r elative h umidity
T	t emperature
TMS	t rimethylsilyl
TOC	t otal o rganic c arbon
UV	u ltraviolet
XRD	X -ray d iffraction

Symbols

Symbol	Meaning	Unit
m	mass	g
M	molar mass	$\text{g}\cdot\text{mol}^{-1}$
n	quantity	mol
θ	diffraction angle	$^{\circ}$

Units and prefixes

A	ampere
AU	astronomical unit (1 AU = 149 597 870 700 m)
bar	bar (1 bar = 100 000 $\text{kg}\cdot\text{m}^{-1}\cdot\text{s}^{-2}$)
bp	base pair

Continued on next page

g	gram
<i>g</i>	gravitational acceleration ($1\text{ g} \approx 9.8\text{ m}\cdot\text{s}^{-2}$)
Ga	giga annum (10^9 years)
Gy	gray ($1\text{ Gy} = 1\text{ m}^2\cdot\text{s}^{-2}$)
h	hour
Hz	hertz (s^{-1})
k[unit]	kilo[unit] (10^3)
kb	kilo (10^3) base pairs
K	Kelvin
L	litre
m	metre
min	minute
mol	mole
m[unit]	milli[unit] (10^{-3})
M	molar ($\text{mol}\cdot\text{L}^{-1}$)
Ma	mega annum (10^6 years)
psi	pound-force per square inch ($1\text{ psi} = 6\,894.76\text{ kg}\cdot\text{m}^{-1}\cdot\text{s}^{-2}$)
rpm	revolution per minute
s	second
U	enzyme quantification unit, defined arbitrary by the provider
V	volt
μ [unit]	micro[unit] (10^{-6})
$^{\circ}\text{C}$	degree Celcius
$^{\circ}$	degree of arc
'	minute of arc ($1^{\circ} = 60'$)
"	second of arc ($1' = 60''$)

Chemicals

Abbreviation	Name	CAS number
AcOEt	ethyl acetate	141-78-6
AcOH	acetic acid	64-19-7
BSTFA	<i>N,O</i> -bis(trimethylsilyl)trifluoroacetamide	25561-30-2
CH_2Cl_2	dichloromethane	75-09-2
Et_2O	diethyl ether	60-29-7
HCl	hydrochloric acid	7647-01-0
iPrOH	isopropyl alcohol	67-63-0
MeOH	methanol	67-56-1
PFO	1 <i>H</i> ,1 <i>H</i> ,2 <i>H</i> ,2 <i>H</i> -perfluorooctan-1-ol	647-42-7

To my parents, grandparents, and sister.

‘Être chercheur, c’est être étudiant à vie.’

Lucia Granieri (2008)

Chapter 1

General introduction

‘What is astrobiology? Which fields does it comprise and what makes an astrobiologist? Ask five scientists and you may end up with six different definitions.’

Noack et al. 2015

Contents

1.1	Brief historical perspective of astrobiology	2
1.2	Mars from an astrobiology perspective	4
1.3	Terrestrial analogues for Mars	7
1.4	Biosignatures	10
1.5	PhD project	12

1.1 Brief historical perspective of astrobiology

Although its definitions are many, astrobiology — called exobiology before 1997 (Dick and Strick 2005a)¹ — is generally used as an umbrella term, designating a multidisciplinary field of science — ranging from astronomy to biology — that aims to study the origin, evolution, and distribution of life in the universe (Des Marais et al. 2003, 2008; Achenbach et al. 2015; Noack et al. 2015; Domagal-Goldman et al. 2016; Horneck et al. 2016).

The University of Glasgow contributed to exobiology research with the late Dr. Graham Cairns-Smith and his clay hypothesis — suggesting that silicate clays played the role of catalysers in the formation of complex molecules that will later lead to life — and by hosting the conference *Clay minerals and the origin of Life* the 18–24 July 1983 (Cairns-Smith 1966; Cairns-Smith and Hartman 1986; Dick and Strick 2005a).² Nowadays, research on the role played by minerals in the origin of life is still undertaken by Prof. Leroy Cronen at the School of Chemistry (e. g. Cooper et al. 2011). More relevant for School of Geographical and Earth Sciences is the work carried out by Prof. Martin Lee on the study of water-mineral interactions in chondrites and martian meteorites (e. g. Lee et al. 2016; Lee and Lindgren 2016; Lee et al. 2018), giving clues about the influence of water during the formation of the Solar System and on early Mars.

This section aims to outline a brief overview of the roots and evolution of astrobiology. For more exhaustive reviews, the reader is referred to Dick (1982), Dick (1999), Dick and Strick (2005a) and Crowe (2008).

1.1.1 The place of Earth in the Universe

Astrobiology finds its roots in the plurality of worlds debate among pre-Socratic Greek philosophers (7th–4th century BC), such as Anaximander, Leucippus, and Democritus. This philosophical debate, based only on cosmological speculations, aimed to establish if Earth was the only planet in the Universe, or just one among others (Dick 1999³, McKirahan 2001).

Although later rejected by more prominent philosophers, such as Plato and Aristotle, the *plurality of worlds* idea survived and developed into a *plurality of inhabited worlds*, thanks to Epicurus (*Letter to Herodotus*⁴ and *Letter to Pythocles*⁵, ca. 300 BC) and Lucretius (*De Rerum Natura*⁶, 1st century BC).

During the Copernician revolution (1510s–1680s) Copernicus changed the geocentrism paradigm to heliocentrism (*De revolutionibus orbium coelestium*, 1543) and improvement of early telescopes by Galileo in the 1610s helped astronomers to discover other planets and moons. These changes in the perception of the world led contemporaries — such as Bruno (*De l'infinito, universo e mondi*, 1584), More (*Democritus Platonissans*, 1646), Fontenelle

¹Chapter *Renaissance: From exobiology to astrobiology*, pp. 202–220.

²Chapter *Exobiology, planetary protection, origin of life*, pp. 56–79.

³Chapter *From the physical world to the biological universe: Democritus to Lowell*, pp. 10–18.

⁴Reported by Diogenes Laërtius, *Lives of the eminent philosophers*, book X, verse 45.

⁵*Ibid.*, verse 89.

⁶Book V, verse 422–431.

(*Entretiens sur la pluralité des mondes*, 1686), and Huygens (*Cosmotheoros*, 1698) — to postulate again about the presence of life on other celestial bodies.

A further development of telescopes in the 19th century combined with the discovery of Uranus and Neptune gave rise to more speculation about the existence of other inhabited worlds by, for example, Flammarion (*La pluralité des mondes habités*, 1862) and Proctor (*Other worlds than ours*, 1870).

1.1.2 A chemical origin of life

Around the same time as Flammarion and Proctor, Darwin suggested — in 1871 — the idea of a *warm little pond* in which prebiotic chemistry would occur (Darwin Correspondence Project 2018).

Similar ideas on the origin of life on Earth were independently reformulated and developed in the 1920s by Oparin (*Происхождение жизни*, 1924)⁷ and Haldane (*The origin of life*, 1929), and summarised as the concept of a *primordial soup*: molecules from a reducing atmosphere, dissolved in water, would gain complexity under ultraviolet radiation. The subsequent synthesis of amino acids in such conditions by Miller and Urey supported Oparin and Haldane's theories (Miller 1953; Miller and Urey 1959).

Following these ideas, a separate chemical origin of life on Mars is possible, if the conditions were met in the past (McKay 2010).

1.1.3 From exobiology to astrobiology

The successful launch of Sputnik, the first artificial satellite, in 1957 marked the beginning of the Space Age. Concerns of biological contamination in future space missions between Earth and other celestial bodies soon appeared, leading to think about, and develop, planetary protection measures for spacecrafts (Lederberg and Cowie 1958; Science 1958). A campaign led by Joshua Lederberg for standardised decontamination methods and the necessity to study life beyond Earth (Wolfe 2002) resulted in the integration at NASA of biological research, designated as exobiology (Lederberg 1960).

Eventually exobiology research was considered too centered on the origin of life and Earth's early evolution. It was then "rebranded" as astrobiology to include both Earth sciences and life sciences in its research objectives (Dick and Strick 2005a).⁸

1.1.4 Astrobiology today

Initially attempting to answer the questions 'how can and how did biology appear?' and 'how is biology sustained?', life sciences now require the help of space and material sciences, these sub-fields of science thus becoming effectively a part of astrobiological research (Dick and Strick 2005a).⁹

⁷The original work in Russian was translated into English in 1967.

⁸Chapter *Renaissance: From exobiology to astrobiology*, pp. 202–220.

⁹*Ibid.*

Today, astrobiology research revolves around three main points: (i) the origin of life (its context and its timescale), (ii) the existence of life beyond Earth, and (iii) the future of life in the Universe (Des Marais et al. 2003, 2008; Achenbach et al. 2015; Horneck et al. 2016; Anglés et al. 2018). As liquid water is one essential requirement for life as we know it, it is considered as a key target for the search for life beyond Earth (Mottl et al. 2007; Schulze-Makuch and Irwin 2008).

1.2 Mars from an astrobiology perspective

In the late 19th century–early 20th century, the so-called "canals" and the seasonal changes observed on the Red Planet by Schiaparelli and Lowell resulted again in speculations about Mars being covered with vegetation, and even possibly being inhabited by intelligent beings (Schiaparelli 1894, 1898; Lowell 1906, 1908).

The existence these of "canals" was disputed at the time they were proposed (Maunder 1894, 1903; Antoniadi 1909). Pictures taken by Mariner 4 in 1965 — and by the following missions — eventually proved that no canals, nor any traces of civilisation, were present on Mars, but revealed the existence of geomorphological features caused by the interaction of water with the landscape (Baker and Milton 1974; Milton 1974; Scott and Tanaka 1986).

A series of missions were sent to assess either directly the possibility of the presence of microbial life on Mars, or the habitability of the planet. Since the Viking landers in the late 1970s, all results about the existence of present or past life on Mars are still considered inconclusive despite Mars showing signs of past habitability (Klein 1999; Quinn et al. 2013; Levin and Straat 2016).

1.2.1 Geological and hydrological history

Age of Mars

No martian samples collected *in situ* have yet been returned to Earth. So the only martian samples available for radioisotopic dating are martian meteorites. Therefore assigning absolute ages to the different areas on Mars can only be done using relative dating techniques, such as crater counting.

The concept for dating stratigraphic layers based on crater counts is based on the Crater Analysis Techniques Working Group (1979). Essentially, crater counts of geologic referent surfaces are compared with the crater size–frequency production distributions from different models. These inferred cratering rates are converted to model-absolute ages (e. g. Tanaka 1986; Hartmann and Neukum 2001; Ivanov 2001; Nyquist et al. 2001; Hartmann 2005; Neukum et al. 2001; Werner and Tanaka 2011; Michael et al. 2012; Platz et al. 2013).

Geomorphological features (Carr and Head 2010), such as volcanism or hydrology, or mineralogy (Bibring et al. 2005; Carr and Head 2010) can also help in assigning relative ages to the different terrains.

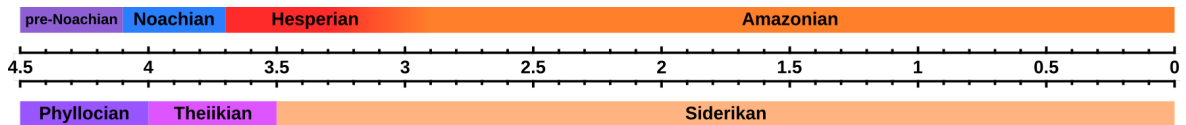


Figure 1.1 – (top) martian geological periods based on crater counting (adapted from Carr and Head 2010). The boundary between the Hesperian and the Amazonian periods is often set at 3 Ga ago for simplification purposes, but it is estimated at 2.9–3.3 Ga ago depending on the model used (Hartmann and Neukum 2001). (bottom) martian geological periods based on mineralogy (adapted from Bibring et al. 2005). Numbers indicate the time (in Ga) before present.

Accretion

Assuming that the condensation of calcium-aluminium-rich inclusions (CAIs) marks the beginning of the formation of the Solar System, Mars’ accretion from the proto-planetary disc was modeled — from ^{182}Hf – ^{182}W chronometry in martian meteorites — to have occurred 2–8 Ma after the formation of CAIs, which means that Mars accreted earlier than Earth (Nimmo and Kleine 2007; Dauphas and Pourmand 2011).

In addition to a quick accretion time, Mars also has a lower mass than predicted by models (e. g. Wetherill 1991, and references within). This small mass has been explained by a lack sufficient material in the circumstellar disc at Mars’ orbit, caused either by a concentration of this material in a narrow annulus between Venus’ and Earth’s orbit (Hansen 2009), or by depletion of the material from Jupiter’s inward, then outward, migration in the Solar System (Walsh et al. 2011). Both these hypotheses suggest that Mars is actually more like a planetary embryo rather than a finished planet.

Pre-Noachian

Following Mars’ accretion, the decay of ^{26}Al within its mantle, combined with impacts at its surface, could have transformed the surface into a magma ocean. This hypothesis is supported by a depletion in siderophile elements observed in martian meteorites (Brandon et al. 2000; Jones et al. 2003). Whether or not mantle convection happened — and if it had an effect on the formation of the north-south crustal dichotomy — remains debated (e.g. Elkins-Tanton et al. 2005; Debaille et al. 2009; Grott et al. 2013; Tosi et al. 2013; Filiberto and Dasgupta 2015).

The discovery of crustal magnetisation by Mars Global Surveyor implies the existence of a dynamo effect (Acuña et al. 1999; Purucker et al. 2000; Acuña et al. 2001). This dynamo effect likely stopped in the Early Noachian, around 4.2–4.0 Ga ago, as magnetic anomalies are mostly restricted to the southern highlands (Lillis et al. 2008). These magnetic anomalies could be explained by tectonic mechanisms, but it is still debated whether or not plate tectonics occurred on Mars (Connerney et al. 1999; Fairén et al. 2002). These anomalies have also been interpreted as a signatures of deep dike swarms (Nimmo 2000).

Noachian

Volcanism was sustained during this period, including the formation of the Tharsis volcanic province (Phillips et al. 2001; Carr and Head 2010).

The Noachian period is mostly characterised by the presence of liquid water at the surface of the planet, forming outflow channels, crater lakes, and possibly an ocean in the northern hemisphere (e.g. Carr and Head 2003; Fassett and Head 2008; Rosenberg and Head 2015; Goudge et al. 2016). Glacial deposits have also been observed in association with this time period (e.g. Fastook and Head 2015; Palumbo et al. 2018). The atmospheric pressure is thought to have varied from around 0.5 to 4 bar (Craddock and Lorenz 2017; Kurokawa et al. 2018).

Hesperian

Volcanism was still ubiquitous during the Hesperian period (e.g. Hiesinger and Head 2004; Williams et al. 2009; Salvatore et al. 2010; Grott et al. 2013). Tectonic stresses caused by the weight of the Tharsis bulge induced deformation and fractures (Plescia and Saunders 1982; Bouley et al. 2018).

These tectonic stresses also contributed to the release of groundwater reservoirs, causing catastrophic floods (Tanaka and Chapman 1990; Dohm et al. 2000; Pacifici et al. 2009). Despite the global decrease in surface water during this time period, a frozen ocean could have persisted in the northern lowlands until the Late Hesperian (Carr and Head 2019).

Amazonian

Volcanism was mostly restricted to Tharsis and Elysium (Grott et al. 2013) and may have persisted until as recently as ~3.0 Ma ago (Werner et al. 2003; Vaucher et al. 2009). Some shield volcanoes produced effusive volcanism.

Some lakes and ponds survived until the late Amazonian (Soare et al. 2008; Hynek et al. 2015). Landforms like sorted clastic stripes and polygons suggest the existence of ground-ice thaw and transient liquid flows (Gallagher et al. 2011; Johnsson et al. 2012; Soare et al. 2016).

1.2.2 Mars today

The surface of Mars at present time is not considered hospitable for life. Due to its weak magnetic field, the solar wind strips the already thin atmosphere from Mars (Rahmati et al. 2014; Jakosky et al. 2015; Jakosky et al. 2017). The low atmospheric pressure (6.6–102 mbar; Schofield et al. 1997; Smith 2008; Taylor et al. 2010; Haberle et al. 2014; Harri et al. 2014b; Martínez et al. 2016; Pla-Garcia et al. 2016) and the low temperatures (181–295 K; Spanovich et al. 2006; Zent et al. 2010) are a primary concern regarding the survival of microorganisms.

UV radiation reaching the surface is blocked by a few millimetres of soil, which are enough to protect potential biomolecules (Ertem et al. 2017; Fornaro et al. 2018). However, solar energetic particles and galactic cosmic rays at the surface are high enough ($76 \text{ mGy} \cdot \text{year}^{-1}$; Hassler et al. 2014) to degrade microorganisms and organic molecules (Pavlov et al. 2002; Dartnell et al. 2007; Dartnell et al. 2010; Pavlov et al. 2012). Additionally, the presence of perchlorates at the surface, causing oxidative stress, would pose a serious threat to potential microorganisms (Quinn et al. 2013; Wadsworth and Cockell 2017).

Water is still present on Mars, mostly as ice in the polar caps, in underground deposits, and in clouds (figure 1.2, a, b, c). However, liquid water was only observed recently and in a transient state (Martín-Torres et al. 2015). Liquid water could nevertheless also persist as brines in the shallow subsurface (Edwards and Piqueux 2016; figure 1.2, d) or at the bottom of subglacial reservoirs (Orosei et al. 2018).

Organic matter is scarce on Mars (Biemann et al. 1977). However, organic molecules were found both in martian meteorites (e.g. Wright et al. 1989; Grady et al. 1994; Sephton et al. 2002; Steele et al. 2012) and on Mars (Freissinet et al. 2015; Eigenbrode et al. 2018). These organics could come from meteoritical and cometary inputs (Flynn 1996), or by reaction of aqueous CO_2 with minerals (Steele et al. 2018). Additionally, methane has been measured seasonally in the martian atmosphere (Webster et al. 2014, 2018).

1.3 Terrestrial analogues for Mars

Terrestrial analogues can be defined as *‘places or spaces on Earth that approximate, in some respect, the geological, environmental and putative biological conditions and/or setting(s) on a particular planetary body, either at the present-day or sometime in the past’* (Osinski et al. 2006).

Analogues serve multiple purposes such as the study of geological formations and processes, the simulation of human or robotic missions, or the study of microbiomes and biosignatures from an astrobiological perspective, in natural environments (Léveillé 2010). Testing material and hypotheses this way helps to improve future space missions. Analogues can also help to answer simpler questions — such as assessing the survival of molecules and microorganisms in extreme conditions, or testing instruments detection limits in field conditions — that do not yet necessitate an actual mission to space, thereby saving time, resources, and money.

Depending on the analogue target (Mars, Venus, icy satellites, ocean worlds, etc.) and on the studied feature (geological, biological, weather system, etc.) different locations on Earth, with different parameters, can be considered (Preston and Dartnell 2014; Martins et al. 2017).

The considerations discussed above also need to be made when focusing on specific aspects of Mars, but emphasis is usually put on dryness and oxidative environment (e.g. Marlow et al. 2011; Pontefract et al. 2017; Cabrol 2018). Below some of the most well-known terrestrial analogues for Mars are discussed.

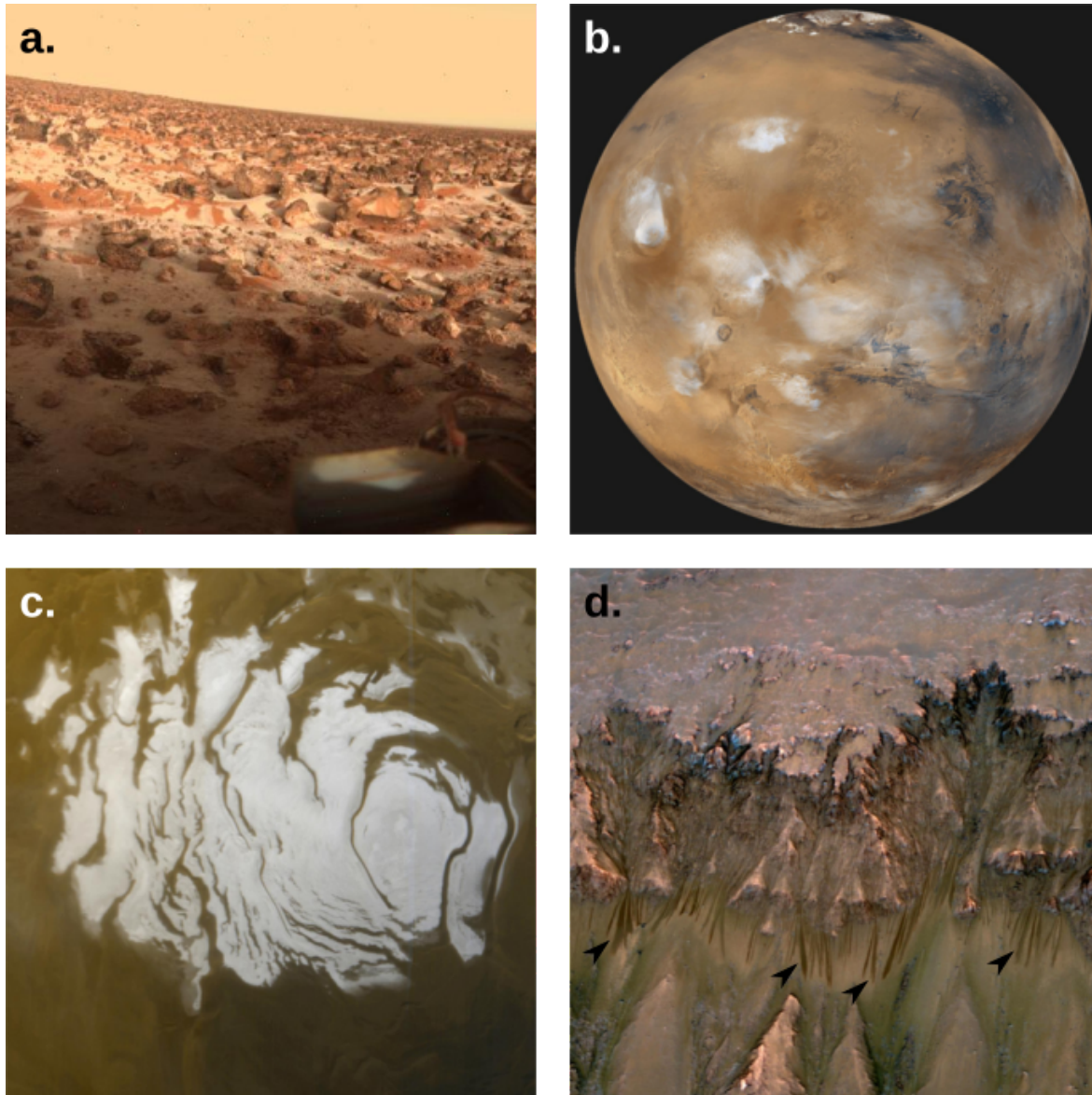


Figure 1.2 – Observations of water on Mars. (a) Water frost at the Viking 2 landing site in *Utopia Planitia* (1979); (b) Water clouds above *Tharsis Montes* and *Valles Marineris*, and ice at the north polar cap (1999); (c) Ice at the south polar cap (2000); (d) Recurring slope lineae at Newton crater (2011). Images adapted from: (a) NASA/JPL, image PIA00571, (b) NASA/JPL/MSSS, image PIA02653, (c) NASA/JPL/MSSS, image PIA02393, (d) NASA/JPL-Caltech/Univ. of Arizona, image PIA14479.

	Atacama	Antarctica	Iceland	Río Tinto	Yellowstone
Aridity	✓	✓			
Cold		✓	✓		
UV radiations	✓	✓			
Perchlorates	✓				
Evaporites	✓				
Acid water			✓	✓	✓
Volcano-ice interactions			✓		
Hydrothermal activity			✓	✓	✓
Silica sinters			✓	✓	✓

Table 1.1 – Features of interest in various planetary analogues for Mars.

Depending on the scientific question asked, specific analogues may be considered over others. The following table (table 1.1) lists different parameters that can be considered when looking for an analogue. Extremophiles are also studied in all analogues. Below are also some brief descriptions of the main analogues used by scientists.

1.3.1 Atacama Desert

The Atacama Desert in Chile is the driest hot natural environment on Earth (Navarro-González et al. 2003; Azua-Bustos et al. 2015). In addition, this environment, like Mars, is also exposed to high levels of UV radiation and contains perchlorates and minimal organic material (e.g. Catling et al. 2010; Fletcher et al. 2012; Calderón et al. 2014; Azua-Bustos et al. 2017; Cordero et al. 2018).

1.3.2 Antarctic Dry Valleys

The McMurdo Dry Valleys in Antarctica are the world's driest cold natural environments (Marchant et al. 1996). Some of the climatic and geomorphological processes observed there can be equated to those occurring on Mars (Horowitz et al. 1972; Marchant and Head 2007). Moreover, microorganisms have been isolated from permafrost environments and some may survive under martian conditions (e.g. Horowitz et al. 1972; Friedmann and Ocampo 1976; Gilichinsky et al. 2007; de Vera et al. 2014; Goordial et al. 2016).

1.3.3 Iceland

Iceland can be used in a variety of ways related to astrobiology research, combining the advantages of having volcanic systems, a cold climate, and the presence of water or ice. The search for microbial extremophiles such as psychrophiles, thermophiles, chemotrophes, and acidophiles, varies depending on sampling location. Caves, geothermal and hydrothermal systems created by volcanic systems can be used as analogues for those existing, or that have existed, on Mars (e.g. Boston et al. 1992; Chapman et al. 2000; Preston et al. 2008; Warner and Farmer 2010; Cousins and Crawford 2011; Beblo-Vranesovic et al. 2017).

1.3.4 Río Tinto

Río Tinto is a Spanish river with an acidic pH and containing high concentrations of heavy metals, iron, and sulfate (e.g. Sánchez-Andrea et al. 2011). Despite this, microbiological communities have developed in the river. This environment is used as an analogue for early Mars (e.g. Amils et al. 2007; Fernández-Remolar et al. 2008; Orgel et al. 2014; Kaplan et al. 2016).

1.3.5 Yellowstone National Park

Yellowstone National Park, located in the United States, is mainly studied for its hot and acidic hydrothermal systems and their associated extremophile microbial communities (e.g. Walter et al. 1972; Bishop et al. 2004; Walker et al. 2005).

1.4 Biosignatures

A biosignature is ‘*any phenomenon produced by life*’ (Steele et al. 2005). These phenomena can be as varied as morphologies, fabrics, biomarkers (i.e. organic molecules), isotopic fractionation, and gases (Farmer and Des Marais 1999; Summons et al. 2011; Röling et al. 2015; Westall et al. 2015).

About two thirds of Mars is covered by Noachian material, formed at a time when the planet could have been habitable. The lower geological activity during the following geological period could have helped to preserve any potential biosignature in Noachian material (Westall et al. 2015). However, biosignatures at shallow depth will have to survive oxidative stress from ionising radiation and perchlorates (Cockell et al. 2000; Dartnell et al. 2010; Pavlov et al. 2012; Quinn et al. 2013; Wadsworth and Cockell 2017). At deeper depth metamorphism may alter the physical or molecular structure of any biosignatures (Bernard 2014; Westall et al. 2015). Moreover, interactions of the biosignatures with their mineral matrix will have an impact on the biosignatures’ preservation, extraction, and analysis (see Röling et al. 2015 for a review). Molecules can be fixed to mineral surface (Summons et al. 2011), trapped in fluid inclusions within minerals (Winters et al. 2013) or in mineralized cells (Orange et al. 2009).

The emphasis here is given to biomarkers (organic molecules) as some of them are stable under geologic conditions (Simoneit et al. 1998).

1.4.1 Lipids

Lipids are considered to be amongst the sturdiest of the biomarkers, because of their rather simple hydrocarbon backbones. Some of them can resist harsh environmental conditions and remain stable over several Ga, under the appropriate conditions (Summons et al. 2008 and references therein). Therefore, some lipids are already used as biosignatures on Earth to detect life records in old samples and in samples from extreme environments (e.g. Summons

et al. 1988; Hart et al. 2011; Kaur et al. 2011; Blanco et al. 2017; Cheng et al. 2017; Wilhelm et al. 2017). Moreover, some of these molecules, like long-chain alkanes and fatty acids, hopanes and steranes, and porphyrins are only derived from molecules produced by living beings (Eglinton et al. 1964). On Mars, under the right conditions, lipid biomarkers dating from the Noachian period could be preserved (Summons et al. 2008).

Hydrocarbons — both alkanes and polycyclic aromatic hydrocarbons (PAHs) — have been reported in meteorite materials, although PAHs were attributed to terrestrial contamination (Monroe and Pizzarello 2011)

1.4.2 Pigments

Pigments can be used in cells to absorb light, and to protect against variable salinity and low temperatures (Mueller et al. 2005). Laboratory simulations under terrestrial atmosphere and temperature have shown a quick degradation of β -carotene under UV radiation despite the protective effect of the martian regolith (Vítek et al. 2009). However, carotenoids have been shown to contribute to the preservation of some desert cyanobacteria *Chroococcidiopsis* under UV-C irradiation (Baqué et al. 2013) and under simulated martian conditions (Baqué et al. 2016).

1.4.3 Amino acid

Amino acid polymers constitute proteins in terrestrial life, but they can also be produced abiotically as monomers or polymers (e.g. Miller 1953; Hartmann et al. 1981; Ménez et al. 2018). A strong enantiomeric excess of either enantiomer could indicate a biogenic origin of the molecules. Whilst amino acids are prone to degradation under current martian conditions, as shown by laboratory simulations (ten Kate et al. 2005; Garry et al. 2006; ten Kate et al. 2006), amino acids produced during the Noachian period could still be preserved today if they were protected from the surface oxidative conditions and from radiation (Kanavarioti and Mancinelli 1990; ten Kate et al. 2005; Kminek and Bada 2006). Moreover, the detection of some amino acids in martian meteorites (Jull et al. 2000; Sephton et al. 2002; Callahan et al. 2013) supports the survival of these molecules on Mars, where the conditions are less extreme than in space, although terrestrial contamination is often more probable (Bada et al. 1998; Glavin et al. 1999).

Whilst a quick collection after the meteorite fall and a storage in an inert atmosphere may limit oxidative reactions and proliferation of terrestrial microbial life within the sample, analysis of the amino acid D/L ratios and of the carbon isotope contents may still help to discriminate martian material from terrestrial contamination (Glavin et al. 1999; Jull et al. 2000; Ehrenfreund et al. 2001; Sephton et al. 2002; Monroe and Pizzarello 2011; Callahan et al. 2013). Study of ^{13}C isotopes also helped to identify extraterrestrial glycine in comet 81P/Wild (Elsila et al. 2009), whilst the same amino acid was identified, with its fragmentation pattern, by mass spectrometry in comet 67P/Churyumov-Gerasimenko (Altwegg et al. 2016).

1.4.4 Nucleic acids

Nucleic acids are damaged by UV radiation (Voet et al. 1963). However, DNA survival has been observed in cells protected by regolith under UV radiation only (Cockell et al. 2005; Baqué et al. 2013), or under simulated martian conditions (Baqué et al. 2016). However, no nucleobases originating from Mars were detected so far in martian meteorites (Callahan et al. 2011, 2013).

1.5 PhD project

1.5.1 Motivation

The ExoMars (ESA and Roscosmos) and the Mars 2020 (NASA) rovers are both scheduled for launch in summer 2020. They will look for signs of extinct or extant life on Mars. Whilst Mars 2020 will focus on collecting surface samples and storing some for a future sample-return mission, ExoMars will be able to collect subsurface samples, as deep as 2 m, thereby reaching depths where potential biosignatures or life forms will be more protected from the extreme surface conditions.

Depending on the amount of radiation received by the martian surface, one simulation indicated that at 10 cm depth complex organic molecules would not persist more than 300 Ma, whilst simple small organic molecules could survive up to 1 Ga (Pavlov et al. 2012). Another simulation predicted a bacterial and spore survival time of 450 000 years at 2 m depth, where the ExoMars rover is supposed to drill (Dartnell et al. 2007). However, further experiments demonstrated that some bacteria were nevertheless able to survive simulated martian cold and radiations under just 30 cm of sediments for up to 100 000 years (Dartnell et al. 2010). Finally, if a depth of 7.5 m may provide enough shielding against radiation (Dartnell et al. 2007), then radioactive decay of long-lived isotopes (^{40}K , ^{232}Th , ^{235}U , and ^{238}U) will still eventually destroy any dormant life (Pavlov et al. 2002).

One key point for the search for life on Mars is the presence or absence of liquid water there. Transient liquid water has been observed (see above, section 1.2.2), surface water sublimates because of low atmospheric pressure and solar radiations, and underground water is frozen. However, in this temperature gradient, there should be a depth range at which the existence of liquid water is theoretically possible — probably varying over time, and depending on other factors like salt composition and concentration. This hypothetical environment, not yet observed by any rover, could serve as the ultimate oasis for martian life today.

By studying terrestrial analogues of past wet environments, or of environments where water ice mostly sublimates to gas and where liquid water is almost non-existent, we can get an idea of the processes that have occurred on Mars in its past and try to determine where and how potential molecular signs of life are preserved in the martian subsurface today.

1.5.2 Contributions

The overall purpose of the following work was to study the nature and repartition of certain organic biosignatures, at shallow depths, in natural terrestrial analogue sites. All these sites were (mostly) barren, so external inputs of material — through wind and rain — would help to enrich the sites in organics. This work was divided in three parts, each with their own objectives.

The first two parts were performed in Chile, in environmental analogues experiencing intense solar irradiation and extreme thermal fluctuations, and where rain is rare and surface liquid water is unstable. Samples were collected along a depth profile, every 2 cm (to be able to see rapid changes in biosignatures or environmental parameters), contrary to most studies which focus on the surface or which have wider gaps between two samples in a profile.

The last part, performed in Iceland in a landscape analogue. Samples were collected at 10 cm depth along a transect in a volcano crater, both in "dry" slopes and in gullies created by water flows.

1. The aim of the first project (chapter 3) was to study biolipids and genetic material through a depth profile in a dry alluvial fan in the Atacama Desert (hot environment).
2. The second project (chapter 4) focused also on the study of biolipids and genetic material, but in four depth profiles along an altitude gradient on the Sairecabur volcano (cold environment). These samples were shared with fellow PhD student Nick Thomas (Thomas 2018), but whilst he focused more on 16S rDNA sequencing, I focus more on biolipids analysis and my approach to genetic material sequencing is different.
3. The third project (chapter 5) focused on a comparative study of microbial and biolipids aeolian inputs and removals along a transect in the Hverfjall volcano.

Chapter 2

Methodology

‘I’ll be honest, we’re throwing science at the wall here to see what sticks. No idea what it’ll do. Probably nothing.’

Cave Johnson, *Portal 2* (2011)

Contents

2.1	Fieldwork	16
2.2	Inorganic content	18
2.3	Organic content	21
2.4	Genomic analyses	24
2.5	ATP activity	27

This chapter describes the methods and techniques used in the thesis. When possible, analyses were chosen to be easy and economical, in order to minimize the experimental costs while maximising collecting more data which could be relevant for the overall interpretation of each site.

Graphs were plotted with PGFPlots (Feuersänger 2018), other figures were created with Inkscape (The Inkscape Project 2015) and GIMP (The GIMP development team 2017). Graphs were either plotted in black and white, or with a colour-blind friendly colour schemes suggested by Tol (2018). All data files can be obtained from the University of Glasgow at the following DOI: [10.5525/gla.researchdata.857](https://doi.org/10.5525/gla.researchdata.857).

Gravimetric analyses were carried out using precision scales. Measurement deviations are thus considered negligible compared to the measurements.

2.1 Fieldwork

2.1.1 Sample collection

Unless otherwise stated in the relevant chapter, soil samples were collected using an ethanol-sanitised trowel, stored in sterile plastic bags and double-bagged. Multiple samples were collected from various depths at each site.

2.1.2 Environmental readings

Temperature and relative humidity Whilst collecting soil samples, air temperature (T) and relative humidity (RH) values were measured. Relative humidity is defined as ‘100 times the partial pressure of water divided by the saturation vapor pressure of water at the same temperature’ (Berger et al. 2003a, equation 2.1).

$$RH = \frac{p_{H_2O}^T}{p_{sat\ H_2O}^T} \cdot 100 \quad (2.1)$$

$$p_{H_2O}^T = \text{partial pressure of water at temperature } T$$

$$p_{sat\ H_2O}^T = \text{saturation vapour pressure of water at temperature } T$$

Measurements were taken approximatively 1.5 m above the ground using a hand held reader (2020R, Digitron).

Surface and underground measurements were also recorded every 10 min for 2 to 3 days following sampling. At ground level, an exposed probe and a sheltered probe were used (iButtons® DS1923, Maxim, or Tinytags Plus 2 TGP-4500, Gemini Data Loggers UK). Underground probes were placed every 5 cm down to 25 cm deep (iButtons® DS1923, Maxim). Data was later downloaded using the 1-Wire® software (Maxim) for iButtons®, and the Tinytag Explorer software (Gemini Data Loggers UK) for Tinytags.

The probes were already calibrated by their manufacturers. In the range of environmental conditions observed, their accuracies were ± 0.50 °C and ± 0.6 % RH for the iButtons® (Maxim Integrated 2015), and ± 0.4 – 0.7 °C and ± 0.3 % RH for the Tinytag (Gemini 2015). Thus, the values recorded should be close to the real ones.

Additionally, T and RH values recorded by iButtons® were automatically corrected by the 1-Wire® software when downloading the data. However, iButtons® RH values needed to be corrected again twice following the manufacturer's instructions (Maxim Integrated 2015).

Firstly, a T-corrected RH (RH') is calculated from the 1-Wire®-corrected T and RH values (equation 2.2).

$$RH' = \frac{RH \cdot K + \alpha \cdot (T - 25) - \beta \cdot (T - 25)^2}{K + \gamma \cdot (T - 25) - \delta \cdot (T - 25)^2} \quad (2.2)$$

RH = measured relative humidity

T = measured temperature

$$K = 30.7 \cdot 10^{-3}$$

$$\alpha = 3.5 \cdot 10^{-3}$$

$$\beta = 4.3 \cdot 10^{-6}$$

$$\gamma = \begin{cases} 10^{-6} & \text{if } T > 15 \\ -5 \cdot 10^{-6} & \text{if } T \leq 15 \end{cases}$$

$$\delta = 0.2 \cdot 10^{-6}$$

Secondly, every hour passed with the iButtons® being continuously exposed to $RH' \geq 70$ % will induce a 1-Wire® saturation drift. A drift-compensated RH (RH'') is calculated using the 1-Wire®-corrected T and the calculated RH' (equation 2.3). To simplify the calculations, RH' values are only considered every hour instead of every 10 min.

$$RH'' = RH'_N - \sum_{n=1}^N \frac{15.6 \cdot 10^{-3} \cdot RH'_n \cdot 2.54^{-0.3502 \cdot n}}{1 + \frac{T_n - 25}{100}} \quad (2.3)$$

$RH'_n = RH'$ at the n^{th} hour with the device continuously exposed to $RH' \geq 70$ %

$T_n = T$ at the n^{th} hour with the device continuously exposed to $RH' \geq 70$ %

N = total number of hours with the device continuously exposed to $RH' \geq 70$ %

$RH'_N = RH'$ reading at the end of the N^{th} hour

T and RH values used in plots are (i) the raw recorded data for Tinytags, and (ii) the 1-Wire®-corrected T and the calculated RH'' data for iButtons®.

Sunrise and sunset times Sunrise and sunset times were calculated at the corresponding dates for each site using the SunCalc program (Agafonkin 2009).

However, the calculation could not take into account the altitude of the site, nor the possible shade induced by surrounding volcanoes.

Ultraviolet radiation Ultraviolet (UV) radiation is classified in different categories based on wavelength: UV-A (315-400 nm), UV-B (280-315 nm), and UV-C (100-280 nm). UV radiation was measured when collecting the soil samples, approximatively 1.5 m above the ground, using a UV203 Radiometer (Macam) equipped with UV-A, UV-B, and UV-C filters (UVA, UVB2 and IF-254 respectively, Macam).

2.2 Inorganic content

2.2.1 Water content

Considering that water is the dominant, if not only, volatile present in the sample that will evaporate at 105 °C, wet soil samples were dried at this temperature for 16 h, then left to cool down in a desiccator.

The masses of wet and dry samples were measured with an AG204 precision scale (Mettler Toledo, deviation: 0.1 mg). The water content of a sample (%H₂O) is expressed as follows:

$$\%_{\text{H}_2\text{O}} = \frac{m_{\text{wet}} - m_{105}}{m_{105}} \cdot 100 \quad (2.4)$$

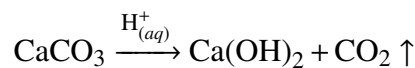
m_{wet} = mass of the wet sample

m_{105} = mass of the same sample dried at 105 °C

2.2.2 Carbonate content

The most common carbonates contain calcium — e.g. calcite and aragonite (CaCO₃), dolomite (CaMgCO₃) —, or metals — e.g. siderite (FeCO₃), malachite (Cu₂CO₃(OH)₂).

An estimate of the samples' carbonate content can be calculated by assuming that calcium carbonate significantly outweighs other carbonates in the samples. Carbonates are removed under acidic conditions, following the reaction



From this equation's stoichiometry we deduce that

$$\begin{aligned} n_{\text{CO}_3^{2-}} &= n_{\text{CO}_2} \\ &= \frac{m_{\text{CO}_2}}{M_{\text{CO}_2}} \end{aligned} \quad (2.5)$$

$n_{\text{CO}_3^{2-}}$ = quantity of carbonate

n_{CO_2} = quantity of carbon dioxide

m_{CO_2} = mass of carbon dioxide

M_{CO_2} = molar mass of carbon dioxide (44.01 g·mol⁻¹)

Inversely, the mass of carbonates is

$$m_{\text{CO}_3^{2-}} = n_{\text{CO}_3^{2-}} \cdot M_{\text{CO}_3^{2-}} \quad (2.6)$$

$m_{\text{CO}_3^{2-}}$ = mass of carbonate

$M_{\text{CO}_3^{2-}}$ = molar mass of carbonate (60.01 g·mol⁻¹)

The mass of CO₂ released during the reaction is

$$m_{\text{CO}_2} = m_{\text{ini}} - m_{\text{fin}} \quad (2.7)$$

m_{ini} = initial dry sample mass, i.e. prior to acidification

m_{fin} = final dry sample mass, i.e. after treatment

Finally, the percentage of carbonate ions initially present in the sample is

$$\%_{\text{CO}_3^{2-}} = \frac{m_{\text{CO}_3^{2-}}}{m_{\text{ini}}} \cdot 100 \quad (2.8)$$

Combining equations (2.5), (2.6), (2.7), and (2.8), we obtain

$$\begin{aligned} \%_{\text{CO}_3^{2-}} &= \frac{(m_{\text{ini}} - m_{\text{fin}}) \cdot M_{\text{CO}_3^{2-}} \cdot 100}{M_{\text{CO}_2} \cdot m_{\text{ini}}} \\ &= \frac{(m_{\text{ini}} - m_{\text{fin}}) \cdot 60.01 \cdot 100}{40.01 \cdot m_{\text{ini}}} \\ &\approx \frac{(m_{\text{ini}} - m_{\text{fin}}) \cdot 150}{m_{\text{ini}}} \end{aligned} \quad (2.9)$$

About 5 g of pre-weighed dry samples were incubated for 24 h with 2 M HCl. Acidified samples were centrifugated (1000 rpm, 10 min) and rinsed with milliQ water. The process was repeated until the rinse water had reached a neutral pH. The samples were then freeze-dried and weighed again. Dry samples' masses were measured with an AG204 precision scale (Mettler Toledo, deviation: 0.1 mg).

2.2.3 pH

About 3 g of soil were resuspended in an equal mass of deionised water. The solution was shaken for 15 min then decanted overnight.

For each soil sample, pH was measured thrice using an MA235 pH metre (Mettler Toledo) calibrated at pH 4.0, 7.0, and 10.0.

2.2.4 Grain size measurement

Depending on the quantity of sample available, approximatively 2–28 g of freeze-dried sediments were sifted through sieves with different mesh-sizes: < 63 μm , 63–125 μm , 125–250 μm , 250–500 μm , 0.5–1 mm, 1–2 mm (BS 410-1, Endecotts Ltd.); 2–4 mm, 4–8 mm, 8–16 mm (BS 410, Endecotts Ltd.).

Particles bigger than 2 mm are designed as gravels; sands range from 2 mm to 63 μm ; particles smaller than 63 μm are grouped as silts and mud (Wentworth 1922).

The mass of each size population is expressed as a percentage of the sample mass.

2.2.5 X-ray diffraction

In a crystal, X-rays are diffracted by atomic lattices. Maximum constructive interference occurs when the wavelengths are proportionnal to interplanar distance of the the crystal lattice (equation 2.10, Bragg and Bragg 1913).

By measuring the angular distance between diffraction peaks, one can calculate the interplanar spacing of the crystal causing the diffraction. These values can then be compared to known minerals in order to identify the unknown mineral causing the diffraction pattern.

$$\forall n \in \mathbb{N}^*, n \cdot \lambda = 2 \cdot d \cdot \sin \theta \quad (2.10)$$

λ = wavelength

d = interplanar distance

θ = diffraction angle

Dry samples were crushed into a fine powder (grain size < 125 μm) and analysed by X-ray diffraction (XRD).

Atacama Desert samples were run at the School of Chemistry (University of Glasgow) on an X'Pert PRO MPD (PANalytical). Data were analysed with the HighScore Plus software (PANalytical).

Samples collected in the Andes were analysed at Advanced Materials Research Laboratory (University of Strathclyde) on a D8 ADVANCE (Bruker). Data were analysed with the DIFFRAC.EVA software (Bruker).

In both cases, monochromatic X-rays were generated by a copper filament (40 kV, 40 mA), and were passed through a 1 mm-wide slit. The intensity of diffracted X-rays was measured

between diffraction angles of 5–85° 2 θ (0.017° increments, 0.5 s steps).

XRD patterns are reported in appendix A (p. 123).

2.2.6 Energy-dispersive X-ray spectroscopy

Energy-dispersive X-ray spectroscopy (EDX) provides the elemental composition of a sample. The sample is irradiated by a high energy electron beam to excite and eject an inner shell atomic electron. An electron from an outer shell then fills the valence gap, releasing energy in the form of an X-ray photon in the process. The energy released corresponds to the energy difference between these outer and inner shells (Goldstein et al. 2018).

An electron beam was generated by an FEI Quanta 200F environmental scanning electron microscope (Quanta) at 20 kV (50 μ m aperture, spot 4). This beam was targetted in low vacuum at sample grains mounted on a sticky carbon stub. Diffracted X-rays were collected by an EDAX silicon-drift detector (Quanta) and analysed with the Edax Genesis software (Quanta). This analysis was performed with the help of Prof. Martin Lee.

2.3 Organic content

2.3.1 Loss on ignition

Loss on ignition (LOI) is a method where ‘*organic matter is oxidised at 500–550 °C to carbon dioxide and ash*’, thereby permitting an evaluation of the organic content of sediments (Heiri et al. 2001).

Depending on the quantity of sample available, around 1.5–10 g of 105 °C-oven-dried sediments were combusted at 550 °C for 16 h. After combustion, samples were left to cool down in a dessicator prior to being weighed. Samples were weighed on a precision balance (AG204, Mettler Toledo, deviation: 0.1 mg). The LOI₅₅₀ is expressed as the percentage of mass lost during combustion at 550 °C, as follows:

$$\text{LOI}_{550} = \frac{m_{105} - m_{550}}{m_{550}} \cdot 100 \quad (2.11)$$

m_{105} = mass of the sample oven-dried at 105 °C

m_{550} = mass of the sample combusted at 550 °C

2.3.2 Organic geochemistry

Any glassware (vials and pipettes) that would come into contact with lipids was wrapped in aluminium foil and heated (450 °C, 8 h) prior to use.

Total lipid extract (TLE)

About 10–15 g of each soil sample was freeze-dried for 72 h ($6 \cdot 10^{-6}$ mbar, -50 °C; Alpha 1-2 LD, Christ) then homogenised.

Lipids were extracted from pre-weighed samples with CH_2Cl_2 :MeOH (9:1, v:v) using an accelerated solvent extractor (1 500 psi, 120 °C, 3×15 min ; Dionex ASE 350, Thermo Scientific). Following the evaporation of the solvent, total lipid extracts (TLEs) were weighted.

Fractions separation

TLEs were then separated into neutral and acid fractions by flash chromatography on an ammonium-coated silica gel column (LC-NH2 SPE silica, Fisher). The neutral fraction was first eluted using CH_2Cl_2 :iPrOH (1:1, v:v), then the acid fraction was eluted with Et_2O :AcOH (24:1, v:v).

Neutral fractions were further separated into four sub-fractions by flash chromatography on silica (230–400 mesh, 35 – 70 μm silica, Fisher). The different neutral sub-fractions, named N1–N4, were eluted with eluents of increasing polarity, in the following order: hexane, CH_2Cl_2 , hexane:AcOEt (3:1, v:v), and MeOH.

Analysis and quantification

The different fractions were run on a gas chromatograph coupled with a flame-ionization detector (GC-FID) to quantify the molecules of interest. To confirm the identity of the molecules, fractions were also run on a gas chromatograph interfaced with a mass spectrometer (GC-MS) using the same program as for the GC-FID analysis. Identification of the molecules was done by comparing the retention times of samples and standards, and by interpreting the ion fragments observed for the selected elution peaks.

To check the reproducibility of measurements and to quantify molecules, an *n*-alkanes standard (NJEPH aliphatic calibration standard, Restek) was measured every six samples. Depending on the molecular weight of a given molecule and its elution time, its detection limit would vary from about ~ 40 $\text{ng}\cdot\text{L}^{-1}$ for the C_{12} *n*-alkane to ~ 60 $\text{ng}\cdot\text{L}^{-1}$ for the C_{40} *n*-alkane. Unless otherwise specified, the molecules reported in this work were present measured above these detection limits.

The identity of the molecules was confirmed using known ion chromatograms and by comparing mass spectral data and GC retention times with published data. The C_{18} *n*-alkane peak of the external standard served as reference to calculate the concentration of compounds observed in the samples.

N1 fractions N1 fractions, containing aliphatic hydrocarbons, were analysed on Shimadzu instruments as described by McColl (2016).

GC-FID analyses were performed on a Shimadzu 2010 GC (Shimadzu) equipped with a BP1 column (60 m \times 250 μm \times 0.25 μm ; SGE Analytical Science). Hydrogen was used as the carrier gas at a 1.2 $\text{mL}\cdot\text{min}^{-1}$ column flow rate. The GC method used a splitless injection

at 320 °C. The oven temperature was programmed as follows: hold at 60 °C for 2 min, ramp up to 120 °C at 30 °C·min⁻¹, then to 350 °C at 3 °C·min⁻¹, then hold at 350 °C for 20 min.

Identification of the molecules by GC-MS was done on a 2010 GC (Shimadzu) interfaced with an OP2010-Plus MS (Shimadzu). The column and program used were the same as above. The interphase temperature was set at 300 °C while the ion source temperature was set at 200 °C. The carrier gas used was helium, at a column flow rate of 1.2 mL·min⁻¹.

N2, N3, N4 fractions, and TLEs Fractions N2 (aromatic hydrocarbons), N3 (alcohols), N4 (polar compounds), and TLEs were analysed on Agilent instruments.

GC-FID analyses were performed on an Agilent 7890B GC system (Agilent) equipped with an Rtx[®]-1 column (60 m × 250 µm × 0.25 µm; Restek).

Hydrogen was used as the carrier gas at a column flow rate of 1.2 mL·min⁻¹. The GC method used splitless injection at 320 °C, and the oven temperature was programmed from 60 °C (hold for 2 min) to 255 °C at 20 °C·min⁻¹, then to 300 °C at 3 °C·min⁻¹, followed by 10 °C·min⁻¹ increase to 320 °C, then hold at 320 °C for 10 min.

Molecules in these samples were identified by GC-MS using the same temperature program as the GC-FID analysis. A GC (7890B Series, Agilent) coupled with a mass spectrometer (5977A GC-EI, Agilent) was used to confirm the identity of the molecules using known ion chromatograms and by comparing mass spectral data and GC retention times with published data.

Prior to being analysed, fractions N3 and N4 had to be derivatised with *N,O*-bis(trimethylsilyl)trifluoroacetamide (BSTFA). TLEs were analysed a first time, then derivatised and reanalysed.

Silylation was performed following the routine method used in the laboratory, adapted from Butts (1972). 40 µL of pyridine (Sigma-Aldrich) and 30 µL of BSTFA containing 1 % trimethylsilyl chloride (Acros Organics) were added to the vial containing the sample. Vials were closed with septum-caps and incubated at 80 °C for 2 h. After evaporation and adjustment of the solvent to the desired volume, samples were run on the GC.

PAHs in N2 fractions Non-anthropogenic sources of polycyclic aromatic hydrocarbons (PAHs) include the combustion of plant materials (e.g. Baumard et al. 1999), the diagenesis of organic matter in sediments (e.g. Wakeham et al. 1980), and possibly the reaction of adsorbed organic material on volcanic plume particles (Raga et al. 2013).

To test for the presence of specific PAHs in N2 fractions, some of these fractions were re-analysed on the Agilent GC-MS setup. Another temperature program, established by Ali Salik was used: splitless injection (300 °C); oven temperature at starting at 55 °C (hold for 10 min) heated up to 180 °C at 10 °C·min⁻¹, then to 320 °C at 30 °C·min⁻¹, and hold for 10 min. Helium was used as a carrier gas at a column flow rate of 2.3 mL·min⁻¹.

Samples were injected a first time analysing the *total ion current*, then a second time using the *single ion mode*. The presence of ions with the following *m/z* ratios, corresponding

to PAH moieties and their derivatives, was investigated: 128.2, 152.2, 154.2, 166.2, 178.2, 202.2, 228.2, 240.2, 252.2, and 276.2. Retention times were compared with a standard (610 PAH Mix, Restek).

Indices

Carbon preference index (CPI) Calculation of the CPI (equation 2.12) gives the relative abundance of odd- and even-carbon-numbered *n*-alkanes in a sample and can be linked to its diagenesis degree (Bray and Evans 1961; Cooper and Bray 1963). The index ranges from C₂₅ to C₃₃ for odd carbon numbers, and from C₂₄ to C₃₄ for even carbon numbers.

$$\text{CPI} = 0.5 \cdot \frac{C_{25} + C_{27} + C_{29} + C_{31} + C_{33}}{C_{24} + C_{26} + C_{28} + C_{30} + C_{32}} + 0.5 \cdot \frac{C_{25} + C_{27} + C_{29} + C_{31} + C_{33}}{C_{26} + C_{28} + C_{30} + C_{32} + C_{34}} \quad (2.12)$$

C_x = concentration of the C_x *n*-alkane

Average chain length (ACL) Calculation of the ACL (equation 2.13) gives the average number of carbon atoms of *n*-alkanes in a sample based on their abundance (Poynter et al. 1989).

$$\text{ACL} = \frac{25 \cdot C_{25} + 27 \cdot C_{27} + 29 \cdot C_{29} + 31 \cdot C_{31} + 33 \cdot C_{33}}{C_{25} + C_{27} + C_{29} + C_{31} + C_{33}} \quad (2.13)$$

C_x = concentration of the C_x *n*-alkane

2.4 Genomic analyses

2.4.1 DNA extraction

This step was performed in William Sloan's laboratory (School of Engineering, University of Glasgow).

Deoxyribonucleic acid (DNA) was extracted from soil samples using a FastDNA Spin kit for soil (MP Biomedical) following the instructions provided by the supplier. This DNA extraction kit was chosen to keep the protocol consistent with the one already used by Thomas (2018) despite some samples possibly giving low extraction yields due to the presence of silts in the samples; the method described by Direito et al. (2012) could be tested to compare yields. About 700-800 mg of each soil sample were processed and DNA was eluted with 50 µL of buffer.

The concentration of recovered DNA was then measured on a QuBit® 2.0 Fluorometer (Life Technologies) using a QuBit® dsDNA HS assay kit (Life Technologies), following the instructions provided by the supplier.

2.4.2 DNA amplification

This step was performed in Linas Mažutis' laboratory (Institute of Biotechnology, Vilnius University).

DNA fragments present in the samples had to be amplified irrespectively of their sequence, i.e. they should not rely on any specific primers. This was performed using digital droplet multiple displacement amplification (ddMDA), a technique recently described (Sidore et al. 2016; Rhee et al. 2016).

Contrary to conventional DNA amplification by polymerase chain reaction, MDA uses randomised primers and amplifies all DNA present in a sample.

Digital droplet is a microfluidic technique which allows the encapsulation of a single DNA molecule in a nanoliter aqueous droplet. The droplet then acts as a compartment in which biological reactions can be performed. Compartmentalisation prevents “*competition*” between the different DNA fragments during amplification contrary to bulk experiments (e.g. Miller et al. 2006).

Microfluidic chips preparation

Chips containing microfluidic devices designed by Linas Mažutis were prepared as described by Mazutis et al. (2013). Chip masters were prepared by Karolis Simutis. These masters were then used as molds to produce microfluidic chips, with the help of Karolis Simutis and Valdemaras Milkus.

PDMS (Dow Corning) and Sylgard® 184 (Dow Corning) were mixed (10:1, m:m) and poured in a Petri dish containing the master. Following degassing in a vacuum desiccator, PDMS was cured overnight at 65 °C.

After cooling to room temperature, the PDMS slab covering the microfluidic devices was gently cut out and holes were punched for the devices' liquid inlets and outlet. The slab was rinsed with iPrOH, then nitrogen-dried.

To attach the PDMS slab to a glass slide, their surfaces to be attached were activated with an oxygen plasma (10 s burst, power 2.5, oxygen level 8–10; Plasma Prep 2, GaLa Instrumente). Following the activation, the PDMS was attached to the glass — making the chip — and incubated at 65 °C for 10 min.

After cooling of the chip to room temperature, its microfluidic channels were treated with Aquapel (Aquapel) to render their surface hydrophobic.

Digital droplet multiple displacement amplification (ddMDA)

Amplification reactions were performed using 5 µL of DNA extract (with a concentration ranging from below detection limit to 10 ng/µL in 50 µL of a reaction mixture containing 2.5 units of Φ29 DNA polymerase (Thermo Scientific) supplemented with 1 × Φ29 buffer, 50 µM of randomised hexamers (Thermo Scientific), 1 mM of each dNTP, 2 mU·µL pyrophosphatase (Thermo Scientific), and 1 % Pluronic F127 (Thermo Scientific).

Samples were emulsified in a fluorinated oil — 1 % EA2 (RAN Biotechnologies) in HFE-7500 (3M) — using a 10 μm nose to produce ~ 4 pL droplets. Flowrates were $50 \mu\text{L}\cdot\text{h}^{-1}$ for the aqueous phase and $150 \mu\text{L}\cdot\text{h}^{-1}$ for the oil phase, hence generating droplets at ~ 3.3 kHz. A layer of mineral oil above the emulsion prevented its coalescence. Emulsions were incubated at 30°C for 16 h. The polymerase was eventually deactivated by heating the samples at 65°C for 10 min.

DNA purification

Following deactivation of the $\Phi 29$ polymerase, excess HFE oil was removed from the tubes prior to pipetting emulsions into new tubes.

To help break the emulsion and to recover the DNA more easily, 20 μL of $\Phi 29$ buffer (Thermo Scientific) and 30 μL of PFO (Fluorochem) were added to the emulsion. Emulsions were broken down by vortexing them and the released HFE oil was pipetted out again.

The remaining aqueous phases were purified with an Agencourt[®] AMPure[®] XP kit (Beckman Coulter) following the recommendation of the supplier.

DNA purity was checked on a NanoDrop[®] ND-1000 Spectrophotometer (Thermo Scientific), and DNA concentration was checked on a Qubit as described above (2.4.1, p. 24).

Polymerase chain reaction (PCR)

Amplification reactions were performed using 0.5 μL of purified DNA in 50 μL of a reaction mixture containing 1.25 units of DreamTaq DNA polymerase (Thermo Scientific), 1 μM of forward primer (Eurogentec), 1 μM of reverse primer (Eurogentec), 200 μM of each dNTP (Thermo Scientific), 1 \times Taq buffer (Thermo Scientific) and were incubated with the following program: heating to 95°C for 3 min, heating to 95°C for 30 s, cooling to 55°C for 30 s, heating to 72°C for 1 min, repetition of the 3 last steps 39 times, heating to 72°C for 10 min, cooling to 4°C . Amplicons were analysed by gel electrophoresis on 1 % agarose.

Bacterial primers were provided by Greta Stonite. \vec{F} : GTT AAT ACC TTT GCT CAT TGA; \overleftarrow{R} : ACC AGG GTA TCT AAT CCT GTT.

Archaeal primers were Arc9F (Kato et al. 2009) and Uni1406R (Kato et al. 2011). Arc9 \vec{F} : CYG GTY GAT CCY GCC RG; Uni1406 \overleftarrow{R} : GAC GGG CRG TGT GTR CAA.

2.4.3 Library preparation and sequencing

DNA libraries were prepared using a Nextera[®] XT Library Prep Kit (Illumina) and a Nextera[®] XT Index Kit v2 Set C (Illumina) following the recommendations of the supplier.

Fragment size was checked with a High Sensitivity DNA Kit (Agilent) on a Bioanalyzer 2100 (Agilent). Sequencing was performed at Vilnius University Hospital, Department of Molecular and Regenerative Medicine, using a MiSeq[®] Reagent Kit v3 (600 cycles) on a MiSeq system. Fragment size checking and sequencing were performed by Juozas Nainys.

DNA sequences were deposited at the NCBI BioProject database under the BioProject identification number PRJNA587227 (<http://www.ncbi.nlm.nih.gov/bioproject/587227>).

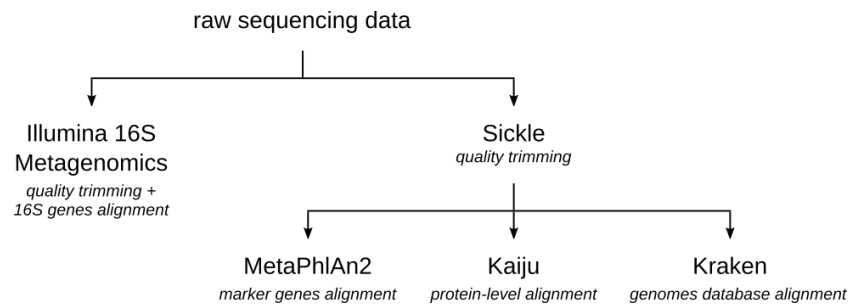


Figure 2.1 – Bioinformatics analysis strategy.

2.4.4 Bioinformatics

To identify the sequences obtained, sequences were analysed with four different programs (figure 2.1). As described below, each of these programs uses a different method to align the DNA sequences, thereby increasing the chances to obtain matches. However these programs focus on microbial genomes, no plant DNA can then be detected.

On one side, raw DNA sequences were processed through the Illumina 16S Metagenomics app (Illumina, Inc.). The algorithm used by this app is derived from Wang et al. 2007.

On another side — and with the help of Umer Ijaz (School of Engineering) — raw DNA sequences were firstly quality-trimmed with Sickle (Joshi and Fass 2011) using the default option for MiSeq sequencing quality and DNA sequence length thresholds (20, for both). Trimmed DNA sequences were then run on three different metagenomics programs: MetaPhlAn2, Kaiju, and Kraken. As these programs use different alignment methods and different gene libraries, their results may be different even though they used the same input.

MetaPhlAn2 outputs the best matches between the analysed DNA sequences and microbial clade-specific marker genes. Its resolution goes down to the species level — or even the strain level in some cases (Truong et al. 2015). However, the number of matches is never output, only the percentage of the total matches.

With Kaiju, the DNA sequences are translated into the six possible reading frames. The amino acid sequences obtained are compared with annotated proteins from microbial reference genomes. The taxon having the maximum exact matches is output (Menzel et al. 2016).

When classifying DNA sequences, Kraken only outputs exact matches against k -mers from a library of microbial genomes (Wood and Salzberg 2014).

2.5 ATP activity

ATP extraction from samples and bioluminescence measurements were performed by Dr David Cullen at the University of Akureyri (Iceland), using the following procedure.

2.5.1 Sample preparation

About 0.5 mL of sample was resuspended in 1 mL of TE buffer (TRIS 100 mM, EDTA 4 mM, pH 7.75), then vortex-mixed. The sample was then placed in boiling water for 5 min, cooled in room temperature water, then vortex-mixed again. The sample was then centrifuged at 9 000 *g*.

2.5.2 Bioluminescence measurement

50 μ L of a sample liquid extract are mixed with 50 μ L of ATP reagent, vortex-mixed for 3 s, then measured immediately on a luminometer.

ATP concentration in samples was deduced by comparing their bioluminescence measurements with the measurements from an ATP calibration curve.

All standard and sample measurements were done in triplicate.

Chapter 3

Atacama

‘I don’t like sand. It’s coarse and rough and irritating and it gets everywhere.’

Anakin Skywalker, *Star Wars: Episode II – Attack of the Clones* (2002)

Contents

3.1	Introduction: The Atacama Desert	30
3.2	Rationale	32
3.3	Hypotheses	33
3.4	Methods	33
3.5	Results	35
3.6	Discussion	49
3.7	Relevance to Mars	56
3.8	Conclusion	56

Abstract

The Atacama Desert is one of the best planetary analogues for Mars. Its extreme dryness and high solar flux make it an excellent environment to test the limits of microbial life. Yet, some parts of this desert still experience occasional rain and flash floods, draining surface molecules underground, thus providing water and nutrients to potential underground microbial communities.

A study of the lipids and the DNA present in a depth profile sampled in the Atacama Desert was performed, and compared with the physio-chemical and environmental conditions. Lipids likely to be of plant origin were observed mainly at the surface and near the bottom of the depth profile. Lipids of an unknown origin were also present in high quantities at 13 cm depth. Little DNA material was recovered throughout the profile and only one sample could be sequenced. The main DNA sequences identified corresponded to bacilli and nitrogen oxidisers. However, these genomics results are to be taken with caution due to the low number of sequence alignment matches.

3.1 Introduction: The Atacama Desert

3.1.1 Climate

The Atacama Desert is located in the north of Chile, 19°S to 29°S, overlapping the Tropic of Capricorn (ecozone NT1303; WWF 2018). The desert lies in the South American dry diagonal, a region receiving less than 500 mm of rain annually (Messerli et al. 1997; Houston and Hartley 2003; Bennett et al. 2016). Houston and Hartley (2003) identified four factors, outlined below, and reported in figure 3.1, contributing to the desert's aridity.

1. Zonal effect: *'[the desert] lies in the subtropical high-pressure belt where descending stable air produced by the Hadley circulation significantly reduces convection and hence precipitation'*;
2. Oceanic effect: *'the cold Peru Current (or Humboldt Current), which upwells along the Atacama coast, inhibits the moisture capacity of onshore winds and creates a persistent inversion that traps any moisture below 800 m'*;
3. Rainshadow effect: *'the proximity of the Andes upwind prevents moisture advection from the east'*;
4. Continentality effect: *'[the desert] lies at a considerable distance (up to 2000 km) from the Amazonia–Atlantic moisture source'*.

In addition, McKay et al. (2009) also points out the effect of the high coastal mountain ranges, which prevent marine fog from going inland.

The extreme aridity of the Atacama Desert makes it one the driest deserts in the world — along with the Dry Valleys in Antarctica (Horowitz et al. 1972) — and an excellent environment in which to test the driest limits of microbial life (Navarro-González et al. 2003). For

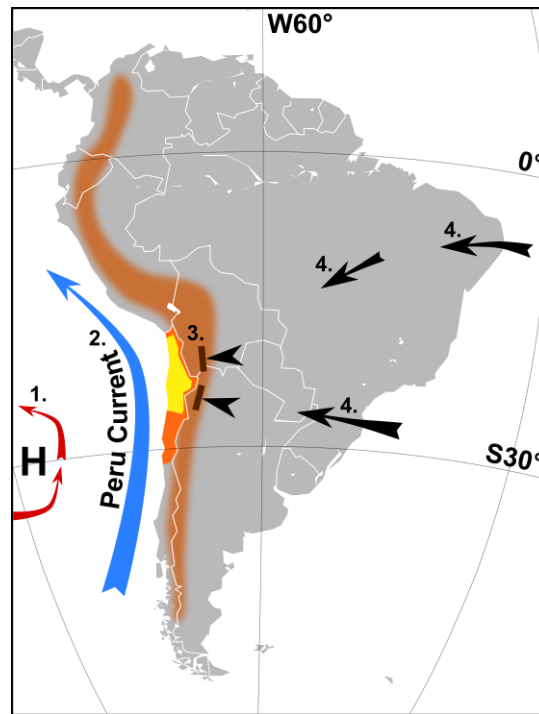


Figure 3.1 – Location of the Chilean part of the Atacama Desert (orange) and its hyper-arid core (yellow), and the Andes Mountains range (brown) in South America. The Pacific high-pressure zone (red) and the Peru Current (blue) are also indicated. Modified from Azua-Bustos et al. (2017).

this reason, the potential of the Atacama Desert as an analogue for Mars has been investigated since the mid-1960s (Edgerton 1966; Dick and Strick 2005b).

More recently, studies in the Atacama region have identified the driest places on Earth to be an area near the abandoned mining town of Yungay (Navarro-González et al. 2003), then the Moctezuma, the Cerritos Bayos, and the María Elena South site (Azua-Bustos et al. 2015).

The Atacama Desert is also the oldest desert on Earth, having continuously experienced arid climates since the late Jurassic (145.0–163.5 Ma; Hartley et al. 2005) or the late Triassic (201.3–237 Ma; Clarke 2006).

In rare events, rainfall does occur in the Atacama Desert. This happened, for example, on 24–25 March 2015 (Di Liberto 2015a; Schulze-Makuch et al. 2018), about a month before fieldwork for this study took place. The high-pressure system usually preventing rainfall in the region had weakened due to ‘a cutoff low off the coast of northern Chile and positive sea surface temperature anomalies over the eastern tropical Pacific’, thus allowing a low-pressure system to move towards the desert (Di Liberto 2015b; Bozkurt et al. 2016).

3.1.2 Life

Despite the extreme aridity, some animals, plants, and microbes have adapted to survive and live in these extreme conditions.

Fauna is mostly concentrated near the few water streams and wetlands, and its composi-

tion varies with the biome. The main predators are *Pseudalopex* foxes and the owl *Tyto alba* (Jaksic et al. 1999). About 1–20 species of mammals and 4–18 species of butterflies were reported to live in areas corresponding to the desert, depending on the specific area (Marquet 1994; Samaniego and Marquet 2009; Despland 2014). In addition, reptiles, amphibians, and scorpions were also reported (Jaksic et al. 1999).

More than 500 species of plants were reported in the Atacama. Plant families vary depending on the biome and water availability. Plant families vary depending on the biome and water availability, including cacti and other succulents, reeds, shrubs, and grasses (Morong 1891; Jaksic et al. 1999; Latorre et al. 2002).

Apart from the rare oases, providing water and nutrients, several microorganisms were still found to be able to survive in the hyperarid core of the desert (see Azua-Bustos et al. 2012 for a review), probably getting their water from mineral deliquescence (Davila et al. 2008). These communities can survive at the surface as endoliths or hypoliths (e. g. Warren-Rhodes et al. 2006; Wierzchos et al. 2006; Azúa-Bustos et al. 2011; Wierzchos et al. 2018), in biological soil crusts (Wang et al. 2017), or buried underground (Parro et al. 2011). Most microorganisms are bacteria (e. g. Navarro-González et al. 2003; Lester et al. 2007; Azua-Bustos et al. 2015; Cámara et al. 2016; Schulze-Makuch et al. 2018), but archaea (e. g. Schulze-Makuch et al. 2018; Wierzchos et al. 2018) and fungi (e. g. Wierzchos et al. 2010; Gonçalves et al. 2016; Schulze-Makuch et al. 2018) were also reported.

3.2 Rationale

Life conditions are particularly challenging in the Atacama Desert. Its extreme aridity makes it one of the driest deserts in the world — along with the Dry Valleys in Antarctica (Horowitz et al. 1972) — and an excellent environment in which to test the driest limits of microbial life (Navarro-González et al. 2003). One study site was even shown to have relative humidity values similar to those observed at Gale Crater by the Mars Science Laboratory (Azua-Bustos et al. 2015). In addition to the dryness, Atacama soils show trace concentrations of organic materials and intense solar UV radiation (e. g. Navarro-González et al. 2003; Azua-Bustos et al. 2015). Moreover, like on the martian surface, perchlorates have also been found in the Atacama (Catling et al. 2010).

Leaving aside the temperatures, these conditions give the Atacama Desert great potential as a natural analogue for Mars. For this reason, investigations in the desert have been going on since the mid-1960s (Edgerton 1966; Dick and Strick 2005b).

The Atacama sampling site was initially planned to serve as the lowest site in an altitude gradient — investigating the changes in biomarkers and in microbial communities — that would go up the Sairecabur volcanic massif (chapter 4). However, going through the area west of San Pedro de Atacama, on the way to the Sairecabur, the field appeared to be less than ideal for sampling. Too many signs of human activity were found, implying an increase in anthropogenic contamination, then the biome evolved quickly into a pre-Puña environment containing plants, whose biosignatures may also overshadow the microbial ones.

Consequently, sampling in the Atacama desert was transformed into a separate study. As the hyperarid core of the desert and the Salar de Atacama (containing halites) would have required more time than we had for a proper field reconnaissance prior to sampling, the Llano de la Piedad (Fig. 3.2.a) was chosen as a compromise between being not too far away from San Pedro de Atacama (where we stayed during fieldwork), being on the edge of the hyperarid core of the desert, and being isolated from human and plant influences. The site chosen presents signs of former water flows. Research was then focused on lipid biomarkers and microbial communities at a dry site which experiences occasional transient liquid water.

3.3 Hypotheses

As the ground surface experiences extreme dryness, and even though microbial communities have been described there, the most important biomass was expected to be found deeper underground, where some moisture from the recent rainfall could still remain (hypothesis 1).

Hypothesis 1: *Microbial concentration and diversity will increase with depth, reaching their highest values where the soil humidity is maximal and constant.*

Some plants were observed nearby the sampling site, having probably grown after the rain. Therefore, an additional hypothesis (hypothesis 2) was added regarding plants inputs in the ground.

Hypothesis 2: *Plant lipids will be found in the samples, and they will be more concentrated at the surface.*

3.4 Methods

3.4.1 Sampling strategy

Sampling site

The sampling site is located in the Llano de la Piedad, a floodplain and a discrete sub-basin of the Salar de Atacama, within the Pre-Andean Depression. The basin is bounded by the Cordillera Domeyko on its western side, and by the Cordillera de la Sal on its eastern side (Jolley et al. 1990; Hartley et al. 1992; Charrier and Reutter 1994). The Llano de la Piedad is located on the edge of the hyper-arid core of the desert. The area has an annual potential evaporation of 2 000 mm and annual precipitation of only 25 mm (Risacher et al. 1999b). Jolley et al. (1990) report that Pascoff (1962) described the area as experiencing an arid climate since the late Cretaceous (66–100.5 Ma), with a temporary wetter period during the Pleistocene glaciation (11.7 ka–2.58 Ma). Surface deposits are identified as Quaternary/Holocene alluvia (present–2.58 Ma, Hartley et al. 1992), with some deposits dating back to the Oligocene (23–30 Ma, Charrier and Reutter 1994). Past ephemeral drainage at the western base of the Cordillera Domeyko is suggested by the presence of alluvial fans (e.g. Carmona et al. 2000; Jolley et al. 1990; Rubilar et al. 2018).

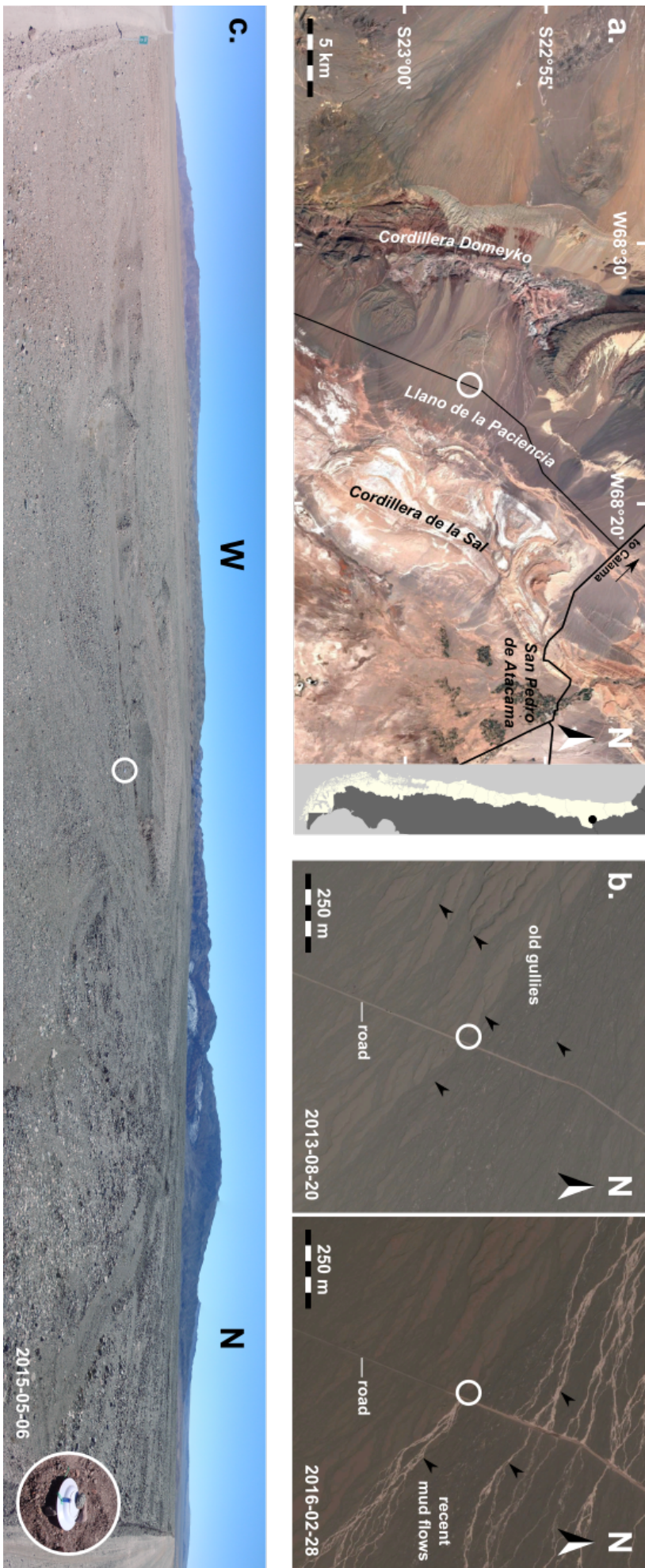


Figure 3.2 – (a) Satellite image of the fieldwork area near San Pedro de Atacama. (b) Close-ups of the field site on the most recent images taken before (August 2013, left) and after (February 2016, right) the March 2015 rain event; older gullies in the alluvial fan (left) are filled with darker material, whilst recent mud flows have a lighter colour (right); the sampling location (white circle) appears to have been unaffected by the rain. (c) Panoramic view of the field site. A close-up of the iButton probe is provided in the bottom right corner. A plate was used to shelter the probe from direct exposure to the sun and the wind. White circles indicate the sampling location. (a, b) Images adapted from Google Earth.

Soil samples

Samples were collected from an alluvial fan, coming west from the *Cordillera Domeyko* (figure 3.2 c). The sediments present in the fan are darker than the surrounding sediments and may have been drained from the cordillera (Cretaceous material, 66–145.5 Ma) and from the hill (non-volcanic Neogene material, 2.58–23.03 Ma) located between the cordillera and the sampling site (Rubilar et al. 2018). It should be noted that, according to the satellite images, our sampling site seems not to have been affected by the mud flows observed after the 2015 rain event (figure 3.2 b).

Soil samples were collected at the surface, and every 2 cm from 1 cm to 21 cm deep — with the help of PhD students Nick Thomas and Rory Porteous, and under the supervision of Prof. Vernon Phoenix.

Plant sample

A stem was collected from a plant (*Tiquilia atacamensis*) growing about 20–30 m from the sampling site. Details can be found in appendix B (sample A).

3.4.2 Planned analyses

Whilst collecting the samples, air temperature (T) and relative humidity (RH), as well as UV radiation, were measured directly at the sampling site. Sensors were also placed in the ground to measure T and RH for about two days. Upon return to Glasgow, samples were analysed following three main themes:

1. Soil physico-chemistry (mineralogy, grain size, water content, carbonate content, pH);
2. Organic content (loss on ignition, total lipid extract, refined lipid fractions);
3. Genetic content (total DNA, metagenomics).

The methodology used for each analysis are described in detail in chapter 2.

3.5 Results

3.5.1 Soil physico-chemistry

Mineralogy

X-ray diffraction (XRD) analysis was performed at the School of Chemistry (University of Glasgow). Samples were prepared and run by Jose Rico under the supervision of Justin Hargreaves. Interpretation of the XRD spectra was done with the help of Claire Wilson. XRD patterns are reported in section A.1 (p. 124).

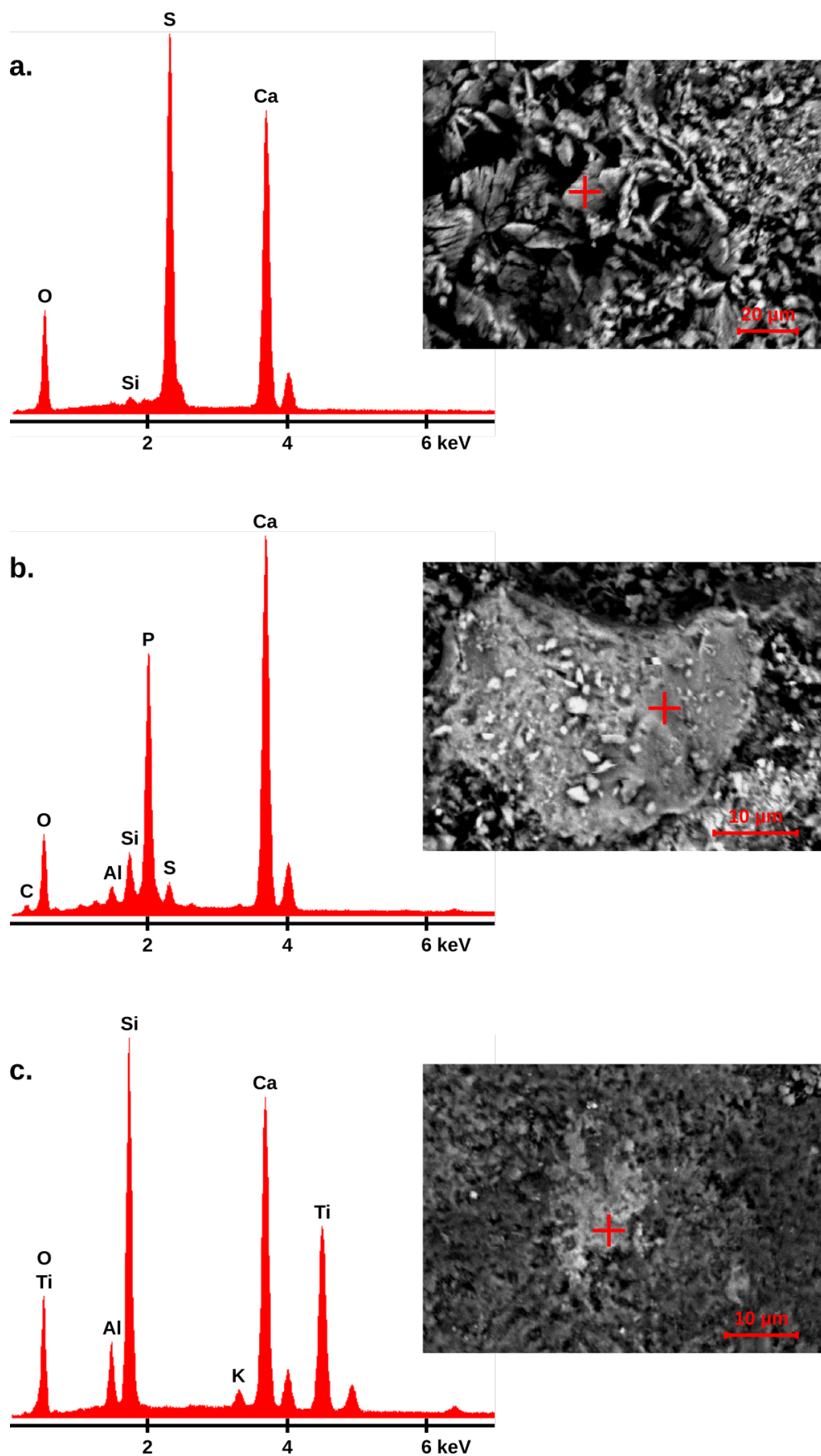


Figure 3.3 – EDX spectra and secondary electron images of mineral samples. Although not identified by XRD, EDX spectra of the samples suggested the presence of (a.) gypsum or anhydrite (CaSO_4), (b.) apatite ($\text{Ca}_5(\text{PO}_4)_3(\text{OH})$), and (c.) perovskite (CaTiO_3) mixed with K-feldspar (KAlSi_3O_8).

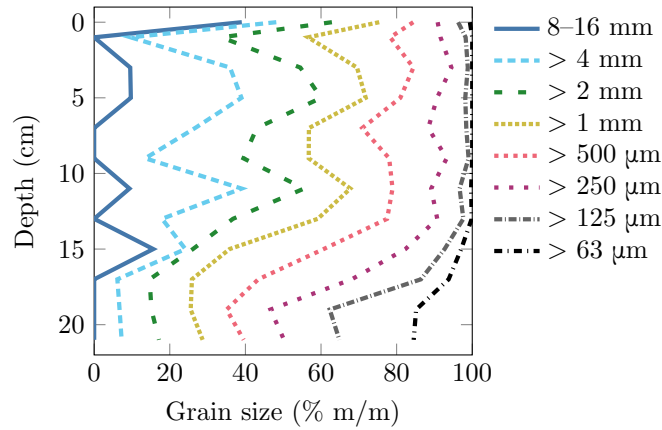


Figure 3.4 – Mass percentage of soil particles for different size thresholds.

To refine the results obtained by XRD and help identify some dubious peaks, energy dispersive X-ray spectroscopy (EDX) was performed on some samples with the help of Martin Lee. Gypsum was identified in samples this way.

XRD and EDX analyses indicate the mineralogy to be consistent through the depth profile. It is dominated by feldspars (mostly plagioclase), with quartz, micas, iron oxides, calcium carbonates, and calcium sulfates.

Grain size

Through the whole depth profile, the soil was composed of loose uncemented material. No hard pan was observed. Samples were sieved to determine the size of the particles (figure 3.4).

Gravels (2–16 mm) represent about 60 % of the surface sediments. This proportion varies between 40 and 60 % for most of the depth profile. Below 13 cm, the concentration of gravels starts decreasing and eventually represents about 15–20 % of the sediments at 17 cm and below.

The proportion of submillimetric particles, representing around 30–40 % of the samples from the surface to 13 cm deep, increases significantly to 60 % at 15 cm deep, then keeps increasing to stabilise around 70–75 % at 17 cm and below.

Very fine sands (63–125 μm), and silts and mud (< 63 μm), follow similar trends. Their proportions, almost negligible through the upper profile, increase to 10 % and 5 %, respectively at 15 cm deep. They keep increasing until 19 cm deep, where they reach around 25 % and 15 %, respectively.

Water-related physico-chemistry

Water and carbonate contents of the soil samples, and their pH are reported in figure 3.5.

At the surface, the water content is about 0.5 % and stays below 1 % down to 11 cm deep (0.89 %). The percentage of water then steadily increases reaching about 3.8 % around 20 cm deep.

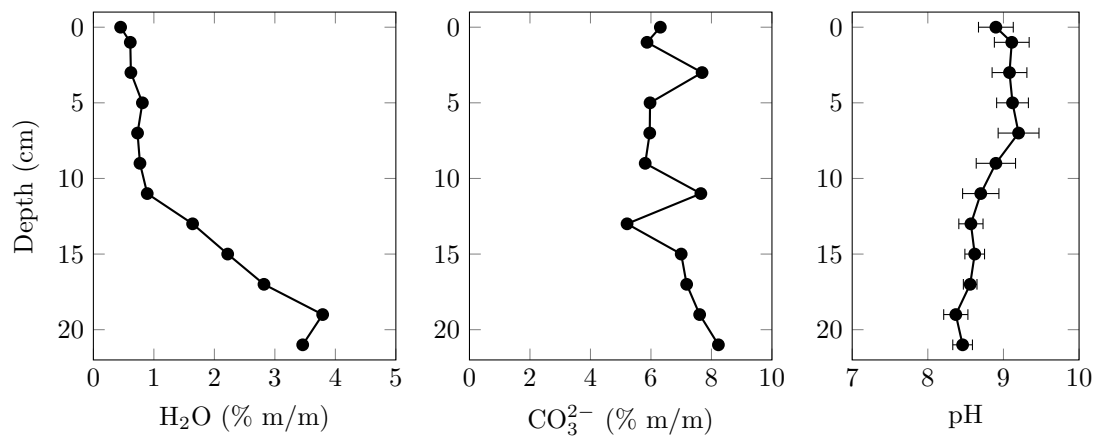


Figure 3.5 – Water-related physico-chemistry. Water and carbonate contents are expressed as a percentage of the sample’s mass. For water and carbonate contents, $n = 1$; for pH, $n = 3$.

Air T	(°C)	22.6
Air RH	(%)	6.4
UV-A	(W·m ⁻²)	19.85
UV-B	(W·m ⁻²)	2.85
UV-C	(mW·m ⁻²)	0.00

Table 3.1 – Environmental parameters measured at the sampling time.

The proportion of carbonate ions is about 6 % from the surface to 9 cm deep, slowly increasing to 8 % at 20 cm deep.

The pH remains alkaline through the whole profile. Around 9 from the surface to 7 cm deep, it then slowly decreases to reach 8.5 around 20 cm deep.

3.5.2 Environmental readings

Air measurements

Whilst collecting the samples, air temperature (T), relative humidity (RH), and ultra-violet (UV) levels for different wavelengths were measured by Prof. Vernon Phoenix. Measurements are reported in table 3.1.

(Under)ground measurements

In addition to air measurements, data were also recorded at the ground surface and underground. Following the collection of samples, probes were installed to measure the soil T and RH, at the surface and underground, for approximatively two days. Measured RH values were corrected as described in section 2.1.2 (p. 16). T and corrected RH are plotted in figure 3.6.

For an easier reading of the measurements, the minimum, maximum, and mean recorded values are also reported in table 3.2. As measurements were recorded for 46 h, the mean

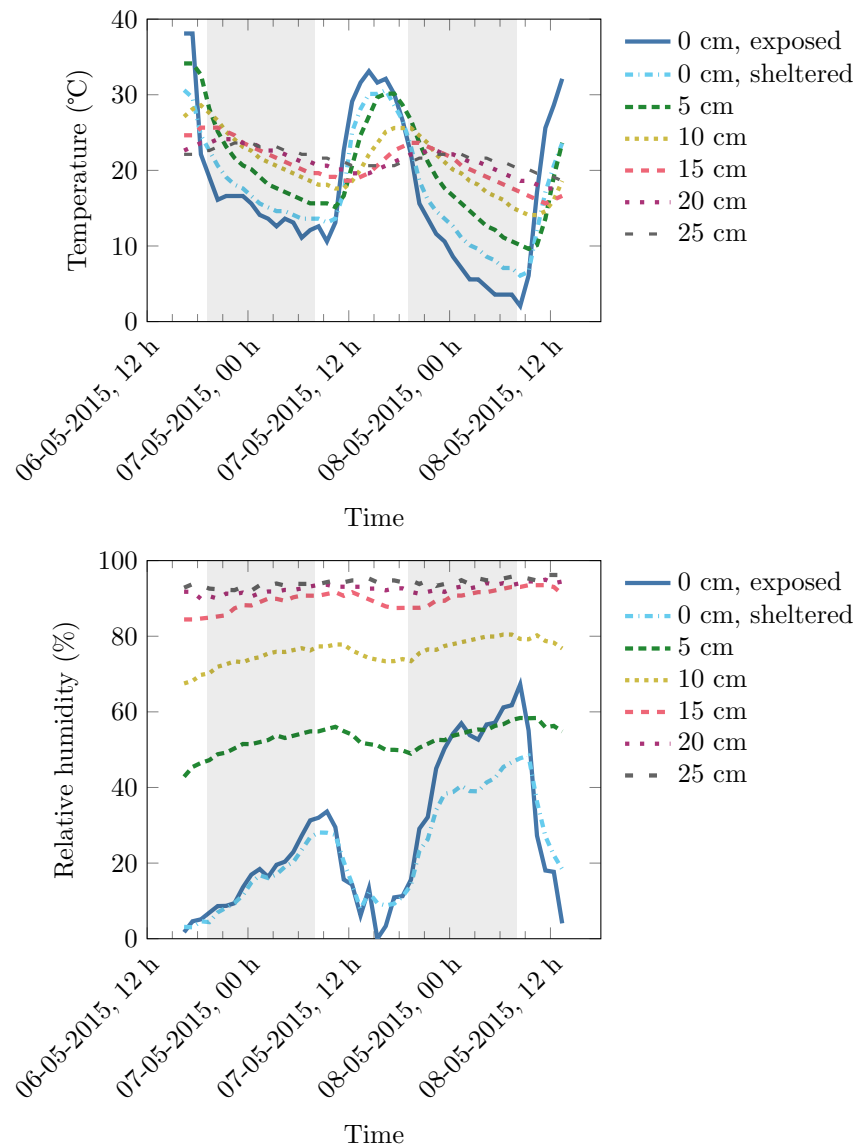


Figure 3.6 – Temperature (top) and relative humidity (bottom) measurements for different depths at the Atacama sampling site. The measurements were recorded, following the collection of soil samples, for about two days. Shaded areas indicate night times, based on the sunrise and sunset times calculated for the sampling site (Agafonkin 2009).

Depth (cm)	T (°C)			RH (%)		
	min	max	mean	min	max	mean
0 <i>exposed</i>	2.1	38.1	18.9	0.0	67.3	20.4
0 <i>sheltered</i>	6.1	30.6	19.2	3.0	48.4	19.5
5	9.6	34.1	21.0	42.8	58.4	52.5
10	14.1	28.6	21.4	67.5	80.4	75.6
15	15.6	25.6	21.2	84.4	93.5	89.5
20	17.6	24.1	21.4	89.9	95.0	92.4
25	18.6	23.6	21.7	92.1	96.2	94.1

Table 3.2 – Minimum, maximum, and mean values for temperature (T) and relative humidity (RH) readings, for different depths, at the Atacama sampling site.

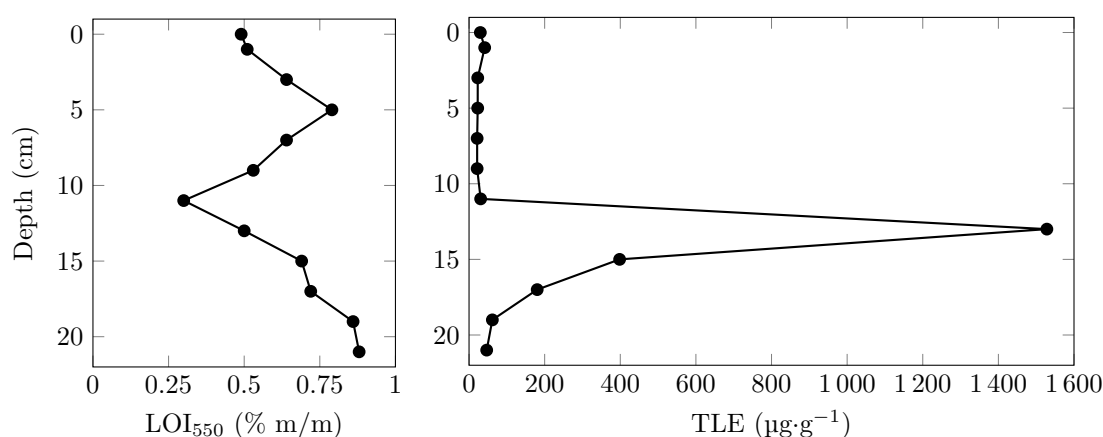


Figure 3.7 – Organic content in the Atacama samples, along the depth profile, estimated by LOI₅₅₀ (left) and TLE concentrations (right). The TLE concentration peak (13 cm depth) is observed just above the depth at which the proportion of submillimetric particles increases significantly (15 cm depth).

value was only calculated for one complete day (24 h), 7 May 2015.

Through the recorded period, surface T ranged between 2.1 and 38.1 °C in the sunlight, and between 6.1 and 30.6 °C in the shade, with daily variations of about 30 °C. At 25 cm deep, T variations were limited to 18.6–23.6 °C. The mean daily T along the whole profile was always close to 20 °C.

During the same time period, RH measurements recorded a negative value for the probe exposed directly to sunlight. This value might have been a measurement artifact and was corrected to 0. Corrected RH at the surface oscillated between 0.0 and 67.3 % in the sunlight, and between 3.0 and 48.4 % in the shade. At 5 cm deep, RH varied between 42.8 and 58.4 %, and at 25 cm deep RH was restricted to 92.1–96.2 %. Mean daily RH was about 20 % at the surface and increased rapidly with depth, reaching about 90 % at 15 cm deep.

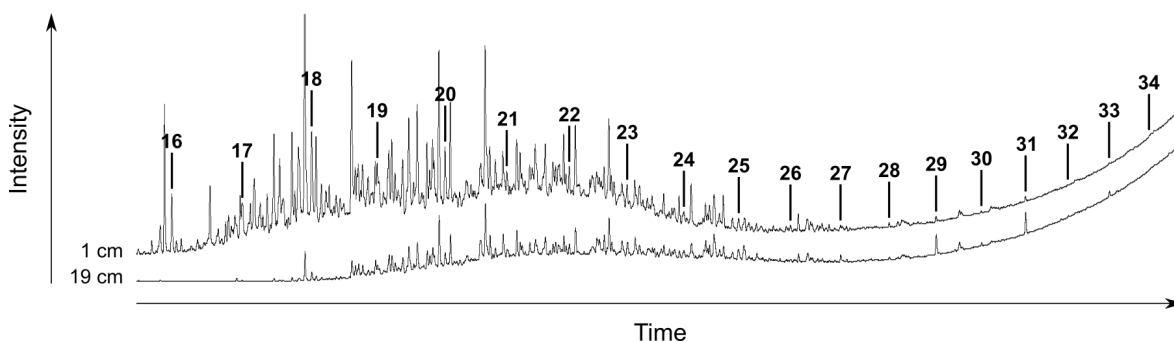


Figure 3.8 – Unresolved complex mixture containing the *n*-alkane molecules for the samples collected at 1 and 19 cm deep. Their position is indicated with their chain length (in carbon atoms number).

3.5.3 Organic content

Loss on ignition

The estimation of organic content in samples by loss on ignition at 550 °C (LOI₅₅₀; figure 3.7, right) yields low values, ranging from 0.30 to 0.88 %. Starting with 0.49 % at the surface, the organic content increases up to 0.79 % at 5 cm deep before decreasing again (0.30 % at 11 cm deep). The percentage of organic content eventually increases again and reaches 0.88 % at 21 cm deep.

Total lipid extract

TLE concentrations varied between 21.4 and 1 528.3 $\mu\text{g}\cdot\text{g}^{-1}$ through the depth profile (figure 3.7, left). At the surface, TLE concentrations are around 30–40 $\mu\text{g}\cdot\text{g}^{-1}$. Between the surface and 11 cm, TLE concentrations are just above 20 $\mu\text{g}\cdot\text{g}^{-1}$. At 13 cm concentration suddenly increases to 1 528.3 $\mu\text{g}\cdot\text{g}^{-1}$, then slowly decreases to reach 50–60 $\mu\text{g}\cdot\text{g}^{-1}$ around 20 cm deep.

TLEs were separated into subfractions, following the protocol described in section 2.3.2 (p. 21) which are discussed below.

N1 fractions

General considerations Fraction N1 contains aliphatic hydrocarbons. Most of the molecules contained in this fraction are part of an unresolved complex mixture (UCM). The main molecules of interest in these fractions are *n*-alkanes, but the elution of most of them within the UCM rendered their quantification challenging (figure 3.8). Depending on the depth of the sample, the *n*-alkanes observed varied between C₁₆ and C₃₄ in carbon chain length, with concentrations ranging from 0.01 to 17.00 $\text{ng}\cdot\text{g}^{-1}$ of soil (figure 3.10).

The abundance of short chain *n*-alkanes (up to C₂₀) significantly outweighs the abundance of longer chain *n*-alkanes. Higher concentrations of even-numbered chain lengths over odd-numbered is observed from C₁₆ to C₂₂, with peak concentrations for C₁₈ (17.00 $\text{ng}\cdot\text{g}^{-1}$ at 1 cm deep and 13.84 $\text{ng}\cdot\text{g}^{-1}$ at 15 cm deep). Short chain *n*-alkanes are almost exclusively

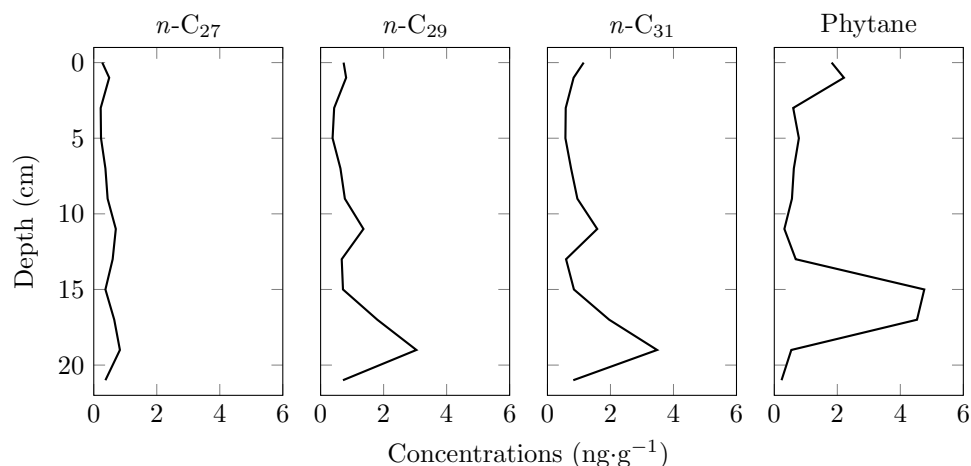


Figure 3.9 – Lipid inputs from higher plants at the Atacama sampling site.

observed at 1 and 15 cm deep. In the paragraphs below, attention is focused on lipids of plant and microbial/diagenetic origin.

Plant inputs Above C₂₆, odd-numbered chain lengths are more concentrated than the even ones. This signature is indicative of the presence of higher plant waxes (e. g. Eglington and Hamilton 1967; Jetter et al. 2006), although their production by microbes has been recently reported (Li et al. 2018).

The highest concentrations for these molecules (figure 3.9) are observed for C₂₉ and C₃₁ (3.04 and 3.48 ng·g⁻¹, respectively, at 19 cm deep). The localisation of these molecules along the depth profile also changes; they are mainly observed at the surface, and at 11 and 19 cm deep.

Pristane (Pr) and phytane (Ph) are isoprenoids, both thought to be diagenesis products of the phytyl side chain of chlorophyll *a* (Curphey 1952; Bendoraitis et al. 1962; Eglington et al. 1964; Brooks et al. 1969; Powell and McKirdy 1973). The Pr/Ph ratio was proposed as an indication of the oxic or anoxic conditions occurring during diagenesis (Powell and McKirdy 1973; Didyk et al. 1978). However, ten Haven et al. (1987) suggested that this ratio rather indicates the oxidative or reductive properties of the medium hosting the molecules at the time of their degradation. A catalysis by clays has also been suggested as a reaction mechanism (see Rontani and Volkman 2003 and references therein). Tocopherols were pointed out as another potential precursor for pristane by Goossens et al. (1984). Their production in plants is however about 10–100 fold less than chlorophyll production (Bucke et al. 1966). Phytanyl chains were also found to originate from archaeal lipids (Corcelli et al. 2000; Lattanzio et al. 2002; Sprott et al. 2003). As both phytane and pristane can have a plant origin, and as plant inputs are likely to outweigh microbial inputs, we will simplify and consider that phytane and pristane both represent plant inputs in soils.

Phytane concentrations ranged from 0.23 to 4.76 ng·g⁻¹ (figure 3.9), but pristane was not detected in the samples. The background concentration for phytane is below 0.8 ng·g⁻¹. Higher concentrations are observed at 0–1 cm deep (about 2 ng·g⁻¹) and at 15–17 cm deep

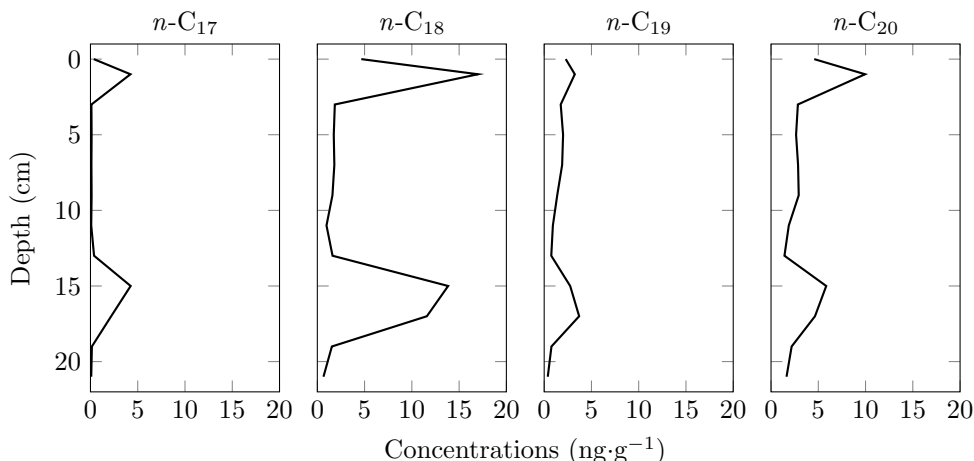


Figure 3.10 – Short chain *n*-alkanes at the Atacama sampling site.

(about $4.6 \text{ ng}\cdot\text{g}^{-1}$).

Degraded material and microbial inputs An even/odd ratio > 1 for short chain *n*-alkanes is a biosignature usually associated with anthropogenic contamination (e. g. Simoneit 1984; Lichtfouse et al. 1997; Brocks et al. 2008), microbial production (e. g. Han and Calvin 1969; Albro 1976), or diagenesis of longer *n*-alkanes (e. g. Goutx and Saliot 1980; Eckmeier and Wiesenberg 2009; Wiesenberg et al. 2009), although this pattern has also been reported for plants (Kuhn et al. 2010).

These results are plotted on figure 3.9 where the concentration dichotomy between odd- and even-numbered *n*-alkanes is clearly visible. The highest concentrations are observed at 1 cm deep and at 15–17 cm deep.

CPI and ACL indices Different indices can be calculated using *n*-alkane concentrations. Two of them can be useful in the context of this study: the carbon preference index (CPI) and the average chain length (ACL). Both indices give indications about the diagenesis of odd-numbered long chain *n*-alkanes. These molecules being associated with plant leaf waxes, it is pre-supposed that molecular inputs of plant origin remain similar at all depths in the soil profile. Details about the calculation of the indices are described in section 2.3.2.

CPI values vary with depth, between 1.55 and 5.28 (figure 3.11, left). ACL values vary between 27.5 and 29.2 and have a mean of around 28 ± 0.5 for most of the depth profile (figure 3.11, right).

N2 fractions

Fraction N2 contains aromatic hydrocarbons, aldehydes, and ketones. A first analysis was conducted to try to identify potential biomarkers. The molecules identified were only polymer-related contaminants, probably coming from the plastic bags that contained the samples. The most abundant was diphenyl sulfone.

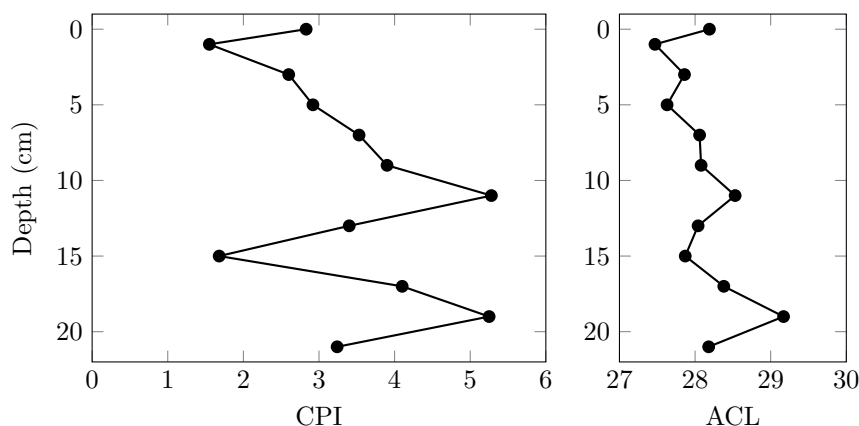


Figure 3.11 – Indices derived from *n*-alkanes concentrations. (left) CPI. (right) ACL.

To restrict the analysis to polycyclic aromatic hydrocarbons (PAHs) only, samples were run again using a different analytic protocol (see section 2.3.2, p. 23). No PAHs were found.

N3 fractions

The only molecules of interest found in fraction N3 were *n*-alkanols. They were identified as their trimethylsilyl (TMS) derivatives (figure 3.12). No archeol — produced by archaea — was identified.

The origin of dodecan-1-ol and tridecan-1-ol, however uncertain, is probably the same given the strong similarities of their concentration profiles in the samples. Production of dodecan-1-ol by bacteria (Dias et al. 2017; Hamilton-Kemp et al. 2005; Liu et al. 2008) and production of tridecan-1-ol by plants have been reported (Oliveira et al. 2012). However, in the latter case the plants described grew in an aquatic environments.

The production of octadecan-1-ol by diverse plants has been reported (Rawat et al. 2017; Faboro et al. 2016; El Gendy et al. 2015; Schröder and Vetter 2012). The molecule can be produced by some bacteria (Gu et al. 2007) and destroyed by others (Chang et al. 1962).

An excess of even long-chain *n*-alkanols (ranging from C₂₀ to C₂₈) is considered to indicate higher plant inputs (Eglinton and Hamilton 1967; Baker 1982; Ficken et al. 2000).

Short-chain *n*-alkanols (C₁₂ and C₁₃) were observed from 1 to 13 cm deep, both with concentrations ranging from 0.32 to 0.59 ng·g⁻¹, and again at 19 and 21 cm deep (0.03–0.18 ng·g⁻¹). The molecules were not detected at other depths.

Octadecan-1-ol is also observed throughout the profile with concentrations ranging from 0.10 to 1.40 ng·g⁻¹.

Even long-chain *n*-alkanols (ranging from C₂₀ to C₂₈) are present between 15 and 21 cm deep. Their peak concentration, always observed at 19 cm deep, ranges from 1.22 to 23.48 ng·g⁻¹, depending on the molecule. The highest concentrations are observed for the hexacosan-1-ol (C₂₆, 23.48 ng·g⁻¹) and the tetracosan-1-ol (C₂₄, 22.90 ng·g⁻¹).

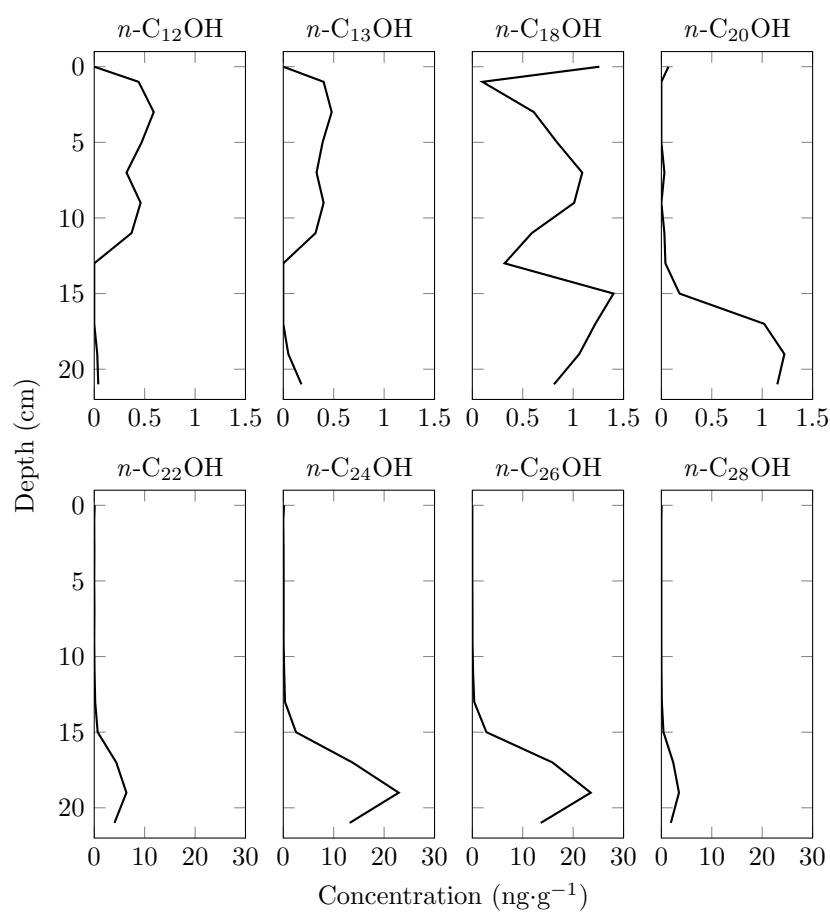


Figure 3.12 – Concentration *n*-alkanol TMS derivatives.

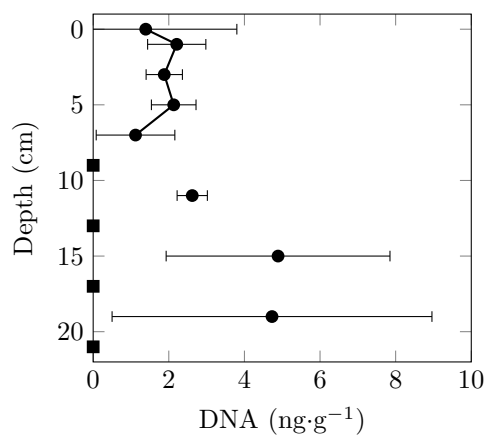


Figure 3.13 – DNA concentrations, normalised to the quantity of soil they were extracted from, as a function of depth ($n = 3$). Squares indicate values below detection limit before normalisation.

N4 fractions

The most polar molecules from the neutral lipid extract are contained in fraction N4. A pilot study was conducted to try to identify trimethylsilyl derivatives of potential biomarkers. None were found.

3.5.4 Plant sample

About 25–30 m from the sampling site, small shrubs of *Tiquilia atacamensis* were growing. A stem was collected from one of them, from which a TLE was extracted and refined into the same subfractions as the soil samples. The n -alkanes composition of this plant sample is reported as sample S in appendix B (p. 133).

The n -alkanes observed ranged from C_{18} to C_{35} in size, with a dominance of odd-numbered long-chain molecules. The combined relative abundances of C_{27} , C_{29} , and C_{31} represented over 70 % of the total n -alkane mass; C_{29} by itself accounting for one third of the total mass.

3.5.5 DNA content

Even though microbial life in the hyperarid core of the Atacama Desert is not as uncommon as initially thought, it still lacks diversity. The main genera identified are *Bacillus* and *Streptomyces* (e.g. Parro et al. 2011; Azua-Bustos et al. 2012; Bull et al. 2016; Paulino-Lima et al. 2013; Paulino-Lima et al. 2016).

Triplicate total DNA extraction from the samples yielded very little material (figure 3.13). Values before conversion and normalisation ranged from below detection limit ($25 \text{ pg} \cdot \mu\text{L}^{-1}$) to $0.17 \text{ ng} \cdot \mu\text{L}^{-1}$. After normalisation to the mass of starting material, DNA concentrations range from 1.12 to $4.89 \text{ ng} \cdot \text{g}^{-1}$ — values below detection limit are defined as 0.

To study the genetic origin of the DNA, its amplification and sequencing were planned.

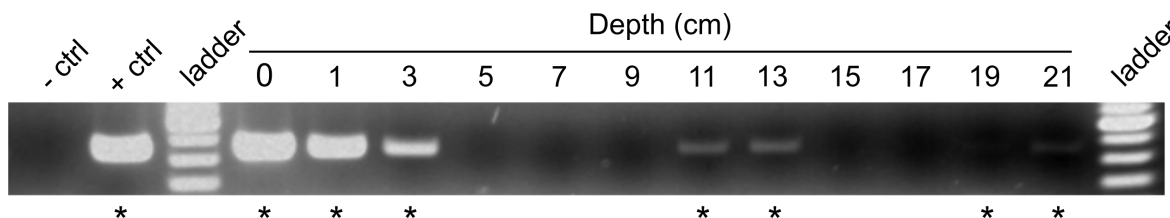


Figure 3.14 – Agarose gel for the bacterial 16S rDNA PCR. Amplification is indicated by an asterisk.

The small amount of DNA material available and the potential degradation of the DNA strands led me to use tools designed to reduce amplification biases. An unbiased amplification on extremely low amounts of genetic material is achieved by using ddMDA — the combination of digital droplet microfluidics (physical separation of each DNA strand) with multiple displacement amplification (aspecific amplification) (Sidore et al. 2016; Rhee et al. 2016).

Following their amplification and purification, DNA samples were prepared for MiSeq sequencing. In parallel, the presence of bacterial and archaeal DNA in the samples was tested by PCR. Bacterial DNA was amplified from the surface to 3 cm deep, and at 11–13 and 19–21 cm deep (figure 3.14). No archaeal DNA was amplified.

After preparation of the DNA for sequencing and purification, only one sample — second DNA set, 15 cm deep — displayed the purity and concentration required for MiSeq sequencing, which was performed by Juozas Nainys (Institute of Biotechnology, Vilnius University). The sequencing generated 3 863 419 raw DNA reads (available on NCBI under the BioSample accession number SAMN13182958).

Raw reads were directly analysed by the Illumina 16S Metagenomics app (algorithm derived from Wang et al. 2007). Only 2 383 reads were identified at the kingdom level, rendering this analysis potentially unrepresentative.

For a second analysis, quality-trimming of the raw sequences — with Sickle (Joshi and Fass 2011) — and further analysis of the trimmed sequences — with MetaPhlAn2 (Truong et al. 2015), Kaiju (Menzel et al. 2016), and Kraken (Wood and Salzberg 2014) — was performed by Umer Ijaz (School of Engineering, University of Glasgow). Kaiju and Kraken results are summarised in table 3.4 and table 3.3, respectively.

MetaPhlAn2 results can be considered to be non-significant as only one bacteria (*Nitrosospora*) and one virus (Dasheen mosaic virus) were matched. Kraken identified 68 367 reads at the kingdom level (table 3.3), whereas Kaiju identified 326 465 reads at the species level (table 3.4). The main genera identified by Kaiju were *Bacillus* and *Nitrosospora* (24 % and 5 % of the hits, respectively).

	Matches	% of total
Global results		
Total (kingdom level only)	68 367	100.00
Classified	65 087	95.20
Unclassified	3 280	4.80
Classified results		
Bacteria	52 770	77.19
Archaea	808	1.18
Other unspecified cellular organisms	252	0.37
Viruses	11 257	16.47

Table 3.3 – Matches output by Kraken for the sample taken at the Atacama sampling site, 15 cm depth.

	Matches	% of total
Global results		
Total	3 862 319	100.00
Classified	813 154	21.05
Unclassified	3 049 165	78.95
Classified results		
Species rank	486 689	12.60
Above species rank	326 465	8.45
Species rank results		
<i>Nitrosospira briensis</i>	9 572	0.25
<i>Bacillus pseudofirmus</i>	8 469	0.22
<i>Flammeovirgaceae bacterium 311</i>	8 031	0.21
<i>Bacillus oceanisediminis</i>	6 612	0.17
<i>Halobacillus halophilus</i>	6 398	0.17
<i>Bacillus cereus</i> group	6 174	0.16
<i>Bacillus halodurans</i>	5 983	0.15
<i>Nitrosospira multiformis</i>	5 550	0.14
<i>Virgibacillus sp. SK37</i>	5 318	0.14
<i>Bacillus cellulosilyticus</i>	5 233	0.14
Others	419 349	10.86

Table 3.4 – Matches output by Kaiju for the sample taken at the Atacama sampling site, 15 cm depth. The ten most abundant species are indicated.



Figure 3.15 – Sediments deposited by the March 2015 rain, about 30 m south-east of the sampling site. A month after the rainfall, darker and wetter sediments can still be observed under the dry surface. The segments removed are ~15–20 cm long. Picture by Rory Porteous.

3.6 Discussion

3.6.1 Soil physico-chemistry

Recent sediment deposits from the last flash flood were observed south-west of the sampling site. They consisted of damp sediments of fine sands and smaller particles. This sediment had a dry crust at its surface, yet signs of humidity (a darker colour) was still observed about 5 mm below the surface (figure 3.15).

Contrary to this recent sediment deposit, our sampling site displayed gravels and coarse sand at the surface (figure 3.4, right), even though it seems to be located in the course of a former water stream. As atmospheric deposits contribute significantly to soil formation processes in the Atacama (Wang et al. 2014, 2015), one hypothesis to explain the grain size observed at our site is that the original water flow also deposited a mud composed of fine particles, which then dried and solidified, and was later covered by sand and gravels brought as aeolian inputs — winds strong enough to carry sand ($100+ \text{ km}\cdot\text{h}^{-1}$) were observed in the past near San Pedro de Atacama (Dingman 1967). Buried at depths where humidity can persist more, the mud could then have eventually desolidified. However, a specific study would be required to test this hypothesis.

Regarding the mineralogy of the grains, carbonates and sulphates could both find their source in evaporites from the nearby Salar de Atacama and from the Cordillera de la Sal (Carmona et al. 2000; Lowenstein et al. 2003; Warren 2016). In addition, sulphate evaporites could also originate from the Domeyko Range (Carmona et al. 2000). Halites — also present in the Salar de Atacama — have not been observed. However their presence in the samples cannot be ruled out.

The water content observed along the depth profile is lower than that reported by Barros

et al. (2008) at 10 cm deep (5–6 %) in the same area and in the Tarapacá region (hyperarid core). It can be noted that the increase in water content follows the increase of submillimetric particles in the samples, potentially making this sand size a threshold for retaining water more efficiently.

The carbonate contents observed at 3, 11, and 13 cm deep may be experimental artefacts due to the presence of a bigger particle in the sample, providing a higher amount of material when crushed: more carbonate minerals at 3 and 11 cm deep, and less carbonate minerals at 13 cm deep. Also, the increase in carbonate content correlates with the increase in water content, but is not as important.

Previously reported pH values were slightly less alkaline (8.0–8.4 at 10 cm deep; Barros et al. 2008).

3.6.2 Environmental readings

The sole weather data found for this area only reports wind patterns (January–March 1993): from the morning till the afternoon, a light ridge lift coming from the east was recorded; in the afternoon it was always replaced by a stronger western katabatic wind, coming down the Cordillera de Domeyko, persisting throughout the night, although progressively losing its strenght from midnight till dawn (Schmidt 1999).

The behaviour of surface T and RH patterns seem to be correlated, one increasing when the other decreases. After sunrise, surface T increases rapidly until the middle of the afternoon. It then starts decreasing, also quite rapidly, probably under the influence of the katabatic wind coming from the Cordillera. After sunset, surface T keeps decreasing but the decrease rate slows down continuously until sunrise. The opposite trend is observed for RH, decreasing rapidly after sunrise until the middle of the afternoon, then steadily rising until sunrise.

T and RH changes followed a wave pattern and were dampened by depth. Depth diminished the wave amplitude and shifted its phase. However, both amplitude and phase changes were more pronounced for T measurements than for RH, suggesting a "low" thermal conductivity of the soil, whilst its components were able to retain humidity quite well.

It should be noted that at depths greater than 10 cm — where RH reaches 80 % — the water content also started to increase (figure 3.5, left). However, these RH values far exceed those recorded in the hyperarid core of the desert (11.1–24.1 % RH at 20 cm deep at the María Elena South site; Azua-Bustos et al. 2015).

3.6.3 Organic content

Loss on ignition

LOI₅₅₀ and total organic carbon (TOC) are two different measures, but their results should be similar. Nevertheless, the results obtained fall within the proportion described in previous results. Indeed, TOC content of nearby sites ranged between 0.17 and 0.62 % m/m (Barros

et al. 2008) whereas TOC in the hyperarid core of the Atacama Desert had a wider range (from below 0.01 % to 2.66 %, see Azua-Bustos et al. 2017 for a review).

It should be pointed out that clays are known to interfere with LOI₅₅₀ measurements, by losing structural water in addition to the organic carbon (Hoogsteen et al. 2015 and references therein). This would affect mostly the measurements done for the samples at 15 cm depth and below, as the others contain only marginal proportions of particles below 63 μm in size. In addition, some carbonates start to decompose around 500–600 °C — which may also lead to overestimating the organic carbon content (Hoogsteen et al. 2018 and references therein). Finally, small sample weights also lead to more inaccurate result (Hoogsteen et al. 2018 and references therein). These combined sources of uncertainty mean that LOI₅₅₀ measurements should be treated as indicative values rather than definitive values.

Total lipid extract

As mentioned in figure. 3.7, the TLE concentration peak is observed at 13 cm depth, just above the depth at which the proportion of submillimetric particles increases significantly (15 cm depth). It should be noted that the TLE concentration keeps decreasing as the proportion of submillimetric particles keeps increasing.

The lack of correlation between the LOI₅₅₀ and TLE results could be explained by the limitations of the LOI measurement mentioned above and by a potential difference in the type of organic molecules present at the different depths.

N1 fractions

Low concentrations of *n*-alkanes are observed at the surface level compared to at 1 cm deep. This could indicate that the molecules are removed by the wind and/or that they percolate to under the surface after being deposited there.

The high concentrations of *n*-alkanes with an even/odd ratio > 1 at 1 cm deep could come from microbial production, diagenesis, or anthropogenic contamination. The presence of the road, about 30 m from the sampling site, could argue in favour of anthropogenic contamination, even though the road did not seem well used. Microbial production is unlikely, because their presence at 3–5 cm deep — according to the PCR results — is not paired with high short-chain *n*-alkane concentrations. The presence of phytane, combined with the extreme T and high UV flux, could point towards a diagenesis of longer molecules.

High concentrations of short-chain *n*-alkanes and phytane are observed again at 15–17 cm deep. These depths correspond to the ones where the amount of submillimetric particles increases significantly. If these sediment layers correspond to muds deposited by a previous water flow, the original molecules could have just been mixed in the sediments at the time of their deposition; the molecules would have then been degraded before being covered by new sediments. Still following this hypothetical scenario, the high concentration of odd-numbered long-chain *n*-alkanes — likely to be of plant origin — observed just below, at 19 cm deep, could correspond to the original undegraded material, preserved under a

thicker layer of sediments.

The presence of odd-numbered long chain *n*-alkanes and of phytane in the samples argues in favour of the presence of plant inputs in the samples, particularly at the deeper depths. Hence, the first part of hypothesis 2 (*Plant lipids will be found in the samples, and they will be more concentrated at the surface*) is verified, whereas its second part is disproved. Both short and long chain *n*-alkanes were also observed recently at another sampling site in the Atacama (Sánchez-García et al. 2018).

CPI values around 3 and higher are generally considered to be an indication of higher plant inputs. Assuming that plant inputs are consistent throughout the whole depth profile, the low CPI values at 1 and 15 cm deep indicate a diagenesis of long chain molecules. These drops in CPI are correlated with the increase of short even *n*-alkanes.

Again assuming consistent plant inputs throughout the depth profile, the maximum ACL value (29.2) at 19 cm deep could either indicate a better preservation of the starting material, or an input of longer molecules.

N3 fractions

The origin of dodecan-1-ol and tridecan-1-ol, however uncertain, is probably the same given the strong similarities of their concentration profiles in the samples. Their shallower peak, at 3 cm deep, overlaps with the one observed for even short-chain *n*-alkanes. However, the peak observed for *n*-alkanes is narrow, therefore a correlation between these two sets is uncertain.

Interpreting the top part of the octadecan-1-ol profile is challenging because it does not really tie in with any other data set. The lower part of the profile, on the other hand, correlates with the peak observed at 15–17 cm deep for even short-chain *n*-alkanes and for phytane, suggesting that octadecan-1-ol could have a microbial origin at this depth.

The concentration peak of even long-chain *n*-alkanols corresponds to the peak observed for odd long-chain *n*-alkanes, confirming their plant origin.

3.6.4 Plant sample

No correlation has been observed between the *n*-alkane profile produced by the plant and the ones observed in the soil samples. This suggests that *Tiquilia atacamensis* is not the dominant source of *n*-alkanes at this site.

3.6.5 DNA content

PCR amplification of bacterial and archaeal 16S rDNA only reveals the presence of the bacterial gene from the surface to 3 cm deep, and at 11–13 cm and 19–21 cm deep. Without any amplification of the archaeal gene, it can be assumed that archaea are not concentrated enough, if present at all, to be detected.

The different methodologies used by each of the bioinformatic programs used may explain the difference between their individual results. In particular, Kaiju only compares DNA

sequences with those from annotated proteins from microbial reference genomes, thereby restraining the number of potential matches by discarding non-microbial DNA and microbial DNA not coding for proteins. Bioinformatic analyses by Kaiju and Kraken — using then various genes to match reads — still suggest that both bacterial and archaeal DNA are still present at 15 cm deep. The absence of significant 16S rDNA gene amplification could mean that the sequenced DNA might have originated from microbial remains instead of living micro-organisms.

Bacilli — with a halotolerant forms (*Halobacillus*)—, one bacteroidetes (*Flammeovirgaceae bacterium 311*), and nitrifying bacteria (*Nitrospira*) were identified by Kaiju. These organisms have been previously reported in the Atacama (e.g. Orlando et al. 2010; Moreno et al. 2012; Azua-Bustos et al. 2015; Schulze-Makuch et al. 2018), so their presence in the sample is not surprising. However, the amount of reads identified (less than 13 % at species level, by Kaiju) is not sufficient to interpret properly the data and definitely draw conclusions. The lack of consistency in the data output formats (all results vs. species-level only results, percentage of matches vs. absolute number of matches) also makes it challenging to interpret and to compare properly the different sets. The lower amount of hits for MetaPhlAn2 and Kraken compared to Kaiju can also be explained by the fact that they output the best matches with microbial clade-specific marker genes (Truong et al. 2015) and the exact matches against *k*-mers from a library of microbial genomes (Wood and Salzberg 2014), respectively, whereas Kaiju compares the six possible reading frames with annotated proteins from microbial proteins and complete genomes on NCBI (Menzel et al. 2016).

If we consider PCR to represent microbial concentration, then the first part of hypothesis 1 (*Microbial concentration and diversity will increase with depth, reaching their highest values where the soil humidity is maximal and constant*) is not verified. As DNA sequencing could only be performed on one sample, the second part of the hypothesis, regarding microbial diversity, remains unanswered.

3.6.6 General discussion

Samples were collected in an alluvial fan, the water stream having probably originated following a flash flood after precipitation on the Cordillera Domeyko, about 8 km north-west and 600 m higher than the sampling site.

The surface currently experiences extreme daily T and RH variations, suggesting inhospitable living conditions for micro-organisms there. In addition the water content of the sediments is lower than one reported by Barros et al. (2008) in a nearby area (5–6 %), but still higher than the ones reported by Schulze-Makuch et al. (2018) in the hyperarid core of the Atacama Desert (mostly < 1 %).

Still, bacterial DNA — already reported in drier parts of the Atacama Desert (e.g. Navarro-González et al. 2003; Lester et al. 2007; Azua-Bustos et al. 2015; Cámara et al. 2016; Schulze-Makuch et al. 2018) — is present in great quantities. The quasi-absence of *n*-alkanes at the surface suggests that the molecules are removed by the wind and/or manage

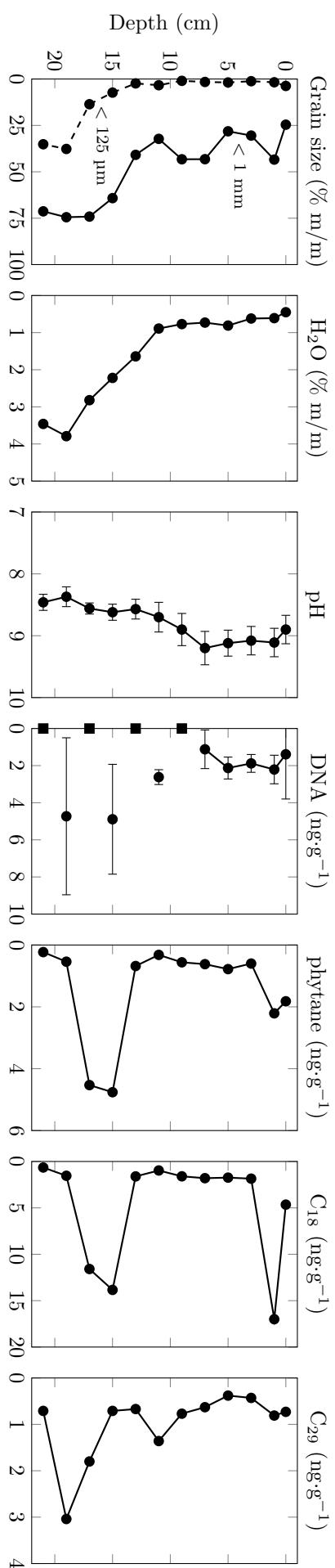


Figure 3.16 – Results summary for the Atacama sampling site.

to percolate to just below the surface.

Great quantities of short-chain *n*-alkanes are found just 1 cm below the surface. These molecules probably originated from the diagenesis of longer molecules, likely of plant origin, under the influence of solar radiation, or as a result of wind inputs from anthropogenic contaminants, like car exhaust. If bacteria were the main producers, similar *n*-alkanes should be observed at neighbouring depth, where bacteria are also found. The presence of phytane also argues in favour of degraded plant material.

Between 10 and 15 cm deep, the RH level is high enough that the percentage of water into the sediments starts to increase. The temperature is also more stable and the pH slightly less alkaline than at the surface. These conditions are probably favourable to the bacteria observed at 11–13 cm deep, but no microbial mat was observed. The quasi-absence of *n*-alkanes until 15 cm below the surface suggests that the percolation of molecules deeper into the soil is limited. The nature and origin of the amount of lipids found 13 cm below the surface is still unknown. It could consist of molecules accumulated over the layer of fine sediments, unable to percolate deeper down, before they got buried in sand. These molecules could still serve as a source of nutrients for the bacteria living at this depth.

At 15 cm deep, the observation of even short-chain *n*-alkanes together with phytane, suggest the presence of degraded plant material. This material was probably accumulated just below the surface of the original fine sediment brought by water. This plant material could have been brought with the sediments by water during the flood, or deposited later as aeolian inputs. The molecules present suggest that the original plant material had enough time to get degraded before being buried by other sediments. Interestingly, no bacterial 16S rDNA was amplified by PCR at this depth, but genomic analysis of the DNA still suggests the presence of bacterial DNA.

The transition between degraded and original molecules is observed 17 cm below the surface, with a decrease in concentration of the molecules observed at 15 cm deep and the appearance of odd long-chain *n*-alkanes, corresponding to pristine higher plant waxes.

At 19 and 21 cm deep, almost exclusively odd long-chain *n*-alkanes are found. These molecules were likely mixed with the mud when it was deposited. These molecules were also preserved from degradation, contrary to the molecules found at 15–17 cm deep. It is worth noting that only about 4 cm of sediment was then able to preserve the molecules from degradation, at a time when they were not yet recovered by sand. Such thin layer of sediment is also predicted to attenuate UV radiation on Mars (Pavlov et al. 2002). The role of water, being retained in a better way by capillarity in fine sediments, remains to be determined. Bacterial 16S rDNA was also amplified from this depth, indicating the presence of bacterial remains.

Overall, the *n*-alkane and DNA concentration ranges observed are consistent with those previously reported for other sampling sites within the Atacama Desert (Azua-Bustos et al. 2015; Sánchez-García et al. 2018). The microorganisms found (bacilli and ammonium oxidising bacteria) are also similar to the ones previously reported in the Atacama (e. g. Orlando et al. 2010; Moreno et al. 2012; Azua-Bustos et al. 2015; Schulze-Makuch et al. 2018).

3.7 Relevance to Mars

Whilst the temperatures recorded at our Atacama site clearly do not compare to those observed on present-day Mars, our relative humidity values are compatible to the martian ones, both for the air (site: 6.4 %; Mars: ~0–49 %, Harri et al. 2014a) and the ground surface (site: 0.0–67.3 %; Mars: < 5 % to saturation, Zent et al. 2010). Additionally the UV-A flux measured ($19.85 \text{ W}\cdot\text{m}^{-2}$) is the same as that recorded on Mars in low atmospheric dust conditions ($\sim 19.5 \text{ W}\cdot\text{m}^{-2}$, Smith et al. 2016).

The ongoing search for organics on Mars revealed both aliphatic and aromatic molecules to be present in samples up to 3 Ga old, without any evidence for a biological origin (Freissinet et al. 2015; Eigenbrode et al. 2018). On Earth, each of the three domains of life produces specific membrane lipids. These lipids and/or their degradation products, which can serve as biomarkers, can even be found in oils and bitumens of Archean age (Dutkiewicz et al. 1998; Brocks et al. 1999), leading in some cases to the identification of specific producers (Brocks et al. 2003b,a). Amongst these molecules, *n*-alkanes can also be considered; their concentration profiles vary depending on their production by biological or abiotic processes (e. g. Georgiou and Deamer 2014). Therefore, future detection of *n*-alkanes on Mars, depending on their concentration profiles and the presence of other molecules, could suggest past life on Mars.

Recurring slope lineae (RSL) are a geological feature on Mars, possibly formed by the action of aqueous solutions (e.g. Ojha et al. 2014; Stillman et al. 2016, 2017; Stillman and Grimm 2018; Schaefer et al. 2019). Regarding the extended period of time during which some lipids can be preserved, if RSL contain any lipids or other organics, the sediments in their outflow channels could become enriched with organic material over time.

3.8 Conclusion

Contrary to what I hypothesised (hypothesis 1, *Microbial concentration and diversity will increase with depth, reaching their highest values where the soil humidity is maximal and constant.*), bacterial communities, seem to be located at the surface as well as deeper down where living conditions are more favourable. Lipids of microbial origin were not clearly identified and seem to be outweighed by degraded plant inputs. Hypothesis 2 (*Plant lipids will be found in the samples, and they will be more concentrated at the surface.*) is then partly verified, as plant lipids are present, but not mainly found at the surface.

As the analysis and interpretation of other data was more advanced than for the genomic data, the latter were set aside and need further analysis. However the low number of matches for the reads and variety of formats used make it challenging to interpret the genomic data. Thus, the part regarding microbial diversity in hypothesis 1 remains unanswered.

The history of the sampling site seems to be more complex than what it looks like from the surface, as biosignatures, likely from different sources, varied significantly along the depth profile.

Should further work be considered at this specific location, sampling at multiple locations down the dry water stream would be interesting, as well as sampling from the former stream bed, near its banks, and outside of the stream bed. Monitoring T and RH over a longer period of time (e. g. a year) would be interesting to have a better understanding of the weather in this part of the Atacama Desert.

The sampling resolution used (every 2 cm) was enough to detect rapid changes in the depth profile without missing anything. However, deeper sampling could be advised in order to try to get past the layer of fine sediments.

Weather can not be forecast months in advance when preparing for such field work, but comparing these results with some others obtained from samples that did not recently experience rain water would also be interesting.

To refine the selection of the sampling sites, a better study of satellite images is advised to pre-select a working zone. The selection could be refined directly on site, by imaging the field with a drone.

Finally, from a planetary analogue perspective — and therefore disregarding the biomarkers source (human, plant, or microbe) — this sampling site could serve as an analogue for Mars around the time of its transition from wet to arid surface conditions in the Late Noachian. It suggests that potential biomarkers contained in fine sediments deposited by water and later covered by aeolian sediments would be more likely to be found just below the boundary between silts/clays and sand, at a centimetre scale.

Chapter 4

Sairecabur

‘Is it possible that the rocks have life?’

James T. Kirk, *Star Trek*, episode 3x14 – *That which survives* (1969)

Contents

4.1	Introduction: The Central Andean Dry Puña	60
4.2	Rationale	61
4.3	Hypotheses	62
4.4	Methods	63
4.5	Results	65
4.6	Discussion	90
4.7	Relevance to Mars	104
4.8	Conclusion	105

Abstract

The Dry Puña in the central part of the Andes experiences environmental conditions that make liquid water unstable and the environment challenging for life. These conditions include lower atmospheric pressure, high solar flux, and cold air temperatures combined with extreme daily temperature gradients. This environment is also similar to that of Mars during its past.

We therefore conducted a study to see if life could survive in this environment. One vegetated site and three non-vegetated sites were studied. At non-vegetated sites, signs of life — biolipids and DNA — were observed several centimetres below the surface at altitudes up to 5 269 m despite the harshness of the environment. However, the specific location of each of these biosignatures in the depth profiles remains difficult to interpret.

4.1 Introduction: The Central Andean Dry Puña

4.1.1 Climate

The Andean dry diagonal is a region receiving less than 500 mm of rain annually, stretching from the Ecuadorian Pacific coastal range to the Patagonian range (Messerli et al. 1997). Within the diagonal, and located east of the Atacama Desert, is the southern part of the Central Andean Dry Puña — *Puña* designates high-elevation grasslands found around 4 000 m altitude — (20–24 °S, ecoregion NT1001, WWF 2018). This region, with less than 200 mm of precipitation and 1 000–1 200 mm of potential evaporation annually, is one of the driest regions of the Andes (Hastenrath and Kutzbach 1985; Messerli et al. 1997; Risacher et al. 1999a; Houston and Hartley 2003; Bennett et al. 2016). Most of the precipitation is received as snowfall (Vuille and Ammann 1997; Schmidt 1999). Recent computations on NASA's Aqua satellite's data indicated precipitation below 10.17 mm each summer in the area over the period 2003–2014 (Cordero et al. 2016).

In addition to extreme dryness, the area also experiences high UV radiation (Schmidt 1999; Piacentini et al. 2003; Cabrol et al. 2014). The high UV levels recorded in this area are due to its tropical latitude, its high elevation, a thinner ozone column, low atmospheric aerosols, and mostly cloudless skies (e. g. Piazena 1996; Blumthaler et al. 1997; Sabburg and Wong 2000; Kim et al. 2013; Cordero et al. 2016; Marzo et al. 2018). The area has an average increase of global UV irradiance of $2 \text{ \%}\cdot\text{km}^{-1}$ above 2 500 m ($2 \text{ \%}\cdot\text{km}^{-1}$ for UV-A, $4 \text{ \%}\cdot\text{km}^{-1}$ for UV-B, Cordero et al. 2016). It is also the location at which the highest UV index ever recorded (43.3) was measured (Cabrol et al. 2014).

The high altitude causes cold air temperatures in the region, and freeze/thaw cycles (corresponding to night/day cycles) occur in the ground's top layer (Schröder et al. 1996; Schröder and Schmidt 1997; Schmidt 1999; Lazar 2005). The area has the highest upper periglacial limit in the world with a mean annual snow line ($0 \text{ }^{\circ}\text{C}$ -isotherm) around 4 500 m (Schröder 1999). Solar irradiance, warming up the ground and surface air, hence creating wind currents, seems to be the main feature controlling the climate there (Schröder and

Schmidt 1997; Schmidt 1999; Richter and Schmidt 2002).

4.1.2 Life

Even though the environmental conditions are particularly inhospitable and challenging in the southern part of the Central Andean Dry Puña, some animal, vegetal, and microbial life forms are still able to survive and develop at high altitude.

Depending on the area, 12–25 species of butterflies and 17–29 species of mammals can be found (Samaniego and Marquet 2009; Despland 2014). The presence of herbivorous animals, like lamoids, can result in two opposite effects in desert areas. On one hand, they contribute to soil eutrophication by leaving their excrement and urine on the ground, thus creating "green oases" if enough water is present for plants to grow. On the other hand, overgrazing can deplete a zone of the few plants living there (Richter 2009). Small mammals and birds have also been reported (Halloy 1991).

A total of only 769 vascular plants is reported by Arroyo et al. (1988). Different plant families can be found, mainly semi-desertic shrubs and succulents, and arid grasslands, varying with the latitude and the altitude (Arroyo et al. 1988; Richter 1996; Richter and Schmidt 2002; Richter 2003). In addition to the overall arid area some locations may receive enough snowmelt water or occasional rain to create and sustain localised wetlands, referred as *bofedales* or highland bogs, which have greater plant productivity than the surrounding arid grasslands (e. g. Ruthsatz 1995; Ruthsatz 2000; Squeo et al. 2006). No plants manage to grow above 5 000 m (Villagrán et al. 1981; Richter 1996; Richter and Schmidt 2002; Richter 2003).

However, even above 5 000 m, some fumaroles, bringing warmth, humidity, and nutrients, can create tiny oases for life, hosting mosses and microbial communities (e. g. Halloy 1991; Costello et al. 2009; Schmidt et al. 2012). Even apart from fumaroles, microbial communities were still reported to live at high altitude in dry conditions, surviving extreme freeze-thaw cycles. These communities can be composed of bacteria and archaea (Demergasso et al. 2010; Bull et al. 2018; Solon et al. 2018), fungi (Schmidt et al. 2012; Pulschen et al. 2015; Vimercati et al. 2016; Schmidt et al. 2017b), algae, and rotifers (Schmidt et al. 2017a).

High-altitude lakes, persisting despite evaporation, also act as oases for microbial ecosystems. These lakes host a diversity of phototroph and heterotroph prokaryote and eukaryote micro-organisms (e. g. Cabrol et al. 2009; Demergasso et al. 2010; Albarracín et al. 2016; Angel et al. 2016a; Toneatti et al. 2017; Aguilar et al. 2018).

4.2 Rationale

The environmental conditions described above — lower atmospheric pressure, high solar and UV flux, negative water balance, cold mean temperatures combined with extreme daily temperature gradients — present some similarities with what Mars could have experienced at

some point during the Noachian period (4.1–3.7 Ga ago) and Hesperian period (3.7–3.0 Ga ago). After the loss of its magnetic field, Mars started to lose its atmosphere and hydrosphere, and its temperature dropped (e. g. Bibring et al. 2005; Mahaffy et al. 2015; Bristow et al. 2017; Jakosky et al. 2017) thereby increasing environmental stress and forcing any potential life forms to adapt to these conditions.

Within this context, the Dry Puña, and more particularly its flanking high-altitude volcanic range, are considered a suitable environmental analogue for Hesperian Mars (Cabrol et al. 2007, 2010; Parro et al. 2018; Schmidt et al. 2018). Studying life in such analogue conditions can provide clues about the survival strategies adopted by Earth-like life forms present on Mars during the Hesperian.

In addition, transient liquid water flows on Earth can be produced at the hours of the day when the solar flux is just high enough to melt snow or ice, without evaporating it directly. These flows, already reported in the Dry Valleys in Antarctica for carving gullies in the sediments, are able to momentarily re-hydrate dry ground, and even temporarily sustain life (Marchant and Head 2007; Head and Marchant 2014). Such transient systems are thought to have been involved in the formation of gullies on Mars until the recent past (1 Ma ago or less; e. g. Christensen 2003; Levy et al. 2010; Morgan et al. 2011). Assuming that life ever appeared on Mars, these systems could have been critical for maintaining a liquid water source for biological systems there.

Most of the work on high altitude lakes has been done by Nathalie Cabrol and collaborators, whilst analysis of the soils were carried out by Steven Schmidt and his team. Focusing on soil analyses, previous genomic studies concentrated on the highest altitudes, without considering the possible effect of an altitude gradient, and had poor depth resolution (4–10 cm), or used samples collected only on the surface. Apart from the work of Nieto-Moreno et al. (2016) the presence of biomarkers was also only investigated in aqueous environments.

This work proposes to compensate for this lack of knowledge in soils by (i) collecting samples over an altitude gradient at high elevation and from high resolution depth profiles (every 2 cm), (ii) analysing both DNA and lipid material, and (iii) comparing the data obtained by environmental and physico-chemical readings of the soil.

4.3 Hypotheses

Considering that the environment will be harsher at higher altitude and at the surface, compared to lower altitudes and in the subsurface, the following hypotheses can be made about microbial communities and biomarkers. The presence of plants at low altitudes is also expected to have an influence.

Hypothesis 3: *Microbial communities are more abundant and diverse with decreasing altitude and increasing depth.*

Hypothesis 4: *Environmental parameters and soil physico-chemistry have the most influence on the composition of microbial communities.*

Hypothesis 5: *Plant biomarkers will predominate at lower altitude, whereas microbial biomarkers will predominate at higher altitude.*

Hypothesis 6: *Biomarker degradation will increase with altitude and decrease with depth.*

4.4 Methods

4.4.1 Sampling strategy

Sampling sites

Samples were collected at the base of, and on, the Sairecabur volcanic massif. This location was chosen to continue the work already done there by Prof. Vernon Phoenix and Nick Thomas in 2014. The Sairecabur was originally selected over other volcanoes for logistical reasons, because a dirt track goes up to the main caldera, thus providing an convenient access to the sampling sites (Phoenix V., personal communication). Whilst not being the highest volcano in the region, the Sairecabur has the advantage of having a long record of environmental conditions through Dieter Schmidt's work (Schmidt 1999), and of never having been studied for its microbial communities.

The Sairecabur volcanic massif is the highest in its homonymous volcanic range. The Sairecabur range, of Pliocene to Quaternary age (5.33 Ma–4.2 ka), spans over 22 km and serves as a natural border between Chile and Bolivia (figure 4.1). Consisting of at least 10 volcanic centres and their associated lava flows, the range is part of the Altiplano-Puña volcanic complex located in the Andean Central Volcanic Zone (Déruelle 1978; Déruelle 1982; Harmon et al. 1984; de Silva 1989; de Silva and Francis 1991).

A primitive stratovolcano reaching approximately 7 km high collapsed, forming a 5 km wide caldera. Following the collapse, the Northern small cone erupted, then the Sairecabur, the latter reaching an altitude of 5 975 m (figure 4.1); the massif is now dormant (Déruelle 1982). The only ongoing geological processes are mainly aeolian and fluvial below 4 000 m, and solifluction above 4 000 m due to the daily freeze-thaw cycles (de Silva and Francis 1991; Schröder 1999).

Despite being located in the aforementioned dry diagonal, Sairecabur's name ironically translates to *mountain of rain* from the Kunza language — the language spoken originally by the Atacama people: *saire/sairi* [sairi], rain; *ckabur/cabur/cahur/caur* [xabur], hill/mountain (Vaïsse et al. 1896; Vilte Vilte and Pérez 2004). The rain here probably refers to the summer precipitation observed in the area. Despite this, potential evaporation still remains higher than precipitation with annual potential evaporation/precipitations values of 1 566 mm/210 mm at 4 270 m, 1 402 mm/635 mm at 4 920 m, and 1 275 mm/390 mm at 5 820 m (Schmidt 1999).

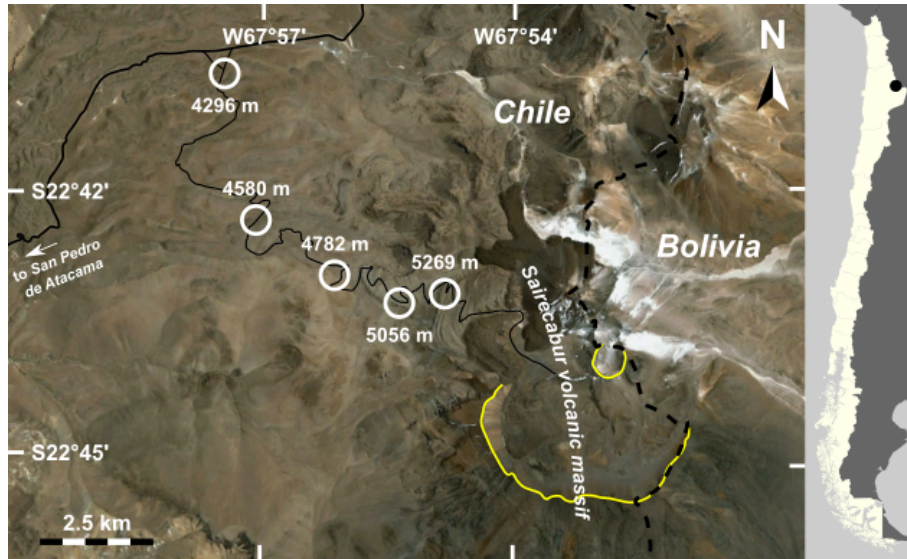


Figure 4.1 – (left) Map indicating the location of the sampling sites along the dirt track (black line) leading to the Sairecabur. The calderas created by the collapse of the primitive cone and of the Northern small cone are outlined in yellow. North of them lies the Sairecabur cone, made of darker lava. The border between Chile and Bolivia is indicated by a dashed line. (right) Location of the area (black dot) within Chile.

Soil samples

The initial plan was to collect samples along an altitude gradient from the vegetated plateau around 4 300 m. This plateau was already used as a reference site by Prof. Vernon Phoenix and Nick Thomas the previous year and had to be used again to duplicate their experiment. The altitude gradient would have then been bidirectional, going up to the summit of the volcano, and going down towards the pre-Puña then the Atacama, with each sampling site being about 500 m higher, or lower, than the previous site. At each sampling site, duplicate depth profiles would have been collected, every 2 cm from the surface to 30 cm deep.

However, the available space and weight to bring back the samples was limited. In addition to this, samples also had to be collected at the surface and at 1, 3, 7, 21, and 37 cm deep in order to reproduce the 2014 experiment. To reduce the number of samples and comply with the constraints, samples were only collected at four sites, following an altitude gradient (figure 4.2), from 4 296 m to 5 269 m. The highest sampling site was initially planned to be around 5 500 m; however the presence of icy *penitentes* (elongated and thin blades of ice) on the ascending track made the driving conditions too hazardous to continue. Samples were then collected at a lower altitude (5 269 m), where it was safer to work. Samples were also collected following a modified depth gradient: at the surface, and every 2 cm from 1 to 21 cm deep. Additional samples were collected at 37 cm deep at the 4 296 m and the 4 782 m sites. Only one set of samples was collected at each site.

The surface geology for the two lowest sites consisted of glacial deposits (Déruelle 1982) — one site was a grassland (4 296 m) whilst the other was barren (4 782 m) — and the two highest sites were barren lava fields (Déruelle 1982; Figueroa and Figueroa 2006) of calc-alkaline (5 056 m) and dacitic lavas (5 269 m). The vegetated site at 4 296 m served as a

control site for biological inputs.

Collection of the soil samples was done with the help of PhD students Nick Thomas and Rory Porteous, and under the supervision of Prof. Vernon Phoenix.

At the control site (4269 m), plant roots were observed starting 9 cm below the surface, even though the nearest plants were about 1 m away. At 5269 m, the ground was completely frozen at around 6 cm deep and had to be gently smashed to collect the 7 cm deep sample; no deeper samples were collected at this altitude.

Plant and lichen samples

In addition to the soil samples, plant and lichen samples were collected to investigate what biomarkers they would produce. These samples were collected within 100 m of the soil sampling sites. Most of these samples were collected at 4296 m, but some were also collected at 4782 m and 5056 m. Two additional plants, not present at the other sites, were sampled at 4580 m (site indicated in figure 4.1). Details can be found in appendix B.

4.4.2 Planned analyses

During fieldwork, air temperature (T) and relative humidity (RH), as well as UV radiation, were measured directly at each sampling site. Sensors were also placed in the ground to measure T and RH for a few days. Upon return to Glasgow, samples were analysed following three main themes:

1. Soil physico-chemistry (mineralogy, grain size, water content, carbonate content, pH);
2. Organic content (loss on ignition, total lipid extract, refined lipid fraction — N1 only);
3. Genetic content (total DNA, metagenomics).

The methodology used for each analysis is described in details in chapter 2.

4.5 Results

4.5.1 Soil physico-chemistry

Mineralogy

X-ray diffraction (XRD) analysis was performed at the Advanced Materials Research Laboratory (University of Strathclyde). Interpretation of the XRD spectra was done with the help of Tiziana Marrocco (University of Strathclyde). XRD patterns are reported in section A.2 (p. 127).

Although the lower sampling sites (4296 m and 4782 m, reddish brown material, glacial deposits) and the higher sampling sites (5056 m and 5269 m, dark brown material, lava field) have different origins and visual aspects, their mineralogical composition, determined



Figure 4.2 – Sampling sites near the Sairecabur volcano.

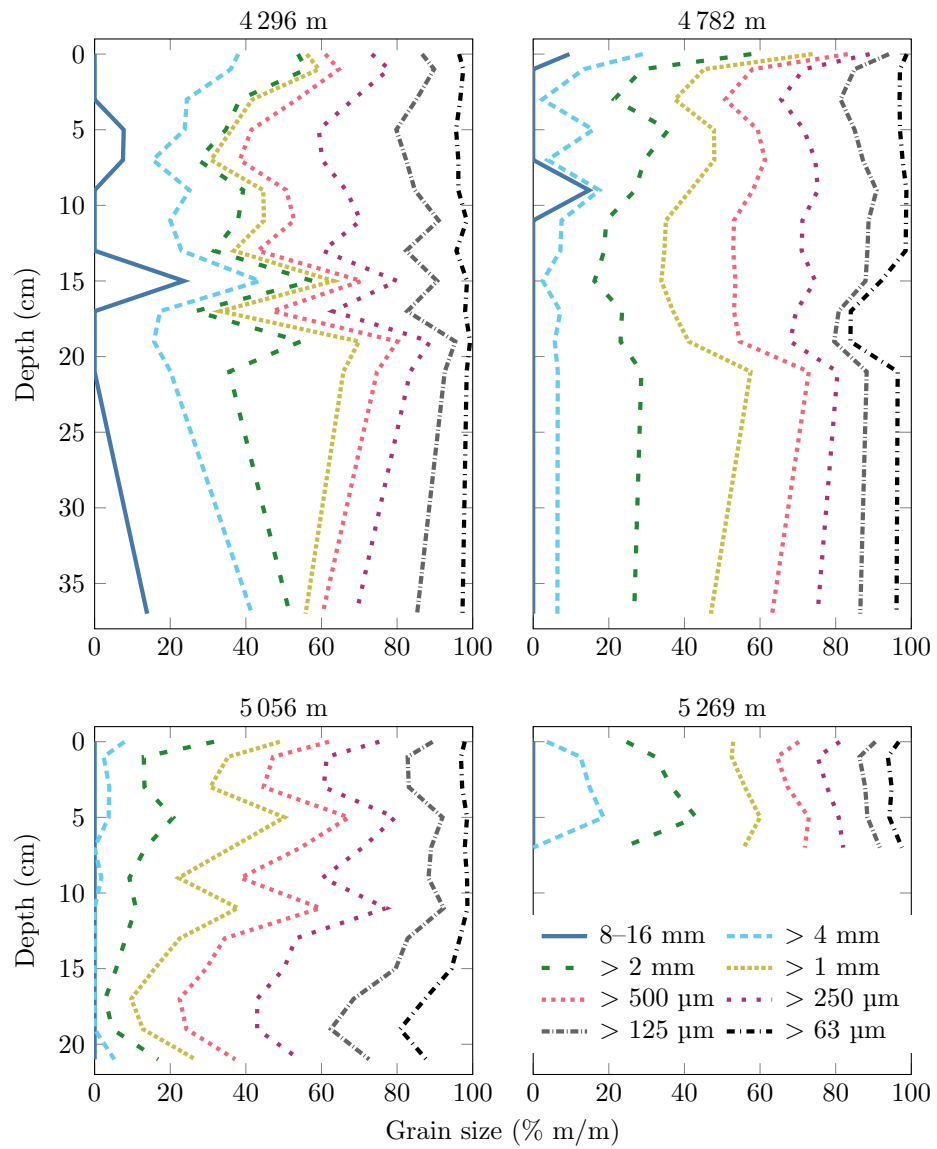


Figure 4.3 – Mass percentage of soil particles for different size thresholds.

by XRD, remains similar. The same observation is made along the different depth profiles. Mineralogy is dominated by feldspars (mostly plagioclase) and, to a lesser extent, by quartz. Traces of calcite, iron oxides, micas, olivine, and pyroxenes are also observed.

Grain size

The soil was composed of unconsolidated material through the whole depth profile at every site. However, at 5 269 m, some of the finer sediments collected below the surface were shaped like 2–3 mm balls, and clustered amongst themselves or with larger sediments in frozen packs of about 5–6 mm. These clusters decomposed upon drying of the sediments. The size of particles composing the dry sediments was determined by dry sifting (figure 4.3).

The relative proportion of the different grain sizes through a given depth profile remains more or less constant at all altitudes, with the exception of 5 056 m, where the proportion of sub-millimetric particles increases with depth. The relative proportion of sub-millimetric

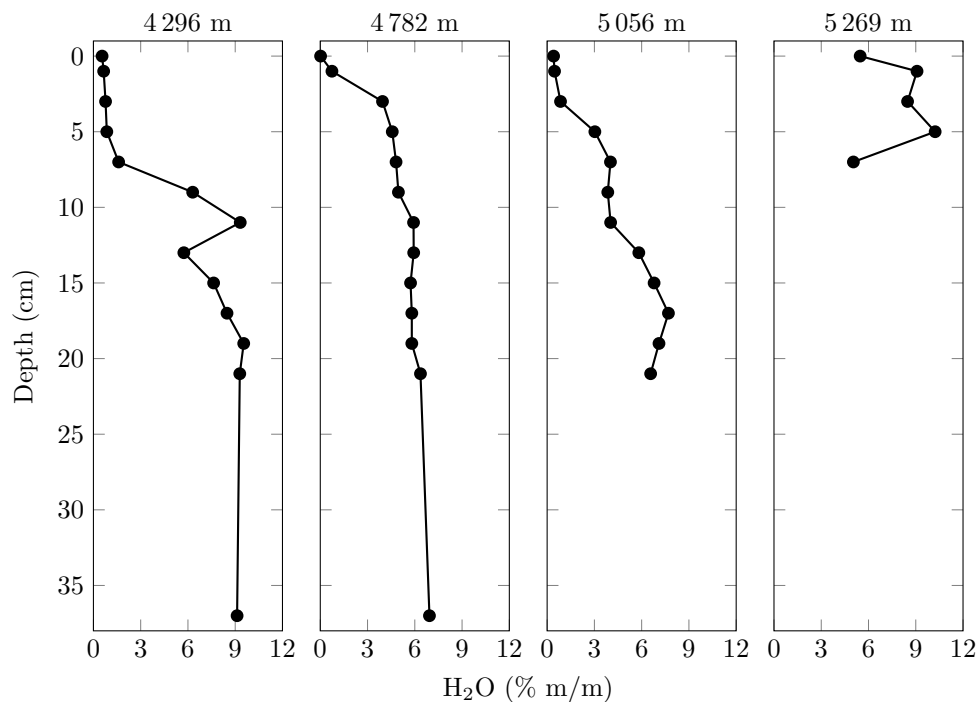


Figure 4.4 – Water content of the different Sairecabur samples. $n = 1$

particles also increases slightly from 4 296 m to 5 056 m (4 296 m: ~30–70 %, 4 782 m: ~40–60 %, 5 056 m: ~50–90 %).

Water-related physico-chemistry

Water content Analysis of the water content (figure 4.4) indicates that all surface samples (0–1 cm deep) from 4 296 m to 5 056 m contained less than 1 % of water. Their water content then increases with depth until stabilising: (i) at 4 296 m the water content surpasses 1 % at 7 cm and stabilises around 9 % at 17 cm deep, (ii) at 4 782 m the water content surpasses 1 % at 3 cm and stabilises around 6 % at 11 cm deep, (iii) at 5 056 m the water content surpasses 1 % at 5 cm, then remains constant at 4 % from 7 to 11 cm deep, then stabilises around 7 % at 15 cm deep. At 5 269 m the water content at the surface and 7 cm below it is lower (~5 %), than for the rest of the depth profile (~9 %).

Carbonate content Small amounts of carbonates (CO_3^{2-}) were observed at all sites (figure 4.5). At 4 296 m the carbonate content remains quite stable through the whole profile and varies between 1.26 and 2.38 %. At 4 782 m it varies between 1.30 and 2.23 % until 21 cm deep. It then increases to 10.55 % at 37 cm deep. At 5 056 m the proportion of carbonate increases steadily from 1.14 % at the surface to 3.83 % at 17 cm deep. It temporarily drops to 1.45 % at 19 cm deep before going up to 3.10 % at 21 cm deep. At 5 269 m the carbonate percentage rises steadily from 1.29 % at the surface to 2.14 % 7 cm below.

pH All sampling sites have an acidic soil pH at the surface (4.6–5.2). pH increases with depth until it stabilises at, or near, neutrality (figure 4.6). At 4 296 m the pH starts at 4.6 at

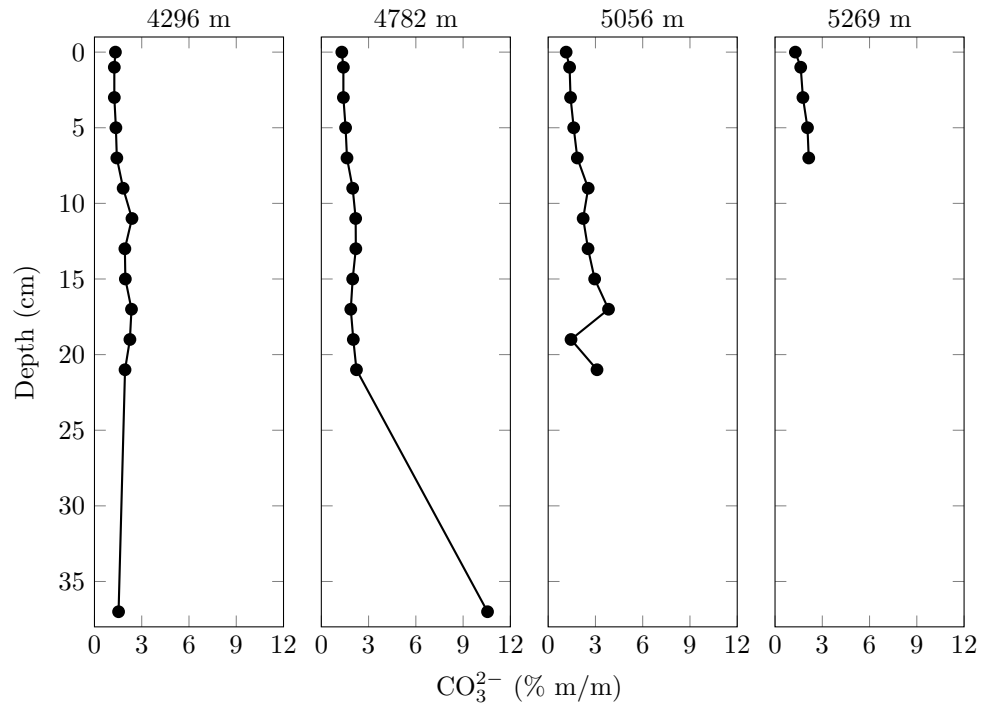
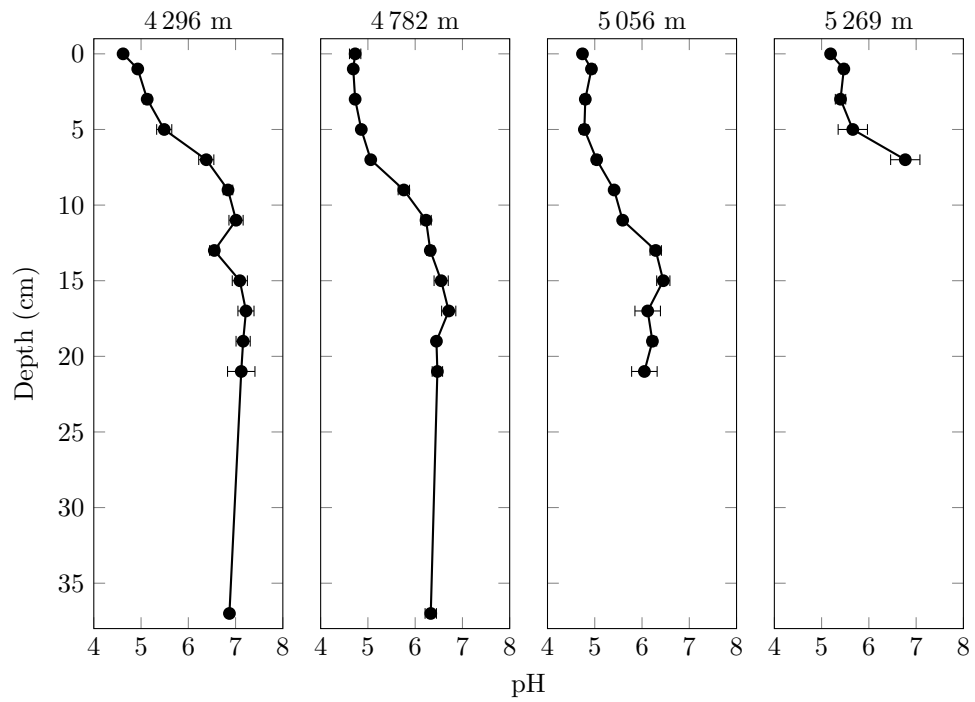


Figure 4.5 – Carbonate content of the different Sairecabur samples.

Figure 4.6 – pH of the different Sairecabur samples. $n = 3$

		4 296 m	4 782 m	5 056 m	5 269 m
Air T	(°C)	17.2	5.0	10.0	0.4
Air RH	(%)	11.6	26.4	18.2	21.4
UV-A	(W·m ⁻²)	22.74	23.60	21.56	22.60
UV-B	(W·m ⁻²)	3.78	3.72	3.29	3.50
UV-C	(mW·m ⁻²)	0.00	0.00	0.00	0.00

Table 4.1 – Values measured for the air temperature and relative humidity, and for the UV irradiance, at the time of the sampling.

the surface and increases until 9 cm deep where it then remains around 7.0 for the rest of the depth profile. At 4 782 m the pH remains below 5 down to 5 cm deep, then increases until 13 cm deep and stays around 6.5 for the rest of the depth profile. At 5 056 m the pH also remains below 5 down to 5 cm deep, then increases until 13 cm deep and oscillates around 6.2 for the rest of the depth profile. At 5 269 m the pH slowly rises from 5.2 at the surface to 5.7 5 cm below. It then suddenly increases to 6.8 at 7 cm deep.

4.5.2 Environmental parameters

Air measurements

Air temperature (T) and relative humidity (RH), and ultra-violet levels were measured by Prof. Vernon Phoenix whilst collecting the samples. Measurements are reported in table 4.1.

(Under)ground measurements

Following the collection of soil samples, probes were installed to record T and RH at the ground surface and underground for 2–3 days at all sites except at the 5 269 m site. Measured RH values were corrected as described in section 2.1.2 (p. 16). T and corrected relative humidity are plotted on figures 4.7 (4 296 m), 4.8 (4 782 m), and 4.9 (5 056 m). Night times, based on the sunrise and sunset times calculated for every sampling site using SunCalc (Agafonkin 2009), are indicated by shaded areas on the different plots. Table 4.2 gives an overview of the minimum, maximum, and mean temperature and relative humidity values.

4.5.3 Organic content

Loss on ignition

For all four sites the estimation of organic content by loss on ignition at 550 °C (LOI₅₅₀; figure 4.10) gives values around 1–2 %.

Samples collected at 4 296 m only lost 1.01–2.11 % of material. Starting at 1.01 % at the surface, values increase to reach a plateau (~1.6 %) between 9 and 15 cm deep. Higher values (~2.1 %) are observed at 17–19 cm, possibly resulting in higher organic content in

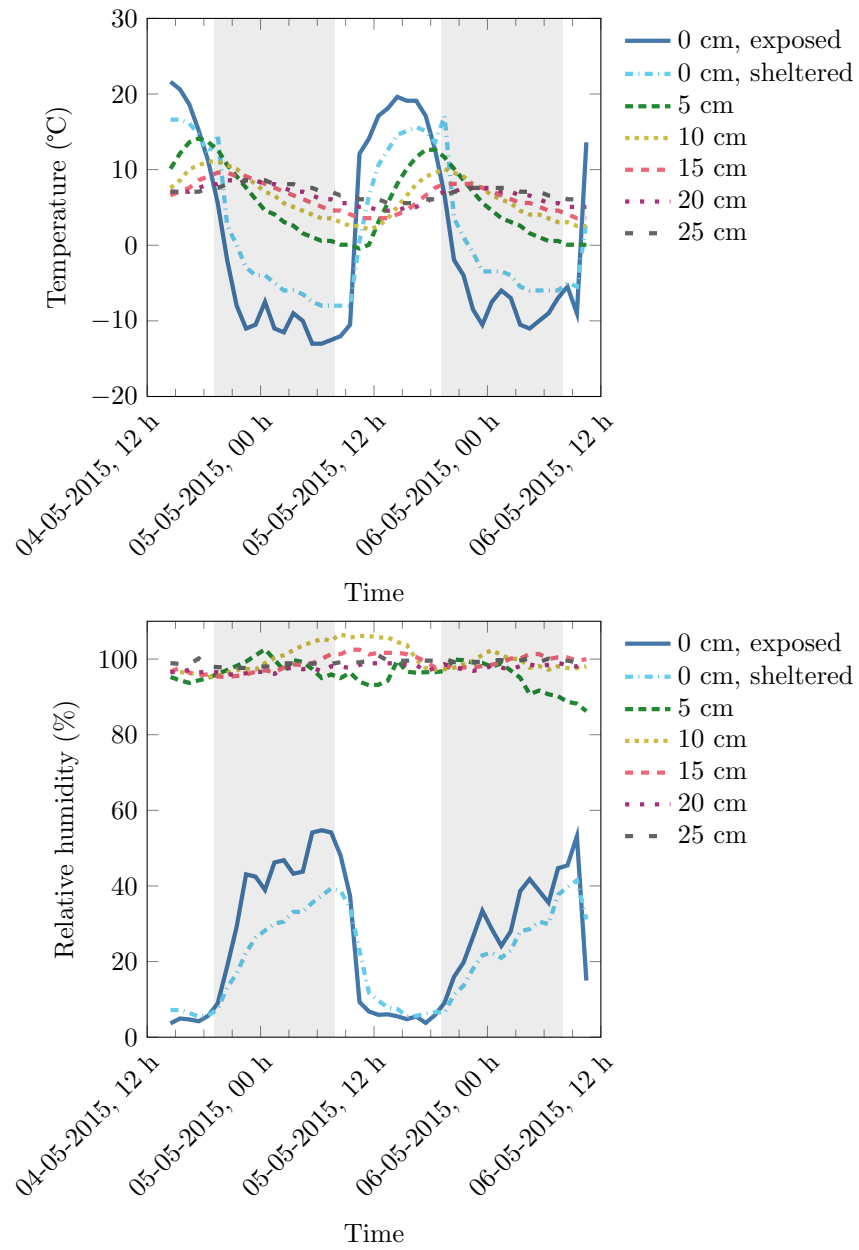


Figure 4.7 – Temperature (top) and relative humidity (bottom) monitored for different depths at the 4 296 m sampling site. Shaded areas indicate night times.

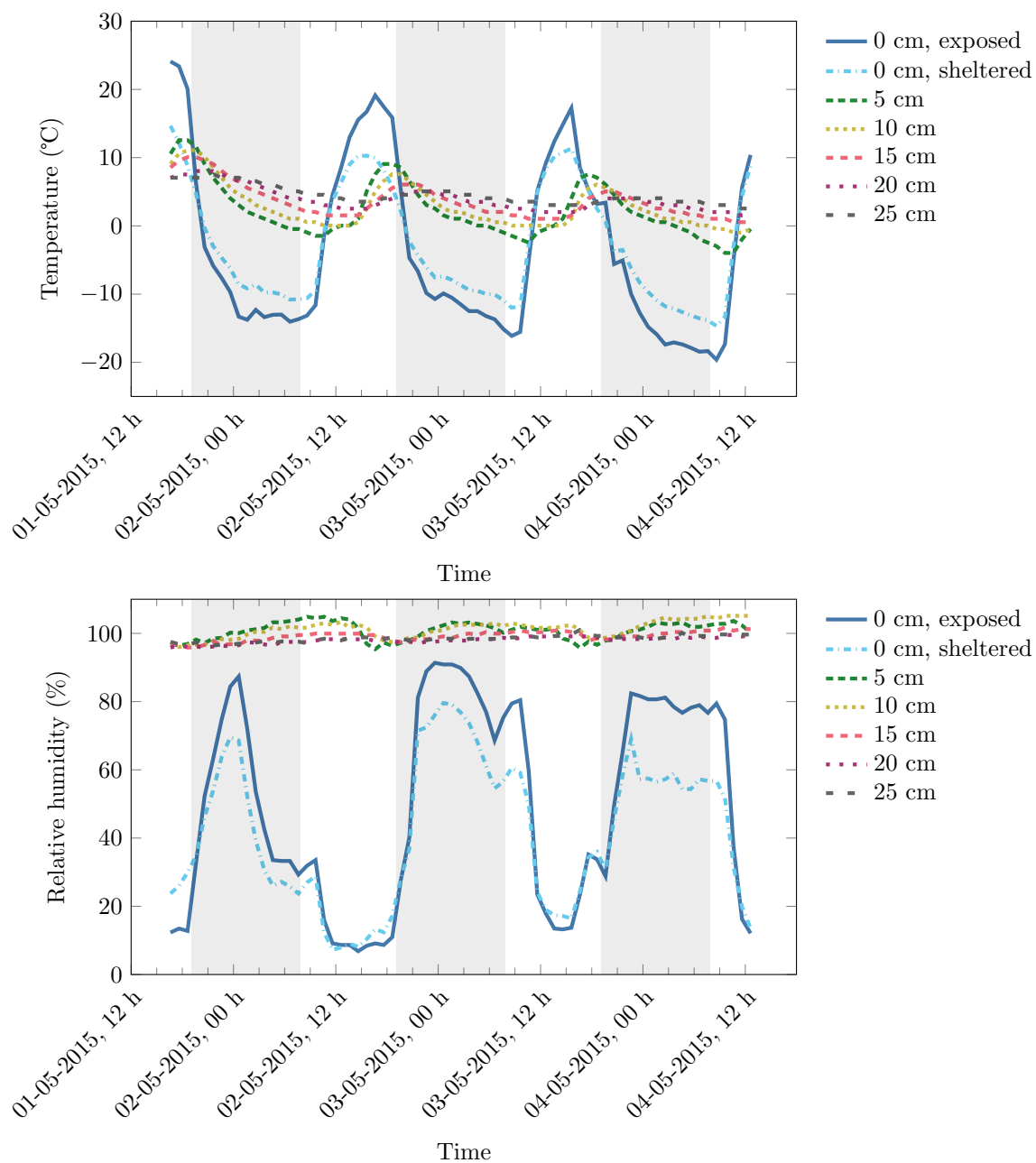


Figure 4.8 – Temperature (top) and relative humidity (bottom) monitored at different depths at the 4782 m sampling site. Shaded areas indicate night times.

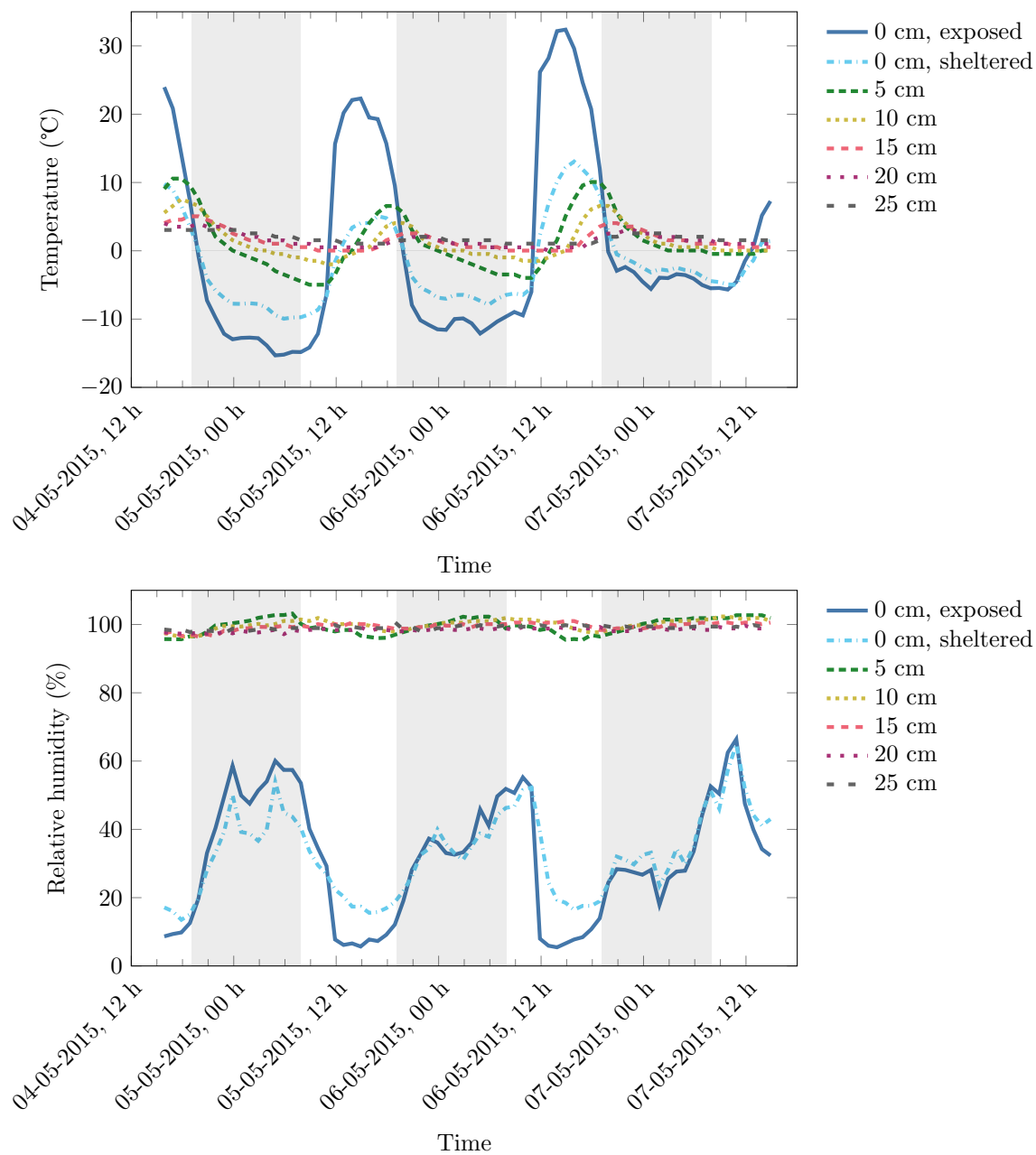


Figure 4.9 – Temperature (top) and relative humidity (bottom) monitored at different depths at the 5 056 m sampling site. Shaded areas indicate night times.

	Depth (cm)	Temperature (°C)			Relative humidity (%)		
		min	max	mean	min	max	mean
4 296 m	0 <i>exposed</i>	−13.0	21.6	0.9	3.6	54.7	26.1
	0 <i>sheltered</i>	−8.0	17.1	2.3	5.4	41.5	20.6
	5	−0.4	14.1	5.2	86.2	102.6	97.2
	10	2.1	11.1	5.8	95.3	106.6	102.2
	15	3.6	9.6	5.9	95.3	102.5	99.6
	20	4.6	8.6	6.3	95.9	99.8	97.8
	25	5.6	8.6	6.8	97.7	101.0	99.2
4 782 m	0 <i>exposed</i>	−19.6	24.1	−2.9	6.8	91.4	46.4
	0 <i>sheltered</i>	−14.7	14.7	−2.4	7.3	79.6	39.6
	5	−4.0	12.6	2.1	95.4	104.9	100.8
	10	−1.0	11.1	2.5	96.0	105.1	101.0
	15	0.5	10.1	3.3	95.8	101.7	99.2
	20	1.5	8.0	3.7	95.8	99.5	98.1
	25	2.6	7.6	4.3	96.4	101.0	98.4
5 056 m	0 <i>exposed</i>	−15.3	32.4	0.9	5.5	66.4	29.9
	0 <i>sheltered</i>	−10.0	13.1	−2.0	13.5	64.9	31.3
	5	−5.0	10.6	0.6	95.5	103.2	99.2
	10	−2.0	7.6	0.9	96.5	102.4	100.0
	15	0.0	5.1	1.2	96.4	101.0	99.7
	20	0.0	4.0	1.2	97.2	99.7	98.5
	25	1.1	3.1	1.6	97.5	100.7	99.2

Table 4.2 – Minimum, maximum, and mean values for temperature and relative humidity readings, for different depths, at the 3 lower sampling sites on the Sairecabur. Mean values are calculated using only data from complete days: 5 May 2015 for 4 296 m, 2–3 May 2015 for 4 782 m, and 5–6 May 2015 for 5 056 m.

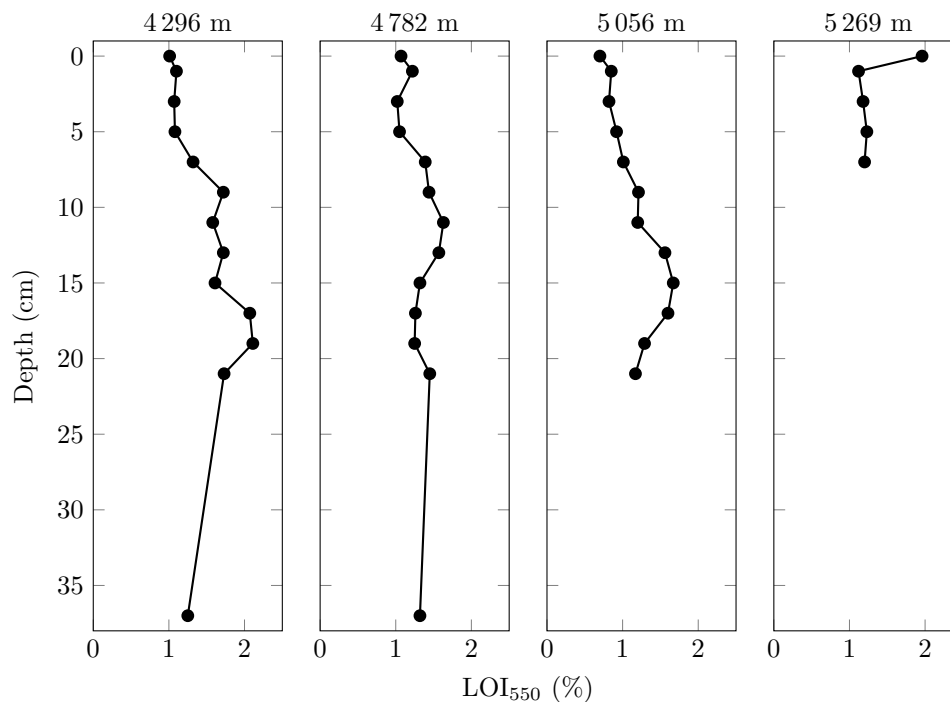


Figure 4.10 – Loss on ignition at 550 °C for the Sairecabur samples.

the soil due to the presence of tiny plant roots and their associated microbiome. The LOI then decreased until 1.25 % at 37 cm deep.

Samples collected at 4 782 m showed the least variation in LOI, with values oscillating between 1.02–1.63 % through the depth profile.

Samples collected at 5 056 m showed an overall range of 0.70–1.67 %. Samples collected near the surface (5 cm deep and above) have loss lower than 1 %. Yet, they increase from the surface (0.70 %) until 15 cm deep (1.67 %), then decrease until 21 cm deep (1.17 %).

The surface sample collected at 5 269 m had the highest surface loss, with 1.96 % of its dry mass combusted. The rest of this depth profile is quite steady with loss of 1.12–1.23 %.

Total lipid extracts

TLE concentrations are reported in figure 4.11. They show no correlation with LOI₅₅₀ values. At 4 296 m (the vegetated site), TLE concentrations are 57.0–116.7 $\mu\text{g}\cdot\text{g}^{-1}$. At 4 782 m TLE concentrations range between 39.8 and 100.3 $\mu\text{g}\cdot\text{g}^{-1}$. The 5 056 m site has the overall lowest TLE concentrations, ranging from 3.5 to 66.0 $\mu\text{g}\cdot\text{g}^{-1}$. At 5 269 m TLE concentrations vary between 40.7 and 73.6 $\mu\text{g}\cdot\text{g}^{-1}$.

Refined lipid data

General considerations All TLE fractions were separated into subfractions (N1 to N4). Focus was given to fraction N1 as they contain aliphatic hydrocarbons, among which *n*-alkanes, hopanes, and steranes can serve as biomarkers. All samples eluted as unresolved complex mixtures (UCM). Within UCM, *n*-alkanes were relatively easy to identify. They

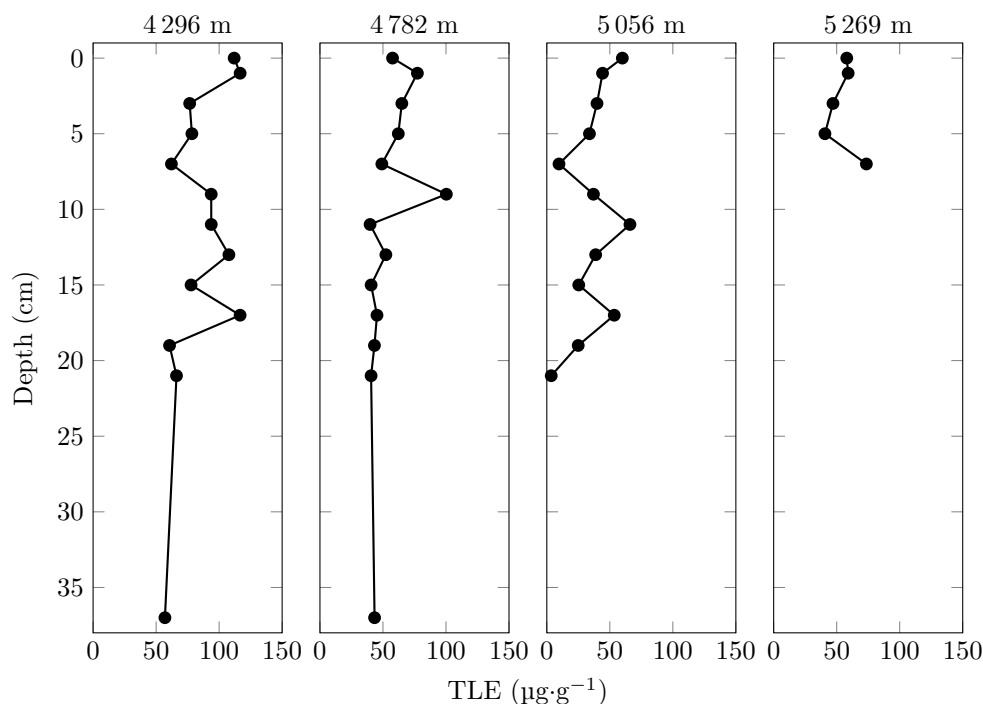


Figure 4.11 – Total lipid extracts of the Sairecabur samples.

were detected and quantified in all samples. Depending on the altitude and the depth of the sample, *n*-alkanes mostly range from C₁₆ to C₃₅, and up to C₄₀ in some cases. Hopanes — produced by bacteria — were sometimes detected, but they were always below detection limit ($\sim 40\text{--}60\text{ ng}\cdot\text{L}^{-1}$ in solution). Steranes — produced by archaea — were not detected. To ease the interpretation of data, only lipids of plant and of microbial/diagenesis origin will be considered.

Fraction N2 — containing aromatic hydrocarbons, aldehydes, and ketones — did not contain any molecules of interest, like polycyclic aromatic hydrocarbons (PAHs), despite searching specifically for them. Only polymer-related contaminants were found. Fractions N3 and N4 were not investigated.

Plant inputs Usually, long chain odd-numbered *n*-alkanes are associated with plant leaf waxes (Eglinton and Hamilton 1967; Jetter et al. 2006). However, they can also be produced by plant roots (Jansen et al. 2006), and have also been attributed to fungi (Oró et al. 1966; Jones 1969; Weete et al. 1970; Weete 1976) and bacteria (Li et al. 2018).

Another molecule likely to originate from plants, by degradation of the phytol side chain of chlorophyll *a* and *b*, is phytane (Curphey 1952; Bendoraitis et al. 1962; Eglinton et al. 1964; Brooks et al. 1969; Powell and McKirdy 1973). A microbial origin has also been suggested for phytane, although mainly in aqueous environments (Han and Calvin 1969; Rowland 1990; Corcelli et al. 2000; Lattanzio et al. 2002; Sprott et al. 2003). Microbial degradation of phytane has also been reported (Jones 1968; Cox et al. 1976; Nakajima et al. 1985; Silva et al. 2007; Prince et al. 2008). No reports of production of phytane in plant roots were found. Synthesis of chlorophyll in roots has been reported in various plants

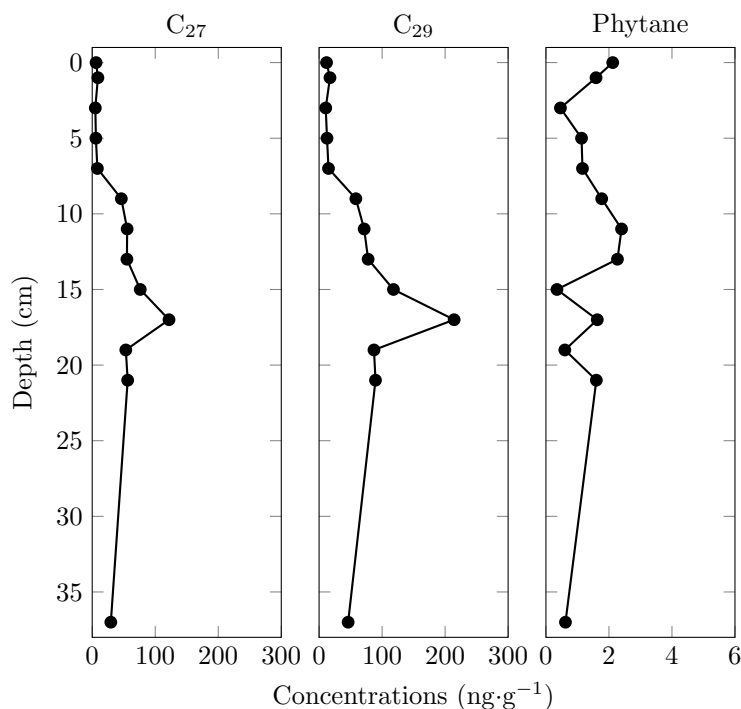


Figure 4.12 – Lipid inputs from higher plants at 4 296 m.

(e. g. Leitgeb 1858; Fadeel 1962; Björn 1965, 1976; Armstrong and Armstrong 1994), but only when the roots were exposed to light.

Depending on the altitude and the depth of the sample, odd-numbered long chain *n*-alkanes could range up to C₃₅. To simplify, only the concentrations of C₂₇ and C₂₉ *n*-alkanes, and of phytane, will be presented here. Depth profiles corresponding to the different altitudes are plotted as follows: 4 296 m (figure 4.12), 4 782 m (figure 4.13), 5 056 m (figure 4.14), and 5 269 m (figure 4.15). For an easier comparison between the different sites, concentration scales are the same for all C₂₇ and C₂₉ plots (except for the 4 296 m site, as the concentrations are much higher), and for all phytane plots.

4 296 m As stated above, the C₂₇ and C₂₉ *n*-alkanes concentrations observed at 4 296 m (figure 4.12) are the highest out of all the sites (up to $121.9 \text{ ng}\cdot\text{g}^{-1}$ for C₂₇ and up to $214.3 \text{ ng}\cdot\text{g}^{-1}$ for C₂₉). Their concentration curves have similar shapes, stable low concentrations down to 7 cm deep, an increase until 17 cm deep, then a decrease until 37 cm deep. For this sampling site, covered with sparse vegetation (figure 4.2) it is reasonable to assume that most of the long chain *n*-alkanes have a plant origin. Surface concentrations are noticeably lower than concentrations observed at deeper depth. Their maximum concentration is also observed at 17 cm deep.

Phytane concentration (figure 4.12) is important at the surface ($2.1 \text{ ng}\cdot\text{g}^{-1}$). It quickly decreases down to $0.5 \text{ ng}\cdot\text{g}^{-1}$ at 3 cm deep before rising again to $2.4 \text{ ng}\cdot\text{g}^{-1}$ at 11 cm deep. It then steadily decreases down to $0.6 \text{ ng}\cdot\text{g}^{-1}$ at 37 cm deep, with two dips at 15 and 19 cm deep (0.4 and $0.6 \text{ ng}\cdot\text{g}^{-1}$, respectively).

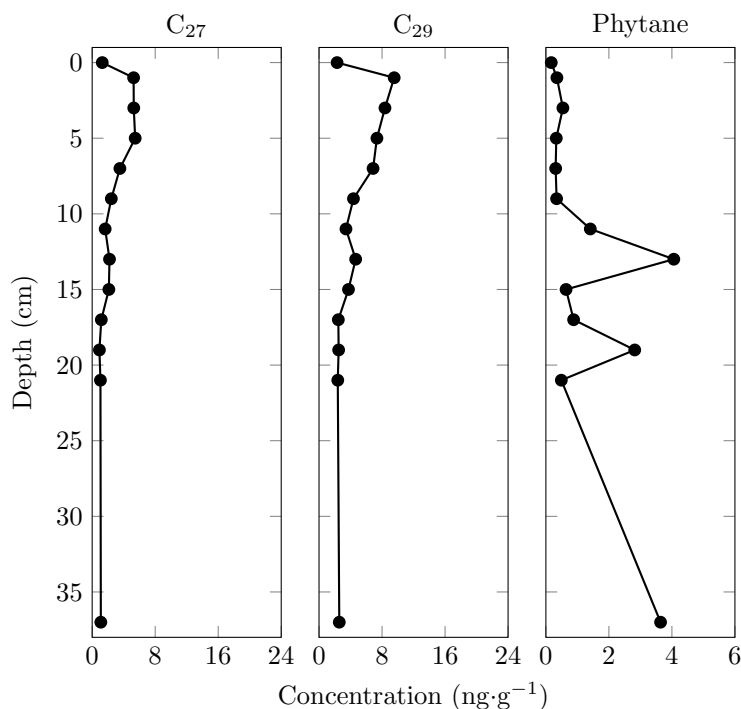


Figure 4.13 – Lipid inputs from higher plants at 4 782 m.

4 782 m At 4 782 m (figure 4.13) the C₂₇ and C₂₉ *n*-alkane profiles have similar shapes to each other. The accumulation of *n*-alkane molecules at 1 cm deep is higher than at the surface (2.3 ng·g⁻¹ at the surface, 9.5 ng·g⁻¹ at 1 cm deep, for C₂₉). The *n*-alkanes concentrations then steadily decrease down to 17 cm deep, then remain constant until the end of the depth profile, 37 cm below the surface.

Phytane concentration (figure 4.13) remains low (0.2–0.5 ng·g⁻¹) until 9 cm deep, then increases up to 4.1 ng·g⁻¹ at 13 cm deep. The concentration decreases between 15 and 17 cm deep (0.6–0.9 ng·g⁻¹). A second and lesser increase at 19 cm deep (2.8 ng·g⁻¹) is immediately followed by a return to a base level concentration (0.5 ng·g⁻¹ at 21 cm deep). The final concentration 37 cm below the surface is high again (3.6 ng·g⁻¹).

5 056 m At 5 056 m, (figure 4.14) the samples corresponding to the 7 cm and 21 cm depths were lost during transfer into vials; hence they could not be properly quantified and are not plotted. The C₂₇ and C₂₉ *n*-alkanes depth profiles still have similar shapes. Their concentrations, not varying much from the surface down to 5 cm deep, suddenly increase, then decrease until 19 cm deep, with a dip in concentration at 11 cm deep.

Phytane concentration (figure 4.14) remains at 0.2–0.7 ng·g⁻¹ from the surface to 9 cm deep. It then rises to reach 2.9 at 13 cm deep, before decreasing to 0.8 ng·g⁻¹ at 19 cm deep, with a concentration dip (0.4 ng·g⁻¹) at 15 cm deep.

5 269 m At 5 269 m, the concentration of C₂₇ (1.4–3.7 ng·g⁻¹) and C₂₉ (4.2–5.4 ng·g⁻¹) *n*-alkanes remains low and relatively constant through the depth profile (figure 4.15) — like the TLE profile, except at 7 cm deep (figure 4.11).

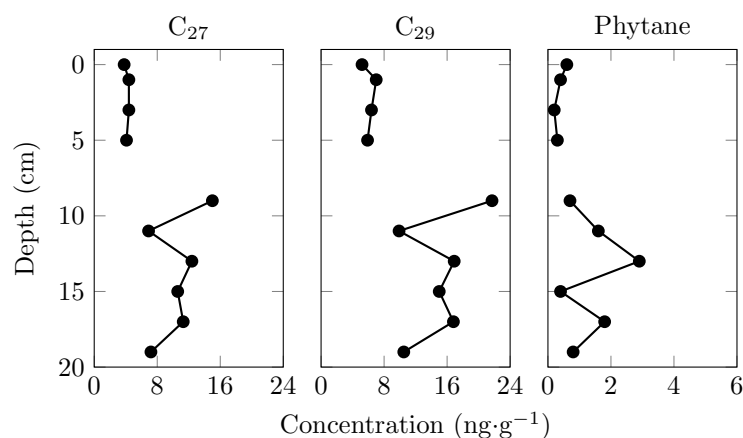


Figure 4.14 – Lipid inputs from higher plants at 5 056 m.

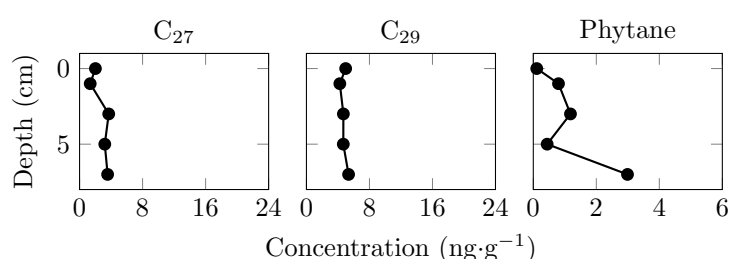


Figure 4.15 – Lipid inputs from higher plants at 5 269 m.

The phytane profile is different (figure 4.15), with a low concentration at the surface ($0.1 \text{ ng}\cdot\text{g}^{-1}$) followed by a slight increase between 1 and 5 cm deep ($0.4\text{--}1.2 \text{ ng}\cdot\text{g}^{-1}$), and finished by a major increase in concentration at 7 cm deep ($3.0 \text{ ng}\cdot\text{g}^{-1}$).

Degraded material and microbial inputs Even-numbered short chain *n*-alkanes ($< \text{C}_{21}$) are associated with anthropogenic contamination (Simoneit 1984; Lichtfouse et al. 1997; Brocks et al. 2008), diagenesis (Goutx and Saliot 1980; Eckmeier and Wiesenberg 2009; Wiesenberg et al. 2009), microbial production — although only reported in aqueous environments (Han and Calvin 1969; Albro 1976) and plant production (Kuhn et al. 2010). Microbial degradation of *n*-alkanes, up to C_{22} in length, has also been reported (Jones and Howe 1968; Amblès et al. 1994). Regarding abiotic reactions, catalytic oxidations of *n*-alkanes on minerals are reported (Huybrechts et al. 1990; Khouw et al. 1994; Faure et al. 2003), but they occur only under specific conditions such as having a specific *n*-alkane, a pure mineral, the presence of peroxides, or high temperatures. Decarboxilation reactions catalysed by minerals have also been reported (Wang and Huang 1987; Huang 1990). Anthropogenic contamination should be minimal at these altitudes, but airborne inputs of organics are still possible (e.g. Beyer et al. 2000; Scheringer 2009; Stres et al. 2013). The *n*-alkane concentrations observed in the depth profiles are reported in figure 4.16 (4 296 m), figure 4.17 (4 782 m), figure 4.18 (5 056 m), and figure 4.19 (5 269 m).

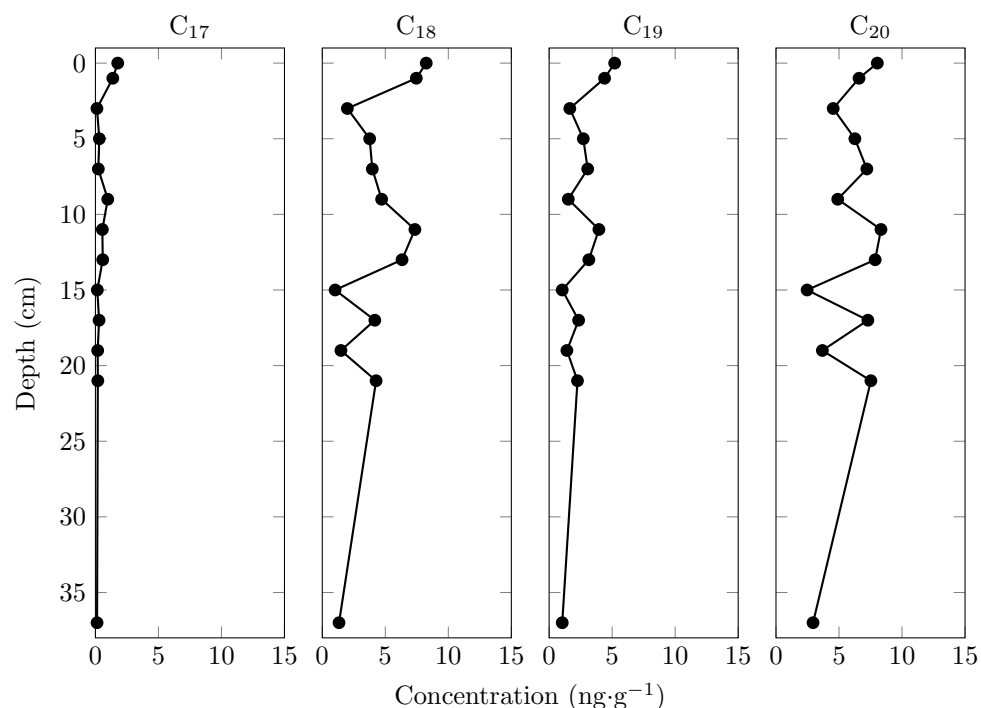


Figure 4.16 – Short chain *n*-alkanes at 4 296 m.

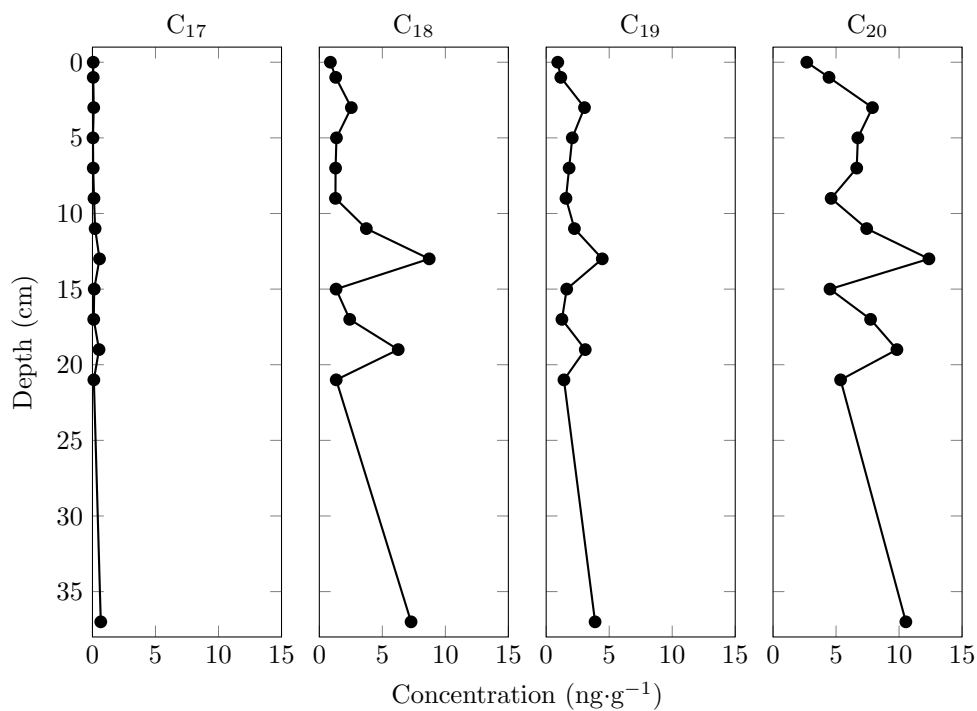
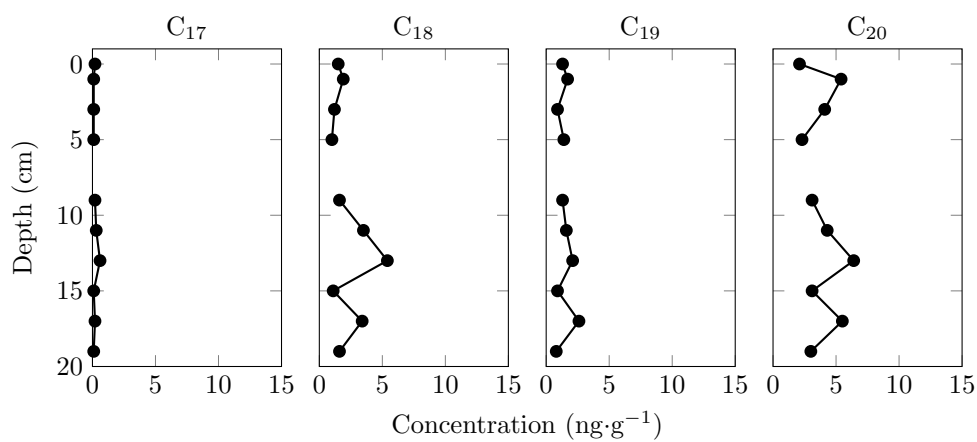
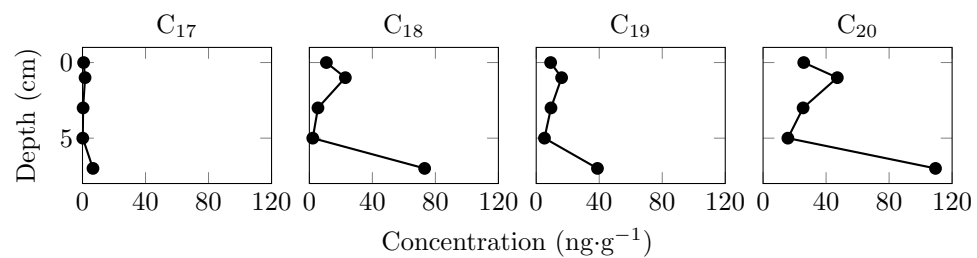
4 296 m At 4 296 m (figure 4.16), the concentration of short chain *n*-alkanes is significantly lower (below $10 \text{ ng}\cdot\text{g}^{-1}$) than the concentration of long chain *n*-alkanes (background around $10 \text{ ng}\cdot\text{g}^{-1}$, maximum values above $200 \text{ ng}\cdot\text{g}^{-1}$, figure 4.12). The concentration profiles of all four molecules are similar and have jigsaw outlines with concentrations globally decreasing with depth. Surface concentrations are the highest. Other noticeable maxima are at 11–13 cm deep (or 9 cm deep, for C_{17}), at 17 cm and 21 cm deep.

4 782 m Concentration profiles of short chain *n*-alkanes at 4 782 m (figure 4.17) also show similar variations with depth. For all short chain *n*-alkanes the surface concentration is the lowest measured in their respective profile, and is slightly below their background concentration; noticeable maxima are observed at 3, 13, 19, and 37 cm deep.

5 056 m Concentrations of short chain *n*-alkanes are the lowest of all the sites at 5 056 m (below $6 \text{ ng}\cdot\text{g}^{-1}$, figure 4.18). Once again, all molecules follow a similar pattern of concentration with depth. Surface concentrations are close to background concentrations. Maxima are observed at 1, 13, and 17 cm deep.

5 269 m Surprisingly, concentration of short chain *n*-alkanes are the highest at 5 269 m (up to $109.5 \text{ ng}\cdot\text{g}^{-1}$, figure 4.19). Concentrations are again lower at the surface, and at 5 cm deep. Maximum concentrations are observed at 1 cm deep, and especially at 7 cm deep.

CPI and ACL indices From the previous results it can be assumed that odd-numbered long chain *n*-alkanes are mostly produced by plants and that these molecules are present at

Figure 4.17 – Short chain *n*-alkanes at 4782 m.Figure 4.18 – Short chain *n*-alkanes at 5056 m.Figure 4.19 – Short chain *n*-alkanes at 5269 m.

all altitudes and depths. Both the carbon preference index (CPI) and the average chain length (ACL) indices can give indications about the preservation state of *n*-alkanes. Diminution of the odd/even *n*-alkanes ratio can be revealed by the CPI (figure 4.20, top) whilst the ACL index (figure 4.20, bottom) will indicate a shortening of the molecules. Details about the calculation of the indices are described in section 2.3.2.

CPI values around 3 and higher are generally considered as an indication of higher plant inputs. This indicates that plant inputs are limited above 8 cm deep and above 10 cm deep at the 4 296 m and 4 782 m sites, respectively. Surface samples are the exception, for which low CPI values suggest a degradation of the molecules at the surface. The opposite trend is observed at 5 056 m, with relatively high CPI values for the whole profile (4.51–5.23), except for the values at 1–5 cm deep (1.12–3.14). This suggests that diagenesis is essentially limited to this zone close to the surface. Values are low at 5 269 m, with 2.60–2.62 near the surface and 1.84–2.00 at 3–7 cm deep. The harsher environmental conditions experienced at this altitude may explain why low values are observed throughout the whole depth profile.

ACL values do not vary much at 4 269 m (28.1–28.7), 4 782 m (27.9–28.6), and 5 056 m (28.3–29.1). Surface values are as low as those observed, for their respective profile, below 10 cm deep (4 296 m) and 15 cm deep (4 782 m). The 5 056 m profile displays the least ACL variation, with the exception of an increase to 29.1 at 11 cm deep. At 5 269 m, ACL values decrease with depth, starting from 28.0 at the surface and reaching 26.6 at 7 cm deep.

4.5.4 Plant and lichen samples

To determine if any plants or lichens present near the different sampling sites contributed significantly to lipid input in soils, plant and lichen samples were collected at 4 296 m, 4 580 m, 4 782 m, and 5 056 m (figure 4.1). No plants or lichens were observed at the 5 269 m site. Other plant types were present below 4 296 m, but were not collected.

The taxonomic identification of all the plants and lichens has not been confirmed for all samples. Their identification started in Chile by comparing the plants collected with the ones present at the archeological museum in San Pedro de Atacama. Upon return to Glasgow, some other plants were identified based on comparison with plants reported by Richter and Schmidt (2002), and with the help of Prof. Claudio Latorre (Pontificia Universidad Católica de Chile).

With the help of undergraduate student Briony Carswell, lipids were extracted from the different samples, separated into sub-fractions, and analysed by GC-FID, following the same procedure as for soil samples. Details about the samples, and their *n*-alkane profiles, are described in appendix B. For every sample, an average of the different plant parts (i.e. leaves, stems, flowers) — with the exception of roots, which were not allowed to be imported — was used when extracting the lipids from every sample.

Briefly, depending on the sample, the observed *n*-alkane distribution ranges between C₁₄ and C₃₇ for plants, and from C₁₈ to C₃₅ for lichens.

The CPI and the ACL indices were calculated following the formula described in sec-

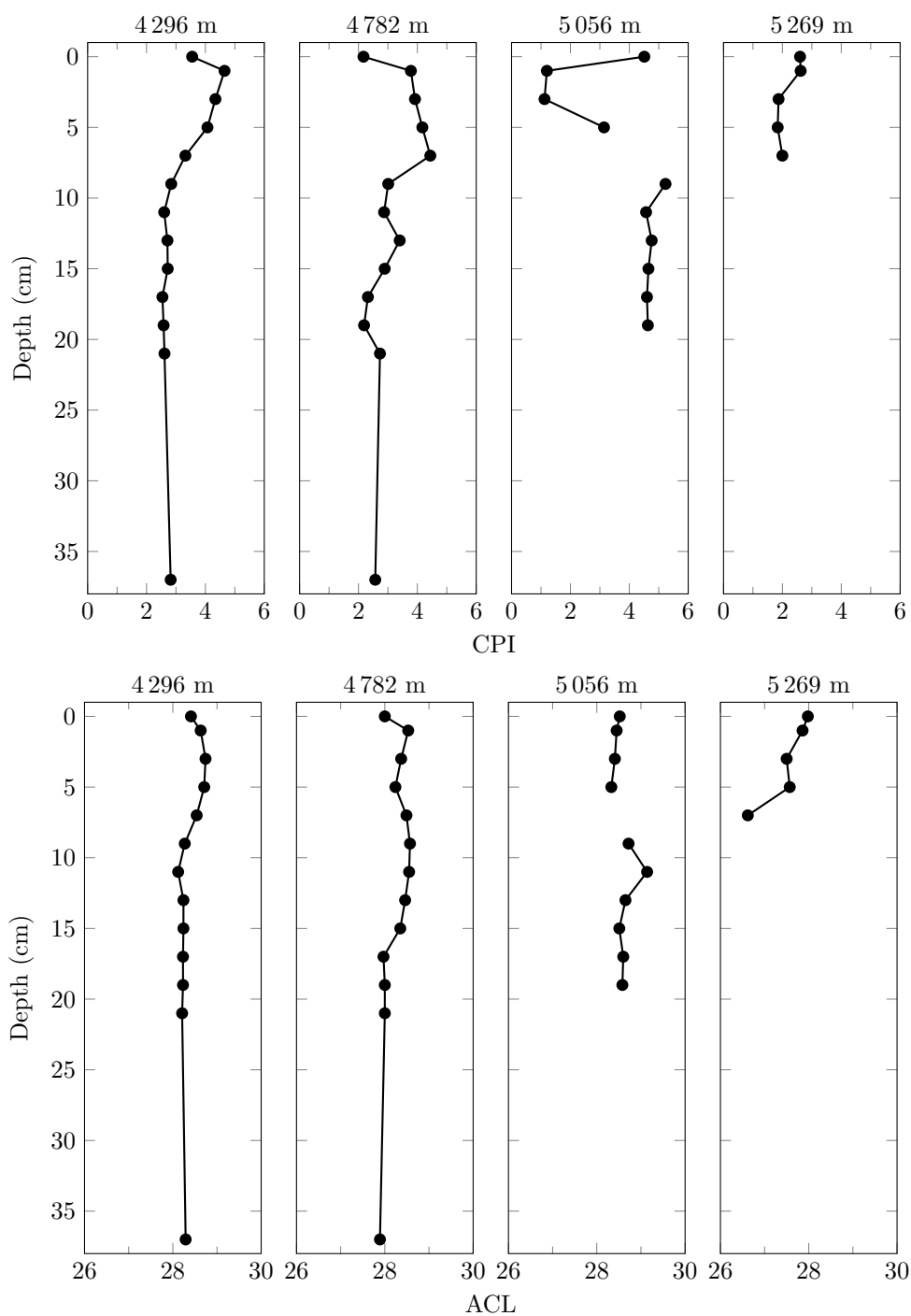


Figure 4.20 – Indices derived from *n*-alkanes concentrations. (top) CPI. (bottom) ACL.

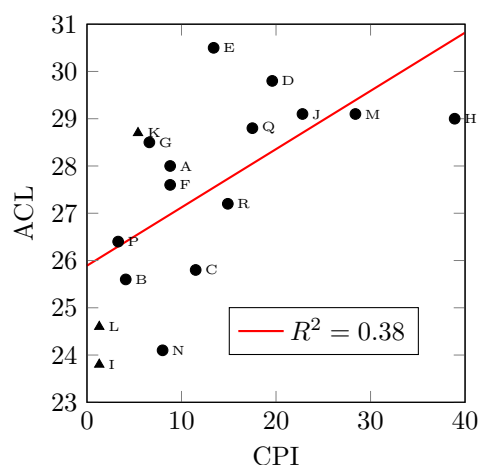


Figure 4.21 – CPI_{19-33} values plotted against ACL_{19-35} values of the plant (●) and the lichen (▲) samples collected on the Sairecabur. The ACL/CPI ratio does not follow a linear trend. Samples are identified by their corresponding letter, as described in appendix B.

tion 2.3.2, but changing the range of odd n -alkane profiles to C_{19} – C_{33} for CPI, and to C_{19} – C_{35} for ACL. The values of these two indices, also reported in appendix B, are plotted against each other in figure 4.21. Plant sample O does not contain even-numbered n -alkanes, hence its CPI could not be calculated. Comparison of CPI and ACL values with the ones observed in soil samples did not help to identify any dominant source of lipids amongst the studied plants and lichens.

The low amount of lichen samples ($n = 3$) may not be representative of the diversity of profiles that could be observed if all different species from the area had been collected. The lichen data obtained yielded low CPI (1.3–5.4), indicating a light excess of odd over even n -alkane chains. Plant CPIs have a broader distribution (3.3–38.9), with sample O not containing any even-numbered n -alkanes. Both lichens and plants have broad ACL values, with 23.8–28.7 for lichens and 24.1–30.5 for plants.

4.5.5 DNA content

Total DNA concentration At dry sites microbial diversity is poor, consisting essentially of *Fungi* and *Actinobacteria* (e.g. Costello et al. 2009; Lynch et al. 2012; Pulschen et al. 2015; Schmidt et al. 2017b; Solon et al. 2018). However, published work lacks proper depth profiles. For this reason, a quantification of the total DNA of all samples from each site was performed. Soil samples were shared with Nick Thomas. Our combined extraction sets give a triplicate total DNA extraction for each sample. Results are plotted on figure 4.22 (top: my extracts alone; bottom: my extracts combined with Nick's). As DNA concentrations vary greatly between the different sites, there is no common scale and each site uses its own. The comments below are made on the combined triplicate sets (figure 4.22, bottom). Values below detection limit ($25 \text{ pg} \cdot \mu\text{L}^{-1}$) before conversion and normalisation were defined as 0 after normalisation.

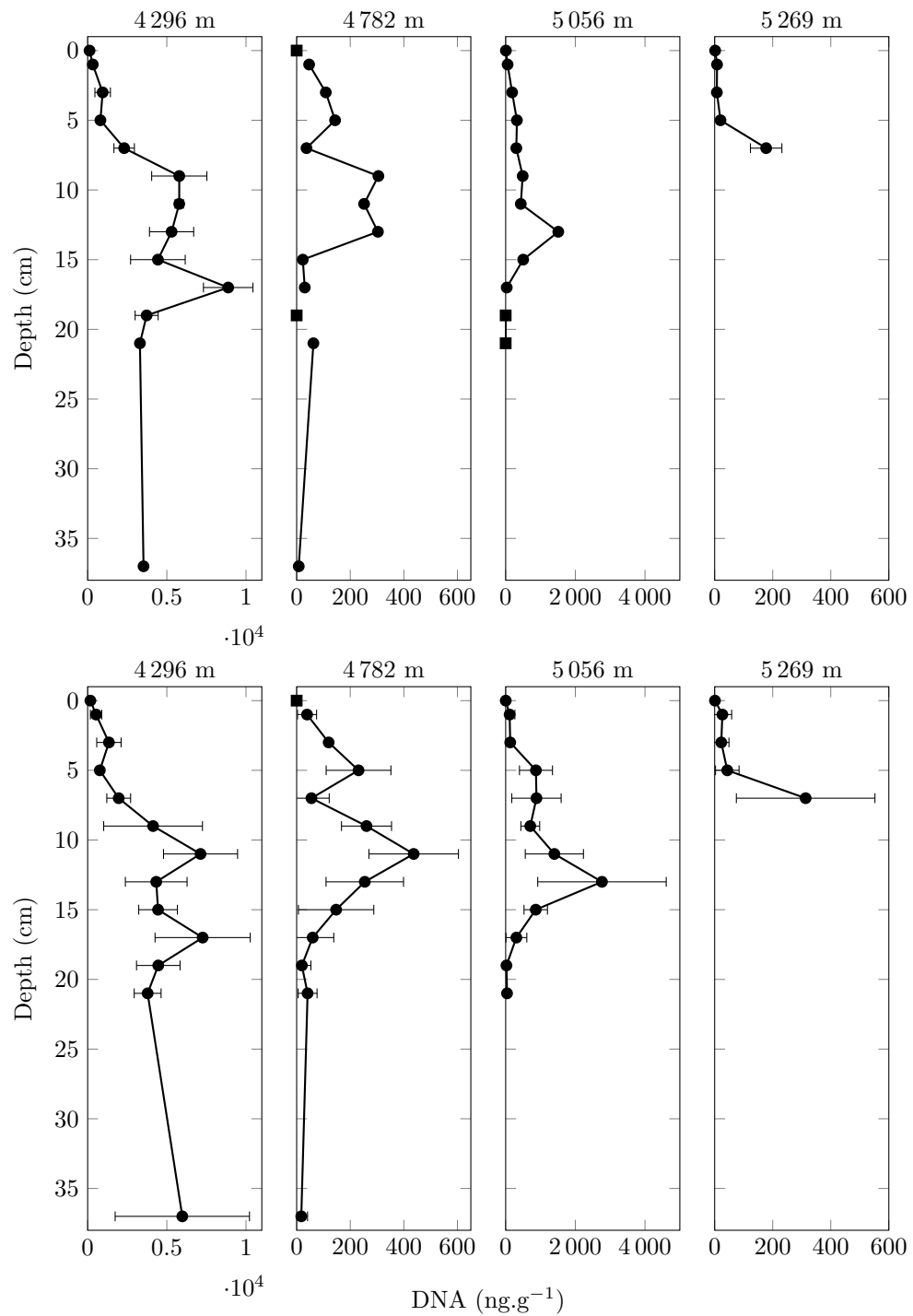


Figure 4.22 – DNA extract, normalised to the quantity of soil, as a function of depth at the sampling site. (top) Values for my extracts alone (4 296 m and 5 269 m, $n = 2$; 4 782 m and 5 056 m, $n = 1$). (bottom) Values for my extracts combined with those obtained by Nick Thomas ($n = 3$ for all samples). Squares indicate values below detection limit before normalisation.

4 296 m The 4 296 m profile displays the highest concentrations. Starting with $0.17 \mu\text{g}\cdot\text{g}^{-1}$ at the surface, DNA concentration rises up to $7.13 \mu\text{g}\cdot\text{g}^{-1}$ at 11 cm deep. After a short decrease at 13–15 cm deep, a new maximum is observed at 17 cm deep ($7.26 \mu\text{g}\cdot\text{g}^{-1}$). A second decrease follows until 22 cm, and then rises to a last maximum at 37 cm deep ($5.98 \mu\text{g}\cdot\text{g}^{-1}$).

4 782 m At 4 782 m DNA concentrations are lower than at 4 296 m. No DNA was detected at the surface. DNA concentration increases to $230.9 \text{ ng}\cdot\text{g}^{-1}$ at 5 cm deep, then briefly decreases to $55.2 \text{ ng}\cdot\text{g}^{-1}$ at 7 cm deep, before increasing again, up to $436.7 \text{ ng}\cdot\text{g}^{-1}$ at 11 cm deep. Finally, concentrations decrease until 19 cm deep, where they remain around $17.2\text{--}40.8 \text{ ng}\cdot\text{g}^{-1}$ until 37 cm deep.

5 056 m DNA concentrations at 5 056 m are higher than at 4 782 m. After a surface concentration of $2.25 \text{ ng}\cdot\text{g}^{-1}$, concentration increases to $113.5\text{--}130.9 \text{ ng}\cdot\text{g}^{-1}$ at 3–5 cm deep. It is then followed by a plateau ($0.71\text{--}0.88 \mu\text{g}\cdot\text{g}^{-1}$) from 5 to 9 cm deep. It then rises up to $2.76 \mu\text{g}\cdot\text{g}^{-1}$ at 13 cm deep before decreasing down to $22.3\text{--}39.1 \text{ ng}\cdot\text{g}^{-1}$ at 19–21 cm deep.

5 269 m Finally, the 5 269 m site, despite having a concentration profile at shallow depth similar to the one observed at 5 056 m, displays a maximum concentration similar to those observed at 4 782 m. With $1.2 \text{ ng}\cdot\text{g}^{-1}$ at the surface, the concentration slowly increases to $43.5 \text{ ng}\cdot\text{g}^{-1}$ at 5 cm deep, then suddenly increases to $238.7 \text{ ng}\cdot\text{g}^{-1}$ at 7 cm deep.

Metagenomics A first metagenomic study of the prokaryotes was performed by Nick Thomas. Sequencing of 16S rDNA revealed microbial communities changing within a few centimeters in the depth profile, and with a domination of bacteria over archaea (Thomas 2018). In order to go beyond the 16S rDNA sequencing, and have an insight into other genes present in the samples, I used the same sequencing approach as for the Atacama samples (section ??).

Briefly, in order to avoid amplification biases, droplet microfluidics–multiple displacement amplification (ddMDA) was used to amplify aspecifically DNA strands separated physically from each other (Sidore et al. 2016; Rhee et al. 2016). This work was performed in Linas Mažutis' laboratory (Institute of Biotechnology, Vilnius University). After DNA amplification, purification, and preparation for sequencing, only a few samples were pure enough to qualify for MiSeq sequencing. Sequencing was performed by Juozas Nainys (Institute of Biotechnology, Vilnius University).

Out of the seven samples sequenced, only three could be retrieved for analysis: 4 296 m, second set, surface; 5 056 m, only set, 1 cm deep; 5 269 m, first set, surface. These three raw sequencing data sets are available on the NCBI BioSample database under their respective accession number: SAMN13182959, SAMN13182960, and SAMN13182961. The raw reads were first analysed with the Illumina 16S Metagenomics app (algorithm derived from Wang et al. 2007). For all three samples, a very low proportion of reads (0.4–1.4 ‰) were identified with the Illumina 16S Metagenomics app.

	Matches	% of total
Global results		
Total (kingdom level only)	57 702	100.00
Classified	57 066	98.90
Unclassified	636	1.10
Classified results		
Bacteria	53 169	92.14
Archaea	1 997	3.46
Other unspecified cellular organisms	116	0.20
Viruses	1 784	3.09

Table 4.3 – Matches output by Kraken for the sample taken at 4 296 m, surface level.

To try to get more detailed results using different programs, Umer Ijaz (School of Engineering, University of Glasgow) quality-trimmed the raw sequences with Sickle (Joshi and Fass 2011) — removing 11–18 % of the reads in the process — before running them separately with the MetaPhlAn2 (Truong et al. 2015), the Kaiju (Menzel et al. 2016), and the Kraken programs (Wood and Salzberg 2014). MetaPhlAn2 failed to match 16S rDNA with known sequences — depending on the sample, only 0–2 hits were obtained.

4 296 m From the initial 7 918 785 raw reads of the 4 296 m surface sample, the Illumina 16S Metagenomics app only identified 3 548 reads at the kingdom level and MetaPhlAn2 matched only one bacteria (*Geodermatophilaceae*) from the trimmed sequences. Kraken and Kaiju results had more hits, with 57 702 reads identified at the kingdom level (Kraken, table 4.3) and 526 498 reads identified at the species level (Kaiju, table 4.4). The main genera identified by Kaiju were *Niastella*, *Candidatus Nitrosotenuis* (an archaea), and *Chitinophaga* (about 10, 5, and 5 % of the hits, respectively).

5 056 m For the 5 056 m 1 cm-depth sample, 3 531 000 raw reads were obtained. The Illumina 16S Metagenomics app only identified 2 741 reads at the kingdom level. MetaPhlAn2 results should be considered non-significant as only two bacteria were matched (*Pseudomonas* and *Hymenobacter*). Kraken identified 24 547 reads at the kingdom level (table 4.5), whereas Kaiju identified 281 667 reads at the species level (table 4.6). The main genera identified by Kaiju were the soil bacteria *Niastella*, *Niabella*, and *Chitinophaga* (about 9, 4, and 4 % of the hits, respectively).

5 269 m For the 5 269 m surface sample, 4 842 706 raw reads were obtained. The Illumina 16S Metagenomics app only identified 6 785 reads at the kingdom level. No correspondence was detected by MetaPhlAn2. However, with 1 837 629 identified reads at the kingdom level for Kraken (table 4.7), and 964 245 identified reads at the species level for Kaiju (table 4.8), this sample has the highest identification proportion of all samples included in my study. Still, the main genera identified by Kaiju were *Escherichia*, *Enterobacter*, and

	Matches	% of total
Global results		
Total	7 912 297	100.00
Classified	1 367 555	17.28
Unclassified	6 544 742	82.72
Classified results		
Species rank	841 057	10.63
Above species rank	526 498	6.65
Species rank results		
<i>Niastella koreensis</i>	50 319	0.64
<i>Candidatus Nitrosotenuis cloacae</i>	27 514	0.35
<i>Chitinophaga pinensis</i>	25 473	0.32
<i>Niabella soli</i>	21 109	0.27
<i>Sphingobacterium</i> sp. 21	17 363	0.22
<i>Pedobacter</i> sp. PACM 27299	16 726	0.21
<i>Pseudopedobacter saltans</i>	15 898	0.20
<i>Pedobacter heparinus</i>	14 338	0.18
<i>Candidatus Nitrosopelagicus brevis</i>	14 142	0.18
<i>Solitalea canadensis</i>	12 959	0.16
Others	625 216	7.90

Table 4.4 – Matches output by Kaiju for the sample taken at 4 296 m, surface level. The ten most abundant species are indicated.

	Matches	% of total
Global results		
Total (kingdom level only)	24 547	100.00
Classified	24 369	99.27
Unclassified	178	0.73
Classified results		
Bacteria	22 540	91.82
Archaea	1 339	5.45
Other unspecified cellular organisms	32	0.13
Viruses	458	1.87

Table 4.5 – Matches output by Kraken for the sample taken at 5 056 m, 1 cm deep.

	Matches	% of total
Global results		
Total	3 529 876	100.00
Classified	727 504	21.61
Unclassified	2 802 372	79.39
Classified results		
Species rank	445 837	12.63
Above species rank	281 667	7.98
Species rank results		
<i>Niastella koreensis</i>	26 020	0.74
<i>Niabella soli</i>	12 508	0.35
<i>Chitinophaga pinensis</i>	11 134	0.32
<i>Candidatus Nitrosotenuis cloacae</i>	8 348	0.24
<i>Candidatus Solibacter usitatus</i>	6 014	0.17
<i>Spirosoma radiotolerans</i>	4 866	0.14
<i>Pedobacter</i> sp. PACM 27299	4 729	0.13
<i>Sphingobacterium</i> sp. 21	4 488	0.13
<i>Candidatus Nitrosopelagicus brevis</i>	4 168	0.12
<i>Dyadobacter fermentans</i>	4 058	0.11
Others	359 504	10.18

Table 4.6 – Matches output by Kaiju for the sample taken at 5 056 m, 1 cm deep. The ten most abundant species are indicated.

	Matches	% of total
Global results		
Total (kingdom level only)	1 837 629	100.00
Classified	1 837 409	99.99
Unclassified	220	0.01
Classified results		
Bacteria	1 829 119	99.54
Archaea	168	0.01
Other unspecified cellular organisms	39	0.00
Viruses	8083	0.44

Table 4.7 – Matches output by Kraken for the sample taken at 5 269 m, surface level.

	Matches	% of total
Global results		
Total	4 840 105	100.00
Classified	1 844 355	38.11
Unclassified	2 995 750	61.89
Classified results		
Species rank	880 110	18.18
Above species rank	964 245	19.92
Species rank results		
<i>Escherichia coli</i>	220 834	4.56
unidentified plasmid	179 774	3.71
<i>Enterobacter cloacae</i> complex	80 191	1.66
<i>Enterobacter cloacae</i>	76 430	1.58
<i>Alteromonas mediterranea</i>	71 126	1.47
<i>Klebsiella pneumoniae</i>	39 403	0.81
<i>Thermanaerovibrio acidaminovorans</i>	27 887	0.58
<i>Rhodococcus aetherivorans</i>	26 641	0.55
<i>Niastella koreensis</i>	5 621	0.12
<i>Chitinophaga pinensis</i>	2 823	0.06
Others	149 380	3.09

Table 4.8 – Matches output by Kaiju for the sample taken at 5 269 m, surface level. The ten most abundant species are indicated.

Alteromonas (about 23, 16, and 7 % of the hits, respectively). Another important hit, only referred to as *unidentified plasmid* by Kaiju, also represented 18.6 % of the hits.

4.6 Discussion

4.6.1 Soil physico-chemistry

At 4 296 m, 4 782 m, and 5 056 m, the soil surface is very dry (< 1 % m/m), likely because of surface water evaporation during the day. This dryness poses a challenge for any microorganism living at the surface, already facing important thermal fluctuations and high UV fluxes. At 5 269 m the lower water content observed at 7 cm deep may be explained by the fact that the ground started to freeze around 6 cm deep, hence preventing liquid water from percolating deeper into the soil. On the other hand, the higher water content observed at the surface, compared to the other sampling sites, may be explained by the presence of snow and ice in the surrounding area.

In addition to dryness the ground surface shows some acidity at all sites. This acidity is probably due to the deposit of eolian sulfur, later oxidised to sulfuric acid. Surface measures of pH are similar to those already described on the Sairecabur (Pulschen et al. 2015) and on nearby volcanoes (Lynch et al. 2012; Solon et al. 2018). This acidity adds another constraint

for the potential microorganisms living there. The pH then increases with depth until it stabilises at, or near, neutrality.

Carbonates rarely occur in igneous rocks and Sairecabur does not produce them (Déruelle 1978; Déruelle 1982; Figueroa and Figueroa 2006), yet they were detected in all samples. The presence of carbonates in the soils there could be explained by (i) aeolian inputs, (ii) reaction of carbene dioxide with minerals (e. g. Risacher et al. 2003), or (iii) biomineralisation of carbon dioxide by microbes (e. g. Lowenstam 1981; Tobler et al. 2011; Anbu et al. 2016). Similar carbonate contents were found in almost all samples. The major outlier is the 37 cm deep sample, at 4 782 m. To explain this result, aeolian inputs of carbonates — possibly originating from the evaporites found at lower altitude in the Salar de Atacama (Carmona et al. 2000; Lowenstein et al. 2003) — could have been drained underground and accumulated over a soil hardpan at this depth. No carbonate excess was observed at the surface, therefore any infiltration of aeolian sediments would not be recent. At 37 cm deep, the soil was composed of unconsolidated sediments (figure 4.3) and no hardpan was observed, discarding this hypothesis. An alternate hypothesis involving the biomineralisation of carbonates by microorganisms could also quickly be discarded; no sign of biomass accumulation was found at this depth and the DNA concentration there is very low (figure 4.22). Conversely, the second major outlier found 19 cm deep at 5 056 m shows a sudden decrease in carbonate content. This drop may be an experimental artifact due to the incomplete reaction of the sample with HCl.

4.6.2 Environmental parameters

Previous data available

Weather data was previously recorded on the Sairecabur by two different teams.

Data from December 1991 to April 1994 was obtained from Michael Richter (Friedrich-Alexander-Universität Erlangen-Nürnberg) after the work of his former PhD student Dieter Schmidt (Technische Universität Dresden; Schmidt 1999). Data was collected as part of the German Research Foundation's former project *Climate-linked ecology: Atacama (Deutsche Forschungsgemeinschaft-Forschungsprojekt: Klimaökologie Atacama)*. Data from the following weather stations is compared to ours: *Jorquencal* (4 270 m), *Yareta* (4 920 m), and *Sairecabur* (5 820 m).

Data from October 2000 to September 2004 was obtained by personnel communication from Scott Paine (Harvard-Smithsonian Center for Astrophysics) and Daniel Marrone (University of Arizona). Their weather station was attached to the Receiver Lab Telescope (5 525 m; Marrone et al. 2004; Marrone et al. 2005).

Although measurements may vary from day to day depending on the weather, both datasets show patterns in the temperature (T) and relative humidity (RH) changes depending on the time of day, the time of year, and the altitude at which the measurements were taken.

Air measurements

A previous report of the mean summer/winter air temperature by Schmidt (1999) gives values of 6.6/0.1 °C (4 270 m), 2.1/−5.2 °C (4 920 m), and −4.8/−13.1 °C (5 820 m). This data also indicates that the temperature we recorded at 4 296 m (17.2 °C) is close to the maximum temperature (17.6 °C) ever recorded for the period 1991–1994 at 4 270 m. The other temperatures we recorded seem to fit the range of temperatures recorded in Schmidt's dataset. However, projecting the 5 269 m temperature (0.4 °C) to 5 525 m using the altitude gradient ($-0.75 \text{ K} \cdot 100 \text{ m}^{-1}$) determined by Schmidt (1999) gives a temperature globally warmer than those recorded by Paine and Marrone (personnal communication) at the same time of year (top limit of the upper quartile, or just above it).

Measured relative humidity values are in agreement with those reported by Schmidt (1999): mean summer/winter relative humidity values of ~50.4/26.3 % (4 270 m), ~55.8/27.5 % (4 920 m), and ~67.5/44.6 % (5 820 m), with mean daily amplitudes of 33.0–46.7 %.

Schmidt (1999) reports UV-A irradiance of ~40–54 $\text{W} \cdot \text{m}^{-2}$ and UV-B irradiance of ~2.6–3.4 $\text{W} \cdot \text{m}^{-2}$ at 5 500 m. Cabrol et al. (2014) report UV-B maxima of 1.3 $\text{W} \cdot \text{m}^{-2}$ in winter and 4.1 $\text{W} \cdot \text{m}^{-2}$ in summer — with a record of ~8.15 $\text{W} \cdot \text{m}^{-2}$ in January 2014. Even though the irradiance values we recorded for UV-A seem to be quite low, those recorded for UV-B are relatively high.

Soil measurements

Temperatures follow a day/night pattern, with a phase delay and amplitude decrease as the depth increases. The temperature increase observed after sunrise stops in the afternoon (14:00–17:00) when a 3-step decrease starts: a fast drop in temperatures is followed by a faster decrease after sunset until around midnight, when the decrease becomes really slow until sunrise.

Schmidt (1999) also reports this decline in temperatures in the afternoon, which is more pronounced at 15 cm deep than 2 m above the ground. The phenomenon is explained by anabatic winds going up the volcano, with increasing temperature and strength as the morning passes, creating turbulence and eventually convection when breaking up the atmospheric boundary layer. This convection cools down air in the warm wind (Schmidt 1999; Richter and Schmidt 2002).

At our 4 296 m site the sheltered probe seemed to be protected enough from the wind to only start to record the temperature decline after sunset.

Even though some depths preserved positive temperatures — 10 cm deep at 4 296 m, 15 cm deep at 4 782 m and 5 056 m (table 4.2) — and thereby enhanced microbial survival during the time of our measurements, temperatures vary all year long. Measurements at 4 270 m suggest that temperatures at 20 cm deep are most favourable for microbial growth and survival (−0.6–19.4 °C for the period 1991–1994, Schmidt 1999). However, at 4 920 m and above, the ground still experiences negative temperatures at 50 cm deep in winter, threatening microbial survival (Schmidt 1999).

Surface relative humidity values between 5 to 50 % were recorded. At 5 cm deep values are already close to saturation.

Theoretical air pressure

Air pressure was not recorded, but theoretical values were calculated at points of interest knowing latitude, longitude, altitude, and temperature (NOAA 1976; equation 4.1):

$$P_A = P_0 \cdot e^{\frac{-g_A \cdot M_{atm} \cdot H_A}{R^* \cdot T}} \quad (4.1)$$

P_A = atmospheric pressure at latitude, longitude, and altitude of point A

P_0 = atmospheric pressure at sea level (1.013 25 bar)

g_A = gravity acceleration at latitude, longitude, and altitude of point A

M_{atm} = atmospheric molar mass (0.028 964 4 kg·mol⁻¹)

H_A = altitude, above sea level, of point A

R^* = ideal gas constant (8.314 459 8 m²·kg·K⁻¹·mol⁻¹·s⁻²)

T_A = temperature at latitude, longitude, and altitude of point A

Using the minimum and maximum temperatures measured on the exposed ground (table 4.2), the atmospheric pressure at ground level is calculated to be 520–577 mbar at the 5 056 m sampling site ($g_A = 9.773 7 \text{ m} \cdot \text{s}^{-2}$; S25W070 GGMplus gravity acceleration map; Hirt et al. 2013). The temperatures recorded by Schmidt for the period 1991–1994 ($T_{\min} = -25.4 \text{ }^\circ\text{C}$, $T_{\max} = 48.4 \text{ }^\circ\text{C}$, Schmidt 1999) give a calculated air pressure of 455–547 mbar at 5 820 m ($g_A = 9.773 2 \text{ m} \cdot \text{s}^{-2}$; S25W070 GGMplus gravity acceleration map; Hirt et al. 2013).

4.6.3 Organic content

Loss on ignition

Surprisingly, all samples had LOI₅₅₀ values of about 1–2 %. These values are remarkably low for the 4 296 m site given the proximity of plants to the sampling site; one would have expected higher levels of organic content in the soil samples. Measurement of the total organic carbon — a more precise method, but also more expensive — contained in the samples, could be used as an alternative for future measurements.

Total lipid extracts

Similarly to LOI₅₅₀ values, TLE concentrations have somehow the same concentration range (50–100 µg·g⁻¹), except at 5 056 m where the concentrations are lower. TLE concentrations show no correlation with LOI₅₅₀ values, suggesting that the lipid fraction of organic content varies in each individual sample. The higher TLE concentrations observed at 4 296 m (the vegetated site) could be attributed to plant degradation products remaining at the surface or

associated with their root system and its associated microbiome. In a similar way, the elevated TLE concentration measured at 7 cm deep at the 5 269 m sampling site could correspond to an accumulation of lipids over the frozen lower soil.

Plant inputs

4 296 m Regarding the C₂₇ and C₂₉ *n*-alkanes, their lower surface concentrations observed at 4 296 m can indicate that (i) leaf wax inputs are negligible compared to root waxes, and/or (ii) surface deposits were drained at lower depth with the last precipitation. However, long chain *n*-alkanes are insoluble in water, so the second option seems less likely (Berger et al. 2003b, pp. 3:298 & 3:434).

At 17 cm deep — the maximum C₂₇ and C₂₉ *n*-alkanes concentration — no particular range of grain size is observed (figure 4.3). The similar amounts of submillimetric particles, which could have adsorbed molecules, are observed above this depth; yet no higher long chain *n*-alkanes concentrations are observed there. Below 17 cm deep, soil particles are coarser, which should help to drain the molecules to a greater depth. The high concentrations are then more likely to be the result of inputs by plant roots.

The high concentration observed at the surface probably results from the decomposition of regular plant material. Higher concentrations observed at deeper depth could be the results of microbial biosynthesis of phytane. Alternatively, phytane could percolate with decreasing concentration within the soil, with localised lower concentrations explained by phytane consumption by micro-organisms. Phytane is hydrophobic (NCBI 2018), and so are its precursors phytol (NCBI 2018) and chlorophyll (Berger et al. 2003b, p. 3:122), which does not favour the water-induced percolation hypothesis. An analysis of microbial population and concentration would help to refine the answer.

4 782 m No plants were present in the vicinity of the sampling site. This data suggests, that these long chain *n*-alkanes come from wind-blown material. The molecules deposited at the surface are more likely to be blown away again; their concentration is hence higher at 1 cm deep, where they are more protected. The rest of the profile suggests a slow percolation of the molecules deeper down, despite the hydrophobicity of the molecules. Interestingly, the *n*-alkanes' concentrations start to stabilise at 17 cm deep, where the percentage of clay-sized particles in the depth profile goes from a background of ~1.5–3.0 % up to 16 % (figure 4.3).

No particular environmental, nor physico-chemical measurement, correlates with the high phytane concentrations observed at 13, 19, and 37 cm deep. If phytane came from aeolian inputs of plant origin, a depth profile shape similar to the ones observed for the *n*-alkanes should be observed. Since that is not the case, the high phytane concentrations may result from microbial production of the molecules. An analysis of microbial population and concentration is necessary at this point to refine the answer.

5 056 m The background and maximum *n*-alkane concentrations are higher for this site than at 4 782 m. After sampling, a couple of plants were found hidden near the site; their

presence near the sampling site may explain the higher background concentrations, but not the higher concentrations observed below 5 cm deep. The increase/decrease of *n*-alkanes observed at 9–11 cm deep correlates with an increase/decrease of particles below 250 μm (40/23 %, figure 4.3). Such particles are also observed in proportions around 40 % at 1–3 cm deep, yet no increase in long chain *n*-alkane concentration is associated with them.

Phytane concentrations are again decoupled from long chain *n*-alkane concentrations. The peak concentration of phytane at 13 cm deep can not be linked to any previous measurement. Biosynthesis of phytane by micro-organisms in the soil is also possible but needs to be verified.

5 269 m No plants were found growing at this altitude, therefore a vegetal origin of the molecules, brought by aeolian inputs, is probable. The hydrophobicity of long chain *n*-alkanes can explain their low percolation in the soil, down to its frozen layer. Indeed, all *n*-alkanes up to C_{26} display an increased concentration at 7 cm deep, whereas higher chain lengths remain at constant concentrations through the depth profile (data not shown).

This last increase corresponds to the TLE increase observed at the same depth (figure 4.11) and may correspond to the accumulation of molecules over the frozen soil.

Summary Surprisingly, the three barren sites have very different depth profiles. In addition, the high concentration of long chain *n*-alkanes observed in the subsurface at 5 056 m can not currently be explained. The same statement goes for the underground phytane concentrations observed at 4 782 and 5 056 m.

Additionally, the concentration range of long chain *n*-alkanes decreases somehow progressively with altitude, except at 5 056 m. The presence of plants in the vicinity of the sampling site may explain this. Phytane concentrations are, on the contrary, similar at all four sites. It is thus difficult to make any conclusions about the plant part of hypothesis 7 (*Plant biomarkers will predominate at lower altitude, whereas microbial biomarkers will predominate at higher altitude*).

Degraded material and microbial inputs

4 296 m The decrease in concentration with depth suggests slow percolation in the soil despite the hydrophobicity of the molecules (Berger et al. 2003b, pp. 3:250, 298, 334, 438). The concentration maxima observed at the surface and at 11–13, 17, and 21 cm deep correlates with the concentration maxima observed for phytane. Therefore, a common origin of short chain *n*-alkanes and phytane is possible. Like for phytane, a microbial analysis of the soil would help determine if microorganisms have any influence on the short chain *n*-alkane concentrations.

4 782 m Again, the short chain *n*-alkanes have concentration profiles similar to the phytane profile, suggesting a similar origin. As already said for phytane, environmental and physico-chemical measurements fail to explain the presence of these high concentration peaks.

5 056 m Contrary to what was observed for the two previous sampling sites, only the 13 and 17 cm deep maxima in short chain *n*-alkanes are also observed for phytane, possibly indicating a different origin for the *n*-alkanes observed at 1 cm deep, than for the ones observed at 13 and 17 cm deep.

5 269 m The high concentrations in short chain *n*-alkanes observed at 7 cm deep compared to those already observed on the TLE (figure 4.11) and the phytane depth profiles. These data suggest an accumulation of molecules over the frozen soil.

Summary Some similarities between the short chain *n*-alkane profiles and the phytane profiles (figures 4.12–4.15) are observed. The overall concentration of short chain *n*-alkanes at each site seems to decrease with altitude, invalidating the microbial part of hypothesis 7 (*Plant biomarkers will predominate at lower altitude, whereas microbial biomarkers will predominate at higher altitude*). No global trend can be identified along all depth profiles; the short chain *n*-alkanes concentrations decreasing with depth at 4 296 m and 5 269 m (except at 7 cm deep), increasing at 4 782 m, and remaining somehow consistent at 5 056 m. This would indicate that, regarding short chain *n*-alkanes, hypothesis 6 (*Biomarker degradation will increase with altitude and decrease with depth*) is not verified.

Indices

CPI CPI values around 3 and higher are generally considered as an indication of higher plant inputs. This suggests that plant inputs are limited above 8 cm deep and above 10 cm deep at the 4 296 m and 4 782 m sites, respectively. Surface samples are the exception, for which low CPI values suggest a degradation of the molecules at the surface. The opposite trend is observed at 5 056 m, with relatively high CPI values for the whole profile (4.51–5.23), except for the values at 1–5 cm deep (1.12–3.14). This suggests that diagenesis is essentially limited to this zone close to the surface. Values are low at 5 269 m, with 2.60–2.62 near the surface and 1.84–2.00 at 3–7 cm deep. The harsher environmental conditions experienced at this altitude may explain why low values are observed throughout the whole depth profile.

ACL Regular inputs of plant leaf waxes at the vegetated site (4 296 m) can help preserve ACL, but the profiles observed at higher altitudes suggest that the degradation of odd-numbered long chain *n*-alkanes is limited. This decrease, which correlates with the increase in concentration for phytane (figure 4.15) and short chain *n*-alkanes (4.19) supports a higher degradation of the molecules at this specific depth. The biotic or abiotic origin of the diagenesis remains to be determined.

Moreover, no CPI or ACL values calculated for soil samples are similar to those calculated for plant and lichen samples. This indicates that *n*-alkane inputs are not dominated by any specific plant or lichen.

Summary Like for long chain *n*-alkanes, the origin of the short chain *n*-alkanes observed underground remains unclear. Whilst a microbial origin is probable, it remains to be confirmed.

No global decrease of CPI and ACL values is observed when increasing the altitude. Moreover, a decrease of CPI and ACL values at the surface compared to the values noted at 1–3 cm deep is observed at 4 296 m and 4 782 m. Yet the opposite trend is observed at 5 056 m and 5 269 m. These observations disprove hypothesis 6 (*Biomarker degradation will increase with altitude and decrease with depth*).

4.6.4 Plant and lichen samples

It seems that no soil samples, from any of the four sites, have had their *n*-alkane profile or their CPI or ACL indices significantly influenced by the any of the plants or lichens analysed.. This was even the case at 4 296 m, where shrubs of *Festuca orthophylla* were growing a few metres away from the sampling site.

The ACL/CPI ratio of plants and lichens does not follow a linear trend ($R^2 = 0.38$; figure 4.21). In contrast to most of the analysed plants, the CPI of lichens were all below 6.

4.6.5 DNA

General considerations The amount of reads identified at the species level by Kaiju for either of the following sites is not sufficient to interpret properly the data and draw definitive conclusions about the microbiome present. Moreover, the lack of consistency in the data output formats (all results vs species-level only results, percentage of matches vs absolute number of matches) also makes it challenging to interpret and to properly compare the different sets. The lower amount of hits for MetaPhlAn2 and Kraken compared to Kaiju can also be explained by the fact that they output the best matches with microbial clade-specific marker genes (Truong et al. 2015) and the exact matches against *k*-mers from a library of microbial genomes (Wood and Salzberg 2014), respectively, whereas Kaiju compares the six possible reading frames with annotated proteins from microbial proteins and complete genomes on NCBI (Menzel et al. 2016).

Supposing that the proportion of prokaryotic DNA is constant in all samples, microbial abundance in the soil could be proportional to DNA concentrations. Samples collected at 4 296 m will probably also contain an increased proportion of plant DNA compared to the other sites because of the presence of plants a few meters away from the sampling spot. When comparing the different sites, a continuous increase of DNA concentrations with depth was not observed. DNA concentrations also do not appear to decrease as the altitude of their collection site increases. This was observed in particular at 5 056 m, where the DNA concentrations are almost an order of magnitude higher than the ones observed at 4 782 m. Thus, the part of hypothesis 3 (*Microbial communities are more abundant and diverse with decreasing altitude and increasing depth*) dealing with microbial abundance can be disproved.

In addition, only three surface samples could be sequenced, with a low identification of the sequences. Hence, the part of hypothesis 3 dealing with microbial diversity can not be answered by this study. For the same reason, hypothesis 4 (*Environmental parameters and soil physico-chemistry have the most influence on the composition of microbial communities*) can not be answered by this study. The findings described by Thomas (2018) report a change of microbial community along the depth profiles at 4 296 m and at 5 056 m, with maximum diversity around the middle of each profile. Soil moisture did not seem to have an influence and pH seems to have a limited influence on microbial communities. Other data available is conflicted: Bryant et al. (2008) and Margesin et al. (2009) report a decrease of diversity with altitude, Siles et al. (2016) reports lower diversity at lower altitude, and Fierer et al. (2011) reports no significant change induced by altitude. Recent works also show that seasons and nutrients (Siles et al. 2016), and plant diversity (Ren et al. 2018) are key factors in shaping soil bacterial communities. Both studies also point out the role played by the soil pH.

4 296 m The high DNA concentrations observed at this altitude are likely due to the presence of nearby plants, their roots and associated microbiome increasing the DNA content in soil. The DNA concentration increases with depth following the thickening of the root horizon.

Both Kraken and Kaiju results indicate that bacteria and archaea are found at this site, with a higher proportion of bacteria. Amongst the 10 main species identified by Kaiju, 8 are bacterial and 2 are archaeal. Bacteria are soil bacteria, amongst which *Chitinophaga pinensis* stands out for being a biomass degrader. Both of the archaea detected (*Candidatus Nitrosotenuis cloacae* and *Candidatus Nitrosopelagicus brevis*) are ammonium oxidisers. These genera differ from the main ones reported by Thomas (2018): *Blastococcus*, *Nakamurella*, and *Jatrophihabitans*. Different methods were used, probably explaining the different results.

4 782 m The DNA peak observed at 5 cm deep does not correlate with any other data. The 11 cm deep maximum is shifted compared to the 13 cm one observed for phytane (figure 4.13) and short chain *n*-alkanes (figure 4.17). So far the presence of these two DNA concentration maxima can not be explained by the other the data sets.

No metagenomics data is available for this site.

5 056 m The DNA concentration peak observed at 13 cm deep corresponds to the peak also observed for phytane (figure 4.14) and short chain *n*-alkanes (figure 4.18), suggesting the presence of a microbial community there.

Bacteria and archaea are also both present at this site, again with a higher proportion of bacteria relative to archaea. The main bacteria genera identified by Kaiju are similar to the ones already observed at 4 296 m, consisting of soil bacteria. The biomass degrader *Chitinophaga pinensis* is present again, but a bacterium resistant to radiation (*Spirosoma radiotolerans*) is part of the main genera observed. The presence of this latter genera may be

due to the increase of UV radiation with altitude reported by Schmidt (1999). Both archaean ammonium oxidisers *Candidatus Nitrosotenuis cloacae* and *Candidatus Nitrosopelagicus brevis* are observed again. These results differ again from the ones reported by Thomas (2018) (*Blastococcus*, *Nakamurella*, and *Jatrophihabitans*), probably because of the different methods used.

5 269 m The high DNA concentration observed at 7 cm deep correlates with the high TLE (figure 4.11), phytane (figure 4.15), and short chain *n*-alkane (figure 4.19) concentrations reported above. The presence of phytane and of short chain *n*-alkanes could suggest a degradation of longer molecules, possibly due to the presence of an active microbial community, indicated by the higher DNA concentration. Alternatively, this DNA could also be degraded material.

Regarding the metagenomics analysis, the important quantity of Kaiju matches with enterobacteria suggest contamination of the sample. However, this barren site was higher than the potential grazing areas used by vicuñas and no animal scat was observed nearby when sampling. Sterile gloves and material were also used when sampling. When preparing the sample, clean and sterile material was used during the whole procedure, hands were cleaned and wearing sterile gloves. The only realistic possibility seems to be contamination by cat hair carried into the lab on clothing at the time of sample preparation. Despite the presence of enterobacteria, *Niastella* and *Chitinophaga* were nonetheless already identified in both previous samples; their presence at 5 269 m is therefore also probable. No previous sequencing data is available from Thomas (2018) for this sampling site, but it may be similar to the microbiome described at 5 056 m due to the similar environmental conditions that both sites experience. Other bacteroidetes were also reported by Costello et al. (2009) at a similar altitude on a nearby volcano.

4.6.6 General discussion

Soil samples were collected near the road leading to the Sairecabur caldera, at four different altitudes (4 296 m, 4 782 m, 5 056 m, and 5 269 m). Even though the sampling areas are different, they share some characteristics. The soil grains and their mineralogy are similar between all sites, despite their different origin (glacial deposit or lava field). Only the 4 296 m sampling site was surrounded by plants; yet, all sites contained long chain *n*-alkanes that are mainly attributed to plant leaf waxes. In a similar way, all sites contained short chain *n*-alkanes that are attributed to anthropogenic contamination, microbial inputs, or diagenesis of longer chains. Airborne transportation is probably how microbes ended up at these high elevations (Stres et al. 2013; Smets et al. 2016).

4 296 m

Samples were collected in a former glacial deposit turned into a grassland. This site served as a positive control for plant inputs in the soil. Despite the presence of nearby plants, the

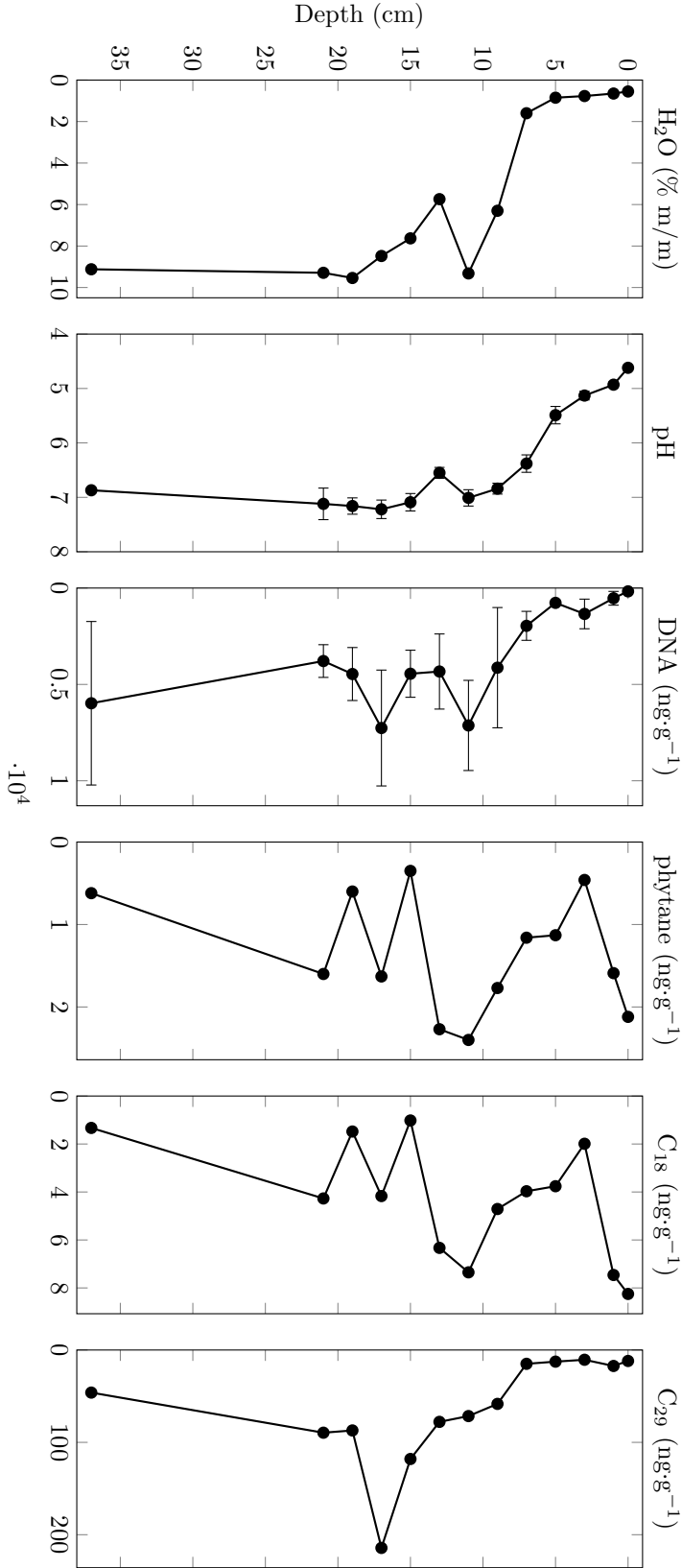


Figure 4.23 – Results summary for the 4 296 m sampling site.

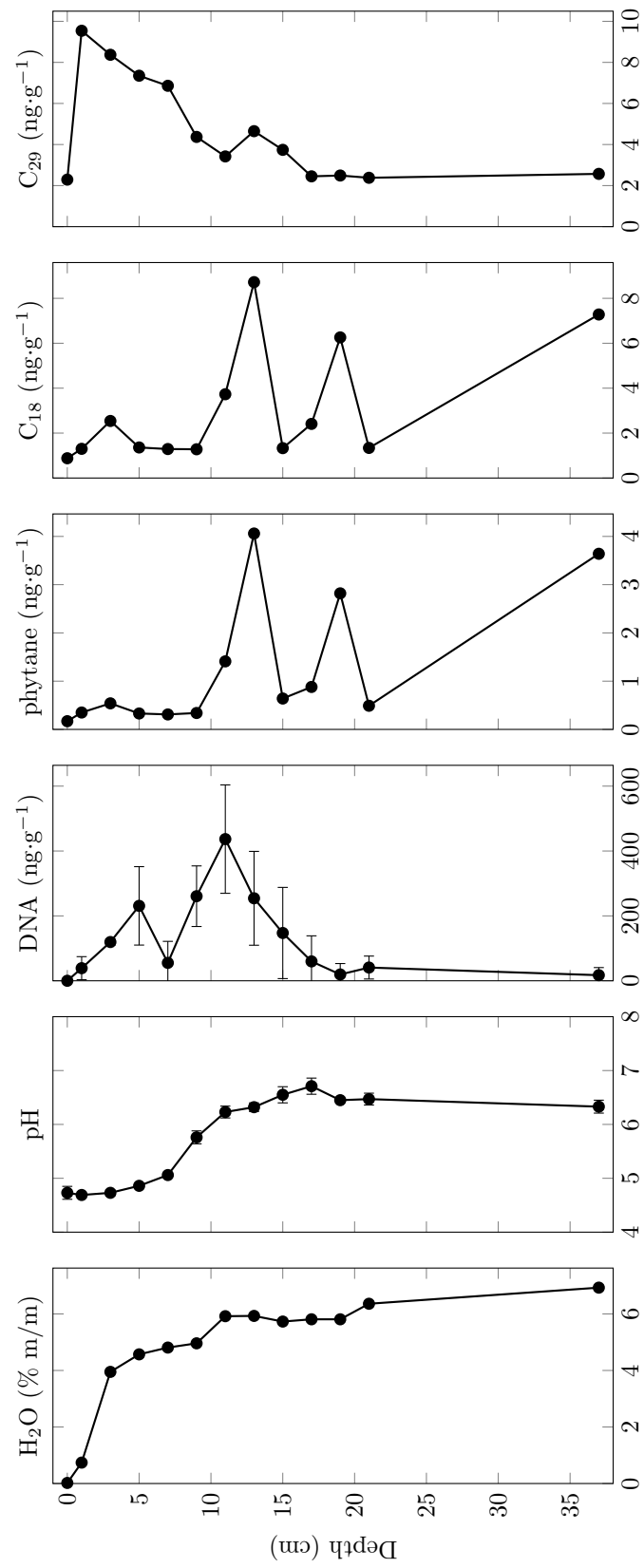


Figure 4.24 – Results summary for the 4782 m sampling site.

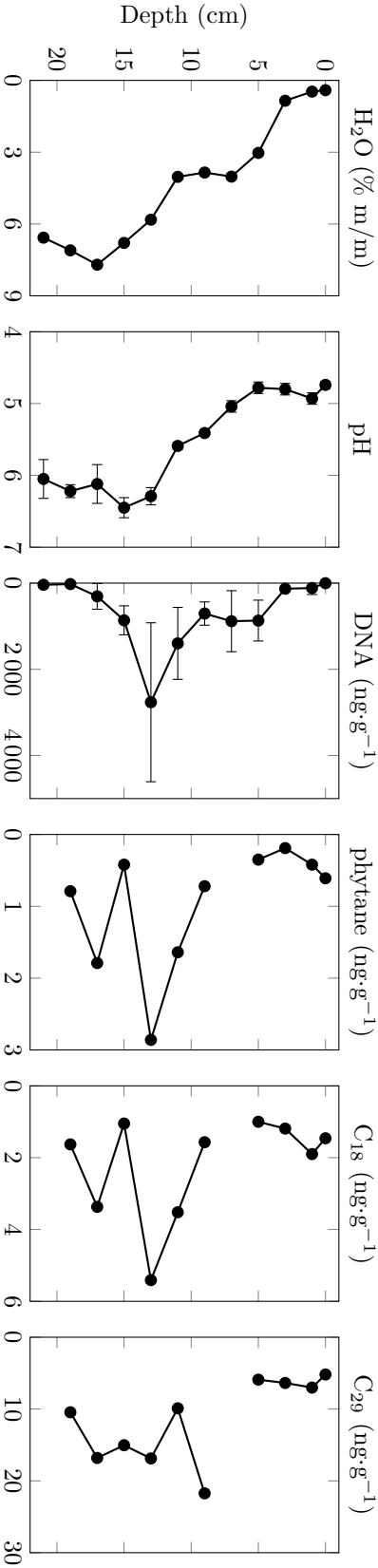


Figure 4.25 – Results summary for the 5 056 m sampling site.

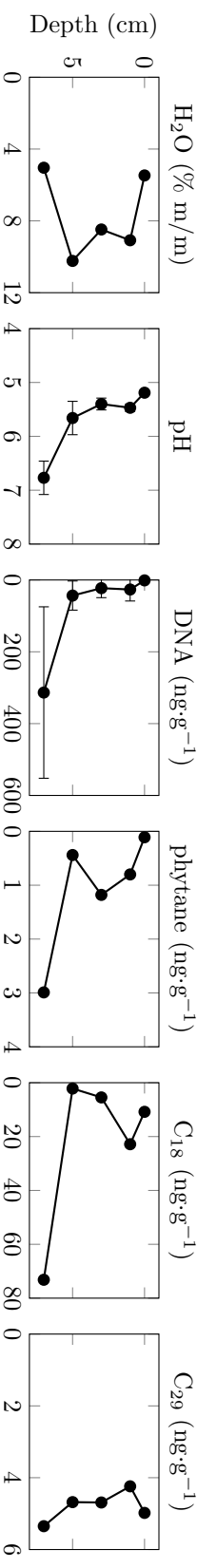


Figure 4.26 – Results summary for the 5 269 m sampling site.

samples collected at this site do not exhibit any enrichment trend in organic content and in lipids compared to the other sites.

The ground surface presents challenging survival conditions for organisms: extreme daily temperature variations, high UV fluxes, particularly low water content, and an acidic pH. Still, T and RH are within the range of those previously reported (Schmidt 1999). Organics show signs of degradation at the ground surface, but it is unclear whether it is due to the environmental conditions or to a microbial activity.

During depth profiling, a plant root system appeared at 9 cm deep and below. At this depth, daily T remain positive at this time of the year (early May), the pH is neutral, and the water content is above 6 %. The influence of this root network may be visible on the long chain odd-numbered *n*-alkanes and on the DNA concentrations. Microbial communities are usually associated with plant roots, even at extremely high altitude (Angel et al. 2016b). However, the proportion of plant vs microbial DNA can not be assessed in these samples due to failure of the metagenomic study.

The main genera of microorganisms observed in the surface soil sample are different than the ones reported by Thomas (2018). The difference in targeted genes and sequencing strategy may explain this difference.

4 782 m

Samples were collected in a barren former glacial deposit. The dry surface quickly became humid with depth, whereas the acidic pH took longer to increase to near neutral.

Long chain *n*-alkane depth profiles suggest a slow percolation of the molecules underground at this site. A DNA concentration peak reaching its maximum concentration at 11 cm deep almost pairs with the short chain *n*-alkane and phytane peaks, possibly indicating signs of microbial activity. At the time of sampling, temperature stayed above zero and the RH was close to saturation, thus also presenting conditions to support life. No microbial mat was observed.

If the environmental conditions are similar to those previously reported in the area by Schmidt (1999), no data from a nearby area is available to compare the geoorganic chemistry results. No DNA sequences were obtained for this site either, preventing again comparison with the results reported by Thomas (2018).

5 056 m

Samples were collected in a barren former lava field with a dry and acidic surface. The environmental conditions experienced at the surface could be similar to those of Mars during the Noachian period.

The main genera of microorganisms observed in the sequenced near-surface sample differ again from those reported by Thomas (2018), probably because of the difference in targeted genes and sequencing strategy. These genera are part of the *Bacteroidetes* phylum for bacteria and of the *Thaumarchaeota* phylum for archaea. If mostly *Actinobacteria* and *Chlo-*

roflexi have been reported in similar sites — nearby volcanoes, similar altitude — (Costello et al. 2009; Lynch et al. 2012; Bull et al. 2018; Thomas 2018), *Thaumarchaeota* correspond to what was previously observed (Lynch et al. 2012).

A high DNA concentration observed at 13 cm deep correlates with the presence of short chain *n*-alkanes and phytane, possibly indicating the presence of an active microbiome. The pH (~6) and the saturated RH both stabilise at this depth and both are more compatible with sustaining life. However the low water content (~6 %) and the temperature barely remaining above 0 °C at this depth at this time of the year (late April) allow for only limited microbial growth. No signs of long chain *n*-alkane diagenesis are observed at this depth.

Accumulation of short chain *n*-alkanes and phytane at 17 cm deep can not be explained by any of the measurements taken during this study.

Also, contrary to what was previously described in the literature (Villagrán et al. 1981; Richter 1996; Richter and Schmidt 2002; Richter 2003), some plants were found to be able to grow at this altitude.

5 269 m

Samples were collected in a barren former lava field, down to 7 cm deep, where the soil was frozen and could not be dug deeper.

Analyses revealed higher concentrations of phytane, short chain *n*-alkanes, and DNA at 7 cm deep, compared to the rest of the depth profile. At this altitude and at this shallow depth, these results could indicate the presence of degraded organic material. Nevertheless, despite the challenging environmental conditions experienced at this depth, the ground could experience transient liquid water because of its proximity to the surface. These results could then suggest a microbial biodegradation of the molecules at 7 cm deep, as supported by the finding of microbial DNA there, mostly originating from *Actinobacteria* (Thomas 2018). A deeper genomic analysis of the DNA present at this depth would help to confirm or reject this interpretation.

The sequencing results from the surface sample, although contaminated, seem to indicate a similar microbiome than the one observed at 5 056 m. However, the contamination forbids to draw definitive conclusions for this sample.

4.7 Relevance to Mars

Air temperature and relative humidity are mild compared to Mars. On Mars, air measurements around 1.5 m above the ground range record temperatures from ~ −86 to ~5 °C (Hess et al. 1976b,a, 1977; Harri et al. 2014a), and between ~0 and ~49 % for relative humidity (Harri et al. 2014a). In comparison, the values recorded on the Sairecabur range from ~ −25 to ~ 9 °C and from below 5 % RH to saturation (100 %) at 5 820 m (Schmidt 1999). On Mars, temperature and relative humidity variations also follow diurnal and seasonal patterns. Observed surface temperatures are 181–295 K (−92–22 °C; Spanovich et al. 2006; Zent et al. 2010) and relative humidity ranges from below 5 % to saturation (Zent et al. 2010). At

5 820 m on the Sairecabur, the surface values are ~ -25 to ~ 48 °C (Schmidt 1999). In low atmospheric dust conditions, UV-A flux is up to ~ 19.5 W·m² (Smith et al. 2016), which corresponds to what we recorded at our sampling site. The current atmospheric pressure on Mars is 6.6–102 mbar (Schofield et al. 1997; Smith 2008; Taylor et al. 2010; Haberle et al. 2014; Harri et al. 2014b; Martínez et al. 2016; Pla-Garcia et al. 2016). However, 4 Ga ago, when the planet is thought to have had suitable conditions to develop life, atmospheric pressure on Mars would have been above 0.5 bar (Kurokawa et al. 2018). Therefore, the Sairecabur is an excellent environmental analogue for a Noachian Mars, at a time when the temperature and pressure started to drop.

Aliphatic and aromatic molecules have recently been found in martian samples up to 3 Ga old, without any evidence for a biological origin (Freissinet et al. 2015; Eigenbrode et al. 2018). Lipids produced on Earth and/or their degradation products can be used as biomarkers. In some cases they have also been found in oils and bitumens of Archean age (Dutkiewicz et al. 1998; Brocks et al. 1999) and even helped to identify their specific producers (Brocks et al. 2003b,a). The concentration profile of small molecules, like *n*-alkanes, can vary depending on their production by biological or abiotic processes (e. g. Georgiou and Deamer 2014). For these reasons, these molecules have been considered as targets of interest when searching for life traces on Mars (Parnell et al. 2007; Westall et al. 2015).

Finally, the site studied at 5 269 m, potentially exposed to transient liquid water and maybe hosting living microorganisms, can be compared to surface aquifers on a Noachian Mars, hypothetically able to sustain life by providing some liquid water between a dried surface and a near-subsurface frozen water reservoir. If future investigations at the 5 269 m site show that the organic material present is just some degraded material accumulated in the frozen ground, then modern-day recurring slope lineae (RSL) on Mars could also serve as a comparison. If the fluid creating the RSLs contain any organic material, they could be able to enrich their outflow channel in organics and thus represent valuable astrobiological targets for future missions to Mars.

4.8 Conclusion

Samples were collected following both an altitude and a depth gradient in an extreme environment. The highest altitude sites experience cold temperatures and extreme daily temperature variations, high UV irradiance, extreme dryness, and low atmospheric pressure that make these sites analogues for a Noachian Mars, a time during which the planet progressively lost its habitability.

Investigating lipid biomarkers at the different sites revealed plant inputs higher than expected, especially at high altitude. Still, the hypothesis "*Plant biomarkers will predominate at lower altitude, whereas microbial biomarkers will predominate at higher altitude*" is partly invalidated because microbial biomarkers do not follow the expected trend. Some lipid variations observed in the depth profiles could not be properly explained by either the environmental and physico-chemical properties of the soils, nor by their biological content.

Hence, the hypothesis "*Biomarker degradation will increase with altitude and decrease with depth*" is not verified. The study of other biomarkers, like carotenoids (Pulschen et al. 2015), or the sequencing of specific microbial genes associated with metabolism — as part of a future study, could still refine our knowledge of the repartition of the different microbial communities in the ground

The attempt to have a deeper insight into the genomic composition of the different microbial communities living in the soil failed. This made the interpretation of lipid biomarkers that could be attributed to microbial activity more difficult. The absence of enough metagenomic data prevented testing the hypothesis "*Environmental parameters and soil physico-chemistry have the most influence on the composition of microbial communities*", the DNA concentrations obtained were sufficient to demonstrate that the hypothesis "*Microbial communities are more abundant and diverse with decreasing altitude and increasing depth*" is at least partly incorrect.

In regards to what an ancient Mars could have been, the presence of DNA at our site — and the confirmation of the existence of microbial communities by Thomas (2018) — suggest that Mars was still able to host life for some time, during its past.

Chapter 5

Iceland

‘Life expands to new territories. Painfully, perhaps even dangerously. But life finds a way.’

Michael Crichton, *Jurassic Park* (1990)

Contents

5.1	Introduction: The Hverfjall crater	108
5.2	Rationale	110
5.3	Hypothesis	111
5.4	Methods	111
5.5	Results	112
5.6	Discussion	115
5.7	Relevance to M ars	117
5.8	Conclusion	118

Abstract

This chapter presents results from a fieldwork carried out as part of the Nordic-EAC-COST Summer School *Biosignatures and the Search for Life on Mars* which took place in Iceland in July 2016. This study aimed to determine if aeolian inputs could be the main driving factor for seeding life in an extinct volcanic crater in Iceland. After analysing a first set of samples for this project, more samples were collected, and all were brought to Glasgow for further analyses.

Samples were sampled across the Hverfjall crater, analysed for microbial activity directly in Iceland; lipid analysis and pH measurement followed in Glasgow. The interpretation of the results was challenging and if wind could play a role in bringing life forms into the crater, its influence can not be observed distinctly.

5.1 Introduction: The Hverfjall crater

Hverfjall is considered as textbook example of a tuff ring volcano (Þórarinnsson 1952b). It is located in the Krafla fissure swarm, within the Northern Volcanic Zone (figure 5.1, inset). It is located about 50 km inland from the north coast of Iceland and 2 km west from Lake Mývatn, Hverfall has a crater ~150 m high, ~10 m deep and ~1 km wide.

The volcano it is believed to have been formed during the Hverfjall Fires around 500 BC, either by a short phreatic explosive eruption (Þórarinnsson 1952a,b; Thorarinnsson 1979), or by a more prolonged phreatomagmatic eruption (Mattsson and Höskuldsson 2011). This age estimation — based on tephrochronology — was later supported by radiodating (^{14}C) of a tephra layer from an Hekla eruption — H₃, located just below the Hverfjall layer — which was dated at 2820 ± 70 years BP (Þórarinnsson 1962) and 2879 ± 34 years BP (Dugmore et al. 1995). The Hverfjall Fires consisted in a fissure eruption with different vents, this fissure passing though the current location of the tuff ring. This volcanic episode had three major phase (the Hverfjall fallout, the Jarðbaðshólar fallout and lava flows, and the Hverfjall base surges; Mattsson and Höskuldsson 2011).

Hverfjall fallouts are relatively poorly sorted and fine grained particles, whereas those produced by the surges are poorly sorted and smaller. Tephra particles have rugged/blocky shapes with low vesicularity. Large fragments can have smaller particles adhering to them and hydration cracks. These features are characteristics of particles generated by phreatomagmatic fragmentation. Tephra contain olivine, plagioclase, clinopyroxene and magnetite phenocrysts. Glass is also present within the deposits (Mattsson and Höskuldsson 2011).

The crater was later completely covered by basaltic tephra from the 1477 Kverkfjöll eruption and, to a lesser extent, from the 1724–1729 Mývatn Fires eruption (Thorarinnsson 1979).

Groundwater flows of cold water have been reported north and south of the crater, flowing from east to west towards the Lake Mývatn (Ólafsson 1979). The only process involving water visible in the crater is the formation of gullies; they are likely formed by landslides

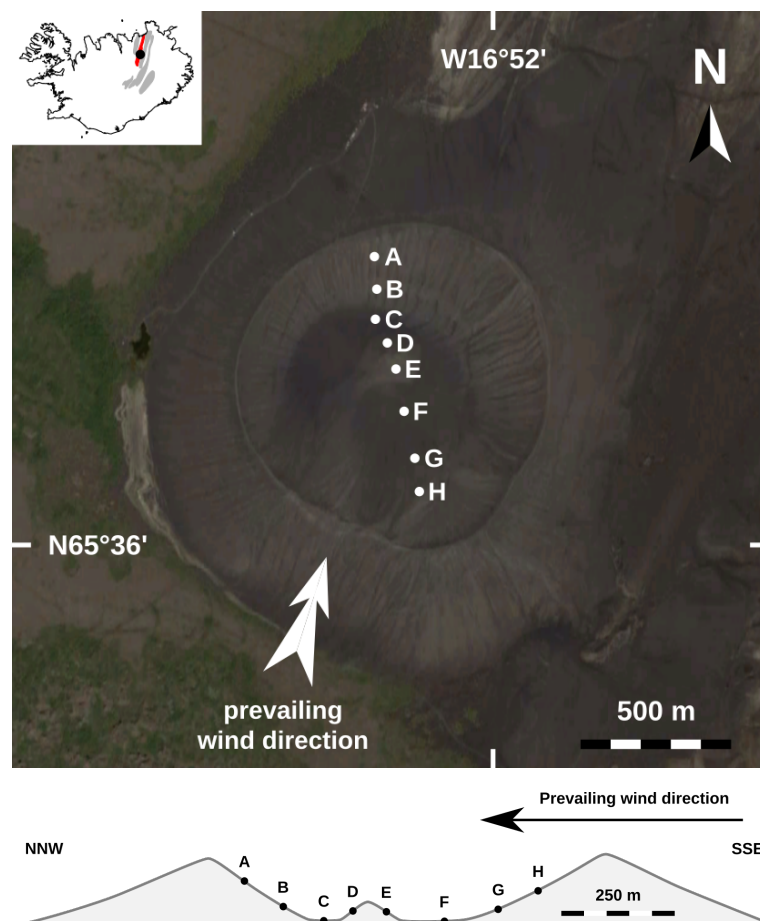


Figure 5.1 – Location of the different sampling points across Hverfjall's crater: top view (top) and cross-section schematics (bottom). The prevailing wind direction is indicated after Björnsson and Jónsson (2004). The top right insert (adapted from Mattsson and Höskuldsson 2011) shows the location of Krafla fissure swarm (red) within the Northern Volcanic Zone (grey). Satellite image modified from Google Earth, cross-section modified from Þórarinnsson (1952a).

caused by rain water.

5.1.1 Climate

Climatic conditions in the Mývatn area are considered to be 'fairly typical for [...] highlands that are at some distance from the coast' (Björnsson and Jónsson 2004). Climatic changes there are connected to the oceanic conditions off the northern coast of Iceland, but in a pattern different from the one associated the North Atlantic Oscillation (Ólafsson 1999; Björnsson and Jónsson 2004).

Throughout the year, mean daily temperatures means can range from -20 to 20 °C, but mean monthly temperatures are milder, only ranging from -5 to 10 °C. The fraction of days receiving at least 0.1 mm of precipitation varies from ~ 0.3 (in May) and ~ 0.45 (in October and November). For the period 1971–2000 the mean daily precipitation range is 0.5 – 5.5 mm \cdot day $^{-1}$. Precipitation appear mostly as rain from May to September, and as snow from September to May. Prevailing winds (indicated on figure 5.1) come from the south,



Figure 5.2 – Example of plants found in Hverfjall's crater

other major wind come from the northwest and the east. Northwesterly winds are mainly observed during summer evenings and are possibly associated with sea breeze (Björnsson and Jónsson 2004).

5.1.2 Life

Despite its age, the interior of Hverfjall contains only sparse vegetation with low diversity (figure 5.2). Plants are mainly present in the gullies and at the bottom of the crater. On the contrary, the area on the western side of the volcano, near Mývatn Lake, is more vegetated and up to 246 species of vascular plants have been identified there (Steindórsson 1932; Jónasson 1937; Löve and Löve 1948; Jónasson 1972).

Colonisation of the crater could be triggered by deposits from the wind, animals, insects, rain droplets, or water streams (gullies). So far, wind dispersal seems to be the most studied mechanism for molecular, microbial, and vegetal material (Beyer et al. 2000; Kuparinen 2006; Scheringer 2009; Stres et al. 2013; Heydel et al. 2014).

As not particular part of the crater contain more plants nor sign of animal passage, the plant density and the potential animal contaminations are considered to be homogeneous within the crater.

Access to the crater rim from its northern side is permitted, but access to within the crater is restricted to scientists only. Despite this, signs of more frequent human passage were present there. For simplification purposes, anthropogenic contamination is considered homogeneous within the crater.

5.2 Rationale

Craters, whether formed by volcanism or meteorite impact, can contain ecosystems which are (somewhat) isolated from the outside environment by the crater rim (Cockell and Lee

2002). Biological seeding of these environments happens through underground migration, water flows, aeolian inputs, as well as animal and anthropogenic contamination. All these factors can be considered to seed life homogeneously throughout the crater, but aeolian inputs may follow the prevailing wind direction.

Rather than focussing on an environmental analogue for Mars, attention is brought to a landscape analogue.

5.3 Hypothesis

Hypothesis 7: *Biological seeding of the Hverfjall crater is mostly triggered by aeolian inputs and follow the prevailing wind direction.*

5.4 Methods

5.4.1 Sampling strategy

Sampling site

Hverfjall is considered as textbook example of a tuff ring volcano (Þórarinnsson 1952b). It is located in the Krafla fissure swarm, within the Northern Volcanic Zone (figure 5.1, inset).

Located 2 km west from Lake Mývatn, Hverfall has a crater ~150 m high, ~10 m deep and ~1 km wide; it is believed to have been formed during the Hverfjall Fires around 500 BC, either by a short phreatic explosive eruption (Þórarinnsson 1952a,b; Thorarinsson 1979), or by a more prolonged phreatomagmatic eruption (Mattsson and Höskuldsson 2011). This estimation — based on tephrochronology — was later supported by radiodating (^{14}C) of a tephra layer from an Hekla eruption — H₃, located just below the Hverfjall layer — which was dated at 2820 ± 70 years BP (Þórarinnsson 1962) and 2879 ± 34 years BP (Dugmore et al. 1995).

The crater was later covered by basaltic tephra from the 1477 Kverkfjöll eruption and, to a lesser extent, from the 1724–1729 Mývatn Fires eruption (Thorarinsson 1979).

Groundwater flows of cold water have been observed north and south of the crater, flowing from east to west towards the Lake Mývatn (Ólafsson 1979).

Tephra samples

Samples were collected on 12th July 2016 along a north-south transect across the crater. The initial sample set (sites B, D, E, and G) was collected under the supervision of Dr David Cullen (Cranfield University) and Prof. Wolf Geppert (Stockholm University), as part of a group project suggested by myself and involving Dr Bo Byloos, Diana Carlsson, Dr Victoria Hartwick, Laura Kotomaa, Đorđe Marković, Dr Carolina Muñoz-Saez, Alex Price, Kaire Veeperv, and Dr Michael Wong. To extend the transect profile, I collected additional samples at sites A, C, F, and H.

For each site duplicate soil samples — composed of a mixture of fine and coarse dark sands — were collected 10 cm below the surface in the same hole. This depth is enough to provide a buffer against surface temperature changes and to keep relative humidity close to saturation (see previous chapters), whilst protecting the soil from new surface contamination.

The spoons used for collecting the samples could not be sterilised prior to the collection of samples, because ethanol could not be obtained prior to sampling. To reduce cross-contamination between sampling sites and to condition the trowel used for collecting the samples, it was repeatedly stuck in the ground, at every site and near the sampling spot, before collecting the samples.

Following the sample collection, triplicate measurements of ATP concentration was performed by Dr David Cullen at the University of Akureyri, as previously described (Barnett et al. 2012; Amador et al. 2015; Gentry et al. 2017). Samples were then brought back to Glasgow for lipid analysis and pH measurements (see chapter 2 for all experimental protocols).

Sampling and export permits were obtained from the Environment Agency of Iceland (Umhverfisstofnun) and from the Icelandic Institute of Natural History (Náttúrufræðistofnun Íslands), respectively.

5.4.2 Planned analyses

Two types of biomarkers are considered in this study: Adenosine-5'-triphosphate (ATP) and lipids. ATP were analysed directly in Iceland, near the field; after exporting the samples to Glasgow, lipids were extracted from them and analysed. The samples' pH was also measured there. Details about the methodology used can be found in chapter 2.

5.5 Results

5.5.1 ATP

ATP serves for storing energy in all cells (Knowles 1980) and can thus be used as a proxy to estimate extant microbial life (Fairbanks et al. 1984).

Mean ATP concentrations for each site are reported in figure 5.3. They indicate a wider range of concentrations for dry sites (107–437 fmol·g⁻¹) than for gullies (132–196 fmol·g⁻¹).

5.5.2 Lipids

Lipids and indices derived from their concentrations can provide an indication about their source and degradation state (see Castañeda and Schouten 2011 for a review). Focus is given on *n*-alkanes here, as they are commonly used biomarkers and serve both aforementioned purposes.

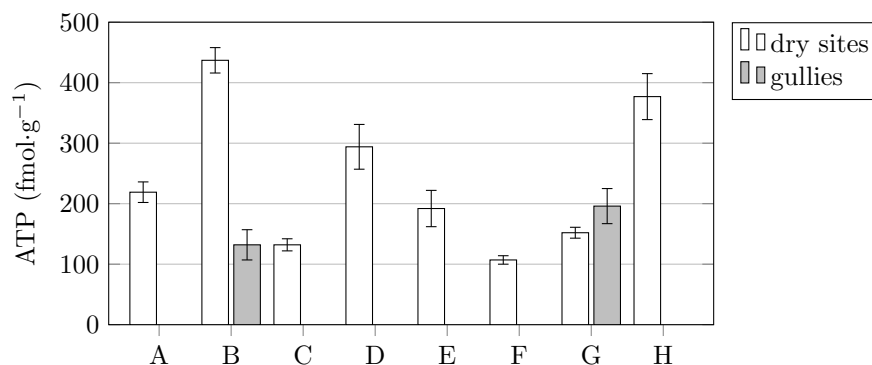


Figure 5.3 – ATP levels measured across the crater.

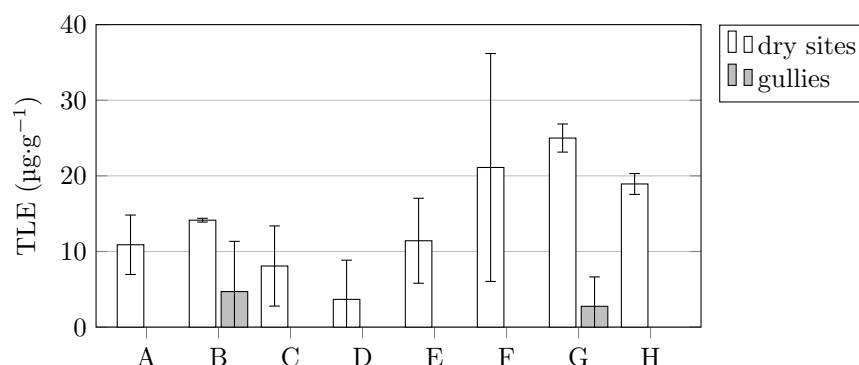


Figure 5.4 – TLE concentrations measured across the crater.

Total lipid extracts

Mean concentrations of total lipid extracts (TLE) are reported for each site on figure 5.4. Again, the concentration range observed at dry sites ($3.7\text{--}25.0\ \mu\text{g}\cdot\text{g}^{-1}$) is wider than the concentrations observed in gullies ($2.8\text{--}4.7\ \mu\text{g}\cdot\text{g}^{-1}$).

n-alkanes

The range of observed *n*-alkanes was $\text{C}_{18}\text{--}\text{C}_{35}$. Mean values were calculated from the duplicate samples.

Plant waxes usually contain odd-numbered long-chain *n*-alkanes. The main representative molecules are the C_{27} , C_{29} , and C_{31} *n*-alkanes. The sum of their percentage can be used as an indication of plant inputs (figure 5.6). All sites, except site A, have percentages around 35–55 %; site A has 15.2 %.

Indices

The average chain length (ACL) and carbon preference index (CPI) were calculated from the previous *n*-alkanes concentrations and are plotted in figure 5.7 and figure 5.8, respectively. Both indices can indicate a degradation of *n*-alkanes, and therefore of organic material.

Most ACL values (figure 5.7) are 29.0–29.4, with one lower value at site A (28.2) and

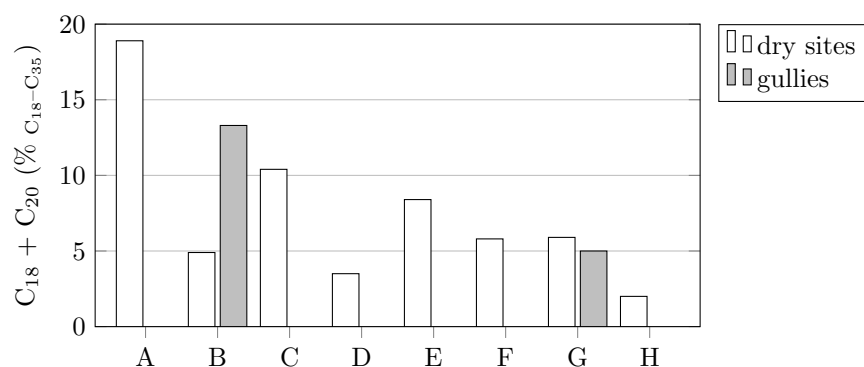


Figure 5.5 – Combined percentage of even-numbered short chain *n*-alkanes (C_{18} and C_{20}) levels measured the crater.

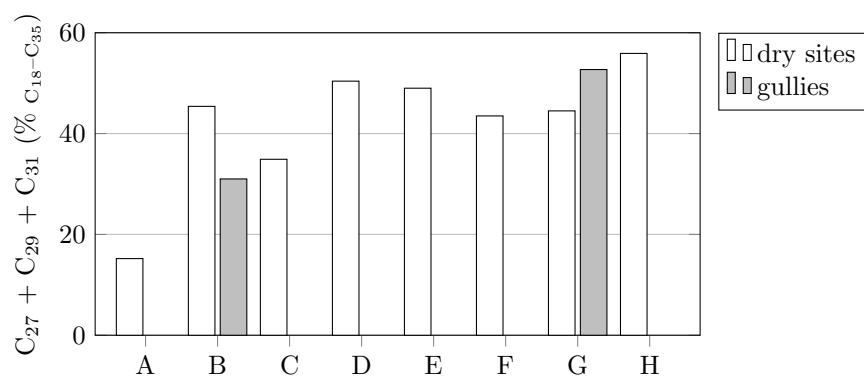


Figure 5.6 – Combined percentage of odd-numbered long chain *n*-alkanes (C_{27} , C_{29} , and C_{31}) across the crater.

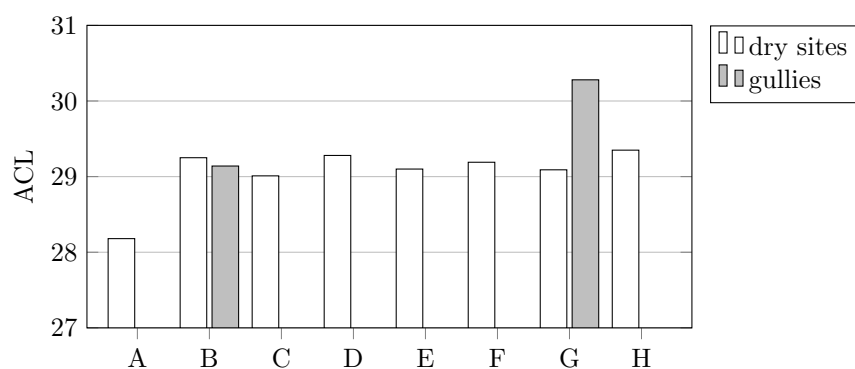


Figure 5.7 – Average chain length (ACL) values across the crater.

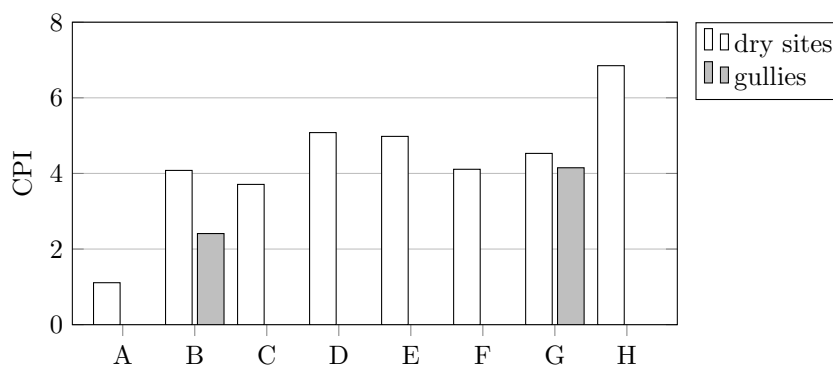


Figure 5.8 – Carbon preference index (CPI) values across the crater.

one higher value at site G (gully, 30.3).

Most CPI values (figure 5.8) are around 4. Lower values are observed at site A (1.1) and B (gully, 2.4). Higher are observed at site D (5.1), E (5.0), and H (6.9).

5.5.3 pH

Triplicate measurements of the samples indicate values closed to neutrality for all sites. Sample G (dry site) has a pH value of 7.0, all the others, dry sites or gullies, have pH values of 7.3–7.5.

5.6 Discussion

ATP and lipid data are discussed here in terms of trends, rather than definitive values, due to the absence of a robust decontamination protocol whilst collecting the samples.

The method used for measuring bioluminescence also measured the total ATP concentration, not only intracellular ATP. However, intracellular ATP is expected to be more abundant than environmental ATP, despite the persistence in the environment of environmental ATP (Fajardo-Cavazos et al. 2008). Microbiota — probably receiving microbial inputs from the same sources — are considered to have similar compositions at all sites; ATP can be thus considered as a reasonable proxy for microbial concentration.

According to the wind-driven seeding hypothesis, ATP concentrations should decrease along the north-south transect, because the southern rim would protect the southern side of the crater against the wind. Such pattern is not observed. Turbulence created by the wind passing just over the rim could potentially enrich site H in microbial content, just inside the southern edge of the crater. Additionally, the lower concentrations observed at sites A, B (gully), and C could be the result of local conditions or soil properties inhibiting microbial growth. Amongst potential conditions, pH can be discarded as an influencing factor, as there was little variation across the whole transect. At this point, additional data are needed to help interpret the ATP data.

Regarding lipid data, TLE concentrations can be a proxy for organic matter inputs. As

no plants nor other "heavy" organic producers were present on the sampling spot, the lipids observed are likely to have been deposited or transported by the wind, as these molecules can be transported across long distances by this mean (e. g. Simoneit 1977; Gagosian and Peltzer 1986; Bendle et al. 2007; Schreuder et al. 2018). The highest concentrations are observed on the southern flank of the crater (dry sites G and H). This can be interpreted either as an enrichment of these sites, or as a depletion at the other sites. However, the low TLE concentration observed at the gully at site G suggests that organic material may be drained down; the same trend is observed at site B. Hence, TLE concentration observed at dry sites G and H are more likely to correspond to a preserved original state whilst the others have seen their material removed. However, if rain helps to drain the lipids — especially in gullies, as stated above — it should affect all dry sites in the same way, which is not what is observed. Another possibility is that the molecules have been blown away by the wind; the southern edge of the crater would then protect the dry sites G and H from the wind influence, whereas all other sites are more exposed, the transition zone being around site F.

Looking more specifically at the lipid data, odd-numbered long chain *n*-alkanes are representative of plant matter (Eglinton and Hamilton 1967; Jetter et al. 2006). A low proportion of these molecules is observed at site A and to a lesser extent at site B (gully) and C (figure 5.6). Plants were spread homogeneously throughout the crater, indicating that shorter *n*-alkanes may represent a higher proportion of the total *n*-alkanes fraction.

The opposite trend is observed for even-numbered short chain *n*-alkanes at the same sites (figure 5.5). These molecules have been associated with molecular diagenesis (Goutx and Salot 1980; Eckmeier and Wiesenberg 2009; Wiesenberg et al. 2009) and with polluting anthropogenic activities (Simoneit 1984; Lichtfouse et al. 1997; Brocks et al. 2008).

Postulating that long chain *n*-alkane inputs are homogeneous throughout the crater, their degradation can be assessed with the indices ACL and CPI. Whilst ACL indicates an overall shortening of *n*-alkanes, CPI indicates a shift in the odd/even *n*-alkane ratio. Site A exhibits signs of molecular diagenesis by a reduction of both indices. A decrease in CPI only, not ACL, is observed for the gully from site B. This profile duality at site B, between the dry site and the gully, could be explained by the shorter molecules being more easily flushed by water into the gully from the dry site (like the light rain, the day preceding the sampling), thus keeping a low amount of short chain *n*-alkanes at the dry site.

Data obtained from *n*-alkane analyses indicates that molecules are degraded at site A and possibly also at site B (gully) and C. At these sites lower ATP concentrations were also observed. Hence the same deleterious conditions may induce the *n*-alkanes degradation and the lower ATP concentrations.

As stated above, pH is constant and neutral along the transect, and can therefore be discarded as the potential cause of the degradation. These sites are all located on the northern side of the crater, which is more exposed to sun-light and to tourist inputs, and steeper than the southern side. However, site B (dry site) is not affected, suggesting that another cause is responsible for the degradation. The reason why dry site B is not affected could nonetheless be explained by the following scenario: the cause of lipid degradation at site A could

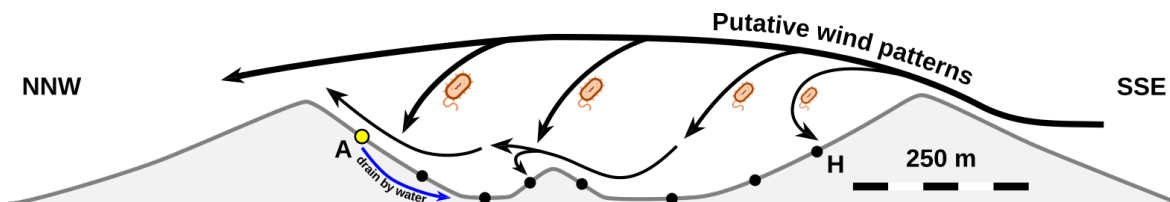


Figure 5.9 – Putative factors influencing the repartition of biomarkers at the Hverfjall volcano. The higher wind flow releases microbial inputs — increasing towards the northern side — whilst ground winds removes the lighter molecules. The unknown factor (possibly of physico-chemical origin) inhibiting microbial growth and degrading lipids at site A (yellow dot) is drained by water in the gullies and eventually reaches the bottom of the crater.

eventually be drained downhill in the gully system through site B; the gullies' content is eventually released at site C. This scenario would also explain the progressive attenuation of the degradation phenomenon. Other factors, like increased salt Rath et al. 2016 or heavy metal (e.g. Fritze et al. 2000; Khan et al. 2010) concentrations, have also been reported to negatively affect microbial growth activity, although they are mainly observed in polluted areas, which not the case here.

To summarise, the prevailing wind direction passing over the volcano may be responsible for the increased microbial colonisation, and the depletion of certain lipids, on the northern side of the crater. Conversely, wind turbulences at site H may cause the accumulation of lipids there. Drainage by water may cause the decrease of lipids in gullies, whilst having no influence on the microbiota living there. An unknown factor, limiting the development of microbes and causing the organics to degrade at site A, could run down the slope via the gully sampled at B, and end up in the basin at site C (figure 5.9). The unknown factor could have a physico-chemical origin (unusual mineralogy, presence of specific ions in the ground) in that environmental conditions would be similar in to whole crater; wind and winter sunlight exposure could also have an influence.

5.7 Relevance to *Mars*

Craters are ubiquitous on Mars, as a result of both volcanoes and hypervelocity impacts.

On Earth, hydrothermal systems, providing heat and nutrients to microorganisms, have been found associated with both volcanoes (e.g. Cabrol et al. 2007; Vick et al. 2010; Cousins et al. 2013) and impact craters (e.g. Cockell and Bland 2005; Osinski et al. 2005, 2013; Simpson et al. 2017).

Evidence of groundwater activity, occasionally reaching the surface, has been observed on Mars (e.g. Andrews-Hanna et al. 2010; Fairén et al. 2010; Ehlmann et al. 2011; Michalski et al. 2013). If life ever appeared on Mars, these underground water reservoirs could potentially serve as a microbiome for a deep microbial biosphere (Michalski et al. 2013). Some of these craters have hosted (or still host) a lacustrine ecosystem (e.g. Licancabur Lake, Cabrol et al. 2009; Ries impact structure, Osinski et al. 2013). Additionally, microorganisms

may influence the geomorphology of their environment over long timescales, thus providing additional evidence of their presence (see Viles 2012 for a review).

Recurring slope lineae (RSL), with formation mechanisms possibly requiring flowing water, have been observed on various crater walls, mainly at mid-latitudes (e.g. Ojha et al. 2014; Stillman et al. 2016, 2017; Stillman and Grimm 2018; Schaefer et al. 2019). If RSL are formed by aqueous solutions containing organics — or even microbial life — they may also be spread out by general wind dispersal or by dust devils. Wind patterns are ubiquitous on Mars (Forget 2004) and dust devils and RSLs have already been reported in the same area inside a crater (Schaefer et al. 2019). As sampling directly in water on Mars would risk biological contamination of martian ecosystems by terrestrial biota, sampling at sites where aeolian processes are likely to have accumulated biosignatures is a valuable alternative.

No ATP activity has ever been measured on Mars. Still, extrapolating ATP half-life under martian conditions gives a persistence time ranging from a couple of sols up to 32 000 sols (about 90 terrestrial years) depending on the exposure to UV radiation (Schuerger et al. 2008), suggesting that the molecule could indeed serve as a biomarker for extant life on Mars.

Simple organic molecules such as *n*-alkanes are also target biomarkers for the search for life on Mars, due to their resilience to extreme conditions (e.g. Parnell et al. 2007; Westall et al. 2015). Aliphatic and aromatic organics have been detected in martian samples, up to 3 Ga old, collected in an ancient lacustrine environment at Gale crater (Freissinet et al. 2015; Eigenbrode et al. 2018). A reanalysis of the results obtained from the Viking Landers also suggests the presence of organics at their landing sites (Navarro-González et al. 2010). However, no indices point toward a biogenic origin for these molecules so far.

5.8 Conclusion

Results indicate that wind may be considered as the major driving force for controlling the seeding and removal of biosignatures in Hverfjall's crater.

To refine the conclusions drawn from the analyses presented here, more samples could be analysed from gullies and other transects, parallel or perpendicular to the one we have. The transect could also be extended to the outer slopes of the volcano and compared with profiles from other nearby craters. Additionally, adding direct diurnal temperature and wind measurements along the transect, could help to understand better the influence of these two parameters on the ATP and lipid profiles.

Chapter 6

Summary



‘Boh, c’est pas si mal.’ [*The Andy Griffith Show* opening theme plays in the background]

David Goodenough, *Joueur du Grenier*, episode *X-perts* (2016)

Contents

6.1	Studied sites	120
6.2	Relevance to Mars exploration	122

6.1 Studied sites

The aim of this thesis was to investigate the nature and repartition of biosignatures contained in soil samples taken from three different terrestrial analogues for Mars. The two Chilean sampling sites — in the Atacama Desert and on the Sairecabur volcano — were chosen for the dryness and the high UV flux they experience to investigate the microbiomes and the lipid biomarkers they contain. In addition, the depth profiles made for this work were the first to have such high spatial resolution for the study of lipids and — along with the work by Thomas (2018), but using a different approach — of DNA content, in the areas studied. The Icelandic site — the Hverfjall tuff ring — was chosen to model potential aeolian input to craters on Mars.

The sampling site in the Atacama Desert presented a hot and dry environment during the day, with a cold and dry environment at night. The high-resolution and shallow depth profile revealed that surface biomarkers were probably due to anthropogenic activities. At depth, the biomarkers had a plant origin, despite the near absence of plants at the surface. However, these rare plants do not appear to be the producers of the lipids observed. It is still unclear if these molecules are old deposits later buried in sand, or surface deposits that were drained by occasional water, but the first hypothesis is favoured. Despite the low DNA concentrations, DNA amplification by PCR revealed traces of genetic material both at the surface, where environmental conditions are extreme, and at deeper depth, where the environmental conditions were milder. However, the quality and quantity of the sequenced DNA was not sufficient to draw any further conclusions.

On the Sairecabur volcano, samples were collected from a cold and dry environment at high altitude, along an altitude gradient from 4 296 to 5 269 m. Four high-resolution shallow depth profiles were collected; one from a vegetated site and three from non-vegetated sites. Compared to the other three sites, the vegetated site showed clear signs of plant biomarker inputs and higher DNA concentrations. With increased altitude, plant biomarker inputs were still predominant compared to other biomarkers, despite the relative absence of plants nearby. Yet, none of the plants or lichens collected on the volcano seemed to be the main source for these biomarkers, as determined by comparing their *n*-alkane profile, their CPI values, and their ACL values, with those observed in the soil samples. DNA concentrations were more important at greater depth, where microbial communities would be more protected from the environmental changes than at the surface. Like the Atacama samples, the quality and quantity of the sequenced DNA was not sufficient to draw any further conclusions on the exact origin of the genetic material. The different geographical settings — especially the varying exposure to winds — of the different sampling sites on the Sairecabur make it challenging to draw general conclusions regarding the effect of the altitude gradient.

In the Hverfjall crater, samples were collected in a cold environment along a transect following the main wind direction. No environmental data was collected there. The repartition of microbial activity and of biolipids along this transect showed that the wind may have a strong influence on bringing and removing these biosignatures from the crater.

	Atacama	4 296 m	Sairecabur			Hverfjall
			4 782 m	5 056 m	5 269 m	
%H ₂ O	0.5–3.8	0.6–9.5	0.0–6.9	0.4–7.7	5.0–10.2	/
pH	8.4–9.2	4.6–7.2	4.7–6.7	4.7–6.5	5.2–6.8	7.0–7.5
TLE (µg·g ⁻¹)	21–14 528	57–117	40–100	4–66	41–74	0–32
% _{short} ^a	18–59	1–18	10–36	4–11	10–36	2–19
% _{long} ^b	5–35	30–66	12–38	23–53	2–10	15–56
DNA (ng·g ⁻¹)	0 ^c –5	172–7 263	0 ^c –437	2–2 765	3–313	/

Table 6.1 – Table comparing for the main results obtained for all sites. Value ranges are indicated. ^a %_{short} = $\frac{C_{18}+C_{20}}{C_{18-35}} \times 100$. ^b %_{long} = $\frac{C_{27}+C_{29}+C_{31}}{C_{18-35}} \times 100$. ^c Samples with a DNA concentration below detection limit were assigned a value of 0.

The lack of duplicate sampling sites at the Chilean sites prevents the Chilean results from being generalised to these sites and to other situations. Both Chilean and Icelandic sampling sites could have benefited from more sampling points, both to refine transect resolutions and to minimise the number of potential analysis artefacts. The geographical and climatic differences between the Atacama, the Central Andean Dry Puña, and Iceland make it more challenging to observe common features between these three areas.

However, similarities could still be found. The main results are summarised in table 6.1. All sites can be considered as isolated environments. Yet, both biomarkers and microbial presence (genetic material or microbial activity) were found at each of these sites. Amongst the observed biomarkers, molecules of plant origin were always present, and usually prevalent, in depth profiles, even at sites considered barren. For the Chilean sites, no dominant input from any of the collected plants was observed within the depth profiles. No human contamination was observed in the lipid samples, but one sequenced DNA sample was contaminated at some stage of its preparation, as evidenced by the presence of enterobacteria.

If the sampling sites are considered as isolated environments, then aeolian inputs may be the dominant factor for spreading biosignatures to these locations. Whilst this was the main working hypothesis for the study in the Hverfjall crater (section 5.3), aeolian input could also explain the presence of plant molecules at Chilean sites with no, or limited, vegetation. Interestingly, the Icelandic sampling site also contained less lipids than the Chilean ones. A possible explanation for this observation is that the interior of the crater was more protected from the wind compared to the open sites in the Atacama and Sairecabur.

As such, the Chilean sites studied may present environmental conditions similar to Mars to study the effects of dryness and UV radiation on biomarkers. However, the residence time of these biomarkers in the soil is unknown. A study of the carbon isotopic fractionation in plant-derived molecules could help to constrain the timescale. In comparison to the Chilean sites, the Hverfjall crater in Iceland may be a more suitable analogue for Mars to investigate for lower concentrations of organics in the soil.

6.2 Relevance to Mars exploration

Considering the results obtained for the analogues studied in this work, the influence of wind should be taken into consideration on Mars if any active biomarker source (i. e. life) were to be identified there. In such a case, downwind sampling could represent an alternative means to sample biomarkers whilst avoiding any direct contamination of their source. This alternative sampling strategy may be an appropriate means to identify extraterrestrial life signs, whilst still complying with planetary protection policies (United Nations 1967; Kminek et al. 2017).

Planetary protection is indeed an important issue as spacecraft decontamination is not perfect. This means that it is impossible to obtain a total absence of spores on each martian lander and rover (Frick et al. 2014). Moreover, simulation experiments have shown that despite the hostile conditions experienced during the journey to Mars, followed by the harsh environmental conditions on Mars, some bacterial spores may still survive (Horneck et al. 2012). A forward contamination of Mars with dormant Earth life is therefore possible. Once on Mars, these spores could be spread over the planet by means of wind and global storms. If any terrestrial spores have already contaminated Mars, their germination there is unlikely, considering that the environmental conditions for their growth are not met. Indeed, spores and bacteria already failed to grow in partially simulated martian environments (e. g. Schuerger and Nicholson 2006; Berry et al. 2010).

In a similar fashion, any organic contamination on the instruments of robots on Mars may be detected as false positives when analysing martian samples for organics. So far, organics coming from the instruments themselves or from other analyses have successfully been identified (Freissinet et al. 2015; Eigenbrode et al. 2018). When bringing martian samples back to Earth in future missions, avoiding their contamination by terrestrial organics will be a primary concern as well (Summons et al. 2014). Therefore, remote and automated handling of samples risks less contamination than direct manipulation by humans. For this reason, and setting aside any other technological or logistical considerations, samples coming from automated sample-return missions, curated and analysed in specifically designed facilities may be less contaminated than samples directly collected and analysed by humans working on Mars in fieldwork conditions. In the near future, both the Rosalind Franklin (ESA) and the Mars 2020 (NASA) rovers will try to answer questions relevant to astrobiology. Yet, only Mars 2020 will collect and store samples that may potentially return to Earth. To date, an aeolian dispersion of potential martian biosignatures has not been taken into account in the rovers' sampling strategy.

Finally, and to put it in simple terms, living beings pose a greater risk of forward contamination to Mars than decontaminated machines. However, as humans are more efficient than rovers at identifying, collecting, and analysing potential samples of interests, the benefits of having a human mission on Mars may outweigh their drawbacks, once enough preliminary data has been obtained with automated missions and analogue experiments.

Appendix A

X-ray diffraction spectra

On the following patterns, the signal intensity is always expressed in arbitrary units (a. u.). The minerals used to identify the samples' content are listed in table A.1.

Some peaks were assigned multiple symbols. This means that either several peaks partly overlap each other, or that the identification of the corresponding mineral is uncertain.

Sometimes, no good match with any powder diffraction file (PDF) could be obtained for certain peaks. The minerals producing them could not be identified.

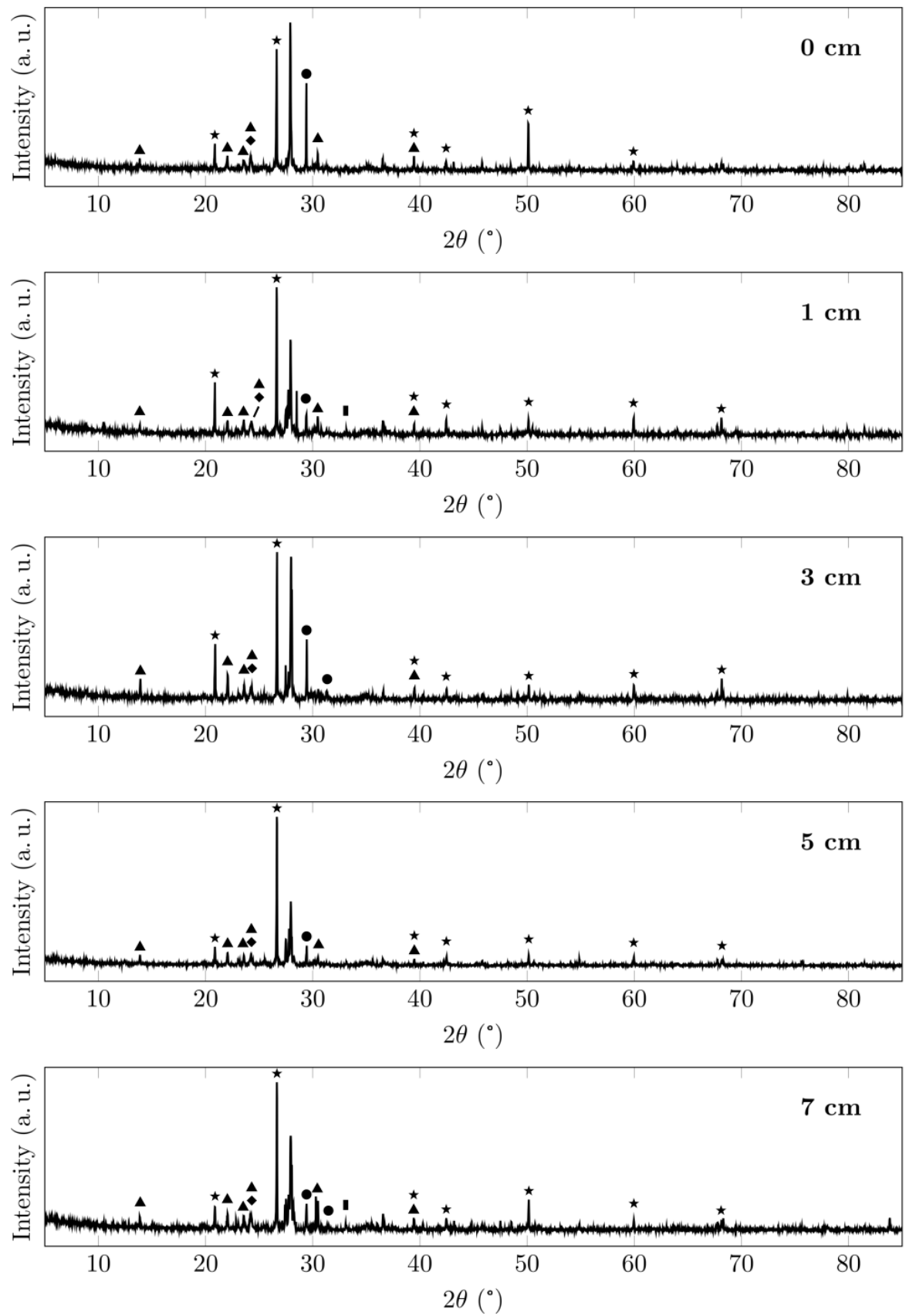
Symbol	Designation	Mineral	PDF number
●	calcite	calcite	00-005-0586
		calcite	00-043-0697
▲	feldspar	albite	00-009-0466
		anorthite	00-018-1202
		orthoclase	00-031-0966
		sanidine	00-019-1227
■	iron oxide	hematite	00-033-0664
		ilmenite	00-029-0733
		iron oxide	01-071-5088
		magnetite	01-075-1374
■	mica	biotite	01-080-1106
		muscovite	00-001-0649
		muscovite	00-019-0814
		muscovite	00-058-2035
◆	olivine	olivine	01-070-2503
▼	pyroxene	clinopyroxene	01-072-3877
		orthopyroxene	01-076-3321
★	quartz	quartz	00-001-0649
		quartz	00-046-1045
		quartz	01-075-8322

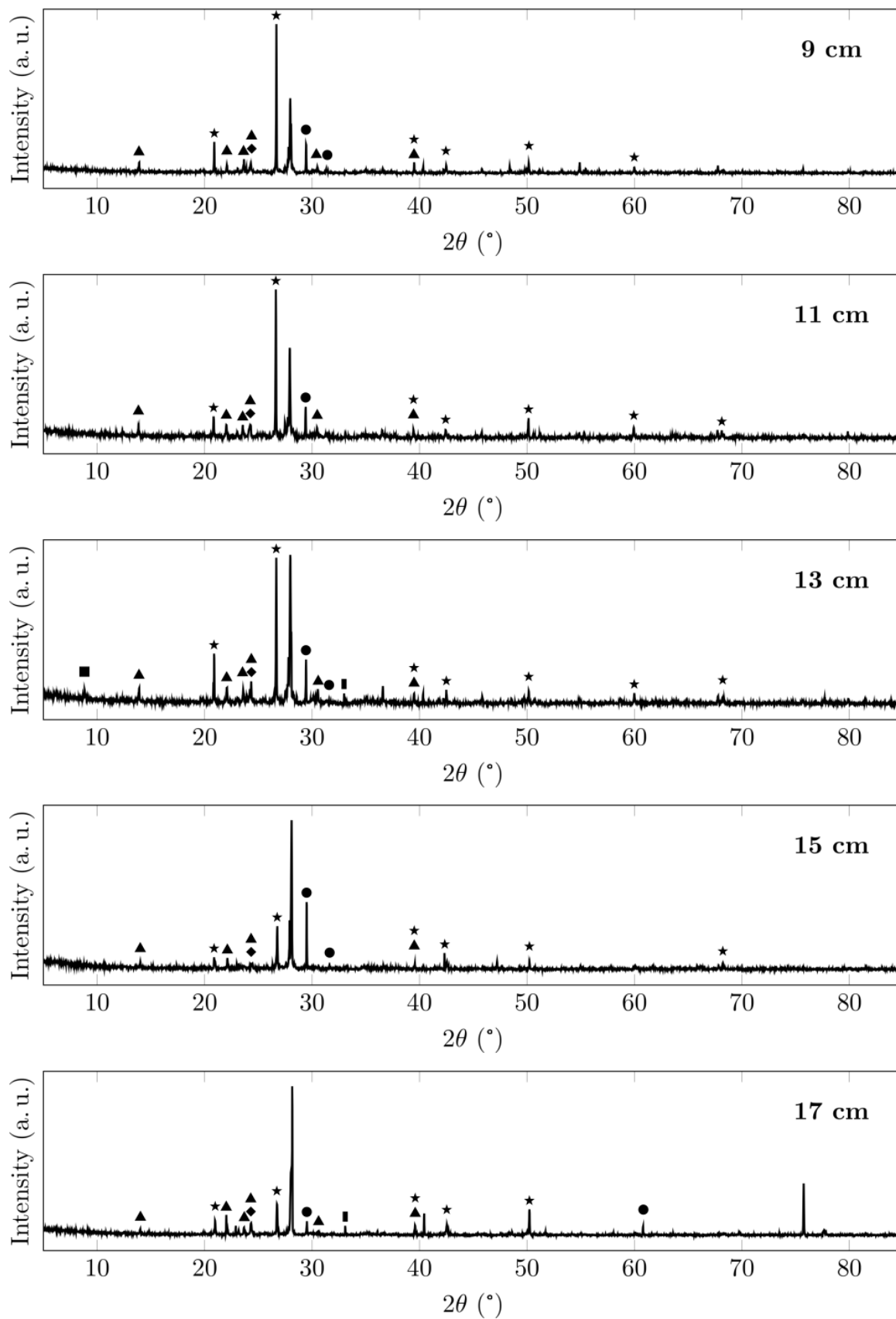
Table A.1 – Minerals, powder diffraction file (PDF), identified by XRD.

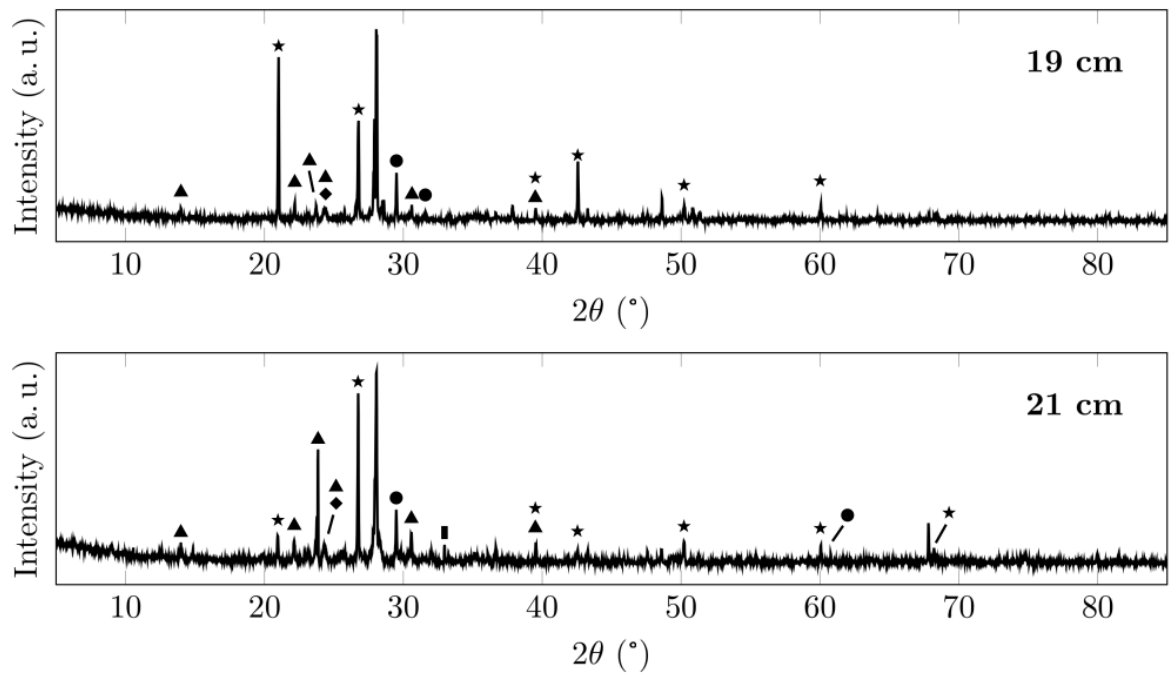
In the following sections, the depth of each sample is reported its corresponding plot.

A.1 Atacama samples

Samples collected in the Atacama Desert were prepared and analysed at the School of Chemistry (University of Glasgow) by Jose Rico, under the supervision of Justin Hargreaves — following the method described in section 2.2.5. Peaks were identified with the help of Claire Wilson (School of Chemistry, University of Glasgow).



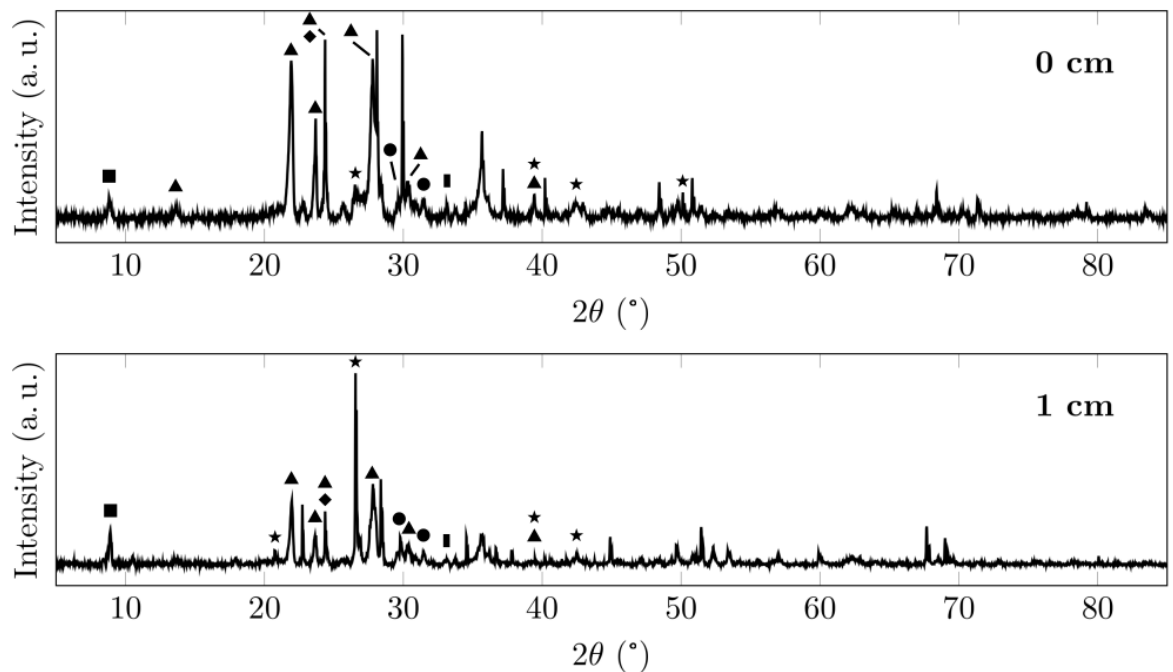


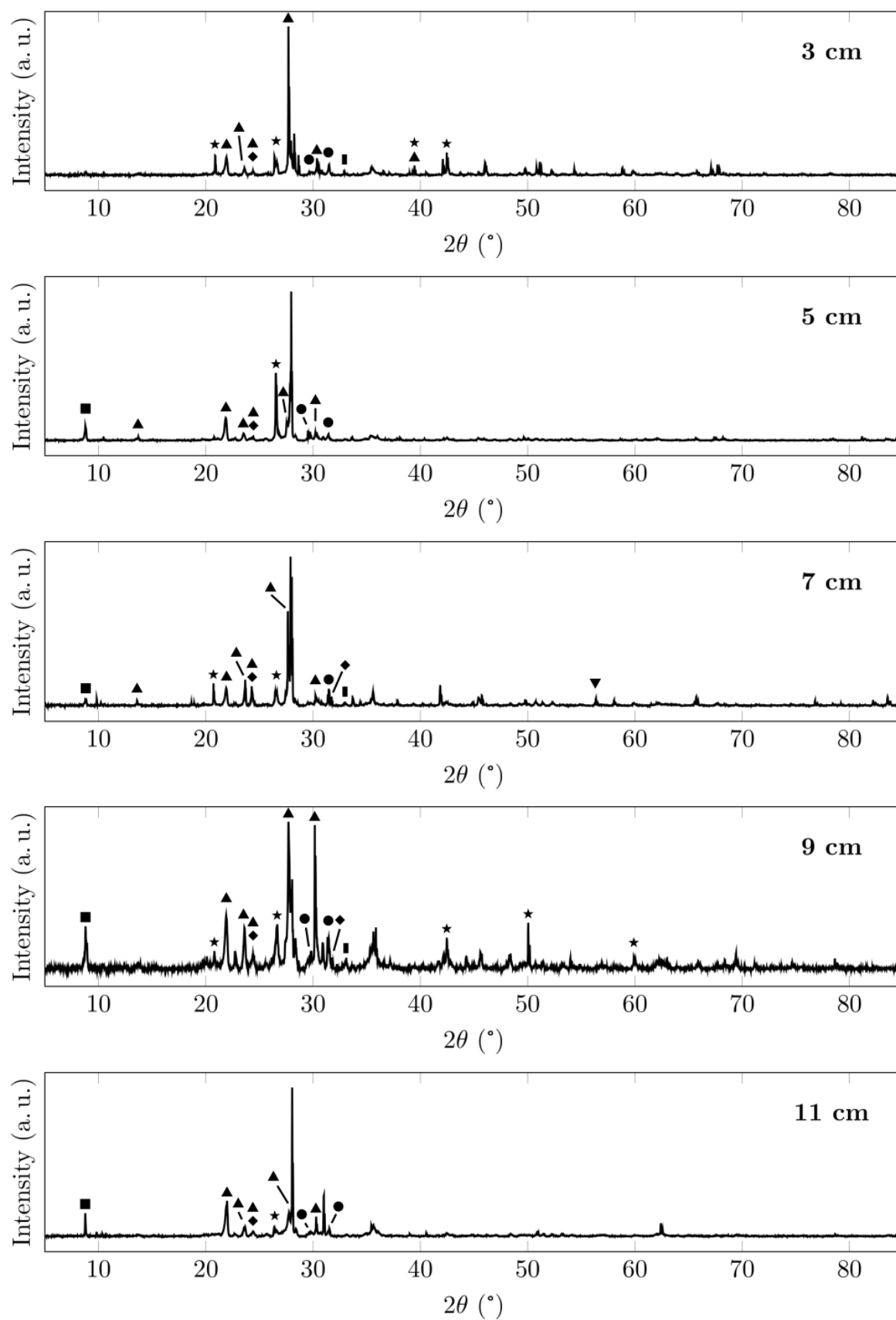


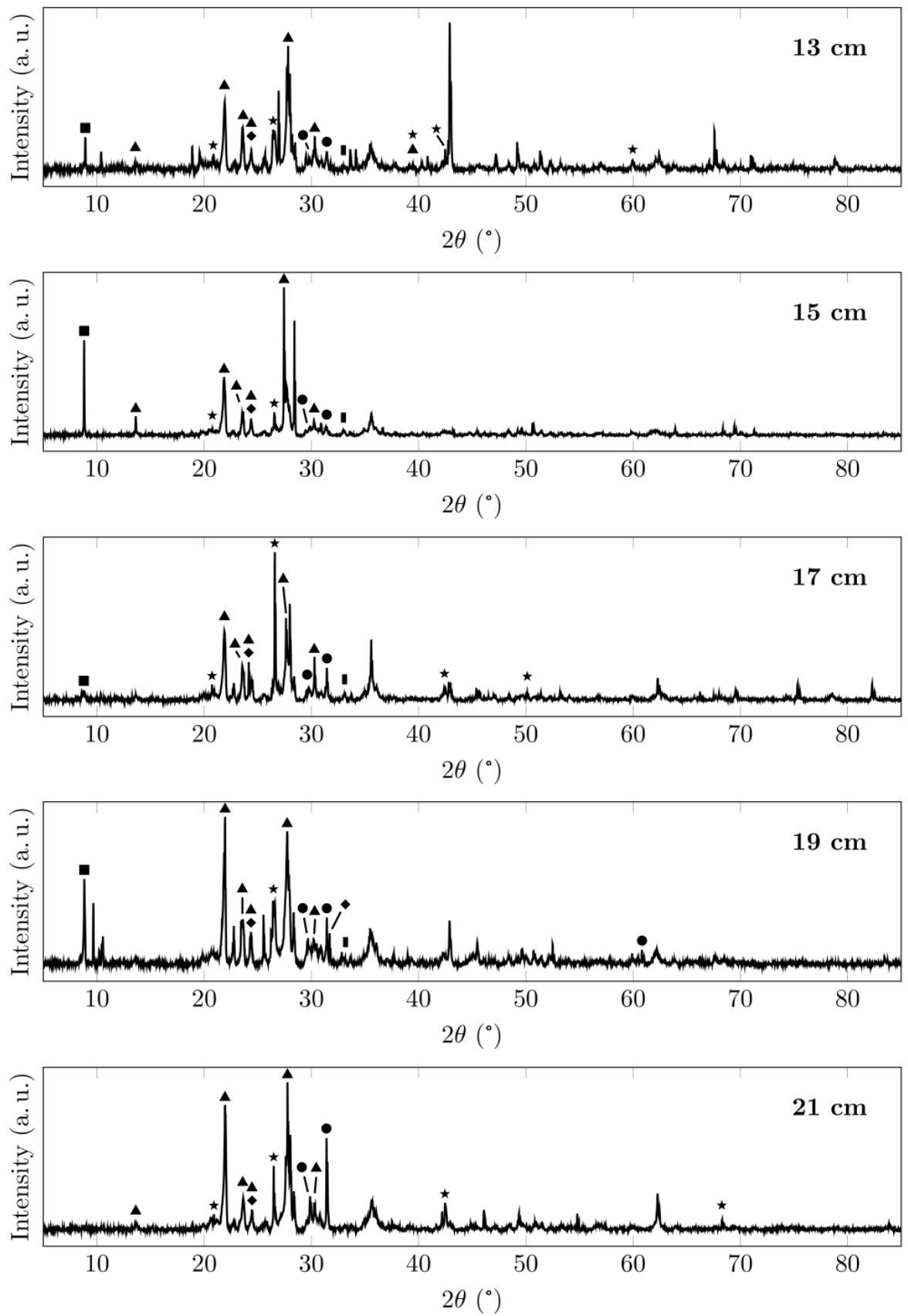
A.2 Sairecabur samples

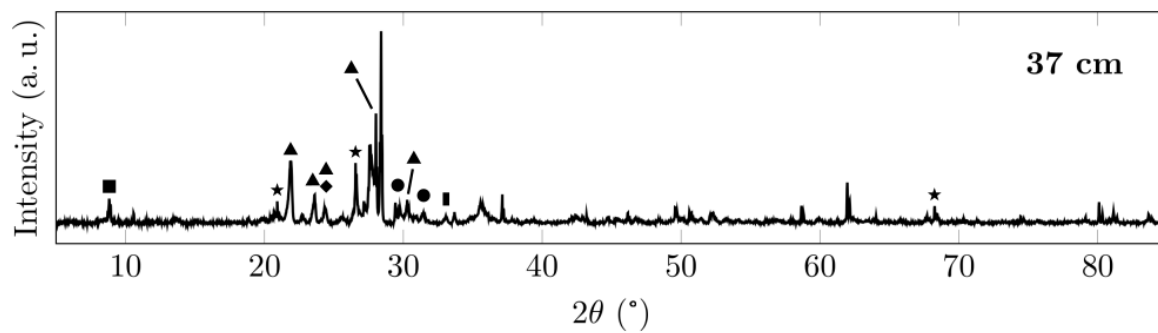
Samples collected on the Sairecabur were analysed at the Advanced Materials Research Laboratory (AMRL, University of Strathclyde), following the method described in section 2.2.5. Peaks were identified with the help of Tiziana Marrocco (AMRL, University of Strathclyde).

A.2.1 4296 m

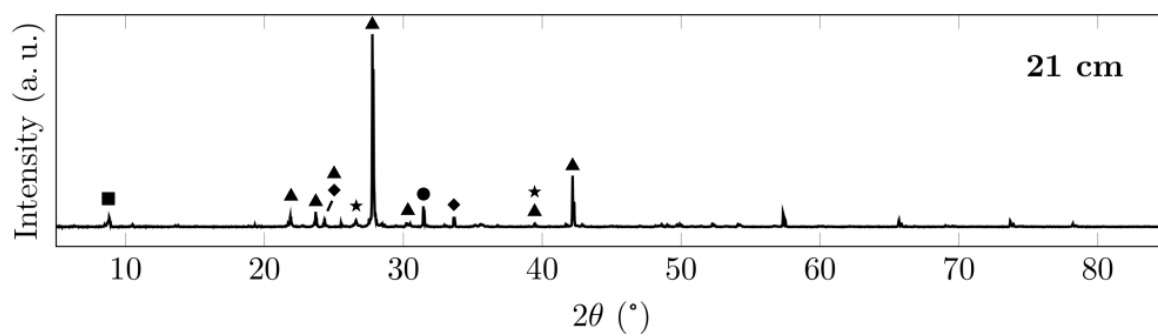
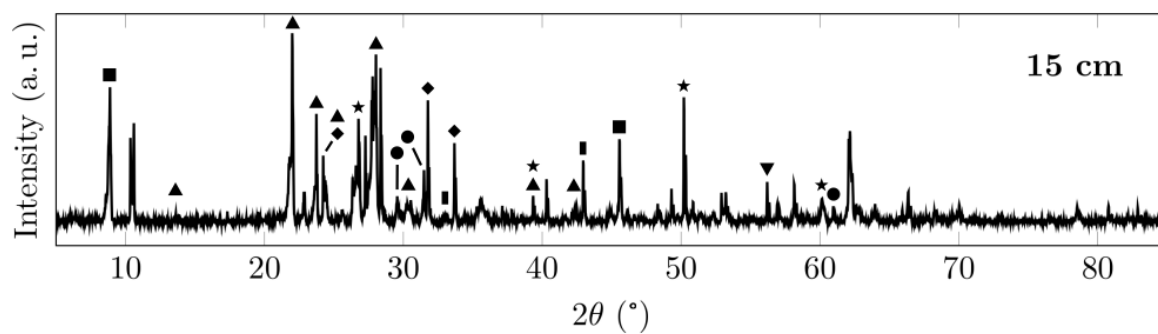
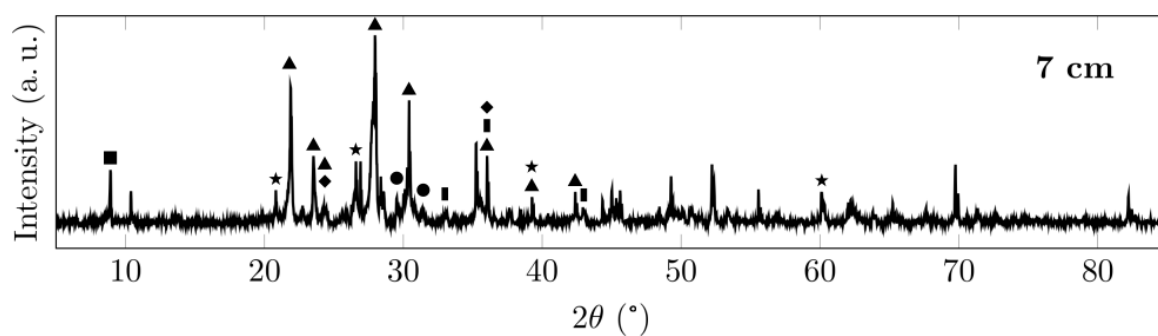
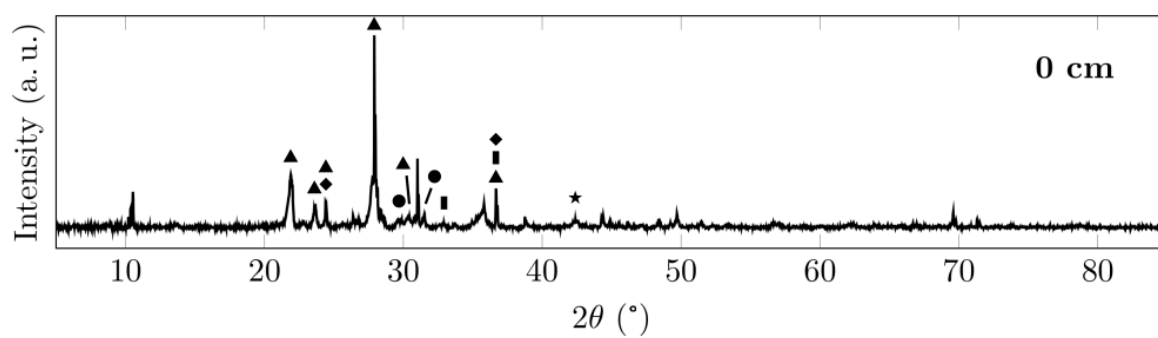


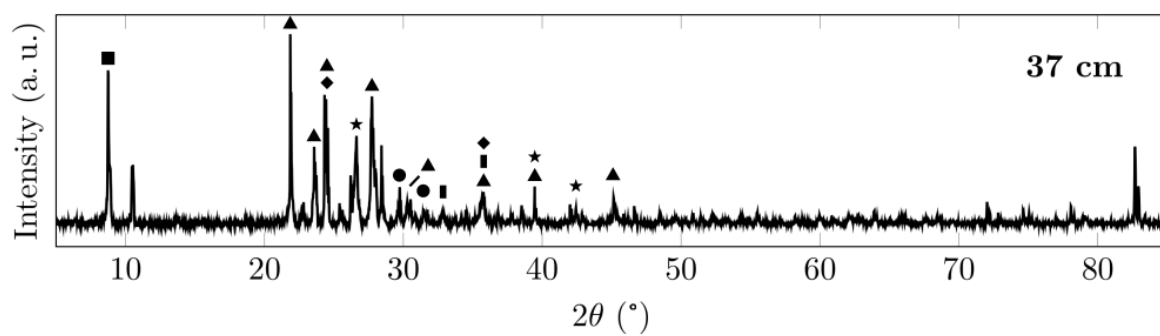




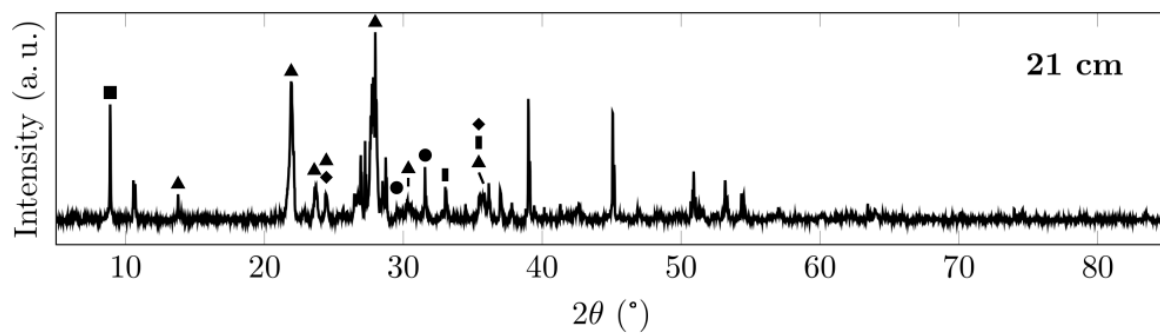
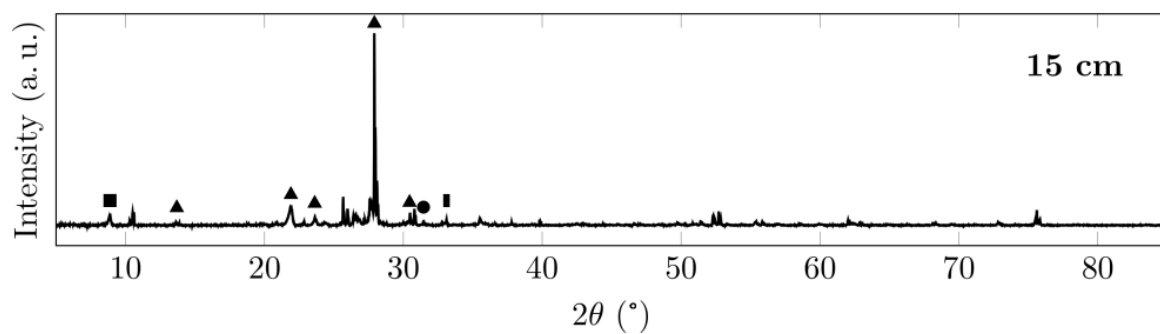
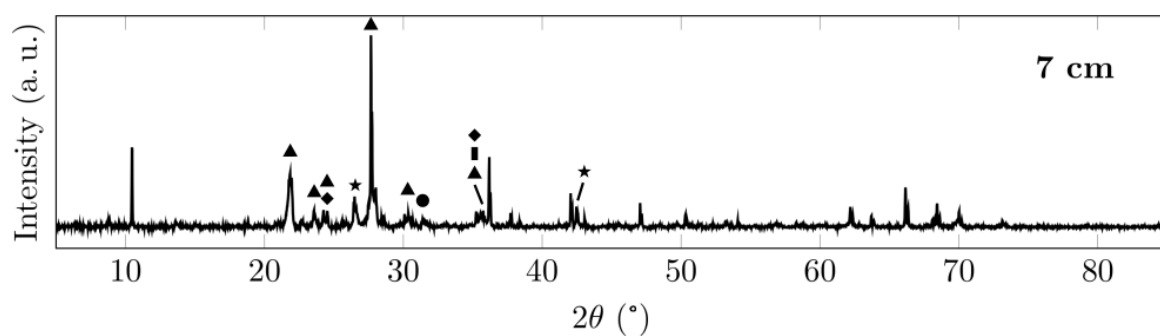
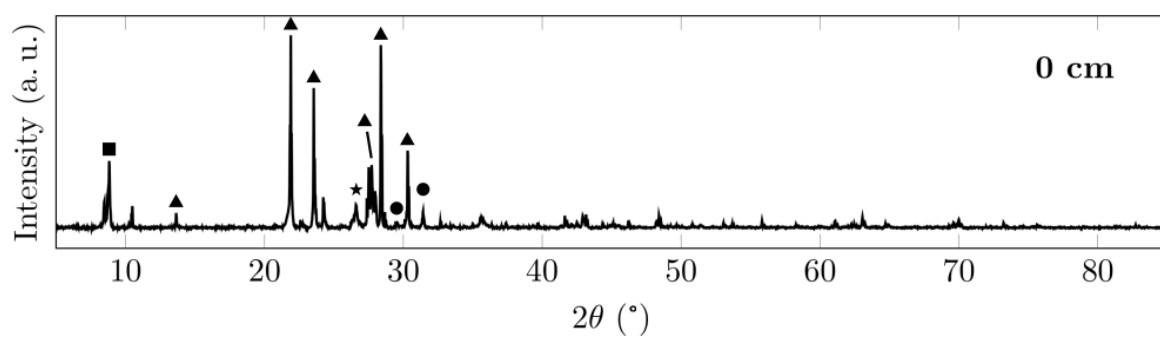


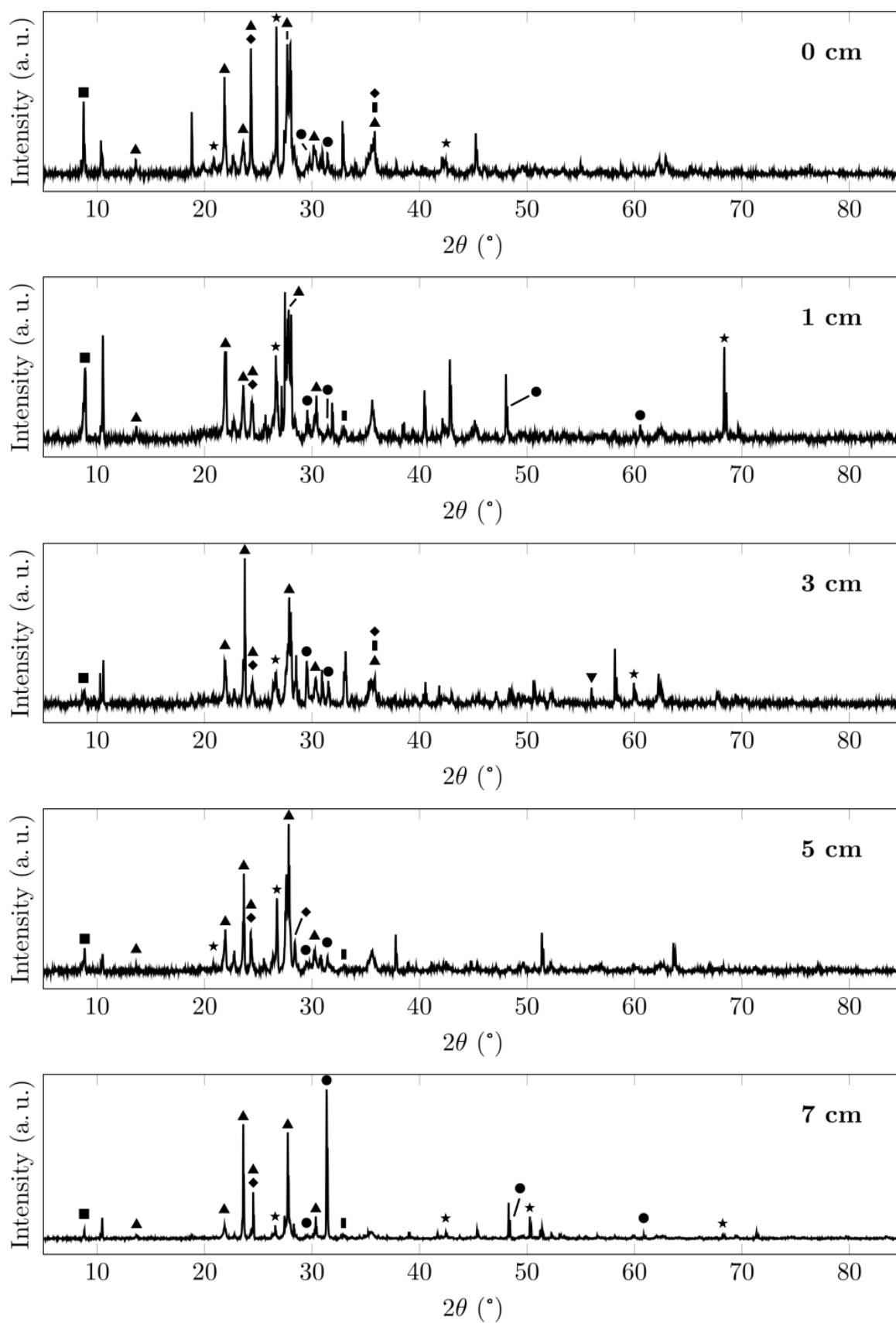
A.2.2 4782 m





A.2.3 5056 m



A.2.4 5269 m

Appendix B

Plant and lichen samples


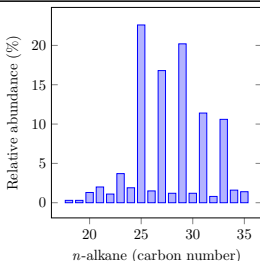

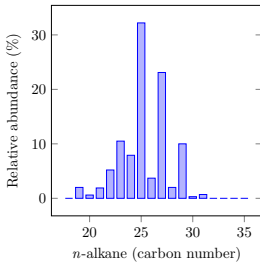
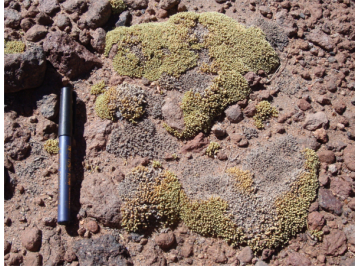
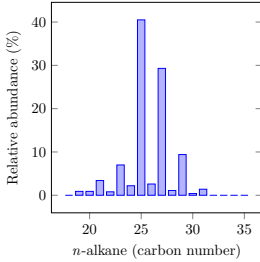
B.1 Sample description

Plant and lichen samples were collected at different altitudes on the Sairecabur (18 samples) and at the Atacama study site (1 sample). With the help of undergraduate student Briony Carswell, lipids were extracted from the different samples, separated into sub-fractions, and analysed by GC-FID following the same procedure as described for soil samples (see section 2.3.2).

Following collection, plants samples were identified by comparing their morphology with the samples displayed at the archeological museum in San Pedro de Atacama (Museo Arqueológico R. P. Gustavo Le Paige) or with the plants identified by Richter and Schmidt (2002), and with the help of Claudio Latorre (Pontificia Universidad Católica de Chile).


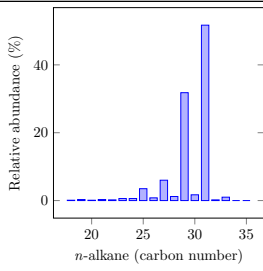

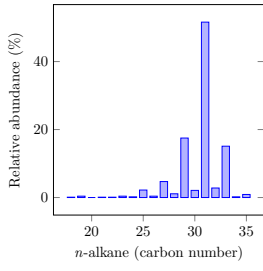

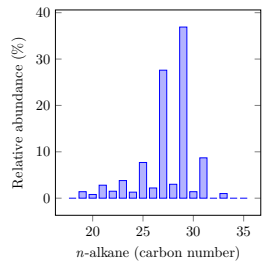

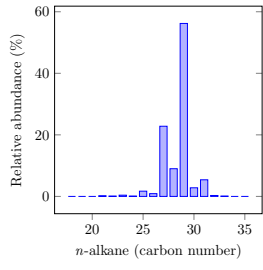

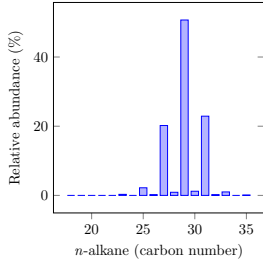

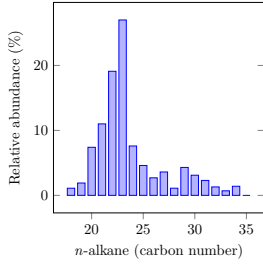
The table below lists the different samples with a suggested identification, the location and altitude at which they were collected, a picture, and the relative abundance of the *n*-alkanes — ranging from C₁₈ to C₃₅ — contained in their respective lipid extract. A name followed by a question mark indicates a provisional identification.

Table B.1 – Analysis of the plant and lichen samples

Sample details	Picture	<i>n</i> -alkanes																																		
<p>Sample A</p> <p><i>Festuca orthophylla</i></p> <p>Sairecabur, 4 296 m</p> <p>CPI_{19–33}: 8.8</p> <p>ACL_{19–35}: 28.0</p>		 <table><caption>Relative abundance (%) of n-alkanes for Sample A</caption><thead><tr><th>n-alkane (carbon number)</th><th>Relative abundance (%)</th></tr></thead><tbody><tr><td>20</td><td>0.5</td></tr><tr><td>21</td><td>1.0</td></tr><tr><td>22</td><td>2.0</td></tr><tr><td>23</td><td>3.0</td></tr><tr><td>24</td><td>4.0</td></tr><tr><td>25</td><td>22.0</td></tr><tr><td>26</td><td>17.0</td></tr><tr><td>27</td><td>10.0</td></tr><tr><td>28</td><td>12.0</td></tr><tr><td>29</td><td>20.0</td></tr><tr><td>30</td><td>11.0</td></tr><tr><td>31</td><td>10.0</td></tr><tr><td>32</td><td>2.0</td></tr><tr><td>33</td><td>1.0</td></tr><tr><td>34</td><td>0.5</td></tr><tr><td>35</td><td>0.5</td></tr></tbody></table>	n-alkane (carbon number)	Relative abundance (%)	20	0.5	21	1.0	22	2.0	23	3.0	24	4.0	25	22.0	26	17.0	27	10.0	28	12.0	29	20.0	30	11.0	31	10.0	32	2.0	33	1.0	34	0.5	35	0.5
n-alkane (carbon number)	Relative abundance (%)																																			
20	0.5																																			
21	1.0																																			
22	2.0																																			
23	3.0																																			
24	4.0																																			
25	22.0																																			
26	17.0																																			
27	10.0																																			
28	12.0																																			
29	20.0																																			
30	11.0																																			
31	10.0																																			
32	2.0																																			
33	1.0																																			
34	0.5																																			
35	0.5																																			
<p>Sample B</p> <p><i>Mulinum crassifolium</i></p> <p>Sairecabur, 4 296 m</p> <p>CPI_{19–33}: 4.1</p> <p>ACL_{19–35}: 25.6</p>		 <table><caption>Relative abundance (%) of n-alkanes for Sample B</caption><thead><tr><th>n-alkane (carbon number)</th><th>Relative abundance (%)</th></tr></thead><tbody><tr><td>20</td><td>0.5</td></tr><tr><td>21</td><td>1.0</td></tr><tr><td>22</td><td>2.0</td></tr><tr><td>23</td><td>3.0</td></tr><tr><td>24</td><td>4.0</td></tr><tr><td>25</td><td>32.0</td></tr><tr><td>26</td><td>10.0</td></tr><tr><td>27</td><td>12.0</td></tr><tr><td>28</td><td>23.0</td></tr><tr><td>29</td><td>10.0</td></tr><tr><td>30</td><td>1.0</td></tr><tr><td>31</td><td>0.5</td></tr><tr><td>32</td><td>0.5</td></tr><tr><td>33</td><td>0.5</td></tr><tr><td>34</td><td>0.5</td></tr><tr><td>35</td><td>0.5</td></tr></tbody></table>	n-alkane (carbon number)	Relative abundance (%)	20	0.5	21	1.0	22	2.0	23	3.0	24	4.0	25	32.0	26	10.0	27	12.0	28	23.0	29	10.0	30	1.0	31	0.5	32	0.5	33	0.5	34	0.5	35	0.5
n-alkane (carbon number)	Relative abundance (%)																																			
20	0.5																																			
21	1.0																																			
22	2.0																																			
23	3.0																																			
24	4.0																																			
25	32.0																																			
26	10.0																																			
27	12.0																																			
28	23.0																																			
29	10.0																																			
30	1.0																																			
31	0.5																																			
32	0.5																																			
33	0.5																																			
34	0.5																																			
35	0.5																																			
<p>Sample C</p> <p><i>Pycnophyllum molle</i></p> <p>Sairecabur, 4 296 m</p> <p>CPI_{19–33}: 11.5</p> <p>ACL_{19–35}: 25.8</p>		 <table><caption>Relative abundance (%) of n-alkanes for Sample C</caption><thead><tr><th>n-alkane (carbon number)</th><th>Relative abundance (%)</th></tr></thead><tbody><tr><td>20</td><td>0.5</td></tr><tr><td>21</td><td>1.0</td></tr><tr><td>22</td><td>2.0</td></tr><tr><td>23</td><td>3.0</td></tr><tr><td>24</td><td>4.0</td></tr><tr><td>25</td><td>40.0</td></tr><tr><td>26</td><td>10.0</td></tr><tr><td>27</td><td>12.0</td></tr><tr><td>28</td><td>29.0</td></tr><tr><td>29</td><td>10.0</td></tr><tr><td>30</td><td>1.0</td></tr><tr><td>31</td><td>0.5</td></tr><tr><td>32</td><td>0.5</td></tr><tr><td>33</td><td>0.5</td></tr><tr><td>34</td><td>0.5</td></tr><tr><td>35</td><td>0.5</td></tr></tbody></table>	n-alkane (carbon number)	Relative abundance (%)	20	0.5	21	1.0	22	2.0	23	3.0	24	4.0	25	40.0	26	10.0	27	12.0	28	29.0	29	10.0	30	1.0	31	0.5	32	0.5	33	0.5	34	0.5	35	0.5
n-alkane (carbon number)	Relative abundance (%)																																			
20	0.5																																			
21	1.0																																			
22	2.0																																			
23	3.0																																			
24	4.0																																			
25	40.0																																			
26	10.0																																			
27	12.0																																			
28	29.0																																			
29	10.0																																			
30	1.0																																			
31	0.5																																			
32	0.5																																			
33	0.5																																			
34	0.5																																			
35	0.5																																			


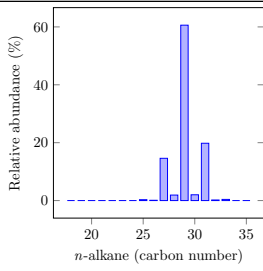
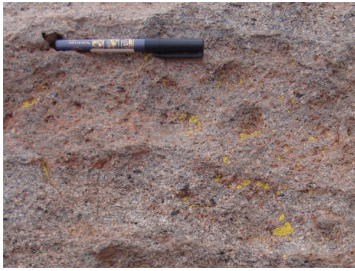
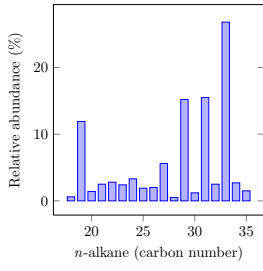

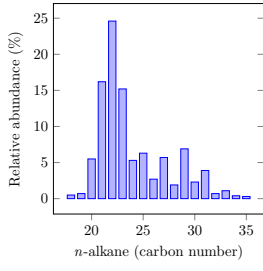

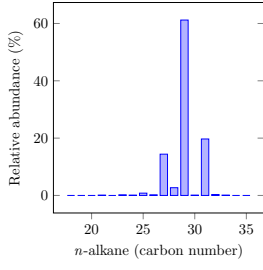

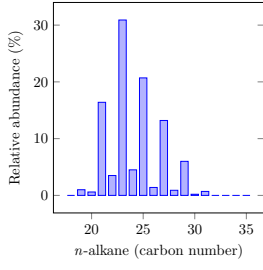

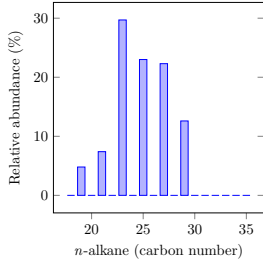
Continued on next page

Table B.1 – Continued from previous page

Sample details	Picture	<i>n</i> -alkanes
<p>Sample D</p> <p><i>Wernaria</i> sp. (?)</p> <p>Sairecabur, 4 296 m</p> <p>CPI_{19–33}: 19.6</p> <p>ACL_{19–35}: 29.8</p>		
<p>Sample E</p> <p><i>Parastrephia quadrangularis</i></p> <p>Sairecabur, 4 296 m</p> <p>CPI_{19–33}: 13.4</p> <p>ACL_{19–35}: 30.5</p>		
<p>Sample F</p> <p><i>Pycnophyllum bryoides</i></p> <p>Sairecabur, 4 296 m</p> <p>CPI_{19–33}: 8.8</p> <p>ACL_{19–35}: 27.6</p>		
<p>Sample G</p> <p><i>Adesmia spinosissima</i></p> <p>Sairecabur, 4 296 m</p> <p>CPI_{19–33}: 6.6</p> <p>ACL_{19–35}: 28.5</p>		
<p>Sample H</p> <p><i>Perezia</i> sp. (?)</p> <p>Sairecabur, 4 782 m</p> <p>CPI_{19–33}: 38.9</p> <p>ACL_{19–35}: 29.0</p>		
<p>Sample I</p> <p><i>Pleopsidium</i> sp. (?)</p> <p>Sairecabur, 4 782 m</p> <p>CPI_{19–33}: 1.3</p> <p>ACL_{19–35}: 23.8</p>		


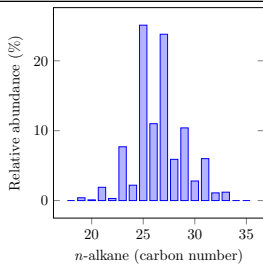

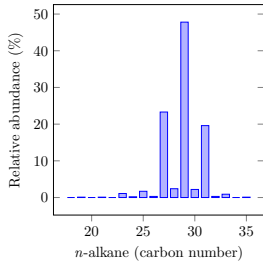

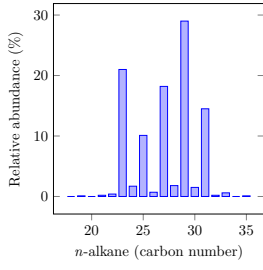

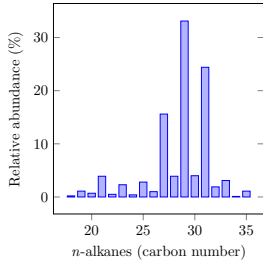
Continued on next page

Table B.1 – Continued from previous page

Sample details	Picture	<i>n</i> -alkanes
<p>Sample J</p> <p><i>Baccharis tola</i></p> <p>Sairecabur, 5 056 m</p> <p>CPI_{19–33}: 22.8</p> <p>ACL_{19–35}: 29.1</p>		
<p>Sample K</p> <p><i>Pleopsidium</i> sp. (?)</p> <p>Sairecabur, 5 056 m</p> <p>CPI_{19–33}: 5.4</p> <p>ACL_{19–35}: 28.7</p>		
<p>Sample L</p> <p><i>Rhizoplaca</i> sp. (?)</p> <p>Sairecabur, 5 056 m</p> <p>CPI_{19–33}: 1.3</p> <p>ACL_{19–35}: 24.6</p>		
<p>Sample M</p> <p><i>Baccharis tola</i></p> <p>Sairecabur, 5 056 m</p> <p>CPI_{19–33}: 28.4</p> <p>ACL_{19–35}: 29.1</p>		
<p>Sample N</p> <p><i>Azorella compacta</i></p> <p>Sairecabur, 4 296 m</p> <p>CPI_{19–33}: 8.0</p> <p>ACL_{19–35}: 24.1</p>		
<p>Sample O</p> <p><i>Mulinum crassifolium</i> (?)</p> <p>Sairecabur, 4 296 m</p> <p>CPI_{19–33}: (odd only)</p> <p>ACL_{19–35}: 24.8</p>		

Continued on next page

Table B.1 – Continued from previous page

Sample details	Picture	<i>n</i> -alkanes
Sample P <i>Ephedra breana</i> Sairecabur, 4 296 m CPI _{19–33} : 3.3 ACL _{19–35} : 26.4		
Sample Q <i>Senecio rahmeri</i> Sairecabur, 4 580 m CPI _{19–33} : 17.5 ACL _{19–35} : 28.8		
Sample R <i>Senecio rahmeri</i> Sairecabur, 4 580 m CPI _{19–33} : 14.9 ACL _{19–35} : 27.2		
Sample S <i>Tiquilia atacamensis</i> Atacama, 2 444 m CPI _{19–33} : 6.9 ACL _{19–35} : 28.6		

B.2 Comments on plants

Identification of all plants is provisional as it is based on morphology alone. Identification could be definitive by sequencing of the chloroplast marker *trnL-F* and the ribosomal *ItS* region, as described by Bell et al. (2012).

Samples Q and R were taken from the same plant species (*Senecio rahmeri*). However, sample Q was taken at a flowering stage of the plant life cycle. Therefore, flowers were included when its lipids were extracted from sample Q. This seasonal change in the plant life cycle may be responsible for the different production of *n*-alkanes in samples Q and R (Huang et al. 2018; Suh and Diefendorf 2018).

B.3 Comments on lichens

Lichens (samples I, K, and L) were sent to Jean-Pierre de Vera (German Aerospace Center (DLR), Berlin, Germany) for identification and cultivation.

Samples I and K are supposed to belong to the same species, yet they exhibit different *n*-alkane profiles. Possible explanations for the observed differences in the relative abundance of *n*-alkanes are: (i) a problem occurred during the lipids extraction, or the lipid fractionation; (ii) lipids were extracted from an insufficient amount of material for sample K, giving erroneous proportions of *n*-alkanes; (iii) the lichens actually belong to different species, producing different *n*-alkanes; (iv) the lichens were experiencing different stages of development, producing different *n*-alkanes; (v) both lichens were exposed to different living conditions, thus producing different *n*-alkanes.

However, (i) no apparent problem occurred during the extraction and the fractionation of lipids; (ii) the same amount of material was used for total lipid extraction each of these two samples (0.04 g); (iii) sample L, which belongs to another lichen species, still has an *n*-alkanes profile similar to the one observed for sample I. (iv) *n*-alkanes profile displayed by plant samples Q and R suggest that plants can produce different waxes at different stages of their life cycle, as also reported by Huang et al. (2018) and Suh and Diefendorf (2018). (v) variations in *n*-alkane production under different conditions has already been reported for plants (e. g. Sachse et al. 2006). Ultimately, hypotheses *iii* and *iv* can not be confirmed, or disproved, based on these observations.

Bibliography

- Achenbach L., Bailey J., Barnes R., Baross J., Bertka C., Boston P., Boyd E., Cable M., Chen I., Ciesla F., Des Marais D., Domagal-Goldman S., Elsila Cook J., Goldman A., Hud N., Lloyd K., Lyons T., Meadows V., Mix L., Mojzsis S., Muller U., Pasek M., Powell M., Robinson T., Rosenzweig F., Schmidt B., Seelig B., Springsteen G., Vance S., Welandar P., Williams L., Wordsworth R., Allwood A., Amend J., Anbar A., Billings L., Blankenship R., Boss A., Braakman R., Cavanaugh C., Copley S., Driscoll P., Ellington A., Erwin D., Falkowski P., Foster J., Fournier G., Ghadiri R., Gleeson D., Grinspoon D., Hecht M., Herbst E., House C., Hud N., Jablonski D., Jacobs D., Johnson C., Johnston D., Kiang N., Knight R., Knowles E., Krakauer D., Laine P., Lyons J., Lyons T., McCubbin F., McCutcheon J., Mullen L., Mumma M., Nicholson W., Oremland R., Patzkowsky M., Pohorille A., Pratt L., Redding K., Reinhard C., Rugheimer S., Schmidt F., Shock E., Sigurdsson S., Singer K., Smirnov A., Smith E., Sniegowski P., Som S., Tice M., Vermaas W., Whittet D. (2015). *Astrobiology strategy*. Ed. by L. Hays. National Aeronautics and Space Administration.
- Acuña M. H., Connerney J. E. P., Ness N. F., Lin R. P., Mitchell D., Carlson C. W., McFadden J., Anderson K. A., Rème H., Mazelle C., Vignes D., Wasilewski P., Cloutier P. (1999). Global distribution of crustal magnetization discovered by the Mars Global Surveyor MAG/ER Experiment. *Science*, Vol. 284 (5415), pp. 790–793.
- Acuña M. H., Connerney J. E. P., Wasilewski P., Lin R. P., Mitchell D., Anderson K. A., Carlson C. W., McFadden J., Rème H., Mazelle C., Vignes D., Bauer S. J., Cloutier P., Ness N. F. (2001). Magnetic field of Mars: Summary of results from the aerobraking and mapping orbits. *Journal of Geophysical Research: Planets*, Vol. 106 (E10), pp. 23403–23417.
- Agafonkin V. (2009). *SunCalc*. URL: <http://suncalc.net/>.
- Aguilar P., Dorador C., Vila I., Sommaruga R. (2018). Bacterioplankton composition in tropical high-elevation lakes of the Andean plateau. *FEMS Microbiology Ecology*, Vol. 94, fty004.
- Albarracín V. H., Gärtner W., Farias M. E. (2016). Forged under the sun: Life and art of extremophiles from Andean lakes. *Photochemistry and Photobiology*, Vol. 92 (1), pp. 14–28.
- Albro P. W. (1976). Bacterial waxes. In: *Chemistry and biochemistry of natural waxes*. Ed. by P. E. Kolattukudy. Amsterdam – Oxford – New York: Elsevier, pp. 419–445.

- Altwegg K., Balsiger H., Bar-Nun A., Berthelier J.-J., Bieler A., Bochslers P., Briois C., Calmonte U., Combi M. R., Cottin H., De Keyser J., Dhooghe F., Fiethe B., Fuselier S. A., Gasc S., Gombosi T. I., Hansen K. C., Haessig M., Jäckel A., Kopp E., Korth A., Le Roy L., Mall U., Marty B., Mousis O., Owen T., Rème H., Rubin M., Sémon T., Tzou C.-Y., Hunter Waite J., Wurz P. (2016). Prebiotic chemicals—amino acid and phosphorus—in the coma of comet 67P/Churyumov-Gerasimenko. *Science Advances*, Vol. 2 (5), e1600285.
- Amador E. S., Cable M. L., Chaudry N., Cullen T., Gentry D., Jacobsen M. B., Murukesan G., Schwieterman E. W., Stevens A. H., Stockton A., Yin C., Cullen D. C., Geppert W. (2015). Synchronous in-field application of life-detection techniques in planetary analog missions. *Planetary and Space Science*, Vol. 106, pp. 1–10.
- Amblès A., Parlanti E., Jambu P., Mayoungou P., Jacquesy J.-C. (1994). *n*-Alkane oxidation in soil. Formation of internal monoalkenes. *Geoderma*, Vol. 64 (1), pp. 111–124.
- Amils R., González-Toril E., Fernández-Remolar D., Gómez F., Aguilera Ángeles, Rodríguez N., Malki M., García-Moyano A., Fairén A. G., de la Fuente V., Sanz J. L. (2007). Extreme environments as Mars terrestrial analogs: The Rio Tinto case. *Planetary and Space Science*, Vol. 55 (3), pp. 370–381.
- Anbu P., Kang C.-H., Shin Y.-J., So J.-S. (2016). Formations of calcium carbonate minerals by bacteria and its multiple applications. *SpringerPlus*, Vol. 5 (1), p. 250.
- Andrews-Hanna J. C., Zuber M. T., Arvidson R. E., Wiseman S. M. (2010). Early Mars hydrology: Meridiani playa deposits and the sedimentary record of Arabia Terra. *Journal of Geophysical Research: Planets*, Vol. 115 (E6), E06002.
- Angel A., Vila I., Herrera V. (2016a). Extremophiles: photosynthetic systems in a high-altitude saline basin (Altiplano, Chile). *International Aquatic Research*, Vol. 8 (2), pp. 91–108.
- Angel R., Conrad R., Dvorsky M., Kopecky M., Kotlínek M., Hiiesalu I., Schweingruber F., Doležal J. (2016b). The root-associated microbial community of the world's highest growing vascular plants. *Microbial Ecology*, Vol. 72 (2), pp. 394–406.
- Anglés A., Arnould J., Billings L., Čápková K. A., Chatzitheodoridis E., Dartnell L., Dunér D., Gargaud M., Geppert W., Hemminger E., Kaňuchová Z., Kereszturi A., Kminek G., Laine P., Losiak A., Martínez-Frías J., Martins Z., Mason N., Melin A., Milligan T., Mitrikeski P. T., Nabulya E., Noack L., Persson E., Ramos S., Smith K., Tirard S., Waltemathe M. (2018). *Astrobiology and society in Europe today*. Ed. by K. A. Čápková, E. Persson, T. Milligan, D. Dunér.
- Antoniadi E. M. (1909). Fifth Interim Report for 1909, dealing with the fact revealed by observation that Prof. Schiaparelli's 'canal' network is the optical product of the irregular minor details diversifying the martian surface. *Journal of the British Astronomical Association*, Vol. 20, pp. 136–141.
- Armstrong J., Armstrong W. (1994). Chlorophyll development in mature lysigenous and schizogenous root aerenchymas provides evidence of continuing cortical cell viability. *New Phytologist*, Vol. 126 (3), pp. 493–497.

- Arroyo M. T. K., Squeo F. A., Armesto J. J., Villagran C. (1988). Effects of aridity on plant diversity in the Northern Chilean Andes: Results of a natural experiment. *Annals of the Missouri Botanical Garden*, Vol. 75 (1), pp. 55–78.
- Azúa-Bustos A., González-Silva C., Mancilla R. A., Salas L., Gómez-Silva B., McKay C. P., Vicuña R. (2011). Hypolithic cyanobacteria supported mainly by fog in the coastal range of the Atacama Desert. *Microbial Ecology*, Vol. 61 (3), pp. 568–581.
- Azua-Bustos A., Urrejola C., Vicuña R. (2012). Life at the dry edge: Microorganisms of the Atacama Desert. *FEBS Letters*, Vol. 586 (18), pp. 2939–2945.
- Azua-Bustos A., Caro-Lara L., Vicuña R. (2015). Discovery and microbial content of the driest site of the hyperarid Atacama Desert, Chile. *Environmental Microbiology Reports*, Vol. 7 (3), pp. 388–394.
- Azua-Bustos A., Carlos G., Corsini G. (2017). The hyperarid core of the Atacama Desert, an extremely dry and carbon deprived habitat of potential interest for the field of carbon science. *Frontiers in Microbiology*, Vol. 8, p. 993.
- Bada J. L., Glavin D. P., McDonald G. D., Becker L. (1998). A search for endogenous amino acids in martian meteorite ALH84001. *Science*, Vol. 279 (5349), pp. 362–365.
- Baker E. A. (1982). Chemistry and morphology of plant epicuticular waxes. In: *The Plant Cuticle, Linnean Society Symposium Series*. Ed. by D. F. Cutler, K. L. Alvin, C. E. Price. Vol. 10. Academic Press, London, pp. 139–165.
- Baker V. R., Milton D. J. (1974). Erosion by catastrophic floods on Mars and Earth. *Icarus*, Vol. 23 (1), pp. 27–41.
- Baqué M., Viaggiu E., Scalzi G., Billi D. (2013). Endurance of the endolithic desert cyanobacterium *Chroococcidiopsis* under UVC radiation. *Extremophiles*, Vol. 17 (1), pp. 161–169.
- Baqué M., Verseux C., Böttger U., Rabbow E., Vera J.-P. P. de, Billi D. (2016). Preservation of Biomarkers from Cyanobacteria Mixed with MarsLike Regolith Under Simulated Martian Atmosphere and UV Flux. *Origins of Life and Evolution of Biospheres*, Vol. 46 (2–3), pp. 289–310.
- Barnett M. J., Pearce D. A., Cullen D. C. (2012). Advances in the in-field detection of microorganisms in Ice. In: *Advances in Applied Microbiology*. Ed. by G. M. Gadd, S. Sariaslani. Vol. 81. Advances in Applied Microbiology. Academic Press, pp. 133–167.
- Barros N., Feijóo S., Salgado J., Ramajo B., García J., Hansen L. (2008). The dry limit of microbial life in the Atacama Desert revealed by calorimetric approaches. *Engineering in Life Sciences*, Vol. 8 (5), pp. 477–486.
- Baumard P., Budzinski H., Garrigues P., Dizer H., Hansen P. (1999). Polycyclic aromatic hydrocarbons in recent sediments and mussels (*Mytilus edulis*) from the Western Baltic Sea: occurrence, bioavailability and seasonal variations. *Marine Environmental Research*, Vol. 47 (1), pp. 17–47.
- Beblo-Vranesevic K., Bohmeier M., Perras A. K., Schwendner P., Rabbow E., Moissl-Eichinger C., Cockell C. S., Pukall R., Vannier P., Marteinson V. T., Monaghan E. P., Ehrenfreund P., Garcia-Descalzo L., Gómez F., Malki M., Amils R., Gaboyer F., Westall F., Cabezas

- P., Walter N., Rettberg P. (Oct. 2017). The responses of an anaerobic microorganism, *Yersinia intermedia* MASE-LG-1 to individual and combined simulated Martian stresses. *PLOS ONE*, Vol. 12 (10), pp. 1–19.
- Bell C. D., Kutschker A., Arroyo M. T. K. (2012). Phylogeny and diversification of Valerianaceae (Dipsacales) in the southern Andes. *Molecular Phylogenetics and Evolution*, Vol. 63 (3), pp. 724–737.
- Bendle J., Kawamura K., Yamazaki K., Niwai T. (2007). Latitudinal distribution of terrestrial lipid biomarkers and *n*-alkane compound-specific stable carbon isotope ratios in the atmosphere over the western Pacific and Southern Ocean. *Geochimica et Cosmochimica Acta*, Vol. 71 (24), pp. 5934–5955.
- Bendoraitis J. G., Brown B. L., Hepner L. S. (1962). Isoprenoid hydrocarbons in petroleum. Isolation of 2,6,10,14-tetramethylpentadecane by high temperature gas-liquid chromatography. *Analytical Chemistry*, Vol. 34 (1), pp. 49–53.
- Bennett M., New M., Marino J., Sillero-Zubiri C. (2016). Climate complexity in the Central Andes: A study case on empirically-based local variations in the Dry Puna. *Journal of Arid Environments*, Vol. 128, pp. 40–49.
- Berger L. I., Covington A. K., Fox R. B., Frederikse H. P. R., Fuhr J. R., Goldberg R. N., Gschneidner K. A., Hammond C. R., Hampson R. F., Holden N. E., Jenkins H. D. B., Kehiaian H. V., Kerr J. A., Kishore N., Lennen R., Lovas F. J., Martin W. C., Miller J. S., Miller T. M., Reader J., Snyder L. E., Stocker D. W., Taylor B. N., Trippe T. G., Vanýsek P., Wiese W. L., Wilks E. S., Wohlfarth C. (2003a). Determination of relative humidity from dew point. In: *CRC handbook of chemistry and physics*. Ed. by D. R. Lide, G. Baysinger, L. I. Berger, R. N. Goldberg, H. V. Kehiaian, K. Kuchitsu, C. C. Lin, G. M. Rosenblatt, A. L. Smith. 84th edition. CRC Press: Boca Raton, 15:24.
- (2003b). Physical constants of organic compounds. In: *CRC handbook of chemistry and physics*. Ed. by D. R. Lide, G. Baysinger, L. I. Berger, R. N. Goldberg, H. V. Kehiaian, K. Kuchitsu, C. C. Lin, G. M. Rosenblatt, A. L. Smith. 84th edition. CRC Press: Boca Raton, 3:1–573.
- Bernard S. (2014). Biosignatures, Effect of Metamorphism. In: *Encyclopedia of Astrobiology*. Ed. by R. Amils, M. Gargaud, J. Cernicharo Quintanilla, H. J. Cleaves, W. M. Irvine, D. Pinti, M. Viso. Berlin, Heidelberg: Springer Berlin Heidelberg, pp. 1–3. ISBN: 978-3-642-27833-4.
- Berry B. J., Jenkins D. G., Schuerger A. C. (2010). Effects of simulated Mars conditions on the survival and growth of *Escherichia coli* and *Serratia liquefaciens*. *Applied and Environmental Microbiology*, Vol. 76 (8), pp. 2377–2386.
- Beyer A., Mackay D., Matthies M., Wania F., Webster E. (2000). Assessing long-range transport potential of persistent organic pollutants. *Environmental Science & Technology*, Vol. 34 (4), pp. 699–703.
- Bibring J.-P., Langevin Y., Gendrin A., Gondet B., Poulet F., Berthé M., Soufflot A., Arvidson R., Mangold N., Mustard J., Drossart P., the OMEGA team (2005). Mars surface di-

- versity as revealed by the OMEGA/Mars Express observations. *Science*, Vol. 307 (5715), pp. 1576–1581.
- Biemann K., Oro J., Toulmin P., Orgel L. E., Nier A. O., Anderson D. M., Simmonds P. G., Flory D., Diaz A. V., Rushneck D. R., Biller J. E., Lafleur A. L. (1977). The search for organic substances and inorganic volatile compounds in the surface of Mars. *Journal of Geophysical Research*, Vol. 82 (28), pp. 4641–4658.
- Bishop J. L., Murad E., Lane M. D., Mancinelli R. L. (2004). Multiple techniques for mineral identification on Mars: a study of hydrothermal rocks as potential analogues for astrobiology sites on Mars. *Icarus*, Vol. 169 (2), pp. 311–323.
- Björn L. O. (1965). Chlorophyll formation in excised wheat roots. *Physiologia Plantarum*, Vol. 18 (4), pp. 1130–1142.
- (1976). The state of protochlorophyll and chlorophyll in corn roots. *Physiologia Plantarum*, Vol. 37 (3), pp. 183–184.
- Björnsson H., Jónsson T. (2004). Climate and climatic variability at Lake Myvatn. *Aquatic Ecology*, Vol. 38 (2), pp. 129–144.
- Blanco Y., Gallardo-Carreño I., Ruiz-Bermejo M., Puente-Sánchez F., Cavalcante-Silva E., Quesada A., Prieto-Ballesteros O., Parro V. (2017). Critical assessment of analytical techniques in the search for biomarkers on Mars: A mummified microbial mat from Antarctica as a best-case scenario. *Astrobiology*, Vol. 17 (10), pp. 984–996.
- Blumthaler M., Ambach W., Ellinger R. (1997). Increase in solar UV radiation with altitude. *Journal of Photochemistry and Photobiology B: Biology*, Vol. 39 (2), pp. 130–134.
- Boston P. J., Ivanov M. V., McKay C. P. (1992). On the possibility of chemosynthetic ecosystems in subsurface habitats on Mars. *Icarus*, Vol. 95 (2), pp. 300–308.
- Bouley S., Baratoux D., Paulien N., Missenard Y., Saint-Bézar B. (2018). The revised tectonic history of Tharsis. *Earth and Planetary Science Letters*, Vol. 488, pp. 126–133.
- Bozkurt D., Rondanelli R., Garreaud R., Arriagada A. (2016). Impact of warmer Eastern tropical pacific SST on the March 2015 Atacama floods. *Monthly Weather Review*, Vol. 144 (11), pp. 4441–4460.
- Bragg W. H., Bragg W. L. (1913). The reflection of X-rays by crystals. *Proceedings of the Royal Society of London A*, Vol. 88 (605), pp. 428–438.
- Brandon A., Walker R., Morgan J., Goles G. (2000). Re-Os isotopic evidence for early differentiation of the Martian mantle. *Geochimica et Cosmochimica Acta*, Vol. 64 (23), pp. 4083–4095.
- Bray E. E., Evans E. D. (1961). Distribution of *n*-paraffins as a clue to recognition of source beds. *Geochimica et Cosmochimica Acta*, Vol. 22 (1), pp. 2–15.
- Bristow T. F., Haberle R. M., Blake D. F., Des Marais D. J., Eigenbrode J. L., Fairén A. G., Grotzinger J. P., Stack K. M., Mischna M. A., Rampe E. B., Siebach K. L., Sutter B., Vaniman D. T., Vasavada A. R. (2017). Low Hesperian P_{CO_2} constrained from in situ mineralogical analysis at Gale Crater, Mars. *Proceedings of the National Academy of Sciences*, Vol. 114 (9), pp. 2166–2170.

- Brocks J. J., Logan G. A., Buick R., Summons R. E. (1999). Archean molecular fossils and the early rise of eukaryotes. *Science*, Vol. 285 (5430), pp. 1033–1036.
- Brocks J. J., Buick R., Summons R. E., Logan G. A. (2003a). A reconstruction of Archean biological diversity based on molecular fossils from the 2.78 to 2.45 billion-year-old Mount Bruce Supergroup, Hamersley Basin, Western Australia. *Geochimica et Cosmochimica Acta*, Vol. 67 (22), pp. 4321–4335.
- Brocks J. J., Buick R., Logan G. A., Summons R. E. (2003b). Composition and syngeneity of molecular fossils from the 2.78 to 2.45 billion-year-old Mount Bruce Supergroup, Pilbara Craton, Western Australia. *Geochimica et Cosmochimica Acta*, Vol. 67 (22), pp. 4289–4319.
- Brocks J. J., Grosjean E., Logan G. A. (2008). Assessing biomarker syngeneity using branched alkanes with quaternary carbon (BAQCs) and other plastic contaminants. *Geochimica et Cosmochimica Acta*, Vol. 72 (3), pp. 871–888.
- Brooks J. D., Gould K., Smith J. W. (1969). Isoprenoid hydrocarbon in coal and petroleum. *Nature*, Vol. 222 (5190), pp. 257–259.
- Bryant J. A., Lamanna C., Morlon H., Kerkhoff A. J., Enquist B. J., Green J. L. (2008). Microbes on mountainsides: Contrasting elevational patterns of bacterial and plant diversity. *Proceedings of the National Academy of Sciences*, Vol. 105 (S1), pp. 11505–11511.
- Bucke C., Leech R. M., Hallaway M., Morton R. A. (1966). The taxonomic distribution of plastoquinone and tocopherolquinone and their intracellular distribution in leaves of *Vicia faba* L. *Biochimica et Biophysica Acta*, Vol. 112 (1), pp. 19–34.
- Bull A. T., Asenjo J. A., Goodfellow M., Gómez-Silva B. (2016). The Atacama desert: Technical resources and the growing importance of novel microbial diversity. *Annual Review of Microbiology*, Vol. 70 (1). PMID: 27607552, pp. 215–234.
- Bull A. T., Idris H., Sanderson R., Asenjo J., Andrews B., Goodfellow M. (2018). High altitude, hyper-arid soils of the Central-Andes harbor mega-diverse communities of actinobacteria. *Extremophiles*, Vol. 22 (1), pp. 47–57.
- Butts W. C. (1972). Two-column gas chromatography of trimethylsilyl derivatives of biochemically significant compounds. *Analytical Biochemistry*, Vol. 46 (1), pp. 187–199.
- Cabrol N. A. (2018). The coevolution of life and environment on Mars: An ecosystem perspective on the robotic exploration of biosignatures. *Astrobiology*, Vol. 18 (1), pp. 1–27.
- Cabrol N. A., McKay C. P., Grin E. A., Kiss K. T., Ács E., Tóth B., Grigorszky I., Szabò K., Fike D. A., Hock A. N., Demergasso C., Escudero L., Galleguillos P., Chong G., Grigsby B. H., Román J. Z., Tambley C. (2007). Signatures of habitats and life in Earth's high-altitude lakes: clues to Noachian aqueous environments on Mars. In: *The geology of Mars: Evidence from Earth-based analogs*. Ed. by M. Chapman. Cambridge University Press, pp. 349–370.
- Cabrol N. A., Grin E. A., Chong G., Minkley E., Hock A. N., Yu Y., Bebout L., Fleming E., Häder D. P., Demergasso C., Gibson J., Escudero L., Dorador C., Lim D., Woosley C., Morris R. L., Tambley C., Gaete V., Galvez M. E., Smith E., Uskin-Peate I., Salazar C.,

- Dawidowicz G., Majerowicz J. (2009). The high-lakes project. *Journal of Geophysical Research: Biogeosciences*, Vol. 114 (G2), G00D06.
- Cabrol N. A., Grin E. A., Chong G., Häder D. P., Minkley E., Yu Y., Demergasso C., Gibson J. A., Lim D. (2010). Dynamics of declining lake habitat in changing climate. In: *Lakes on Mars*. Ed. by N. A. Cabrol, E. A. Grin. Amsterdam: Elsevier, pp. 347–369. ISBN: 978-0-444-52854-4.
- Cabrol N. A., Feister U., Häder D.-P., Piazena H., Grin E. A., Klein A. (2014). Record solar UV irradiance in the tropical Andes. *Frontiers in Environmental Science*, Vol. 2, p. 19.
- Cairns-Smith A. G. (1966). The origin of life and the nature of the primitive gene. *Journal of Theoretical Biology*, Vol. 10 (1), pp. 53–88.
- Cairns-Smith A. G., Hartman H. (1986). *Clay minerals and the origin of life*. Cambridge: Cambridge University Press. ISBN: 978-0521324083.
- Calderón R., Palma P., Parker D., Molina M., Godoy F. A., Escudey M. (2014). Perchlorate levels in soil and waters from the Atacama Desert. *Archives of Environmental Contamination and Toxicology*, Vol. 66 (2), pp. 155–161.
- Callahan M. P., Smith K. E., Cleaves H. J., Ruzicka J., Stern J. C., Glavin D. P., House C. H., Dworkin J. P. (2011). Carbonaceous meteorites contain a wide range of extraterrestrial nucleobases. *Proceedings of the National Academy of Sciences*, Vol. 108 (34), pp. 13995–13998.
- Callahan M. P., Burton A. S., Elsila J. E., Baker E. M., Smith K. E., Glavin D. P., Dworkin J. P. (2013). A search for amino acids and nucleobases in the Martian meteorite Roberts Massif 04262 using liquid chromatography-mass spectrometry. *Meteoritics & Planetary Science*, Vol. 48 (5), pp. 786–795.
- Cámara B., Souza-Egipsy V., Ascaso C., Artieda O., De Los Ríos A., Wierzchos J. (2016). Biosignatures and microbial fossils in endolithic microbial communities colonizing Ca-sulfate crusts in the Atacama Desert. *Chemical Geology*, Vol. 443, pp. 22–31.
- Carmona V., Pueyo J., Taberner C., Chong G., Thirlwall M. (2000). Solute inputs in the Salar de Atacama (N. Chile). *Journal of Geochemical Exploration*, Vol. 69–70, pp. 449–452.
- Carr M., Head J. (2019). Mars: Formation and fate of a frozen Hesperian ocean. *Icarus*, Vol. 319, pp. 433–443.
- Carr M. H., Head J. W. (2003). Oceans on Mars: An assessment of the observational evidence and possible fate. *Journal of Geophysical Research: Planets*, Vol. 108 (E5), p. 5042.
- (2010). Geologic history of Mars. *Earth and Planetary Science Letters*, Vol. 294 (3), pp. 185–203.
- Castañeda I. S., Schouten S. (2011). A review of molecular organic proxies for examining modern and ancient lacustrine environments. *Quaternary Science Reviews*, Vol. 30 (21), pp. 2851–2891.
- Catling D. C., Claire M. W., Zahnle K. J., Quinn R. C., Clark B. C., Hecht M. H., Kounaves S. (2010). Atmospheric origins of perchlorate on Mars and in the Atacama. *Journal of Geophysical Research: Planets*, Vol. 115, E00E11.

- Chang S. L., McClanahan M. A., Kabler P. W. (1962). Effect of bacterial decomposition of hexadecanol and octadecanol in monolayer films on the suppression of evaporation loss of water. In: *Retardation of Evaporation by Monolayers*. Ed. by V. K. La Mer. New York: Academic Press, pp. 119–131. ISBN: 978-1-4832-2947-8.
- Chapman M. G., Allen C. C., Gudmundsson M. T., Gulick V. C., Jakobsson S. P., Lucchitta B. K., Skilling I. P., Waitt R. B. (2000). Volcanism and ice interactions on Earth and Mars. In: *Environmental effects on volcanic eruptions: From deep oceans to deep space*. Ed. by J. R. Zimbelman, T. K. P. Gregg. Boston, MA: Springer US, pp. 39–73.
- Charrier R., Reutter K.-J. (1994). The Purilactis Group of Northern Chile: Boundary between arc and backarc from late Cretaceous to Eocene. In: *Tectonics of the Southern Central Andes*. Ed. by K.-J. Reutter, E. Scheuber, P. J. Wigger. Berlin: Springer, pp. 189–202.
- Cheng Z., Xiao L., Wang H., Yang H., Li J., Huang T., Xu Y., Ma N. (2017). Bacterial and archaeal lipids recovered from subsurface evaporites of Dalangtan Playa on the Tibetan plateau and their astrobiological implications. *Astrobiology*, Vol. 17 (11), pp. 1112–1122.
- Christensen P. R. (2003). Formation of recent martian gullies through melting of extensive water-rich snow deposits. *Nature*, Vol. 422 (6927), pp. 45–48.
- Clarke J. D. (2006). Antiquity of aridity in the Chilean Atacama Desert. *Geomorphology*, Vol. 73 (1), pp. 101–114.
- Cockell C., Lee P. (2002). The biology of impact craters – a review. *Biological Reviews*, Vol. 77 (3), pp. 279–310.
- Cockell C. S., Bland P. A. (2005). The evolutionary and ecological benefits of asteroid and comet impacts. *Trends in Ecology & Evolution*, Vol. 20 (4), pp. 175–179.
- Cockell C. S., Catling D. C., Davis W. L., Snook K., Kepner R. L., Lee P., McKay C. P. (2000). The ultraviolet environment of Mars: Biological implications. Past, present, and future. *Icarus*, Vol. 146 (2), pp. 343–359.
- Cockell C. S., Schuerger A. C., Billi D., Friedmann E. I., Panitz C. (2005). Effects of a simulated martian UV flux on the cyanobacterium, *Chroococcidiopsis* sp. 029. *Astrobiology*, Vol. 5 (2), pp. 127–140.
- Connerney J., Acuña M., Wasilewski P., Ness N., Rème H., Mazelle C., Vignes D., Lin R., Mitchell D., Cloutier P. (1999). Magnetic lineations in the ancient crust of Mars. *Science*, Vol. 284 (5415), pp. 794–800.
- Cooper G. J. T., Kitson P. J., Winter R., Zagnoni M., Long D.-L., Cronin L. (2011). Modular Redox-Active Inorganic Chemical Cells: iCHELLs. *Angewandte Chemie International Edition*, Vol. 50 (44), pp. 10373–10376.
- Cooper J. E., Bray E. E. (1963). A postulated role of fatty acids in petroleum formation. *Geochimica et Cosmochimica Acta*, Vol. 27 (11), pp. 1113–1127.
- Corcelli A., Colella M., Mascolo G., Fanizzi F. P., Kates M. (2000). A novel glycolipid and phospholipid in the purple membrane. *Biochemistry*, Vol. 39 (12), pp. 3318–3326.
- Cordero R. R., Damiani A., Seckmeyer G., Jorquera J., Caballero M., Rowe P., Ferrer J., Mubarak R., Carrasco J., Rondanelli R., Matus M., Laroze D. (2016). The solar spectrum in the Atacama Desert. *Scientific Reports*, Vol. 6, p. 22457.

- Cordero R. R., Damiani A., Jorquera J., Sepúlveda E., Caballero M., Fernandez S., Feron S., Llanillo P. J., Carrasco J., Laroze D., Labbe F. (2018). Ultraviolet radiation in the Atacama Desert. *Antonie van Leeuwenhoek*, Vol. 111 (8), pp. 1301–1313.
- Costello E. K., Halloy S. R. P., Reed S. C., Sowell P., Schmidt S. K. (2009). Fumarole-supported islands of biodiversity within a hyperarid, high-elevation landscape on Socoma Volcano, Puna de Atacama, Andes. *Applied and Environmental Microbiology*, Vol. 75 (3), pp. 735–747.
- Cousins C. R., Crawford I. A. (2011). Volcano-ice interaction as a microbial habitat on Earth and Mars. *Astrobiology*, Vol. 11 (7). PMID: 21877914, pp. 695–710.
- Cousins C., Crawford I., Carrivick J., Gunn M., Harris J., Kee T., Karlsson M., Carmody L., Cockell C., Herschy B., Joy K. (2013). Glaciovolcanic hydrothermal environments in Iceland and implications for their detection on Mars. *Journal of Volcanology and Geothermal Research*, Vol. 256, pp. 61–77.
- Cox R. E., Maxwell J. R., Myers R. N. (1976). Monocarboxylic acids from oxidation of acyclic isoprenoid alkanes by *Mycobacterium fortuitum*. *Lipids*, Vol. 11 (1), pp. 72–76.
- Craddock R. A., Lorenz R. D. (2017). The changing nature of rainfall during the early history of Mars. *Icarus*, Vol. 293, pp. 172–179.
- Crater Analysis Techniques Working Group (1979). Standard techniques for presentation and analysis of crater size-frequency data. *Icarus*, Vol. 37 (2), pp. 467–474.
- Crowe M. J. (2008). *The extraterrestrial life debate, Antiquity to 1915: A source book*. Notre Dame IN: University of Notre Dame.
- Curphey E. (1952). Possible reactions in the geosynthesis of petroleum. *Petroleum (London)*, Vol. 15, p. 297.
- Dartnell L. R., Desorgher L., Ward J. M., Coates A. J. (2007). Modelling the surface and subsurface Martian radiation environment: Implications for astrobiology. *Geophysical Research Letters*, Vol. 34 (2), p. L02207.
- Dartnell L. R., Hunter S. J., Lovell K. V., Coates A. J., Ward J. M. (2010). Low-temperature ionizing radiation resistance of *Deinococcus radiodurans* and Antarctic Dry Valley bacteria. *Astrobiology*, Vol. 10 (7), pp. 717–732.
- Darwin Correspondence Project (2018). *Letter no. 7471*. URL: <https://www.darwinproject.ac.uk/>.
- Dauphas N., Pourmand A. (2011). Hf–W–Th evidence for rapid growth of Mars and its status as a planetary embryo. *Nature*, Vol. 473 (7348), pp. 489–492.
- Davila A. F., Gómez-Silva B., de los Rios A., Ascaso C., Olivares H., McKay C. P., Wierzchos J. (2008). Facilitation of endolithic microbial survival in the hyperarid core of the Atacama Desert by mineral deliquescence. *Journal of Geophysical Research: Biogeosciences*, Vol. 113, G01028.
- de Silva S. L. (1989). Altiplano-Puna volcanic complex of the central Andes. *Geology*, Vol. 17 (12), pp. 1102–1106.
- de Silva S. L., Francis P. W. (1991). Escalante and Sairecabur. In: *Volcanoes of the Central Andes*. Springer-Verlag: Berlin, pp. 78–80.

- de Vera J.-P., Schulze-Makuch D., Khan A., Lorek A., Koncz A., Möhlmann D., Spohn T. (2014). Adaptation of an Antarctic lichen to Martian niche conditions can occur within 34 days. *Planetary and Space Science*, Vol. 98. Planetary evolution and life, pp. 182–190.
- Debaille V., Brandon A. D., O'Neill C., Yin Q.-Z., Jacobsen B. (2009). Early martian mantle overturn inferred from isotopic composition of nakhlite meteorites. *Nature Geoscience*, Vol. 2, pp. 548–552.
- Demergasso C., Dorador C., Meneses D., Blamey J., Cabrol N., Escudero L., Chong G. (2010). Prokaryotic diversity pattern in high-altitude ecosystems of the Chilean Altiplano. *Journal of Geophysical Research: Biogeosciences*, Vol. 115 (G2), G00D09.
- Déruelle B. (1982). Sairecabur volcano, a Plio-Quaternary calc-alkaline massif of the Andes of Atacama: petrology. In: *III Congreso Geológico Chileno – Concepción, Chile*. Vol. 2, pp. D20–D40.
- Déruelle B. (1978). Calc-alkaline and shoshonitic lavas from five Andean volcanoes (between latitudes 21°45' and 24°30'S) and the distribution of the Plio-Quaternary volcanism of the south-central and southern Andes. *Journal of Volcanology and Geothermal Research*, Vol. 3 (3), pp. 281–298.
- Des Marais D. J., Allamandola L. J., Benner S. A., Boss A. P., Deamer D., Falkowski P. G., Farmer J. D., Hedges S. B., Jakosky B. M., Knoll A. H., Liskowsky D. R., Meadows V. S., Meyer M. A., Pilcher C. B., Nealson K. H., Spormann A. M., Trent J. D., Turner W. W., Woolf N. J., Yorke H. W. (2003). The NASA astrobiology roadmap. *Astrobiology*, Vol. 3 (2), pp. 219–235.
- Des Marais D. J., Nuth J. A., Allamandola L. J., Boss A. P., Farmer J. D., Hoehler T. M., Jakosky B. M., Meadows V. S., Pohorille A., Runnegar B., Spormann A. M. (2008). The NASA astrobiology roadmap. *Astrobiology*, Vol. 8 (4), pp. 715–730.
- Despland E. (2014). Butterflies of the high-altitude Atacama Desert: habitat use and conservation. *Frontiers in Genetics*, Vol. 5, p. 334.
- Di Liberto T. (Apr. 2015a). *Flooding in Chile's Atacama Desert after years' worth of rain in one day*. National Oceanic and Atmospheric Administration. URL: <https://www.climate.gov>.
- (Apr. 2015b). *Flooding in the Atacama Desert: How did that happen?* National Oceanic and Atmospheric Administration. URL: <https://www.climate.gov>.
- Dias M. P., Bastos M. S., Xavier V. B., Cassel E., Astarita L. V., Santarém E. R. (2017). Plant growth and resistance promoted by *Streptomyces* spp. in tomato. *Plant Physiology and Biochemistry*, Vol. 118, pp. 479–493.
- Dick S. J. (1982). *Plurality of worlds: The extraterrestrial life debate from Democritus to Kant*. Ed. by C. U. Press. Cambridge.
- Dick S. J. (1999). *The biological universe: The twentieth century extraterrestrial life debate and the limits of science*. Cambridge: Cambridge University Press.
- Dick S. J., Strick J. E. (2005a). *The living universe: NASA and the development of astrobiology*. Rutgers University Press: New Brunswick, New Jersey, London.

- (2005b). Viking to Mars. In: *The living universe: NASA and the development of astrobiology*. Rutgers University Press: New Brunswick, New Jersey, London, pp. 80–102.
- Didyk B. M., Simoneit B. R. T., Brassel S. C., Eglington G (1978). Organic geochemical indicators of palaeoenvironmental conditions of sedimentation. *Nature*, Vol. 272 (5650), pp. 216–222.
- Dingman R. J. (1967). Geology and ground-water resources of the northern part of the Salar de Atacama, Antofagasta Province, Chile. *United States Geological Survey Bulletin*, Vol. 1219, pp. 1–49.
- Direito S. O., Marees A., Röling W. F. (2012). Sensitive life detection strategies for low-biomass environments: Optimizing extraction of nucleic acids adsorbing to terrestrial and Mars analogue minerals. *FEMS Microbiology Ecology*, Vol. 81 (1), pp. 111–123.
- Dohm J. M., Anderson R. C., Baker V. R., Ferris J. C., Hare T. M., Strom R. G., Rudd L. P., Rice J. W., Casavant R. R., Scott D. H. (2000). System of Gigantic Valleys northwest of Tharsis, Mars: Latent catastrophic flooding, northwest watershed, and implications for Northern Plains Ocean. *Geophysical Research Letters*, Vol. 27 (21), pp. 3559–3562.
- Domagal-Goldman S. D., Wright K. E., Adamala K., Rubia L. Arina de la, Bond J., Dartnell L. R., Goldman A. D., Lynch K., Naud M.-E., Paulino-Lima I. G., Singer K., Walter-Antonio M., Abrevaya X. C., Anderson R., Arney G., Atri D., Azúa-Bustos A., Bowman J. S., Brazelton W. J., Brennecka G. A., Carns R., Chopra A., Colangelo-Lillis J., Crockett C. J., DeMarines J., Frank E. A., Frantz C., Fuente E. de la, Galante D., Glass J., Gleeson D., Glein C. R., Goldblatt C., Horak R., Horodyskyj L., Kaçar B., Kereszturi A., Knowles E., Mayeur P., McGlynn S., Miguel Y., Montgomery M., Neish C., Noack L., Rugheimer S., Stüeken E. E., Tamez-Hidalgo P., Walker S. I., Wong T. (2016). The Astrobiology Primer v2.0. *Astrobiology*, Vol. 16 (8), pp. 561–653.
- Dugmore A. J., Cook G. T., Shore J. S., Newton A. J., Edwards K. J., Larsen G. (1995). Radiocarbon dating tephra layers in Britain and Iceland. *Radiocarbon*, Vol. 37 (2), pp. 379–388.
- Dutkiewicz A., Rasmussen B., Buick R. (1998). Oil preserved in fluid inclusions in Archaean sandstones. *Nature*, Vol. 395, pp. 885–888.
- Eckmeier E., Wiesenberger G. L. B. (2009). Short-chain *n*-alkanes (C_{16–20}) in ancient soils are useful molecular markers for prehistoric biomass burning. *Journal of Archaeological Science*, Vol. 36 (7), pp. 1590–1596.
- Edgerton K. E. (1966). *Driest desert to aid life-on-Mars study*. California Digital Newspaper Collection (*San Bernardino Sun*, 22 May 1966, p. 3). URL: <https://cdnc.ucr.edu/>.
- Edwards C. S., Piqueux S. (2016). The water content of recurring slope lineae on Mars. *Geophysical Research Letters*, Vol. 43 (17), pp. 8912–8919.
- Eglington G., Hamilton R. J. (1967). Leaf epicuticular waxes. *Science*, Vol. 156 (3780), pp. 1322–1335.
- Eglington G., Scott P. M., Belsky T., Burlingame A. L., Calvin M., Cloud P. E. J. (1964). Hydrocarbon of biological origin from a one-billion year old sediment. *Science*, Vol. 145 (3629), pp. 263–264.

- Ehlmann B. L., Mustard J. F., Murchie S. L., Bibring J.-P., Meunier A., Fraeman A. A., Langevin Y. (2011). Subsurface water and clay mineral formation during the early history of Mars. *Nature*, Vol. 479, pp. 53–60.
- Ehrenfreund P., Glavin D. P., Botta O., Cooper G., Bada J. L. (2001). Extraterrestrial amino acids in Orgueil and Ivuna: Tracing the parent body of CI type carbonaceous chondrites. *Proceedings of the National Academy of Sciences*, Vol. 98 (5), pp. 2138–2141.
- Eigenbrode J. L., Summons R. E., Steele A., Freissinet C., Millan M., Navarro-González R., Sutter B., McAdam A. C., Franz H. B., Glavin D. P., Archer P. D., Mahaffy P. R., Conrad P. G., Hurowitz J. A., Grotzinger J. P., Gupta S., Ming D. W., Sumner D. Y., Szopa C., Malespin C., Buch A., Coll P. (2018). Organic matter preserved in 3-billion-year-old mudstones at Gale crater, Mars. *Science*, Vol. 360 (6393), pp. 1096–1101.
- El Gendy A. G., El Gohary A. E., Omer E. A., Hendawy S. F., Hussein M. S., Petrova V., Stancheva I. (2015). Effect of nitrogen and potassium fertilizer on herbage and oil yield of chervil plant (*Anthriscus cerefolium* L.) *Industrial Crops and Products*, Vol. 69, pp. 167–174.
- Elkins-Tanton L. T., Hess P. C., Parmentier E. M. (2005). Possible formation of ancient crust on Mars through magma ocean processes. *Journal of Geophysical Research: Planets*, Vol. 110, E12S01.
- Elsila J. E., Glavin D. P., Dworkin J. P. (2009). Cometary glycine detected in samples returned by Stardust. *Meteoritics & Planetary Science*, Vol. 44 (9), pp. 1323–1330.
- Ertem G., Ertem M. C., McKay C. P., Hazen R. M. (2017). Shielding biomolecules from effects of radiation by Mars analogue minerals and soils. *International Journal of Astrobiology*, Vol. 16 (3), pp. 280–285.
- Faboro E. O., Wei L., Liang S., McDonald A. G., Obafemi C. A. (2016). Characterization of dichloromethane and methanol extracts from the leaves of a medicinal plant: *Globimetula oreophila*. *Industrial Crops and Products*, Vol. 83, pp. 391–399.
- Fadeel A. A. (1962). Location and properties of chloroplasts and pigment determination in roots. *Physiologia Plantarum*, Vol. 15 (1), pp. 130–146.
- Fairbanks B., Woods L., Bryant R., Elliott E., Cole C., Coleman D. (1984). Limitations of ATP estimates of microbial biomass. *Soil Biology and Biochemistry*, Vol. 16 (6), pp. 549–558.
- Fairén A. G., Ruiz J., Anguita F. (2002). An origin for the linear magnetic anomalies on Mars through accretion of terranes: Implications for dynamo timing. *Icarus*, Vol. 160 (1), pp. 220–223.
- Fairén A. G., Chevrier V., Abramov O., Marzo G. A., Gavin P., Davila A. F., Tornabene L. L., Bishop J. L., Roush T. L., Gross C., Kneissl T., Uceda E. R., Dohm J. M., Schulze-Makuch D., Rodríguez J. A. P., Amils R., McKay C. P. (2010). Noachian and more recent phyllosilicates in impact craters on Mars. *Proceedings of the National Academy of Sciences*, Vol. 107 (27), pp. 12095–12100.
- Fajardo-Cavazos P., Schuerger A. C., Nicholson W. L. (2008). Persistence of biomarker ATP and ATP-generating capability in bacterial cells and spores contaminating spacecraft ma-

- terials under Earth conditions and in a simulated martian environment. *Applied and Environmental Microbiology*, Vol. 74 (16), pp. 5159–5167.
- Farmer J. D., Des Marais D. J. (1999). Exploring for a record of ancient Martian life. *Journal of Geophysical Research: Planets*, Vol. 104 (E11), pp. 26977–26995.
- Fassett C. I., Head J. W. (2008). Valley network-fed, open-basin lakes on Mars: Distribution and implications for Noachian surface and subsurface hydrology. *Icarus*, Vol. 198 (1), pp. 37–56.
- Fastook J. L., Head J. W. (2015). Glaciation in the Late Noachian Icy Highlands: Ice accumulation, distribution, flow rates, basal melting, and top-down melting rates and patterns. *Planetary and Space Science*, Vol. 106, pp. 82–98.
- Faure P., Schlepp L., Burkle-Vitzthum V., Elie M. (2003). Low temperature air oxidation of *n*-alkanes in the presence of Na-smectite. *Fuel*, Vol. 82 (14), pp. 1751–1762.
- Fernández-Remolar D. C., Prieto-Ballesteros O., Rodríguez N., Gómez F., Amils R., Gómez-Elvira J., Stoker C. R. (2008). Underground habitats in the Río Tinto basin: A model for subsurface life habitats on Mars. *Astrobiology*, Vol. 8 (5), pp. 1023–1047.
- Feuersänger C. (2018). *PGFPlots - A \LaTeX package to create normal/logarithmic plots in two and three dimensions (version 1.16)*. URL: <http://sourceforge.net/projects/pgfplots/>.
- Ficken K. J., Li B, Swain D. L., Eglinton G (2000). An *n*-alkane proxy for the sedimentary input of submerged/floating freshwater aquatic macrophytes. *Organic Geochemistry*, Vol. 31 (7), pp. 745–749.
- Fierer N., McCain C. M., Meir P., Zimmermann M., Rapp J. M., Silman M. R., Knight R. (2011). Microbes do not follow the elevational diversity patterns of plants and animals. *Ecology*, Vol. 92 (4), pp. 797–804.
- Figueroa J. C., Figueroa O. A. (2006). Petrografía y geoquímica de las lavas del volcán Saicabur, Andes Centrales, Chile [in Spanish]. In: *XI Congreso Geológico Chileno – Antofagasta, Chile*, pp. 459–462.
- Filiberto J., Dasgupta R. (2015). Constraints on the depth and thermal vigor of melting in the Martian mantle. *Journal of Geophysical Research: Planets*, Vol. 120 (1), pp. 109–122.
- Fletcher L. E., Valdivia-Silva J. E., Perez-Montaña S., Condori-Apaza R. M., Conley C. A., McKay C. P. (2012). Variability of organic material in surface horizons of the hyper-arid Mars-like soils of the Atacama Desert. *Advances in Space Research*, Vol. 49 (2), pp. 271–279.
- Flynn G. J. (1996). The delivery of organic matter from asteroids and comets to the early surface of Mars. *Earth, Moon, and Planets*, Vol. 72 (1–3), pp. 469–474.
- Forget F. (2004). Alien Weather at the Poles of Mars. *Science*, Vol. 306 (5700), pp. 1298–1299.
- Fornaro T., Boosman A., Brucato J. R., ten Kate I. L., Siljeström S., Poggiali G., Steele A., Hazen R. M. (2018). UV irradiation of biomarkers adsorbed on minerals under Martian-like conditions: Hints for life detection on Mars. *Icarus*, Vol. 313, pp. 38–60.

- Freissinet C., Glavin D. P., Mahaffy P. R., Miller K. E., Eigenbrode J. L., Summons R. E., Brunner A. E., Buch A., Szopa C., Archer P. D., Franz H. B., Atreya S. K., Brinckerhoff W. B., Cabane M., Coll P., Conrad P. G., Des Marais D. J., Dworkin J. P., Fairén A. G., François P., Grotzinger J. P., Kashyap S., Kate I. L., Leshin L. A., Malespin C. A., Martin M. G., Martin-Torres F. J., McAdam A. C., Ming D. W., Navarro-González R., Pavlov A. A., Prats B. D., Squyres S. W., Steele A., Stern J. C., Sumner D. Y., Sutter B., Zorzano M.-P., the MSL Science Team (2015). Organic molecules in the Sheepbed Mudstone, Gale Crater, Mars. *Journal of Geophysical Research: Planets*, Vol. 120 (3), pp. 495–514.
- Frick A., Mogul R., Stabekis P., Conley C. A., Ehrenfreund P. (2014). Overview of current capabilities and research and technology developments for planetary protection. *Advances in Space Research*, Vol. 54 (2), pp. 221–240.
- Friedmann E. I., Ocampo R. (1976). Endolithic blue-green algae in the Dry Valleys: Primary producers in the Antarctic desert ecosystem. *Science*, Vol. 193 (4259), pp. 1247–1249.
- Fritze H., Pennanen T., Haimi J., Siira-Pietikäinen A., Vanhala P. (2000). Effects of heavy metals on soil microflora. In: *Forest Condition in a Changing Environment: The Finnish Case*. Ed. by E. Mälikönen. Dordrecht: Springer Netherlands, pp. 260–265. ISBN: 978-94-015-9373-1.
- Gagosian R. B., Peltzer E. T. (1986). The importance of atmospheric input of terrestrial organic material to deep sea sediments. *Organic Geochemistry*, Vol. 10 (4), pp. 661–669.
- Gallagher C., Balme M., Conway S., Grindrod P. (2011). Sorted clastic stripes, lobes and associated gullies in high-latitude craters on Mars: Landforms indicative of very recent, polycyclic ground-ice thaw and liquid flows. *Icarus*, Vol. 211 (1), pp. 458–471.
- Garry J. R. C., Kate I. L. ten, Martins Z., Nørnberg P., Ehrenfreund P. (2006). Analysis and survival of amino acids in Martian regolith analogs. *Meteoritics & Planetary Science*, Vol. 41 (3), pp. 391–405.
- Gemini (2015). *Data sheet – Tinytag Plus 2 dual channel temperature/relative humidity (–25 to +85°C/0 to 100% RH): TGP-4500 – (Issue 13 : 9th August 2019)*. Ed. by Gemini. URL: <https://www.geminidataloggers.com>.
- Gentry D. M., Amador E. S., Cable M. L., Chaudry N., Cullen T., Jacobsen M. B., Murukesan G., Schwieterman E. W., Stevens A. H., Stockton A., Tan G., Yin C., Cullen D. C., Geppert W. (2017). Correlations between life-detection techniques and implications for sampling site selection in pPlanetary analog missions. *Astrobiology*, Vol. 17 (10), pp. 1009–1021.
- Georgiou C. D., Deamer D. W. (2014). Lipids as Universal Biomarkers of Extraterrestrial Life. *Astrobiology*, Vol. 14 (6), pp. 541–549.
- Gilichinsky D., Wilson G., Friedmann E., McKay C., Sletten R., Rivkina E., Vishnivetskaya T., Erokhina L., Ivanushkina N., Kochkina G., Shcherbakova V., Soina V., Spirina E., Vorobyova E., Fyodorov-Davydov D., Hallet B., Ozerskaya S., Sorokovikov V., Laurinavichyus K., Shatilovich A., Chanton J., Ostroumov V., Tiedje J. (2007). Microbial populations in antarctic permafrost: Biodiversity, state, age, and implication for astrobiology. *Astrobiology*, Vol. 7 (2), pp. 275–311.

- Glavin D. P., Bada J. L., Brinton K. L. F., McDonald G. D. (1999). Amino acids in the Martian meteorite Nakhla. *Proceedings of the National Academy of Sciences*, Vol. 96 (16), pp. 8835–8838.
- Goldstein J. I., Newbury D. E., Michael J. R., Ritchie N. W., Scott J. H. J., Joy D. C. (2018). Energy dispersive X-ray spectroscopy: Physical principles and user-selected parameters. In: *Scanning Electron Microscopy and X-Ray Microanalysis*. 4th edition. Springer-Verlag, New York, pp. 209–234.
- Gonçalves V. N., Cantrell C. L., Wedge D. E., Ferreira M. C., Soares M. A., Jacob M. R., Oliveira F. S., Galante D., Rodrigues F., Alves T. M. A., Zani C. L., Junior P. A. S., Murta S., Romanha A. J., Barbosa E. C., Kroon E. G., Oliveira J. G., Gomez-Silva B., Galetovic A., Rosa C. A., Rosa L. H. (2016). Fungi associated with rocks of the Atacama Desert: taxonomy, distribution, diversity, ecology and bioprospection for bioactive compounds. *Environmental Microbiology*, Vol. 18 (1), pp. 232–245.
- Goordial J., Davila A., Lacelle D., Pollard W., Marinova M. M., Greer C. W., DiRuggiero J., McKay C. P., Whyte L. G. (2016). Nearing the cold-arid limits of microbial life in permafrost of an upper dry valley, Antarctica. *The ISME Journal*, Vol. 10, pp. 1613–1624.
- Goossens H., de Leeuw J. W., Schenck P. A., Brassell S. C. (1984). Tocopherols as likely precursors of pristane in ancient sediments and crude oils. *Nature*, Vol. 312, pp. 440–442.
- Goudge T. A., Fassett C. I., Head J. W., Mustard J. F., Aureli K. L. (2016). Insights into surface runoff on early Mars from paleolake basin morphology and stratigraphy. *Geology*, Vol. 44 (6), p. 419.
- Goutx M., Saliot A (1980). Relationship between dissolved and particulate fatty acids and hydrocarbons, chlorophyll *a* and zooplankton biomass in Villefranche Bay, Mediterranean Sea. *Marine Chemistry*, Vol. 8 (4), pp. 299–318.
- Grady M. M., Wright I. P., Douglas C., Pillinger C. T. (1994). Carbon and nitrogen in ALH 84001. *Meteoritics*, Vol. 29 (4), p. 469.
- Grott M., Baratoux D., Hauber E., Sautter V., Mustard J., Gasnault O., Ruff S. W., Karato S.-I., Debaille V., Knapmeyer M., Sohl F., Van Hoolst T., Breuer D., Morschhauser A., Toplis M. J. (2013). Long-term evolution of the martian crust-mantle system. *Space Science Reviews*, Vol. 174 (1), pp. 49–111.
- Gu Y.-Q., Mo M.-H., Zhou J.-P., Zou C.-S., Zhang K.-Q. (2007). Evaluation and identification of potential organic nematocidal volatiles from soil bacteria. *Soil Biology and Biochemistry*, Vol. 39 (10), pp. 2567–2575.
- Haberle R. M., Gómez-Elvira J., Torre Juárez M., Harri A.-M., Hollingsworth J. L., Kahanpää H., Kahre M. A., Lemmon M., Martín-Torres F. J., Mischna M., Moores J. E., Newman C., Rafkin S. C. R., Rennó N., Richardson M. I., Rodríguez-Manfredi J. A., Vasavada A. R., Zorzano-Mier M.-P., the REMS/MSL Science Team (2014). Preliminary interpretation of the REMS pressure data from the first 100 sols of the MSL mission. *Journal of Geophysical Research: Planets*, Vol. 119 (3), pp. 440–453.

- Halloy S. (1991). Islands of life at 6000 m altitude: The environment of the highest autotrophic communities on Earth (Socompa Volcano, Andes). *Arctic and Alpine Research*, Vol. 23 (3), pp. 247–262.
- Hamilton-Kemp T., Newman M., Collins R., Elgaali H., Yu K., Archbold D. (2005). Production of the long-chain alcohols octanol, decanol, and dodecanol by *Escherichia coli*. *Current Microbiology*, Vol. 51 (2), pp. 82–86.
- Han J., Calvin M. (1969). Hydrocarbon distribution of algae and bacteria, and microbiological activity in sediments. *Proceedings of the National Academy of Sciences*, Vol. 64 (2), pp. 436–443.
- Hansen B. M. S. (2009). Formation of the terrestrial planets from a narrow annulus. *The Astrophysical Journal*, Vol. 703 (1), pp. 1131–1140.
- Harmon R. S., Barreiro B. A., Moorbath S., Hoefs J., Francis P. W., Thorpe R. S., Déruelle B., McHugh J., Viglino J. A. (1984). Regional O-, Sr-, and Pb-isotope relationships in late Cenozoic calc-alkaline lavas of the Andean Cordillera. *Journal of the Geological Society*, Vol. 141 (5), pp. 803–822.
- Harri A.-M., Genzer M., Kemppinen O., Gomez-Elvira J., Haberle R., Polkko J., Savijärvi H., Rennó N., Rodriguez-Manfredi J. A., Schmidt W., Richardson M., Siili T., Paton M., Torre-Juarez M. de la, Mäkinen T., Newman C., Rafkin S., Mischna M., Merikallio S., Haukka H., Martin-Torres J., Komu M., Zorzano M.-P., Peinado V., Vazquez L., Urqui R. (2014a). Mars Science Laboratory relative humidity observations: Initial results. *Journal of Geophysical Research: Planets*, Vol. 119 (9), pp. 2132–2147.
- Harri A.-M., Genzer M., Kemppinen O., Kahanpää H., Gomez-Elvira J., Rodriguez-Manfredi J. A., Haberle R., Polkko J., Schmidt W., Savijärvi H., Kauhanen J., Atlaskin E., Richardson M., Siili T., Paton M., Torre Juarez M., Newman C., Rafkin S., Lemmon M. T., Mischna M., Merikallio S., Haukka H., Martin-Torres J., Zorzano M.-P., Peinado V., Urqui R., Lapinette A., Scodary A., Mäkinen T., Vazquez L., Rennó N., the REMS/MSL Science Team (2014b). Pressure observations by the Curiosity rover: Initial results. *Journal of Geophysical Research: Planets*, Vol. 119 (1), pp. 82–92.
- Hart K. M., Szpak M. T., Mahaney W. C., Dohm J. M., Jordan S. F., Frazer A. R., Allen C. C., Kelleher B. P. (2011). A bacterial enrichment study and overview of the extractable lipids from paleosols in the Dry Valleys, Antarctica: implications for future Mars reconnaissance. *Astrobiology*, Vol. 11 (4), pp. 303–321.
- Hartley A. J., Chong G., Houston J., Mather A. E. (2005). 150 million years of climatic stability: evidence from the Atacama Desert, northern Chile. *Journal of the Geological Society*, Vol. 162 (3), pp. 421–424.
- Hartley A., Flint S., Turner P., Jolley E. (1992). Tectonic controls on the development of a semi-arid alluvial basin as reflected in the stratigraphy of the Purilactis Group (upper cretaceous-eocene), northern Chile. *Journal of South American Earth Sciences*, Vol. 5 (3), pp. 275–296.
- Hartmann J., Brand M. C., Dose K. (1981). Formation of specific amino acid sequences during thermal polymerization of amino acids. *Biosystems*, Vol. 13 (3), pp. 141–147.

- Hartmann W. K. (2005). Martian cratering 8: Isochron refinement and the chronology of Mars. *Icarus*, Vol. 174 (2), pp. 294–320.
- Hartmann W. K., Neukum G. (2001). Cratering Chronology and the Evolution of Mars. *Space Science Reviews*, Vol. 96 (1), pp. 165–194.
- Hassler D. M., Zeitlin C., Wimmer-Schweingruber R. F., Ehresmann B., Rafkin S., Eigenbrode J. L., Brinza D. E., Weigle G., Böttcher S., Böhm E., Burmeister S., Guo J., Köhler J., Martin C., Reitz G., Cucinotta F. A., Kim M.-H., Grinspoon D., Bullock M. A., Posner A., Gómez-Elvira J., Vasavada A., Grotzinger J. P., the MSL Science Team (2014). Mars' surface radiation environment measured with the Mars Science Laboratory's Curiosity rover. *Science*, Vol. 343 (6169), p. 1244797.
- Hastenrath S., Kutzbach J. (1985). Late Pleistocene climate and water budget of the south American Altiplano. *Quaternary Research*, Vol. 24 (3), pp. 249–256.
- Head J. W., Marchant D. R. (2014). The climate history of early Mars: Insights from the Antarctic McMurdo Dry Valleys hydrologic system. *Antarctic Science*, Vol. 26 (6), pp. 774–800.
- Heiri O., Lotter A. F., Lemcke G. (2001). Loss on ignition as a method for estimating organic and carbonate content in sediments: reproducibility and comparability of results. *Journal of Paleolimnology*, Vol. 25, pp. 101–110.
- Hess S. L., Henry R. M., Leovy C. B., Mitchell J. L., Ryan J. A., Tillman J. E. (1976a). Early meteorological results from the Viking 2 lander. *Science*, Vol. 194 (4271), pp. 1352–1353.
- Hess S. L., Henry R. M., Leovy C. B., Ryan J. A., Tillman J. E., Chamberlain T. E., Cole H. L., Dutton R. G., GRreene G. C., Simon W. E., Mitchell J. L. (1976b). Mars Climatology from Viking 1 after 20 Sols. *Science*, Vol. 194 (4260), pp. 78–81.
- Hess S. L., Henry R. M., Leovy C. B., Ryan J. A., Tillman J. E. (1977). Meteorological results from the surface of Mars: Viking 1 and 2. *Journal of Geophysical Research*, Vol. 82 (28), pp. 4559–4574.
- Heydel F., Cunze S., Bernhardt-Römermann M., Tackenberg O. (2014). Long-distance seed dispersal by wind: disentangling the effects of species traits, vegetation types, vertical turbulence and wind speed. *Ecological Research*, Vol. 29 (4), pp. 641–651.
- Hiesinger H., Head J. W. (2004). The Syrtis Major volcanic province, Mars: Synthesis from Mars Global Surveyor data. *Journal of Geophysical Research: Planets*, Vol. 109, E01004.
- Hirt C., Claessens S., Fecher T., Kuhn M., Pail R., Rexer M. (2013). New ultrahigh-resolution picture of Earth's gravity field. *Geophysical Research Letters*, Vol. 40 (16), pp. 4279–4283.
- Hoogsteen M. J. J., Lantinga E. A., Bakker E. J., Groot J. C. J., Tittonell P. A. (2015). Estimating soil organic carbon through loss on ignition: Effects of ignition conditions and structural water loss. *European Journal of Soil Science*, Vol. 66 (2), pp. 320–328.
- Hoogsteen M. J. J., Lantinga E. A., Bakker E. J., Tittonell P. A. (2018). An evaluation of the loss-on-ignition method for determining the soil organic matter content of calcareous soils. *Communications in Soil Science and Plant Analysis*, Vol. 49 (13), pp. 1541–1552.

- Horneck G., Moeller R., Cadet J., Douki T., Mancinelli R. L., Nicholson W. L., Panitz C., Rabbow E., Rettberg P., Spry A., Stackebrandt E., Vaishampayan P., Venkateswaran K. J. (2012). Resistance of bacterial endospores to outer space for planetary protection purposes—Experiment PROTECT of the EXPOSE-E mission. *Astrobiology*, Vol. 12 (5), pp. 445–456.
- Horneck G., Walter N., Westall F., Grenfell J. L., Martin W. F., Gomez F., Leuko S., Lee N., Onofri S., Tsiganis K., Saladino R., Pilat-Lohinger E., Palomba E., Harrison J., Rull F., Muller C., Strazzulla G., Brucato J. R., Rettberg P., Capria M. T. (2016). AstRoMap European Astrobiology Roadmap. *Astrobiology*, Vol. 16 (3), pp. 201–243.
- Horowitz N. H., Cameron R. E., Hubbard J. S. (1972). Microbiology of the Dry Valleys of Antarctica. *Science*, Vol. 176 (4032), pp. 242–245.
- Houston J., Hartley A. J. (2003). The central Andean west-slope rainshadow and its potential contribution to the origin of hyper-aridity in the Atacama Desert. *International Journal of Climatology*, Vol. 23 (12), pp. 1453–1464.
- Huang P. M. (1990). Role of soil minerals in transformation of natural organics and xenobiotics in soil. In: *Soil biochemistry*, 6th edition. Ed. by J.-M. Bollag, G. Stotzky. New York – Basel: Marcel Dekker, Inc, pp. 29–116.
- Huang X., Zhao B., Wang K., Hu Y., Meyers P. A. (2018). Seasonal variations of leaf wax *n*-alkane molecular composition and δD values in two subtropical deciduous tree species: Results from a three-year monitoring program in central China. *Organic Geochemistry*, Vol. 118, pp. 15–26.
- Huybrechts D. R. C., Bruycker L. D., Jacobs P. A. (1990). Oxyfunctionalization of alkanes with hydrogen peroxide on titanium silicalite. *Nature*, Vol. 345, pp. 240–242.
- Hynek B. M., Osterloo M. K., Kierein-Young K. S. (2015). Late-stage formation of Martian chloride salts through ponding and evaporation. *Geology*, Vol. 43 (9), pp. 787–790.
- Ivanov B. A. (2001). Mars/Moon Cratering Rate Ratio Estimates. *Space Science Reviews*, Vol. 96 (1–4), pp. 87–104.
- Jakosky B. M., Slipski M., Benna M., Mahaffy P., Elrod M., Yelle R., Stone S., Alsaeed N. (2017). Mars' atmospheric history derived from upper-atmosphere measurements of $^{38}\text{Ar}/^{36}\text{Ar}$. *Science*, Vol. 355 (6332), pp. 1408–1410.
- Jakosky B. M., Grebowsky J. M., Luhmann J. G., Brain D. A. (2015). Initial results from the MAVEN mission to Mars. *Geophysical Research Letters*, Vol. 42 (21), pp. 8791–8802.
- Jaksic F. M., Torres-Mura J. C., Cornelius C., Marquet P. A. (1999). Small mammals of the Atacama Desert (Chile). *Journal of Arid Environments*, Vol. 42 (2), pp. 129–135.
- Jansen B., Nierop K. G., Hageman J. A., Cleef A. M., Verstraten J. M. (2006). The straight-chain lipid biomarker composition of plant species responsible for the dominant biomass production along two altitudinal transects in the Ecuadorian Andes. *Organic Geochemistry*, Vol. 37 (11), pp. 1514–1536.
- Jetter R., Kunst L., Samuels A. L. (2006). Composition of plant cuticular waxes. In: *Biology of the Plant Cuticle, Annual Plant Reviews*. Ed. by M. Riederer, C. Müller. Vol. 23. Blackwell: Oxford, pp. 145–181.

- Johnsson A., Reiss D., Hauber E., Zanetti M., Hiesinger H., Johansson L., Olvmo M. (2012). Periglacial mass-wasting landforms on Mars suggestive of transient liquid water in the recent past: Insights from solifluction lobes on Svalbard. *Icarus*, Vol. 218 (1), pp. 489–505.
- Jolley E. J., Turner P., Williams G. D., Hartley A. J., Flint S. (1990). Sedimentological response of an alluvial system to Neogene thrust tectonics, Atacama Desert, northern Chile. *Journal of the Geological Society*, Vol. 147 (5), pp. 769–784.
- Jónasson H. (1937). Gróður í Slúttnessi [in Icelandic]. *Náttúrufræðingurinn*, Vol. 7, p. 150.
- Jónasson H. (1972). Flóra Mývatnssveitar [in Icelandic]. *Acta Botanica Islandica*, Vol. 1, pp. 32–42.
- Jones D. F. (1968). Microbiological oxidation of long-chain aliphatic compounds. Part II. Branched-chain alkanes. *Journal of the Chemical Society C: Organic*, pp. 2809–2815.
- Jones D. F., Howe R. (1968). Microbiological oxidation of long-chain aliphatic compounds. Part I. Alkanes and alk-1-enes. *Journal of the Chemical Society C: Organic* (0), pp. 2801–2808.
- Jones J. G. (1969). Studies on lipids of soil micro-organisms with particular reference to hydrocarbons. *Microbiology*, Vol. 59 (2), pp. 145–152.
- Jones J. H., Neal C. R., Ely J. C. (2003). Signatures of the highly siderophile elements in the SNC meteorites and Mars: a review and petrologic synthesis. *Chemical Geology*, Vol. 196 (1), pp. 5–25.
- Joshi N. A., Fass J. N. (2011). *Sickle: A sliding-window, adaptive, quality-based trimming tool for FastQ files (Version 1.33)*. URL: <https://github.com/najoshi/sickle>.
- Jull A., Beck J., Burr G. (2000). Isotopic evidence for extraterrestrial organic material in the Martian meteorite, Nakhla. *Geochimica et Cosmochimica Acta*, Vol. 64 (21), pp. 3763–3772.
- Kanavarioti A., Mancinelli R. L. (1990). Could organic matter have been preserved on Mars for 3.5 billion years? *Icarus*, Vol. 84 (1), pp. 196–202.
- Kaplan H. H., Milliken R. E., Fernández-Remolar D., Amils R., Robertson K., Knoll A. H. (2016). Orbital evidence for clay and acidic sulfate assemblages on Mars based on mineralogical analogs from Rio Tinto, Spain. *Icarus*, Vol. 275, pp. 45–64.
- Kato S., Kobayashi C., Kakegawa T., Yamagishi A. (2009). Microbial communities in iron-silica-rich microbial mats at deep-sea hydrothermal fields of the Southern Mariana Trough. *Environmental Microbiology*, Vol. 11, pp. 2094–2111.
- Kato S., Itoh T., Yamagishi A. (2011). Archaeal diversity in a terrestrial acidic spring field revealed by a novel PCR primer targeting archaeal 16S rRNA genes. *FEMS Microbiology Letters*, Vol. 319 (34–43).
- Kaur G., Mountain B. W., Hopmans E. C., Pancost R. D. (2011). Preservation of microbial lipids in geothermal sinters. *Astrobiology*, Vol. 11 (3), pp. 259–274.
- Khan S., El-Latif Hesham A., Qiao M., Rehman S., He J.-Z. (2010). Effects of Cd and Pb on soil microbial community structure and activities. *Environmental Science and Pollution Research*, Vol. 17 (2), pp. 288–296.

- Khouw C. B., Dartt C. B., Labinger J. A., Davis M. E. (1994). Studies on the Catalytic-Oxidation of Alkanes and Alkenes by Titanium Silicates. *Journal of Catalysis*, Vol. 149 (1), pp. 195–205.
- Kim J., Cho H.-K., Mok J., Yoo H. D., Cho N. (2013). Effects of ozone and aerosol on surface UV radiation variability. *Journal of Photochemistry and Photobiology B: Biology*, Vol. 119, pp. 46–51.
- Klein H. P. (1999). Did Viking discover life on Mars? *Origins of Life and Evolution of the Biosphere*, Vol. 29 (6), pp. 625–631.
- Kminek G., Conley C., Yano H. (2017). COSPAR's planetary protection policy. *Space Research Today*, Vol. 200, pp. 12–25.
- Kminek G., Bada J. L. (2006). The effect of ionizing radiation on the preservation of amino acids on Mars. *Earth and Planetary Science Letters*, Vol. 245 (1), pp. 1–5.
- Knowles J. R. (1980). Enzyme-catalyzed phosphoryl transfer reactions. *Annual Review of Biochemistry*, Vol. 49 (1), pp. 877–919.
- Kuhn T. K., Krull E. S., Bowater A., Grice K., Gleixner G. (2010). The occurrence of short chain *n*-alkanes with an even over odd predominance in higher plants and soils. *Organic Geochemistry*, Vol. 41 (2), pp. 88–95.
- Kuparinen A. (2006). Mechanistic models for wind dispersal. *Trends in Plant Science*, Vol. 11 (6), pp. 296–301.
- Kurokawa H., Kurosawa K., Usui T. (2018). A lower limit of atmospheric pressure on early Mars inferred from nitrogen and argon isotopic compositions. *Icarus*, Vol. 299, pp. 443–459.
- Latorre C., Betancourt J. L., Rylander K. A., Quade J. (2002). Vegetation invasions into absolute desert: A 45 000 yr rodent midden record from the Calama–Salar de Atacama basins, northern Chile (lat 22°–24°S). *GSA Bulletin*, Vol. 114 (3), pp. 349–366.
- Lattanzio V. M., Corcelli A., Mascolo G., Oren A. (2002). Presence of two novel cardiolipins in the halophilic archaeal community in the crystallizer brines from the salterns of Margherita di Savoia (Italy) and Eilat (Israel). *Extremophiles*, Vol. 6 (6), pp. 437–444.
- Lazar R. (2005). Konzept für eine bioklimatische Bewertung eines Expeditions- und Trekkinggebietes in mittleren und großen Höhen [in German]. *Wiener Medizinische Wochenschrift*, Vol. 155 (7), pp. 176–187.
- Lederberg J. (1960). Exobiology: Approaches to life beyond the Earth. *Science*, Vol. 132 (3424), pp. 393–400.
- Lederberg J., Cowie D. B. (1958). Moondust. *Science*, Vol. 127 (3313), pp. 1473–1475.
- Lee M. R., Lindgren P. (2016). Aqueous alteration of chondrules from the Murchison CM carbonaceous chondrite: Replacement, pore filling, and the genesis of polyhedral serpentine. *Meteoritics & Planetary Science*, Vol. 51 (6), pp. 1003–1021.
- Lee M. R., Daly L., Cohen B. E., Hallis L. J., Griffin S., Trimby P., Boyce A., Mark D. F. (2018). Aqueous alteration of the Martian meteorite Northwest Africa 817: Probing fluid–rock interaction at the nakhlite launch site. *Meteoritics & Planetary Science*, Vol. 53 (11), pp. 2395–2412.

- Lee M. R., Lindgren P., King A. J., Greenwood R. C., Franchi I. A., Sparkes R. (2016). Elephant Moraine 96029, a very mildly aqueously altered and heated CM carbonaceous chondrite: Implications for the drivers of parent body processing. *Geochimica et Cosmochimica Acta*, Vol. 187, pp. 237–259.
- Leitgeb H. (1858). Die Haftwurzeln des Epheu. *Sitzungsberichte der kaiserlichen Akademie der Wissenschaften, Mathematisch-Naturwissenschaftliche Classe*, Vol. 29 (10), pp. 350–361.
- Lester E. D., Satomi M., Ponce A. (2007). Microflora of extreme arid Atacama Desert soils. *Soil Biology and Biochemistry*, Vol. 39 (2), pp. 704–708.
- Léveillé R. (2010). A half-century of terrestrial analog studies: From craters on the Moon to searching for life on Mars. *Planetary and Space Science*, Vol. 58 (4), pp. 631–638.
- Levin G. V., Straat P. A. (2016). The case for extant life on Mars and its possible detection by the Viking labeled release experiment. *Astrobiology*, Vol. 16 (10), pp. 798–810.
- Levy J., Head J., Dickson J., Fassett C., Morgan G., Schon S. (2010). Identification of gully debris flow deposits in Protonilus Mensae, Mars: Characterization of a water-bearing, energetic gully-forming process. *Earth and Planetary Science Letters*, Vol. 294 (3), pp. 368–377.
- Li G., Li L., Tarozo R., Longo W. M., Wang K. J., Dong H., Huang Y. (2018). Microbial production of long-chain *n*-alkanes: Implication for interpreting sedimentary leaf wax signals. *Organic Geochemistry*, Vol. 115, pp. 24–31.
- Lichtfouse E., Bardoux G., Mariotti A., Balesdent J., Ballentine D. C., Macko S. A. (1997). Molecular, ^{13}C , and ^{14}C evidence for the allochthonous and ancient origin of $\text{C}_{16}\text{--C}_{18}$ *n*-alkanes in modern soils. *Geochimica et Cosmochimica Acta*, Vol. 61, pp. 1891–1898.
- Lillis R. J., Frey H. V., Manga M., Mitchell D. L., Lin R. P., Acuña M. H., Bougher S. W. (2008). An improved crustal magnetic field map of Mars from electron reflectometry: Highland volcano magmatic history and the end of the martian dynamo. *Icarus*, Vol. 194 (2), pp. 575–596.
- Liu W., Mu W., Zhu B., Liu F. (2008). Antifungal activities and components of VOCs produced by *Bacillus subtilis* G₈. *Current Research in Bacteriology*, Vol. 1 (1), pp. 28–34.
- Löve A., Löve D. (1948). Jurtir í Slúttnessi [in Icelandic]. *Náttúrufræðingurinn*, Vol. 18, pp. 23–26.
- Lowell P. L. (1906). *Mars and its canals*. London: MacMillan & Co.
- (1908). *Mars as the abode of life*. New York: The MacMillan Company.
- Lowenstam H. A. (1981). Minerals formed by organisms. *Science*, Vol. 211 (4487), pp. 1126–1131.
- Lowenstein T. K., Hein M. C., Bobst A. L., Jordan T. E., Ku T.-L., Luo S. (2003). An assessment of stratigraphic completeness in climate-sensitive closed-basin lake sediments: Salar de Atacama, Chile. *Journal of Sedimentary Research*, Vol. 73 (1), pp. 91–104.
- Lynch R. C., King A. J., Farías M. E., Sowell P., Vitry C., Schmidt S. K. (2012). The potential for microbial life in the highest-elevation (>6000 m.a.s.l.) mineral soils of the Atacama region. *Journal of Geophysical Research: Biogeosciences*, Vol. 117 (G2), G02028.

- Mahaffy P. R., Webster C. R., Stern J. C., Brunner A. E., Atreya S. K., Conrad P. G., Domagal-Goldman S., Eigenbrode J. L., Flesch G. J., Christensen L. E., Franz H. B., Freissinet C., Glavin D. P., Grotzinger J. P., Jones J. H., Leshin L. A., Malespin C., McAdam A. C., Ming D. W., Navarro-Gonzalez R., Niles P. B., Owen T., Pavlov A. A., Steele A., Trainer M. G., Williford K. H., Wray J. J., the MSL science team (2015). The imprint of atmospheric evolution in the D/H of Hesperian clay minerals on Mars. *Science*, Vol. 347 (6220), pp. 412–414.
- Marchant D. R., Head J. W. (2007). Antarctic dry valleys: Microclimate zonation, variable geomorphic processes, and implications for assessing climate change on Mars. *Icarus*, Vol. 192 (1), pp. 187–222.
- Marchant D. R., Denton G. H., Swisher C. C., Potter N. (1996). Late Cenozoic Antarctic paleoclimate reconstructed from volcanic ashes in the Dry Valleys region of southern Victoria Land. *GSA Bulletin*, Vol. 108 (2), pp. 181–194.
- Margesin R., Jud M., Tscherko D., Schinner F. (2009). Microbial communities and activities in alpine and subalpine soils. *FEMS Microbiology Ecology*, Vol. 67 (2), pp. 208–218.
- Marlow J. J., Martins Z., Sephton M. A. (2011). Organic host analogues and the search for life on Mars. *International Journal of Astrobiology*, Vol. 10 (1), pp. 31–44.
- Marquet P. A. (1994). Diversity of small mammals in the Pacific coastal desert of Peru and Chile and in the adjacent Andean area: Biogeography and community structure. *Australian Journal of Zoology*, Vol. 42, pp. 527–542.
- Marrone D. P., Blundell R., Gibson H., Paine S., Papa D. C., Tong C.-Y. E. (2004). Characterization and status of a terahertz telescope. In: *Proceedings of the Fifteenth International Symposium on Space Terahertz Technology – Northampton, Massachusetts, USA*, p. 426.
- Marrone D. P., Blundell R., Tong E., Paine S. N., Loudkov D., Kawamura J. H., Lühr D., Barrientos C. (2005). Observations in the 1.3 and 1.5 THz atmospheric windows with the Receiver Lab Telescope. In: *Sixteenth International Symposium on Space Terahertz Technology – Göteborg, Sweden*, pp. 64–67.
- Martín-Torres F. J., Zorzano M.-P., Valentín-Serrano P., Harri A.-M., Genzer M., Kemppinen O., Rivera-Valentin E. G., Jun I., Wray J., Bo Madsen M., Goetz W., McEwen A. S., Hardgrove C., Renno N., Chevrier V. F., Mischna M., Navarro-González R., Martínez-Frías J., Conrad P., McConnochie T., Cockell C., Berger G., R. Vasavada A., Sumner D., Vaniman D. (2015). Transient liquid water and water activity at Gale crater on Mars. *Nature Geoscience*, Vol. 8, pp. 357–361.
- Martínez G. M., Fischer E., Rennó N. O., Sebastián E., Kemppinen O., Bridges N., Borlina C. S., Meslin P.-Y., Genzer M., Harri A.-H., Vicente-Retortillo A., Ramos M., de la Torre Juárez M., Gómez F., AsenjoGómez-Elvira J. A., the REMS Team (2016). Likely frost events at Gale crater: Analysis from MSL/REMS measurements. *Icarus*, Vol. 280, pp. 93–102.
- Martins Z., Cottin H., Kotler J. M., Carrasco N., Cockell C. S., de la Torre Noetzel R., Demets R., de Vera J.-P., d'Hendecourt L., Ehrenfreund P., Elsaesser A., Foing B., Onofri S., Quin R., Rabbow E., Rettberg P., Ricco A. J., Slenza K., Stalport F., ten Kate I. L., van Loon

- J. J.W. A., Westall F. (2017). Earth as a tool for astrobiology—A European perspective. *Space Science Reviews*, Vol. 209 (1–4), pp. 43–81.
- Marzo A., Ferrada P., Beiza F., Besson P., Alonso-Montesinos J., Ballestrín J., Román R., Portillo C., Escobar R., Fuentealba E. (2018). Standard or local solar spectrum? Implications for solar technologies studies in the Atacama desert. *Renewable Energy*, Vol. 127, pp. 871–882.
- Mattsson H. B., Höskuldsson A. (2011). Contemporaneous phreatomagmatic and effusive activity along the Hverfjall eruptive fissure, north Iceland: Eruption chronology and resulting deposits. *Journal of Volcanology and Geothermal Research*, Vol. 201 (1), pp. 241–252.
- Maunder E. W. (1894). The canals of Mars. *Knowledge*, Vol. 17, pp. 249–252.
- (1903). The canals of Mars. *Knowledge*, Vol. 26, pp. 249–251.
- Maxim Integrated (2015). *DS1923 – iButton Hygrochron temperature/humidity logger with 8KB datalog memory*. Maxim Integrated. URL: <https://www.maximintegrated.com>.
- Mazutis L., Gilbert J., Ung W. L., Weitz D. A., Griffiths A. D., Heyman J. A. (2013). Single-cell analysis and sorting using droplet-based microfluidics. *Nature Protocols*, Vol. 8 (5), pp. 870–891.
- McColl J. L. (2016). Climate variability of the last 1000 years in the NW Pacific: high resolution, multi-biomarker records from Lake Toyoni. PhD thesis. University of Glasgow: School of Geographical and Earth Sciences.
- McKay C. P. (2010). An origin of life on Mars. *Cold Spring Harbor Perspectives in Biology*, Vol. 2 (4), a003509.
- McKay C. P., Molaro J. L., Marinova M. M. (2009). High-frequency rock temperature data from hyper-arid desert environments in the Atacama and the Antarctic Dry Valleys and implications for rock weathering. *Geomorphology*, Vol. 110 (3), pp. 182–187.
- McKirahan R. (2001). Anaximander's Infinite Worlds. In: *Essays in Ancient Greek Philosophy VI – Before Plato*. Ed. by A. Preus. Albany: State University of New York Press, pp. 49–65.
- Ménez B., Pisapia C., Andreani M., Jamme F., Vanbellinghen Q. P., Brunelle A., Richard L., Dumas P., Réfrégiers M. (2018). Abiotic synthesis of amino acids in the recesses of the oceanic lithosphere. *Nature*, in press.
- Menzel P., Ng K. L., Krogh A. (2016). Fast and sensitive taxonomic classification for metagenomics with Kaiju. *Nature Communications*, Vol. 7, p. 11257.
- Messerli B., Grosjean M., Vuille M. (1997). Water availability, protected areas, and natural resources in the Andean Desert Altiplano. *Mountain Research and Development*, Vol. 17 (3), pp. 229–238.
- Michael G., Platz T., Kneissl T., Schmedemann N. (2012). Planetary surface dating from crater size–frequency distribution measurements: Spatial randomness and clustering. *Icarus*, Vol. 218 (1), pp. 169–177.

- Michalski J. R., Cuadros J., Niles P. B., Parnell J., Deanne Rogers A., Wright S. P. (2013). Groundwater activity on Mars and implications for a deep biosphere. *Nature Geoscience*, Vol. 6, pp. 133–138.
- Miller O. J., Bernath K., Agresti J. J., Amitai G., Kelly B. T., Mastrobattista E., Taly V., Magdassi S., Tawfik D. S., Griffiths A. D. (2006). Directed evolution by *in vitro* compartmentalization. *Nature Methods*, Vol. 3, pp. 561–570.
- Miller S. L. (1953). Production of amino acids under possible primitive Earth conditions. *Science*, Vol. 117 (3046), pp. 528–529.
- Miller S. L., Urey H. C. (1959). Organic compound synthesis on the primitive Earth. *Science*, Vol. 130 (3370), pp. 245–251.
- Milton D. J. (1974). *Geologic map of the Lunae Palus Quadrangle of Mars (IMAP 894)*. Ed. by USGS.
- Monroe A. A., Pizzarello S. (2011). The soluble organic compounds of the Bells meteorite: Not a unique or unusual composition. *Geochimica et Cosmochimica Acta*, Vol. 75 (23), pp. 7585–7595.
- Moreno M. L., Piubeli F., Bonfá M. R. L., García M. T., Durrant L. R., Mellado E. (2012). Analysis and characterization of cultivable extremophilic hydrolytic bacterial community in heavy-metal-contaminated soils from the Atacama Desert and their biotechnological potentials. *Journal of Applied Microbiology*, Vol. 113 (3), pp. 550–559.
- Morgan G. A., Head J. W., Marchant D. R. (2011). Preservation of Late Amazonian Mars ice and water-related deposits in a unique crater environment in Noachis Terra: Age relationships between lobate debris tongues and gullies. *Icarus*, Vol. 211 (1), pp. 347–365.
- Morong T. (1891). The Flora of the Desert of Atacama. *Bulletin of the Torrey Botanical Club*, Vol. 18 (2), pp. 39–48.
- Mottl M. J., Glazer B. T., Kaiser R. I., Meech K. J. (2007). Water and astrobiology. *Chemie der Erde*, Vol. 67 (4), pp. 253–282.
- Mueller D. R., Vincent W. F., Bonilla S., Laurion I. (2005). Extremotrophs, extremophiles and broadband pigmentation strategies in a high arctic ice shelf ecosystem. *FEMS Microbiology Ecology*, Vol. 53 (1), pp. 73–87.
- Nakajima K., Sato A., Takahara Y., Iida T. (1985). Microbial oxidation of isoprenoid alkanes, phytane, norpristane and farnesane. *Agricultural and Biological Chemistry*, Vol. 49 (7), pp. 1993–2002.
- Navarro-González R., Rainey F. A., Molina P., Bagaley D. R., Hollen B. J., de la Rosa J., Small A. M., Quinn R. C., Grunthaner F. J., Cáceres L., Gomez-Silva B., McKay C. P. (Nov. 2003). Mars-like soils in the Atacama Desert, Chile, and the dry limit of microbial life. *Science*, Vol. 302 (5647), pp. 1018–1021.
- Navarro-González R., Vargas E., de la Rosa J., Raga A. C., McKay C. P. (2010). Reanalysis of the Viking results suggests perchlorate and organics at midlatitudes on Mars. *Journal of Geophysical Research: Planets*, Vol. 115 (E12), E12010.
- NCBI (2018). *PubChem*. National Center for Biotechnology Information. URL: <https://pubchem.ncbi.nlm.nih.gov/>.

- Neukum G., Ivanov B., Hartmann W. (2001). Cratering Records in the Inner Solar System in Relation to the Lunar Reference System. *Space Science Reviews*, Vol. 96 (1–4), pp. 55–86.
- Nieto-Moreno V., Rohrmann A., Meer M. T. van der, Damsté J. S. S., Sachse D., Tofelde S., Niedermeyer E. M., Strecker M. R., Mulch A. (2016). Elevation-dependent changes in *n*-alkane δD and soil GDGTs across the South Central Andes. *Earth and Planetary Science Letters*, Vol. 453, pp. 234–242.
- Nimmo F., Kleine T. (2007). How rapidly did Mars accrete? Uncertainties in the Hf–W timing of core formation. *Icarus*, Vol. 191 (2), pp. 497–504.
- Nimmo F. (2000). Dike intrusion as a possible cause of linear Martian magnetic anomalies. *Geology*, Vol. 28 (5), pp. 391–394.
- NOAA (1976). *U.S. standard atmosphere, 1976*. Tech. rep. NOAA—S/T 76–1562. Washington D.C.: National Oceanic and Atmospheric Administration, National Aeronautics and Space Administration, United States Air Force.
- Noack L., Verseux C., Serrano P., Musilova M., Nauny P., Samuels T., Schwendner P., Simoncini E., Stevens A. (2015). Astrobiology from early-career scientists' perspective. *International Journal of Astrobiology*, Vol. 14 (4), pp. 533–535.
- Nyquist L., Bogard D., Shih C.-Y., Greshake A., Stöffler D., Eugster O. (2001). Ages and geologic histories of Martian meteorites. *Space Science Reviews*, Vol. 96 (1), pp. 105–164.
- Ojha L., McEwen A., Dundas C., Byrne S., Mattson S., Wray J., Masse M., Schaefer E. (2014). HiRISE observations of Recurring Slope Lineae (RSL) during southern summer on Mars. *Icarus*, Vol. 231, pp. 365–376.
- Ólafsson J. (1979). Physical characteristics of Lake Mývatn and the river Láxa. *Oikos*, Vol. 32, pp. 38–66.
- (1999). Connections between oceanic conditions off N-Iceland, Lake Mývatn temperature, regional wind direction variability and the North Atlantic Oscillation. *Rit Fiskideildar*, Vol. 16, pp. 41–57.
- Oliveira V., Santos A. L., Aguiar C., Santos L., Salvador Â. C., Gomes N. C., Silva H., Rocha S. M., Almeida A., Cunha Â. (2012). Prokaryotes in salt marsh sediments of Ria de Aveiro: Effects of halophyte vegetation on abundance and diversity. *Estuarine, Coastal and Shelf Science*, Vol. 110. Coastal Lagoons in a changing environment: understanding, evaluating and responding, pp. 61–68.
- Orange F., Westall F., Disnar J.-R., Prieur D., Bienvenu N., Le Romancer M., Défarge C. (2009). Experimental silicification of the extremophilic Archaea *Pyrococcus abyssi* and *Methanocaldococcus jannaschii*: applications in the search for evidence of life in early Earth and extraterrestrial rocks. *Geobiology*, Vol. 7 (4), pp. 403–418.
- Orgel C., Kereszturi Á., Váczi T., Groemer G., Sattler B. (2014). Scientific results and lessons learned from an integrated crewed Mars exploration simulation at the Rio Tinto Mars analogue site. *Acta Astronautica*, Vol. 94 (2), pp. 736–748.

- Orlando J., Alfaro M., Bravo L., Guevara R., Carú M. (2010). Bacterial diversity and occurrence of ammonia-oxidizing bacteria in the Atacama Desert soil during a "desert bloom" event. *Soil Biology and Biochemistry*, Vol. 42 (7), pp. 1183–1188.
- Oró J., Laseter J. L., Weber D. (1966). Alkanes in fungal spores. *Science*, Vol. 154 (3747), pp. 399–400.
- Orosei R., Lauro S. E., Pettinelli E., Cicchetti A., Coradini M., Cosciotti B., Di Paolo F., Flamini E., Mattei E., Pajola M., Soldovieri F., Cartacci M., Cassenti F., Frigeri A., Giuppi S., Martufi R., Masdea A., Mitri G., Nenna C., Noschese R., Restano M., Seu R. (2018). Radar evidence of subglacial liquid water on Mars. *Science*, in press.
- Osinski G. R., Lee P., Parnell J., Spray J. G., Baron M. (2005). A case study of impact-induced hydrothermal activity: The Haughton impact structure, Devon Island, Canadian High Arctic. *Meteoritics & Planetary Science*, Vol. 40 (12), pp. 1859–1877.
- Osinski G. R., Léveillé R., Berinstain A., Lebeuf M., Bamsey M. (2006). Terrestrial analogues to Mars and the Moon: Canada's role. *Geoscience Canada*, Vol. 33 (4), pp. 175–188.
- Osinski G. R., Tornabene L. L., Banerjee N. R., Cockell C. S., Flemming R., Izawa M. R., McCutcheon J., Parnell J., Preston L. J., Pickersgill A. E., Pontefract A., Sapers H. M., Southam G. (2013). Impact-generated hydrothermal systems on Earth and Mars. *Icarus*, Vol. 224 (2). Terrestrial Analogs for Mars: Mars Science Laboratory and Beyond, pp. 347–363.
- Pacifici A., Komatsu G., Pondrelli M. (2009). Geological evolution of Ares Vallis on Mars: Formation by multiple events of catastrophic flooding, glacial and periglacial processes. *Icarus*, Vol. 202 (1), pp. 60–77.
- Palumbo A. M., Head J. W., Wordsworth R. D. (2018). Late Noachian Icy Highlands climate model: Exploring the possibility of transient melting and fluvial/lacustrine activity through peak annual and seasonal temperatures. *Icarus*, Vol. 300, pp. 261–286.
- Parnell J., Cullen D., Sims M. R., Bowden S., Cockell C. S., Court R., Ehrenfreund P., Gaubert F., Grant W., Parro V., Rohmer M., Sephton M., Stan-Lotter H., Steele A., Toporski J., Vago J. (2007). Searching for life on Mars: Selection of molecular targets for ESA's Aurora ExoMars mission. *Astrobiology*, Vol. 7 (4), pp. 578–604.
- Parro V., de Diego-Castilla G., Moreno-Paz M., Blanco Y., Cruz-Gil P., Rodríguez-Manfredi J. A., Fernández-Remolar D., Gómez F., Gómez M. J., Rivas L. A., Demergasso C., Echeverría A., Urtuvia V. N., Ruiz-Bermejo M., García-Villadangos M., Postigo M., Sánchez-Román M., Chong-Díaz G., Gómez-Elvira J. (2011). A microbial oasis in the hypersaline Atacama subsurface discovered by a life detector chip: Implications for the search for life on Mars. *Astrobiology*, Vol. 11 (10), pp. 969–996.
- Parro V., Blanco Y., Puente-Sánchez F., Rivas L. A., Moreno-Paz M., Echeverría A., Chong-Díaz G., Demergasso C., Cabrol N. A. (2018). Biomarkers and Metabolic Patterns in the Sediments of Evolving Glacial Lakes as a Proxy for Planetary Lake Exploration. *Astrobiology*, Vol. 18 (5), pp. 586–606.

- Pascoff R. (1962). Note préliminaire sur certaines analogies du Quaternaire chilien avec le Quaternaire marocain [in French]. *Comptes Rendus des séances mensuelles de la Société des Sciences Naturelles et Physiques du Maroc*, Vol. 28 (7), pp. 129–131.
- Paulino-Lima I. G., Azua-Bustos A., Vicuña R., González-Silva C., Salas L., Teixeira L., Rosado A., Costa Leitaó A. A. da, Lage C. (2013). Isolation of UVC-tolerant bacteria from the hyperarid Atacama Desert, Chile. *Microbial Ecology*, Vol. 65 (2), pp. 325–335.
- Paulino-Lima I. G., Fujishima K., Navarrete J. U., Galante D., Rodrigues F., Azua-Bustos A., Rothschild L. J. (2016). Extremely high UV-C radiation resistant microorganisms from desert environments with different manganese concentrations. *Journal of Photochemistry and Photobiology B: Biology*, Vol. 163, pp. 327–336.
- Pavlov A. A., Vasilyev G., Ostryakov V. M., Pavlov A. K., Mahaffy P. (2012). Degradation of the organic molecules in the shallow subsurface of Mars due to irradiation by cosmic rays. *Geophysical Research Letters*, Vol. 39 (13), p. L13202.
- Pavlov A., Blinov A., Konstantinov A. (2002). Sterilization of Martian surface by cosmic radiation. *Planetary and Space Science*, Vol. 50 (7), pp. 669–673.
- Phillips R. J., Zuber M. T., Solomon S. C., Golombek M. P., Jakosky B. M., Banerdt W. B., Smith D. E., Williams R. M. E., Hynek B. M., Aharonson O., II S. A. H. (2001). Ancient geodynamics and global-scale hydrology on Mars. *Science*, Vol. 291 (5513), pp. 2587–2591.
- Piacentini R. D., Cede A., Bárcena H. (2003). Extreme solar total and UV irradiances due to cloud effect measured near the summer solstice at the high-altitude desertic plateau Puna of Atacama (Argentina). *Journal of Atmospheric and Solar-Terrestrial Physics*, Vol. 65 (6), pp. 727–731.
- Piazena H. (1996). The effect of altitude upon the solar UV-B and UV-A irradiance in the tropical Chilean Andes. *Solar Energy*, Vol. 57 (2), pp. 133–140.
- Pla-García J., Rafkin S. C. R., Kahre M., Gomez-Elvira J., Hamilton V. E., Navarro S., Torres J., Marín M., Vasavada A. R. (2016). The meteorology of Gale crater as determined from rover environmental monitoring station observations and numerical modeling. Part I: Comparison of model simulations with observations. *Icarus*, Vol. 280, pp. 103–113.
- Platz T., Michael G., Tanaka K. L., Skinner J. A., Fortezzo C. M. (2013). Crater-based dating of geological units on Mars: Methods and application for the new global geological map. *Icarus*, Vol. 225 (1), pp. 806–827.
- Plescia J. B., Saunders R. S. (1982). Tectonic history of the Tharsis Region, Mars. *Journal of Geophysical Research: Solid Earth*, Vol. 87 (B12), pp. 9775–9791.
- Pontefract A., Zhu T. F., Walker V. K., Hepburn H., Lui C., Zuber M. T., Ruvkun G., Carr C. E. (2017). Microbial diversity in a hypersaline sulfate lake: A terrestrial analog of ancient Mars. *Frontiers in Microbiology*, Vol. 8, p. 1819.
- Powell T. G., McKirdy D. M. (1973). Relationship between ratio of pristane to phytane, crude oil composition and geological environment in Australia. *Nature Physical Science*, Vol. 243, pp. 37–39.

- Poynter J. G., Farrimond P., Robinson N., Eglinton G. (1989). Aeolian-derived higher plant lipids in the marine sedimentary record: Links with palaeoclimate. In: *Paleoclimatology and paleometeorology: Modern and past patterns of global atmospheric transport*. Ed. by M. Leinen, M. Sarnthein. Vol. 282. NATO ASI series C: Mathematical and physical sciences. Kluwer Academic Publishing: Dordrecht, pp. 435–462.
- Preston L. J., Benedix G. K., Genge M. J., Sephton M. A. (2008). A multidisciplinary study of silica sinter deposits with applications to silica identification and detection of fossil life on Mars. *Icarus*, Vol. 198 (2), pp. 331–350.
- Preston L. J., Dartnell L. R. (2014). Planetary habitability: Lessons learned from terrestrial analogues. *International Journal of Astrobiology*, Vol. 13 (1), pp. 81–98.
- Prince R. C., Haitmanek C., Lee C. C. (2008). The primary aerobic biodegradation of biodiesel B20. *Chemosphere*, Vol. 71 (8), pp. 1446–1451.
- Pulschen A. A., Rodrigues F., Duarte R. T. D., Araujo G. G., Santiago I. F., Paulino-Lima I. G., Rosa C. A., Kato M. J., Pellizari V. H., Galante D. (2015). UV-resistant yeasts isolated from a high-altitude volcanic area on the Atacama Desert as eukaryotic models for astrobiology. *MicrobiologyOpen*, Vol. 4 (4), pp. 574–588.
- Purucker M., Ravat D., Frey H., Voorhies C., Sabaka T., Acuña M. (2000). An altitude-normalized magnetic map of Mars and its interpretation. *Geophysical Research Letters*, Vol. 27 (16), pp. 2449–2452.
- Quinn R. C., Martucci H. F., Miller S. R., Bryson C. E., Grunthaner F. J., Grunthaner P. J. (2013). Perchlorate radiolysis on Mars and the origin of martian soil reactivity. *Astrobiology*, Vol. 13 (6), pp. 515–520.
- Raga G. B., Baumgardner D., Ulke A. G., Torres Brizuela M., Kucienska B. (2013). The environmental impact of the Puyehue–Cordon Caulle 2011 volcanic eruption on Buenos Aires. *Natural Hazards and Earth System Sciences*, Vol. 13 (9), pp. 2319–2330.
- Rahmati A., Cravens T. E., Nagy A. F., Fox J. L., Bougher S. W., Lillis R. J., Ledvina S. A., Larson D. E., Dunn P., Croxell J. A. (2014). Pickup ion measurements by MAVEN: A diagnostic of photochemical oxygen escape from Mars. *Geophysical Research Letters*, Vol. 41 (14), pp. 4812–4818.
- Rath K. M., Maheshwari A., Bengtson P., Rousk J. (2016). Comparative toxicities of salts on microbial processes in soil. *Applied and Environmental Microbiology*, Vol. 82 (7), pp. 2012–2020.
- Rawat P., Singh P. K., Kumar V. (2017). Evidence based traditional anti-diarrheal medicinal plants and their phytochemicals. *Biomedicine & Pharmacotherapy*, Vol. 96, pp. 1453–1464.
- Ren B., Hu Y., Chen B., Zhang Y., Thiele J., Shi R., Liu Miao and Bu R. (2018). Soil pH and plant diversity shape soil bacterial community structure in the active layer across the latitudinal gradients in continuous permafrost region of Northeastern China. *Scientific Reports*, Vol. 8, p. 5619.

- Rhee M., Light Y. K., Meagher R. J., Singh A. K. (2016). Digital droplet multiple displacement amplification (ddMDA) for whole genome sequencing of limited DNA samples. *PLOS ONE*, Vol. 11 (5), e0153699.
- Richter M. (1996). Klimatologische und pflanzenmorphologische Vertikalgradienten in Hochgebirgen [in German]. *Erdkunde*, Vol. 50 (3), pp. 205–237.
- (2003). Using plant functional types as climatic indicators in the Cordilleras. *Lyonia*, Vol. 4 (1), pp. 1–18.
- (2009). To what extent do natural disturbances contribute to Andean plant diversity? A theoretical outline from the wettest and driest parts of the tropical Andes. *Advances in Geosciences*, Vol. 22, pp. 95–105.
- Richter M., Schmidt D. (2002). Cordillera de la Atacama – Das trockenste Hochgebirge der Welt [in German]. *Petermanns Geographische Mitteilungen*, Vol. 146, pp. 48–57.
- Risacher F., Alonso H., Salazar C. (1999a). Volumen I – Síntesis [in Spanish]. In: *Geoquímica de aguas en cuencas cerradas: I, II y III regiones, Chile*. Dirección General de Aguas – Universidad Católica del Norte – Institut de Recherche pour le Developpement.
- (1999b). Volumen III – Estudio de la cuencas de la II región [in Spanish]. In: *Geoquímica de aguas en cuencas cerradas: I, II y III regiones, Chile*. Dirección General de Aguas – Universidad Católica del Norte – Institut de Recherche pour le Developpement.
- Risacher F., Alonso H., Salazar C. (2003). The origin of brines and salts in Chilean salars: a hydrochemical review. *Earth-Science Reviews*, Vol. 63 (3), pp. 249–293.
- Röling W. F., Aerts J. W., Patty C. L., ten Kate I. L., Ehrenfreund P., Direito S. O. (2015). The significance of microbe-mineral-biomarker interactions in the detection of life on Mars and beyond. *Astrobiology*, Vol. 15 (6), pp. 492–507.
- Rontani J.-F., Volkman J. K. (2003). Phytol degradation products as biogeochemical tracers in aquatic environments. *Organic Geochemistry*, Vol. 34 (1), pp. 1–35.
- Rosenberg E. N., Head J. W. (2015). Late Noachian fluvial erosion on Mars: Cumulative water volumes required to carve the valley networks and grain size of bed-sediment. *Planetary and Space Science*, Vol. 117, pp. 429–435.
- Rowland S. J. (1990). Production of acyclic isoprenoid hydrocarbons by laboratory maturation of methanogenic bacteria. *Organic Geochemistry*, Vol. 15 (1), pp. 9–16.
- Rubilar J., Martínez F., Arriagada C., Becerra J., Bascuñán S. (2018). Structure of the Cordillera de la Sal: A key tectonic element for the Oligocene-Neogene evolution of the Salar de Atacama basin, Central Andes, northern Chile. *Journal of South American Earth Sciences*, in press.
- Ruthsatz B. (2000). Die Hartpolstermoore der Hochanden und ihre Artenvielfalt [in German]. *Berichte der Reinhold-Tüxen-Gesellschaft*, Vol. 12, pp. 351–371.
- Ruthsatz B. (1995). Vegetation und Ökologie tropischer Hochgebirgsmoore in den Anden Nord-Chiles [in German]. *Phytocoenologia*, Vol. 25 (2), pp. 185–234.
- Sabburg J., Wong J. (2000). The effect of clouds on enhancing UVB irradiance at the Earth's surface: A one year study. *Geophysical Research Letters*, Vol. 27 (20), pp. 3337–3340.

- Sachse D., Radke J., Gleixner G. (2006). δD values of individual *n*-alkanes from terrestrial plants along a climatic gradient – Implications for the sedimentary biomarker record. *Organic Geochemistry*, Vol. 37 (4), pp. 469–483.
- Salvatore M. R., Mustard J. F., Wyatt M. B., Murchie S. L. (2010). Definitive evidence of Hesperian basalt in Acidalia and Chryse planitiae. *Journal of Geophysical Research: Planets*, Vol. 115, E07005.
- Samaniego H., Marquet P. A. (2009). Mammal and butterfly species richness in Chile: taxonomic covariation and history. *Revista Chilena de Historia Natural*, Vol. 82, pp. 135–151.
- Sánchez-Andrea I., Rodríguez N., Amils R., Sanz J. L. (2011). Microbial diversity in anaerobic sediments at Río Tinto, a Naturally Acidic Environment with a High Heavy Metal Content. *Applied and Environmental Microbiology*, Vol. 77 (17), pp. 6085–6093.
- Sánchez-García L., Aeppli C., Parro V., Fernández-Remolar D., García-Villadangos M., Chong-Díaz G., Blanco Y., Carrizo D. (2018). Molecular biomarkers in the subsurface of the Salar Grande (Atacama, Chile) evaporitic deposits. *Biogeochemistry*, Vol. 140 (1), pp. 31–52.
- Schaefer E., McEwen A., Sutton S. (2019). A case study of recurring slope lineae (RSL) at Tivat crater: Implications for RSL origins. *Icarus*, Vol. 317, pp. 621–648.
- Scheringer M. (2009). Long-range transport of organic chemicals in the environment. *Environmental Toxicology and Chemistry*, Vol. 28 (4), pp. 677–690.
- Schiaparelli G. (1894). The planet Mars. Trans. by W. H. Pickering. *Astronomy and Astrophysics*, pp. 635–640, 714–723.
- (1898). La vie sur la planète Mars. *Bulletin de la Société astronomique de France*, Vol. 12, pp. 423–429.
- Schmidt D. (1999). Das Extremklima der nordchilenischen Hochatacama unter besonderer Berücksichtigung der Höhengradienten [*in German*]. *Dresdener geographische Beiträge*, Vol. 4, pp. 1–122.
- Schmidt S. K., Naff C. S., Lynch R. C. (2012). Fungal communities at the edge: Ecological lessons from high alpine fungi. *Fungal Ecology*, Vol. 5 (4), pp. 443–452.
- Schmidt S. K., Darcy J. L., Sommers P., Gunawan E., Knelman J. E., Yager K. (2017a). Freeze–thaw revival of rotifers and algae in a desiccated, high-elevation (5500 meters) microbial mat, high Andes, Perú. *Extremophiles*, Vol. 21 (3), pp. 573–580.
- Schmidt S. K., Gendron E. M. S., Vincent K., Solon A. J., Sommers P., Schubert Z. R., Vimercati L., Porazinska D. L., Darcy J. L., Sowell P. (2018). Life at extreme elevations on Atacama volcanoes: the closest thing to Mars on Earth? *Antonie van Leeuwenhoek*, Vol. 111 (8), pp. 1389–1401.
- Schmidt S. K., Vimercati L., Darcy J. L., Arán P., Gendron E. M., Solon A. J., Porazinska D., Dorador C. (2017b). A Naganishia in high places: functioning populations or dormant cells from the atmosphere? *Mycology*, Vol. 8 (3), pp. 153–163.

- Schofield J. T., Barnes J. R., Crisp D., Haberle R. M., Larsen S., Magalhães J. A., Murphy J. R., Seiff A., Wilson G. (1997). The Mars Pathfinder Atmospheric Structure Investigation/Meteorology (ASI/MET) experiment. *Science*, Vol. 278 (5344), pp. 1752–1758.
- Schreuder L. T., Stuut J.-B. W., Korte L. F., Damsté J. S. S., Schouten S. (2018). Aeolian transport and deposition of plant wax n-alkanes across the tropical North Atlantic Ocean. *Organic Geochemistry*, Vol. 115, pp. 113–123.
- Schröder H. (1999). Vergleichende Periglazialmorphologie im Sommerregengebiet der Atacama [in German]. *Erdkunde*, Vol. 53 (2), pp. 119–135.
- Schröder H., Schmidt D. (1997). Klimamorphologie und Morphogenese des Llullaillaco (Chile/ Argentinien) [in German]. *Mitteilungen der Fränkischen Geographischen Gesellschaft*, Vol. 44, pp. 225–258.
- Schröder H., Makki M., Ciutura M. (1996). Die Zusammensetzung und morphologische Wirksamkeit der Salze in der ariden Höhenregion der Atacama (Chile) [in German]. *Mitteilungen der Fränkischen Geographischen Gesellschaft*, Vol. 43, pp. 259–274.
- Schröder M., Vetter W. (2012). Investigation of unsaponifiable matter of plant oils and isolation of eight phytosterols by means of high-speed counter-current chromatography. *Journal of Chromatography A*, Vol. 1237, pp. 96–105.
- Schuerger A. C., Nicholson W. L. (2006). Interactive effects of hypobaria, low temperature, and CO₂ atmospheres inhibit the growth of mesophilic *Bacillus* spp. under simulated martian conditions. *Icarus*, Vol. 185 (1), pp. 143–152.
- Schuerger A. C., Fajardo-Cavazos P., Clausen C. A., Moores J. E., Smith P. H., Nicholson W. L. (2008). Slow degradation of ATP in simulated martian environments suggests long residence times for the biosignature molecule on spacecraft surfaces on Mars. *Icarus*, Vol. 194 (1), pp. 86–100.
- Schulze-Makuch D., Irwin L. N. (2008). Life and the need for a solvent. Expectations and Constraints. In: *Life in the Universe*. Second edition. Springer-Verlag Berlin Heidelberg, pp. 109–132.
- Schulze-Makuch D., Wagner D., Kounaves S. P., Mangelsdorf K., Devine K. G., de Vera J.-P., Schmitt-Kopplin P., Grossart H.-P., Parro V., Kaupenjohann M., Galy A., Schneider B., Airo A., Frösler J., Davila A. F., Arens F. L., Cáceres L., Cornejo F. S., Carrizo D., Dartnell L., DiRuggiero J., Flury M., Ganzert L., Gessner M. O., Grathwohl P., Guan L., Heinz J., Hess M., Keppler F., Maus D., McKay C. P., Meckenstock R. U., Montgomery W., Oberlin E. A., Probst A. J., Sáenz J. S., Sattler T., Schirmack J., Sephton M. A., Schlöter M., Uhl J., Valenzuela B., Vestergaard G., Wörmer L., Zamorano P. (2018). Transitory microbial habitat in the hyperarid Atacama Desert. *Proceedings of the National Academy of Sciences*, Vol. 115 (11), pp. 2670–2675.
- Science (1958). News of Science: Development of international efforts to avoid contamination of extraterrestrial bodies. *Science*, Vol. 128 (3329), pp. 887–891.
- Scott D. H., Tanaka K. L. (1986). *Geologic map of the western equatorial region of Mars (IMAP 1802)*. Ed. by USGS.

- Sephton M., Wright I., Gilmour I., Leeuw J. de, Grady M., Pillinger C. (2002). High molecular weight organic matter in martian meteorites. *Planetary and Space Science*, Vol. 50 (7), pp. 711–716.
- Sidore A. M., Lan F., Lim S. W., Abate A. R. (2016). Enhanced sequencing coverage with digital droplet multiple displacement amplification. *Nucleic Acids Research*, Vol. 44, e66.
- Siles J. A., Cajthaml T., Minerbi S., Margesin R. (2016). Effect of altitude and season on microbial activity, abundance and community structure in Alpine forest soils. *FEMS Microbiology Ecology*, Vol. 92 (3), fiw008.
- Silva R. A., Grossi V., Alvarez H. M. (2007). Biodegradation of phytane (2,6,10,14-tetramethylhexadecane) and accumulation of related isoprenoid wax esters by *Mycobacterium ratisbonense* strain SD4 under nitrogen-starved conditions. *FEMS Microbiology Letters*, Vol. 272 (2), pp. 220–228.
- Simoneit B. R. T. (1984). Organic matter of the troposphere—III. Characterization and sources of petroleum and pyrogenic residues in aerosols over the western United States. *Atmospheric Environment*, Vol. 18 (1), pp. 51–67.
- Simoneit B. R. T., Summons R. E., Jahnke L. L. (1998). Biomarkers as tracers for life on early Earth and Mars. *Origins of Life and Evolution of the Biosphere*, Vol. 28 (4), pp. 475–483.
- Simoneit B. R. (1977). Organic matter in eolian dusts over the Atlantic Ocean. *Marine Chemistry*, Vol. 5 (4). Concepts in Marine Organic Chemistry, pp. 443–464.
- Simpson S., Boyce A., Lambert P., Lindgren P., Lee M. (2017). Evidence for an impact-induced biosphere from the $\delta^{34}\text{S}$ signature of sulphides in the Rochechouart impact structure, France. *Earth and Planetary Science Letters*, Vol. 460, pp. 192–200.
- Smets W., Moretti S., Denys S., Lebeer S. (2016). Airborne bacteria in the atmosphere: Presence, purpose, and potential. *Atmospheric Environment*, Vol. 139, pp. 214–221.
- Smith M. D. (2008). Spacecraft Observations of the Martian Atmosphere. *Annual Review of Earth and Planetary Sciences*, Vol. 36 (1), pp. 191–219.
- Smith M. D., Zorzano M.-P., Lemmon M., Martín-Torres J., Mendaza de Cal T. (2016). Aerosol optical depth as observed by the Mars Science Laboratory REMS UV photodiodes. *Icarus*, Vol. 280. MicroMars to MegaMars, pp. 234–248.
- Soare R. J., Osinski G. R., Roehm C. L. (2008). Thermokarst lakes and ponds on Mars in the very recent (late Amazonian) past. *Earth and Planetary Science Letters*, Vol. 272 (1), pp. 382–393.
- Soare R., Conway S., Gallagher C., Dohm J. (2016). Sorted (clastic) polygons in the Argyre region, Mars, and possible evidence of pre- and post-glacial periglaciation in the Late Amazonian Epoch. *Icarus*, Vol. 264, pp. 184–197.
- Solon A. J., Vimercati L., Darcy J. L., Arán P., Porazinska D., Dorador C., Farías M. E., Schmidt S. K. (2018). Microbial Communities of High-Elevation Fumaroles, Penitentes, and Dry Tephra “Soils” of the Puna de Atacama Volcanic Zone. *Microbial Ecology*, Vol. 76 (2), pp. 340–351.

- Spanovich N., Smith M., Smith P., Wolff M., Christensen P., Squyres S. (2006). Surface and near-surface atmospheric temperatures for the Mars Exploration Rover landing sites. *Icarus*, Vol. 180 (2), pp. 314–320.
- Sprott G. D., Larocque S., Cadotte N., Dicaire C. J., McGee M., Brisson J. R. (2003). Novel polar lipids of halophilic eubacterium *Planococcus* H8 and archaeon *Haloferax volcanii*. *Biochimica et Biophysica Acta*, Vol. 1633 (3), pp. 179–188.
- Squeo F. A., Warner B. G., Aravena R., Espinoza D. (2006). Bofedales: high altitude peatlands of the central Andes. *Revista Chilena de Historia Natural*, Vol. 79, pp. 245–255.
- Steele A., Beaty D., Amend J., Anderson R., Beegle L., Benning L., Bhattacharya J., Blake D., Brinckerhoff W., Biddle J., Cady S., Conrad P., Lindsay J., Mancinelli R., Mungas G., Mustard J., Oxnevad K., Toporski J., Waite H. (2005). *The Astrobiology Field Laboratory*. White paper. MEPAG Astrobiology Field Laboratory Science Steering Group (AFL-SSG).
- Steele A., McCubbin F. M., Fries M., Kater L., Boctor N. Z., Fogel M. L., Conrad P. G., Glamoclija M., Spencer M., Morrow A. L., Hammond M. R., Zare R. N., Vicenzi E. P., Siljeström S., Bowden R., Herd C. D. K., Mysen B. O., Shirey S. B., Amundsen H. E. F., Treiman A. H., Bullock E. S., Jull A. J. T. (2012). A reduced organic carbon component in martian basalts. *Science*, Vol. 337 (6091), pp. 212–215.
- Steele A., Benning L. G., Wirth R., Siljeström S., Fries M. D., Hauri E., Conrad P. G., Rogers K., Eigenbrode J., Schreiber A., Needham A., Wang J. H., McCubbin F. M., Kilcoyne D., Rodriguez Blanco J. D. (2018). Organic synthesis on Mars by electrochemical reduction of CO₂. *Science Advances*, Vol. 4 (10).
- Steindórsson S. (1932). Gróður í Slúttnessi [in Icelandic]. *Náttúrufræðingurinn*, Vol. 2, pp. 90–92.
- Stillman D. E., Grimm R. E. (2018). Two pulses of seasonal activity in martian southern mid-latitude recurring slope lineae (RSL). *Icarus*, Vol. 302, pp. 126–133.
- Stillman D. E., Michaels T. I., Grimm R. E., Hanley J. (2016). Observations and modeling of northern mid-latitude recurring slope lineae (RSL) suggest recharge by a present-day martian briny aquifer. *Icarus*, Vol. 265, pp. 125–138.
- Stillman D. E., Michaels T. I., Grimm R. E. (2017). Characteristics of the numerous and widespread recurring slope lineae (RSL) in Valles Marineris, Mars. *Icarus*, Vol. 285, pp. 195–210.
- Stres B., Sul W. J., Murovec B., Tiedje J. M. (2013). Recently deglaciated high-altitude soils of the Himalaya: Diverse environments, heterogenous bacterial communities and long-range dust inputs from the upper troposphere. *PLOS ONE*, Vol. 8 (9), e76440.
- Suh Y. J., Diefendorf A. F. (2018). Seasonal and canopy height variation in n-alkanes and their carbon isotopes in a temperate forest. *Organic Geochemistry*, Vol. 116, pp. 23–34.
- Summons R., Sessions A., Allwood A., Barton H., Beaty D., Blakkolb B., Canham J., Clark B., Dworkin J., Lin Y., Mathies R., Milkovich S., Steele A. (2014). Planning considerations related to the organic contamination of martian samples and implications for the Mars 2020 rover. *Astrobiology*, Vol. 14 (12). PMID: 25495496, pp. 969–1027.

- Summons R. E., Brassell S. C., Eglinton G., Evans E., Horodyski R. J., Robinson N., Ward D. M. (1988). Distinctive hydrocarbon biomarkers from fossiliferous sediment of the Late Proterozoic Walcott Member, Chuar Group, Grand Canyon, Arizona. *Geochimica et Cosmochimica Acta*, Vol. 52 (11), pp. 2625–2637.
- Summons R. E., Albrecht P., McDonald G., Moldowan J. M. (2008). Molecular biosignatures. *Space Science Reviews*, Vol. 135 (1), pp. 133–159.
- Summons R. E., Amend J. P., Bish D., Buick R., Cody G. D., Des Marais D. J., Dromart G., Eigenbrode J. L., Knoll A. H., Sumner D. Y. (2011). Preservation of martian organic and environmental records: Final report of the Mars Biosignature Working Group. *Astrobiology*, Vol. 11 (2), pp. 157–181.
- Tanaka K. L. (1986). The stratigraphy of Mars. *Journal of Geophysical Research: Solid Earth*, Vol. 91 (B13), E139–E158.
- Tanaka K. L., Chapman M. G. (1990). The relation of catastrophic flooding of Mangala Valles, Mars, to faulting of Memnonia Fossae and Tharsis Volcanism. *Journal of Geophysical Research: Solid Earth*, Vol. 95 (B9), pp. 14315–14323.
- Taylor P. A., Kahanpää H., Weng W., Akingunola A., Cook C., Daly M., Dickinson C., Harri A.-M., Hill D., Hipkin V., Polkko J., Whiteway J. (2010). On pressure measurement and seasonal pressure variations during the Phoenix mission. *Journal of Geophysical Research: Planets*, Vol. 115 (E3), E00E15.
- ten Haven H. L. and de Leeuw J. W., Rullkötter J., Sinninghe Damsté J. S. (1987). Restricted utility of the pristane/phytane ratio as a palaeoenvironmental indicator? *Nature*, Vol. 330, pp. 641–643.
- ten Kate I. L., Garry J. R. C., Peeters Z., Quinn R., Foing B., Ehrenfreund P. (2005). Amino acid photostability on the Martian surface. *Meteoritics & Planetary Science*, Vol. 40 (8), pp. 1185–1193.
- ten Kate I. L., Garry J. R., Peeters Z., Foing B., Ehrenfreund P. (2006). The effects of Martian near surface conditions on the photochemistry of amino acids. *Planetary and Space Science*, Vol. 54 (3), pp. 296–302.
- The GIMP development team (2017). *GNU Image Manipulation Program (version 2.8.22)*. URL: <https://www.gimp.org/>.
- The Inkscape Project (2015). *Inkscape (version 0.91)*. The Inkscape Project. URL: <https://inkscape.org/>.
- Thomas N. R. (2018). Preservation and detection of molecular signs of life under Mars analogue conditions. PhD thesis. University of Glasgow: School of Geographical and Earth Sciences.
- Thorarinsson S. (1979). The postglacial history of the Mývatn area. *Oikos*, Vol. 32 (1/2), pp. 17–28.
- Þórarinnsson S. (1952a). Hverfall. I. Gerd Hverfalls [*in Icelandic*]. *Náttúrufræðingurinn*, Vol. 22 (3), pp. 113–129.
- (1952b). Hverfall. II. Aldur Hverfalls og myndun [*in Icelandic*]. *Náttúrufræðingurinn*, Vol. 22 (4), pp. 145–172.

- (1962). Trjáför í Hverfjalls- og Hekluvík [in Icelandic]. *Náttúrufræðingurinn*, Vol. 32 (3), pp. 124–131.
- Tobler D. J., Cuthbert M. O., Greswell R. B., Riley M. S., Renshaw J. C., Handley-Sidhu S., Phoenix V. R. (2011). Comparison of rates of ureolysis between *Sporosarcina pasteurii* and an indigenous groundwater community under conditions required to precipitate large volumes of calcite. *Geochimica et Cosmochimica Acta*, Vol. 75 (11), pp. 3290–3301.
- Tol P. (22nd Sept. 2018). *Qualitative colour schemes*. URL: <https://personal.sron.nl/~pault/>.
- Toneatti D. M., Albarracín V. H., Flores M. R., Polerecky L., Farías M. E. (2017). Stratified bacterial diversity along physico-chemical gradients in high-altitude modern stromatolites. *Frontiers in Microbiology*, Vol. 8, p. 646.
- Tosi N., Plesa A.-C., Breuer D. (2013). Overturn and evolution of a crystallized magma ocean: A numerical parameter study for Mars. *Journal of Geophysical Research: Planets*, Vol. 118 (7), pp. 1512–1528.
- Truong D. T., Franzosa E. A., Tickle T. L., Scholz M., Weingart G., Pasolli E., Tett A., Huttenhower C., Segata N. (2015). MetaPhlAn2 for enhanced metagenomic taxonomic profiling. *Nature Methods*, Vol. 12, pp. 902–903.
- United Nations (1967). *Treaty on principles governing the activities of states in the exploration and use of outer space, including the Moon and other celestial bodies, General Assembly resolution 2222 (XXI)*. Ed. by United Nations. New-York.
- Vaïsse E. F., Hoyos F. S., Echeverría y Reyes A. (1896). *Diccionario de la lengua Atacameña [in Spanish]*. Cervantes.
- Vaucher J., Baratoux D., Mangold N., Pinet P., Kurita K., Grégoire M. (2009). The volcanic history of central Elysium Planitia: Implications for martian magmatism. *Icarus*, Vol. 204 (2), pp. 418–442.
- Vick T. J., Dodsworth J. A., Costa K. C., Shock E. L., Hedlund B. P. (2010). Microbiology and geochemistry of Little Hot Creek, a hot spring environment in the Long Valley Caldera. *Geobiology*, Vol. 8 (2), pp. 140–154.
- Viles H. A. (2012). Microbial geomorphology: A neglected link between life and landscape. *Geomorphology*, Vol. 157–158, pp. 6–16.
- Villagrán C., Armesto J. J., Kalin Arroyo M. T. (1981). Vegetation in a high Andean transect between Turi and Cerro León in Northern Chile. *Vegetatio*, Vol. 48 (1), pp. 3–16.
- Vilte Vilte J., Pérez C. (2004). *Kunza – diccionario kunza-español / español-kunza – lengua del pueblo lickan antai o atacameño*. Ed. by B. Stevenson. Santiago: Ograma S. A. ISBN: 956-8072-03-9.
- Vimercati L., Hamsher S., Schubert Z., Schmidt S. K. (2016). Growth of high-elevation *Cryptococcus* sp. during extreme freeze–thaw cycles. *Extremophiles*, Vol. 20 (5), pp. 579–588.
- Vítek P., Jehlička J., Bezděk J., Francøu E. (2009). Degradation of β -carotene under UV-rich irradiation conditions: Implications for martian environment. In: *40th Lunar and Planetary Science Conference* –, p. 1970.

- Voet D., Gratzer W. B., Cox R. A., Doty P. (1963). Absorption spectra of nucleotides, polynucleotides, and nucleic acids in the far ultraviolet. *Biopolymers*, Vol. 1 (3), pp. 193–208.
- Vuille M., Ammann C. (1997). Regional snowfall patterns in the high, arid Andes. *Climatic Change*, Vol. 36 (3–4), pp. 413–423.
- Wadsworth J., Cockell C. S. (2017). Perchlorates on Mars enhance the bacteriocidal effects of UV light. *Scientific Reports*, Vol. 7, p. 4662.
- Wakeham S. G., Schaffner C., Giger W. (1980). Diagenetic polycyclic aromatic hydrocarbons in Recent sediments: Structural information obtained by high performance liquid chromatography. *Physics and Chemistry of the Earth*, Vol. 12. Proceedings of the Ninth International Meeting on Organic Geochemistry, pp. 353–363.
- Walker J. J., Spear J. R., Pace N. R. (2005). Geobiology of a microbial endolithic community in the Yellowstone geothermal environment. *Nature*, Vol. 434, 1011–1014.
- Walsh K. J., Morbidelli A., Raymond S. N., O'Brien D. P., Mandell A. M. (2011). A low mass for Mars from Jupiter's early gas-driven migration. *Nature*, Vol. 475, pp. 206–209.
- Walter M. R., Bauld J., Brock T. D. (1972). Siliceous algal and bacterial stromatolites in hot spring and geyser effluents of Yellowstone National Park. *Science*, Vol. 178 (4059), pp. 402–405.
- Wang F., Michalski G., Seo J. hye, Ge W. (2014). Geochemical, isotopic, and mineralogical constraints on atmospheric deposition in the hyper-arid Atacama Desert, Chile. *Geochimica et Cosmochimica Acta*, Vol. 135, pp. 29–48.
- Wang F., Michalski G., Seo J.-H., Granger D. E., Lifton N., Caffee M. (2015). Beryllium-10 concentrations in the hyper-arid soils in the Atacama Desert, Chile: Implications for arid soil formation rates and El Niño driven changes in Pliocene precipitation. *Geochimica et Cosmochimica Acta*, Vol. 160, pp. 227–242.
- Wang F., Michalski G., Luo H., Caffee M. (2017). Role of biological soil crusts in affecting soil evolution and salt geochemistry in hyper-arid Atacama Desert, Chile. *Geoderma*, Vol. 307, pp. 54–64.
- Wang M. C., Huang P. M. (1987). Polycondensation of pyrogallol and glycine and the associated reactions as catalyzed by birnessite. *Science of The Total Environment*, Vol. 62, pp. 435–442.
- Wang Q., Garrity G. M., Tiedje J. M., Cole J. R. (2007). Naïve Bayesian classifier for rapid assignment of rRNA sequences into the new bacterial taxonomy. *Applied and Environmental Microbiology*, Vol. 73 (16), pp. 5261–5267.
- Warner N. H., Farmer J. D. (2010). Subglacial hydrothermal alteration minerals in jökulhlaup deposits of southern Iceland, with implications for detecting past or present habitable environments on Mars. *Astrobiology*, Vol. 10 (5), pp. 523–545.
- Warren J. K. (2016). Sabkhas, saline mudflats and aans. In: *Evaporites: A geological compendium*. Springer, pp. 207–302.
- Warren-Rhodes K. A., Rhodes K. L., Pointing S. B., Ewing S. A., Lacap D. C., Gómez-Silva B., Amundson R., Friedmann E. I., McKay C. P. (2006). Hypolithic cyanobacteria,

- dry limit of photosynthesis, and microbial ecology in the hyperarid Atacama Desert. *Microbial Ecology*, Vol. 52 (3), pp. 389–398.
- Webster C. R., Mahaffy P. R., Atreya S. K., Flesch G. J., Mischna M. A., Meslin P.-Y., Farley K. A., Conrad P. G., Christensen L. E., Pavlov A. A., Martín-Torres J., Zorzano M.-P., McConnochie T. H., Owen T., Eigenbrode J. L., Glavin D. P., Steele A., Malespin C. A., Archer P. D., Sutter B., Coll P., Freissinet C., McKay C. P., Moores J. E., Schwenzer S. P., Bridges J. C., Navarro-Gonzalez R., Gellert R., Lemmon M. T., the MSL Science Team (2014). Mars methane detection and variability at Gale crater. *Science*.
- Webster C. R., Mahaffy P. R., Atreya S. K., Moores J. E., Flesch G. J., Malespin C., McKay C. P., Martinez G., Smith C. L., Martin-Torres J., Gomez-Elvira J., Zorzano M.-P., Wong M. H., Trainer M. G., Steele A., Archer D., Sutter B., Coll P. J., Freissinet C., Meslin P.-Y., Gough R. V., House C. H., Pavlov A., Eigenbrode J. L., Glavin D. P., Pearson J. C., Keymeulen D., Christensen L. E., Schwenzer S. P., Navarro-Gonzalez R., Pla-García J., Rafkin S. C. R., Vicente-Retortillo Á., Kahanpää H., Viudez-Moreiras D., Smith M. D., Harri A.-M., Genzer M., Hassler D. M., Lemmon M., Crisp J., Sander S. P., Zurek R. W., Vasavada A. R. (2018). Background levels of methane in Mars' atmosphere show strong seasonal variations. *Science*, Vol. 360 (6393), pp. 1093–1096.
- Weete J. D. (1976). Algal and fungal waxes. In: *Chemistry and Biochemistry of Natural Waxes*. Ed. by P. E. Kolattukudy. Amsterdam – Oxford – New York: Elsevier, pp. 349–418.
- Weete J. D., Weber D. J., Le Tourneau D. (1970). Hydrocarbons, free fatty acids, and amino acids of sclerotia of *Sclerotinia sclerotiorum*. *Archiv für Mikrobiologie*, Vol. 75 (1), pp. 59–66.
- Wentworth C. K. (1922). A scale of grade and class terms for clastic sediments. *The Journal of Geology*, Vol. 30 (5), pp. 377–392.
- Werner S. C., Gasselt S. van, Neukum G. (2003). Continual geological activity in Athabasca Valles, Mars. *Journal of Geophysical Research: Planets*, Vol. 108 (E12), p. 8081.
- Werner S., Tanaka K. (2011). Redefinition of the crater-density and absolute-age boundaries for the chronostratigraphic system of Mars. *Icarus*, Vol. 215 (2), pp. 603–607.
- Westall F., Foucher F., Bost N., Bertrand M., Loizeau D., Vago J. L., Kminek G., Gaboyer F., Campbell K. A., Bréhéret J.-G., Gautret P., Cockell C. S. (2015). Biosignatures on Mars: What, where, and how? Implications for the search for martian life. *Astrobiology*, Vol. 15 (11), pp. 998–1029.
- Wetherill G. W. (1991). Why isn't Mars as big as Earth? In: *XXII Lunar and Planetary Sciences Conference – Houston TX, USA*, pp. 1495–1496.
- Wierzchos J., Cámara B., de los Ríos A., Davila A. F., Sánchez Almazo I. M., Artieda O., Wierzchos K., Gómez-Silva B., McKay C., Ascaso C. (2010). Microbial colonization of Ca-sulfate crusts in the hyperarid core of the Atacama Desert: Implications for the search for life on Mars. *Geobiology*, Vol. 9 (1), pp. 44–60.

- Wierzchos J., Ascaso C., McKay C. P. (2006). Endolithic cyanobacteria in halite rocks from the hyperarid core of the Atacama Desert. *Astrobiology*, Vol. 6 (3). PMID: 16805697, pp. 415–422.
- Wierzchos J., Casero M. C., Artieda O., Ascaso C. (2018). Endolithic microbial habitats as refuges for life in polyextreme environment of the Atacama Desert. *Current Opinion in Microbiology*, Vol. 43. Environmental Microbiology * The New Microscopy, pp. 124–131.
- Wiesenberg G. L. B., Lehdorff E., Schwark L. (2009). Thermal degradation of rye and maize straw: Lipid pattern changes as a function of temperature. *Organic Geochemistry*, Vol. 40 (2), pp. 167–174.
- Wilhelm M. B., Davila A. F., Eigenbrode J. L., Parenteau M. N., Jahnke L. L., Liu X.-L., Summons R. E., Wray J. J., Stamos B. N., O'Reilly S. S., Williams A. (2017). Xeropreservation of functionalized lipid biomarkers in hyperarid soils in the Atacama Desert. *Organic Geochemistry*, Vol. 103, pp. 97–104.
- Williams D. A., Greeley R., Fergason R. L., Kuzmin R., McCord T. B., Combe J.-P., Head J. W., Xiao L., Manfredi L., Poulet F., Pinet P., Baratoux D., Plaut J. J., Raitala J., Neukum G. (2009). The Circum-Hellas Volcanic Province, Mars: Overview. *Planetary and Space Science*, Vol. 57 (8), pp. 895–916.
- Winters Y., Lowenstein T., Timofeeff M. (2013). Identification of Carotenoids in Ancient Salt from Death Valley, Saline Valley, and Searles Lake, California, Using Laser Raman Spectroscopy. *Astrobiology*, Vol. 13 (11). PMID: 24283928, pp. 1065–1080.
- Wolfe A. J. (2002). Germs in space. Joshua Lederberg, exobiology, and the public imagination, 1958-1964. *Isis*, Vol. 93 (2), pp. 183–205.
- Wood D. E., Salzberg S. L. (2014). Kraken: ultrafast metagenomic sequence classification using exact alignments. *Genome Biology*, Vol. 15 (3), R46.
- Wright I. P., Grady M. M., Pillinger C. T. (1989). Organic materials in a martian meteorite. *Nature*, Vol. 340, pp. 220–222.
- WWF (2018). *Terrestrial ecoregions*. World Wildlife Fund. URL: <https://www.worldwildlife.org/>.
- Zent A. P., Hecht M. H., Cobos D. R., Wood S. E., Hudson T. L., Milkovich S. M., DeFlores L. P., Mellon M. T. (2010). Initial results from the thermal and electrical conductivity probe (TECP) on Phoenix. *Journal of Geophysical Research*, Vol. 115 (E3), E00E14.